Title

PLATINUM SURFACE CHEMISTRY STUDIED BY THERMAL DESORPTION SPECTROMETRY AND NEAR EDGE X-RAY ABSORPTION FINE STRUCTURE: ADSORBATE EFFECTS

Author

Johnson, A.L.

Publication Date

1986

Lawrence Berkeley Laboratory
UNIVERSITY OF CALIFORNIA

Materials & Molecular Research Division

PLATINUM SURFACE CHEMISTRY STUDIED BY THERMAL DESORPTION SPECTROMETRY AND NEAR EDGE X-RAY ABSORPTION FINE STRUCTURE: ADSORBATE EFFECTS

A.L. Johnson
(Ph.D. Thesis)

January 1986

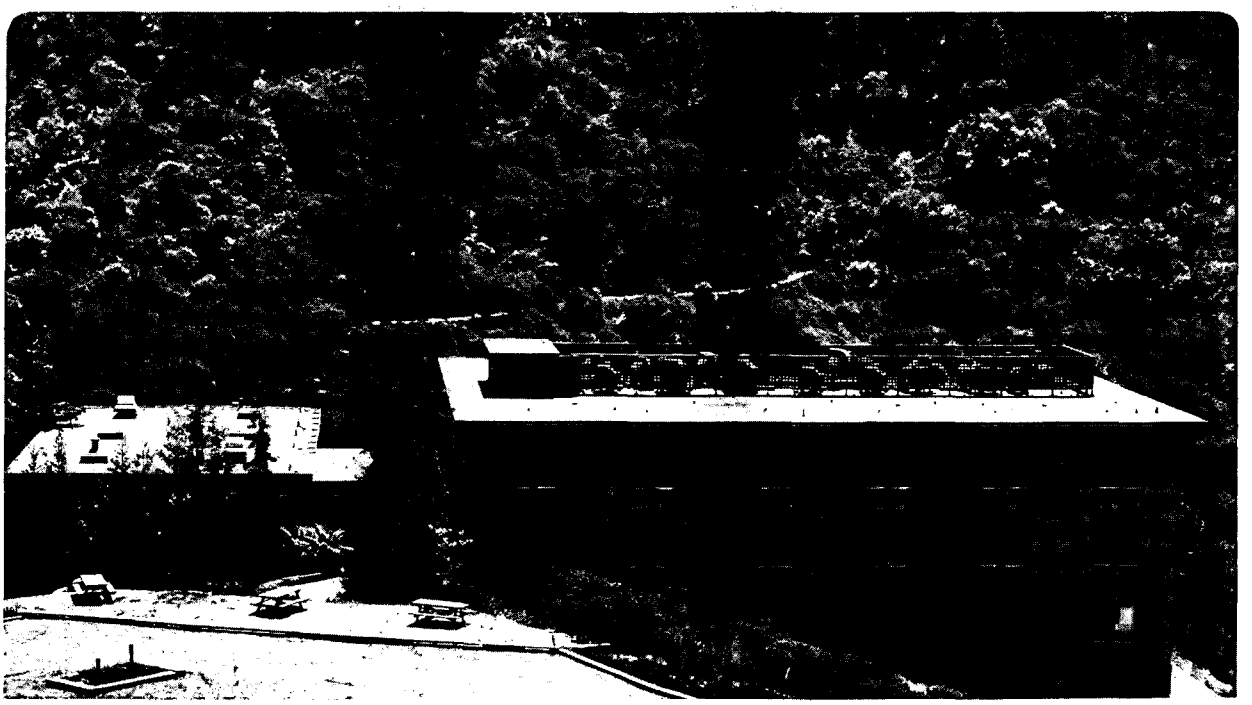

Prepared for the U.S. Department of Energy under Contract DE-AC03-76SF00098

DISCLAIMER

LBL-20964

Platinum Surface Chemistry Studied by Thermal Desorption Spectrometry and Near Edge X-ray Absorption Fine Structure: Adsorbate Effects

Allen Lewis Johnson
Ph.D. Thesis

Lawrence Berkeley Laboratory
University of California
Berkeley, California 94720

January 1986

Platinum Surface Chemistry Studied by Thermal Desorption Spectrometry and Near Edge X-ray Absorption Fine Structure: Adsorbate Effects

By

Allen Lewis Johnson

ABSTRACT

The surface chemistry of hydrocarbons, particularly aromatic hydrocarbons, adsorbed on Pt(111) was investigated by Thermal Desorption Spectrometry (TDS) and Near Edge X-ray Absorption Fine Structure (NEXAFS). The utility of NEXAFS in the investigation of reactive systems of molecules of moderate complexity is demonstrated.

Benzene chemisorption was studied as a function of temperature. Below the decomposition temperature benzene is parallel to the surface and π coordinated. At higher temperatures the benzene loses hydrogen, but maintains its parallel orientation. A benzyne-like surface state is proposed.

The fluorinated benzenes were investigated to determine the effects of shifts in energy of the HOMO and LUMO levels of the adsorbate on the chemisorption energy. The observed trend was not monotonic in either the HOMO or the LUMO energies and a steric effect is suggested. The fluorinated benzenes are found to chemisorb with a parallel orientation at temperatures below decomposition, similar to benzene.

The pyridine chemisorption state at low temperatures was oriented with its ring plane parallel to the surface which at higher temperatures became oriented with the ring plane normal to the surface. The transition is motivated by the formation of an α-pyridyl.

Thiophene, in common with all of the aromatic molecules studied, chemisorbed parallel to the surface. A low temperature extrusion of sulfur was demonstrated and an intermediate leading to hydrocarbon production was proposed.

The C_4 through C_8 cyclic unsaturated hydrocarbons were investigated

to determine the effects of aromaticity on chemisorption. The C_5, C_6, and C_7 molecules were flat and π coordinated to the Pt(111) surface, while the C_4 and C_8 rings were not, indicating the importance of gas phase aromaticity in hydrocarbon chemisorption on Pt(111).

Diatomics and pseudo diatomics were studied to determine under which conditions they might be oriented parallel (e.g. ethylene) or normal (e.g. CO) to the surface. All of the molecules except CO adsorbed nearly parallel to the surface at low temperature. A novel electron induced decomposition of acetonitrile is reported and a mechanism is proposed.

Finally, the future of NEXAFS is discussed and extensions to the present work suggested.

Neil A. Stirley
1/8/86

TABLE OF CONTENTS

ACKNOWLEDGEMENTS

The author wishes to acknowledge the support of the many people who made this work possible. Dr. Earl Muetterties provided a work environment and support that was an honor to work under. He will be missed. Dr. David Shirley helped me in a difficult situation and gave invaluable guidance as to the basic nature of the spectrometry. Dr. J. Stöhr was tolerant when I was learning the basics of synchrotron radiation work and was kind, thoughtful, and enthusiastic during our collaboration. Dr. C. M. Friend provided the opportunity to do work at the National Synchrotron Light Source.

I also wish to thank co-workers and others: Dr. F. Sette and Dr. J. Gland, for aid and support during the NEXAFS investigations; the Muetterties and Shirley research group members, for discussions and friendship; and my friends at Berkeley without whom I would not have been able to finish my graduate career.

Funding for this work came from the Director, Office of Energy Research, Office of Basic Energy Science, Chemical Sciences Division of the U. S. Department of Energy under contract No. DE-AC03-76SF00098. I also wish to acknowledge the support for travel money during some of this work the Dean of the Graduate School, the University of California, Berkeley, and the NSLS-HFBR Faculty and Student Support program of the Department of Energy. Most of the NEXAFS work done here was done at the Stanford Synchrotron Radiation Laboratory which is supported by the Office of Basic Energy Sciences of DOE and the Division of Materials Research of the National Science Foundation.

"Chemistry: `the art or practice of the chemist'; at first probably contemptuous,...

3. That branch of physical science and research, which deals with the several elementary substances, or forms of matter, of which all bodies are composed, the laws that regulate the combination of these elements in the formation of compound bodies, and the various phenomena that accompany their exposure to diverse physical conditions."[1]

I INTRODUCTION

This thesis describes kinetic, spectroscopic, and structural studies of the chemisorption of organic molecules of modest complexity to (primarily) the Pt(111) surface. The relationship of structure and reactivity studies can be visualized in terms of the generalized reaction diagram (figure 1). Structural studies require a sample that stays unchanged during the course of the measurement. If the structure of the molecule changes during the measurement then an average molecular structure is observed. States at local minima in the potential energy surface (intermediates) are those which have lifetimes long enough to be directly investigated by most spectrometries (although there is recent work with ultra fast measurements on the nano to pico second time scale to investigate species with very short lifetimes). Reactivity, on the other hand, is controlled by the path potential energy local maxima (transition states). Transition states are generally of low concentration and of short lifetime in a reacting system and are therefore not generally accessible to direct measurement.

We have focused on the interactions of unsaturated hydrocarbons with the platinum (111) and (100) surfaces. Unsaturated molecules chemisorb to the Pt(111) surface and exhibit interesting chemistry. We have investigated diatomic, pseudo diatomic, and aromatics chemisorbed species. Diatomics are suited to investigations of the basic nature of surface chemistry because of their relative simplicity. Aromatic molecules are particularly well suited to investigation of the effects of chemical modification of the adsorbate on chemisorption because of extensive investigations of substituent effects in the gas and solution phase (to derive the linear free energy relations, amongst others) and

because the extraordinary stability of aromatic molecules makes it more likely that the molecule will be weakly perturbed from the gas phase and thus extrapolations between members of the family both with respect to gas phase behavior and in comparing members of the family in their chemisorption behavior is better founded. Strongly chemisorbed molecules, and in particular those which undergo extensive structural change on chemisorption, require explicit inclusion of metal orbitals in their theoretical description and so use of the implicitly first order treatment of the systematic trends in terms of adsorbate electronic and structural changes will be significantly in error.

The choice of the platinum surfaces for investigation was predicated upon several factors. First, platinum surfaces (in particular the thermally most stable [111] surface) exhibit both associative and dissociative chemisorption and allow the study of both the surface chemical bond and surface chemical reactivity. The platinum (111) surface is the predominate surface plane in platinum particles created by the preparation of annealed dispersed platinum catalysts and is therefore a good model for a common heterogeneous catalyst. Lastly, platinum has been one of the most intensively studied transition metals and there is a large body of previous work that provides such information as Auger calibrations, core binding energies and other parameters that make theoretical understanding of the specifics of platinum surface chemistry possible.

Here we will present results derived primarily from thermal desorption spectrometry (TDS, sometimes referred to as temperature programed reaction spectrometry, TPRS) and Near Edge X-ray Absorption

Fine Structure (NEXAFS; NEXAFS is the surface analog of X-ray Absorption Near Edge Structure [XANES]) studies of organic molecules adsorbed on low Miller index platinum surfaces under ultra high vacuum conditions (i.e. pressures $< 10^{-7}$torr).

Thermal desorption spectrometry is a tool to investigate reaction kinetics - it is essentially the ultra high vacuum equivalent of a batch reactor. Thermal desorption can be used to derive plausible structures using the principle of least motion (maximize entropy) and maximal bonding (minimize enthalpy) during the course of reaction; but these structures are inferred and not directly observed. Utilization of isotope labeling and investigation of families of molecules, in a manner similar to that used in physical organic studies, allows one to investigate the effects of electronic and structural changes of the adsorbate on the surface reaction and thus derive information about the relevant parameters of the surface transition state.

NEXAFS is a spectroscopic technique that is suited to investigations of the molecular structure of large molecular species adsorbed in a partially disordered fashion on surfaces. Structural studies allow one to directly observe the effect of electronic and structural changes of the adsorbate on the surface chemical bond as reflected by changes in chemisorption geometry. NEXAFS can also indicate that structural changes have occurred in a molecule during a surface reaction and thus indicate molecular reactivity, in a sense by acting as a detector during a thermal desorption experiment. This capability is very important since thermal desorption experiments generally use mass spectrometric detection and so are limited to observation of gas phase products.

NEXAFS, being a relatively new tool in surface science, should be put into proper perspective with respect to other methods of structural analysis of adsorbates on well characterized single crystal surfaces. NEXAFS allows the determination of parameters such as bond length and tilt with respect to the surface for adsorbates that are only weakly ordered, for example reaction intermediates. Additionally one can examine each type of atom separately in a heteroatomic adsorbate (given that photons of the appropriate energy and polarization are available) independently of the other atoms, thus getting molecular parameters in the region of the atom being studied and allowing the possibility of studies of coadsorption without direct interference in the spectra.

Other direct structural methods being used for surface studies include low energy electron diffraction (LEED), high resolution electron energy loss (HREELS), angle resolved photoelectron spectrometry (ARPES), angle resolved photoelectron extended fine structure (ARPEFS), surface extended x-ray absorption fine structure (SEXAFS), Rutherford backscattering, azimuthal photoelectron diffraction (APD), grazing angle x-ray diffraction, electron (and photon) stimulated desorption of ions angular distribution (ESDIAD), and scanning tunneling microscopy. These techniques can be divided into two types: those that examine the long range ordering of the adsorbate/substrate pair and those that don't. All of these methods with the exception of HREELS, ESDIAD, ARPES, and scanning tunneling microscopy examine the ordering of the adsorbate/substrate pair. This characteristic is one of the strengths of these methods - the dependence on ordering gives direct dependence on the specific surface site of the adsorbate and thus can give registry to

the surface. However, this leaves ARPES, HREELS, ESDIAD, and scanning tunneling microscopy as possible general tools for the investigation of systems of large (and potentially disordered) adsorbates.

Scanning tunneling microscopy is the newest of the techniques and potentially one of the most powerful, giving as it does the potential for direct imaging of the surface under investigation[2a,b]. Concomitant, however, with direct imaging is the possibility of perturbation of the state visualized[2c]. Tunneling microscopes use fields greater than 10^7V/cm to create the tunneling current and it has not been shown to image potentially mobile adsorbates.

ESDIAD examines the direction of desorption of ions created by either photon or electron excitation. If electronic motion is rapid with respect to nuclear motion (which in general is expected to be true) then in the model where bonding is essentially two center the repulsive state produced relaxes by ejection of the ion along the bond vector direction. If the ensemble of adsorbed molecules have bonds which are distributed anisotropically then the ion emission will be anisotropic and so surface orientation can be derived. This technique requires that there be facile ion production for the bond of interest and has to account for the subsequent perturbation by the surface of the departing ion trajectories[3]. ESDIAD is however in general insensitive to the presence of coadsorbed species and has been recently used to investigate the effects of surface modifiers on the surface chemical bond.

HREELS has gained popularity as a method to determine the structure of adsorbates. These studies have relied on several types of analysis. At the lowest level of analysis there is determination of local symmetry of the adsorbate by counting the number of mode seen and using symmetry

constraints for the dipole excited vibrations. This kind of study requires that the adsorbate vibrations be correctly assigned and that the adsorbate be in a highly symmetric surface site[4]. The second form of analysis utilizes appropriate structural models for the adsorbate (either gas phase or metal coordination compounds) and derives a reasonable structure. If a model compound close to the projected structure can be found then the suggested structure can be classified as plausible or implausible[5]. One of the more recent forms of analysis attempted was an investigation of the intensity of the observed vibrations, and utilizing the surface dipole selection rule for molecular vibrations one determines a surface tilt. It has been recently noted that this form of analysis requires a knowledge of the intrinsic intensity of the two transitions being compared, which may be strongly perturbed by the surface[6]. It should be noted that HREELS remains the method of choice for investigations of the behavior of hydrogens, particularly in hydrocarbons, due to its high sensitivity and selectivity for the hydrogen vibrational modes.

ARPES examines the angular distribution of the photoelectrons emitted by the valence levels of the chemisorbed molecule. It therefore requires detailed knowledge of the actual electronic state of the chemisorbed species, which for complex molecules is quite difficult. The signal may also be obscured by the effects of emission from the substrate.

In addition there are indirect methods for structural determinations. As indicated above, the use of model compounds in HREELS is an indirect method. The appearance and relative shifts of

electronic transitions (detected by electron energy loss spectrometry in the 1 to 10 eV range and by UV photoelectron spectrometry) and by core level shifts (observed by X-ray photoelectron spectrometry) are common indirect tools to determine surface structure. The difficulty with these techniques is that the interpretation of the spectra in terms of structural parameters requires the ability to determine the electronic shifts induced by structural features, which is at present not generally possible.

NEXAFS has its limitations as a surface tool. In many cases there is no direct information as to the particular surface register that the adsorbate occupies. The resonances in the near edge region are stronger than those seen for SEXAFS but the resonances are not in general sharp enough to resolve the various chemical identities in the chemisorbed molecules. Similarly, the orientation detected by the technique is an averaged orientation - if there is more than one surface species then the observed structural parameters are an average of all the surface species (which in some cases may be an advantage - small amounts of decomposition or minority product can (to first order) be ignored). Bond lengths are derived from the energy position of the sigma resonances. Recently a linear correlation between bond length and shape resonance position has been proposed experimentally but theoretical treatments of the effect give a linear correlation as a limiting case and thus each determination must be examined carefully to determine if it is justified (particularly when the molecule is highly symmetric)[7]. In the case of strongly chemisorbed molecules (in particular those with metal-carbon sigma bonding) the spectra can be interpreted in detail only with quantum mechanical calculations, at some cost and difficulty[8].

The detection methods currently available to investigate the first row elements (some variant on electron yield, generally) give low signal to background intensity and thus background subtraction and normalization become difficult. Lastly, NEXAFS investigations require time on a synchrotron radiation facility. The synchrotron facilities in the United States that are capable of supporting NEXAFS studies are at present very oversubscribed with respect to available beam time. The NEXAFS experiments described here were carried out at the Stanford Synchrotron Radiation Laboratory on beam line I-1 except where indicated.

In summary we will present the results of studies of diatomic, pseudo diatomic (such as acetylene and the nitriles), aromatic and substituted aromatic carbon containing molecules chemisorbed to platinum (primarily platinum (111)) studied by NEXAFS and thermal desorption spectrometry.

I.1 FIGURES

Figure 1

This figure shows a generalized diagram of a chemical reaction. Points A, C, and E are at local minima of the potential energy surface and are intermediates. Points B and D are at local maxima along the reaction coordinate and at minima along paths near the reaction coordinate.

The meaning of "Reaction Pathway" and reaction coordinate deserves further comment. The plot is supposed to describe the potential that a molecule experiences while it is undergoing reaction. Thus the reaction pathway or the reaction coordinate refers to the "progress" of reaction, i.e. the extent of the molecular distortions that lead to the products. The implication of the thermodynamic treatment of the diagram is that the path is in some sense a local minima at all points i.e. that any path close to the reaction path traces a higher energy pathway. Thus the points B and D are saddle points of the full potential energy surface. This model is reasonable for molecules in solution or adsorbed to surfaces: they are in contact with a condensed phase that provides a thermodynamic sink and thus the reacting species are in equilibrium at each point on the potential energy surface. This is in contrast to the gas phase, where unless some method is available to redistribute energy a molecule at point C must have excess internal energy equal to E_B-E_C or E_D-E_C and thus the molecular trajectory is not controlled solely by the potential.

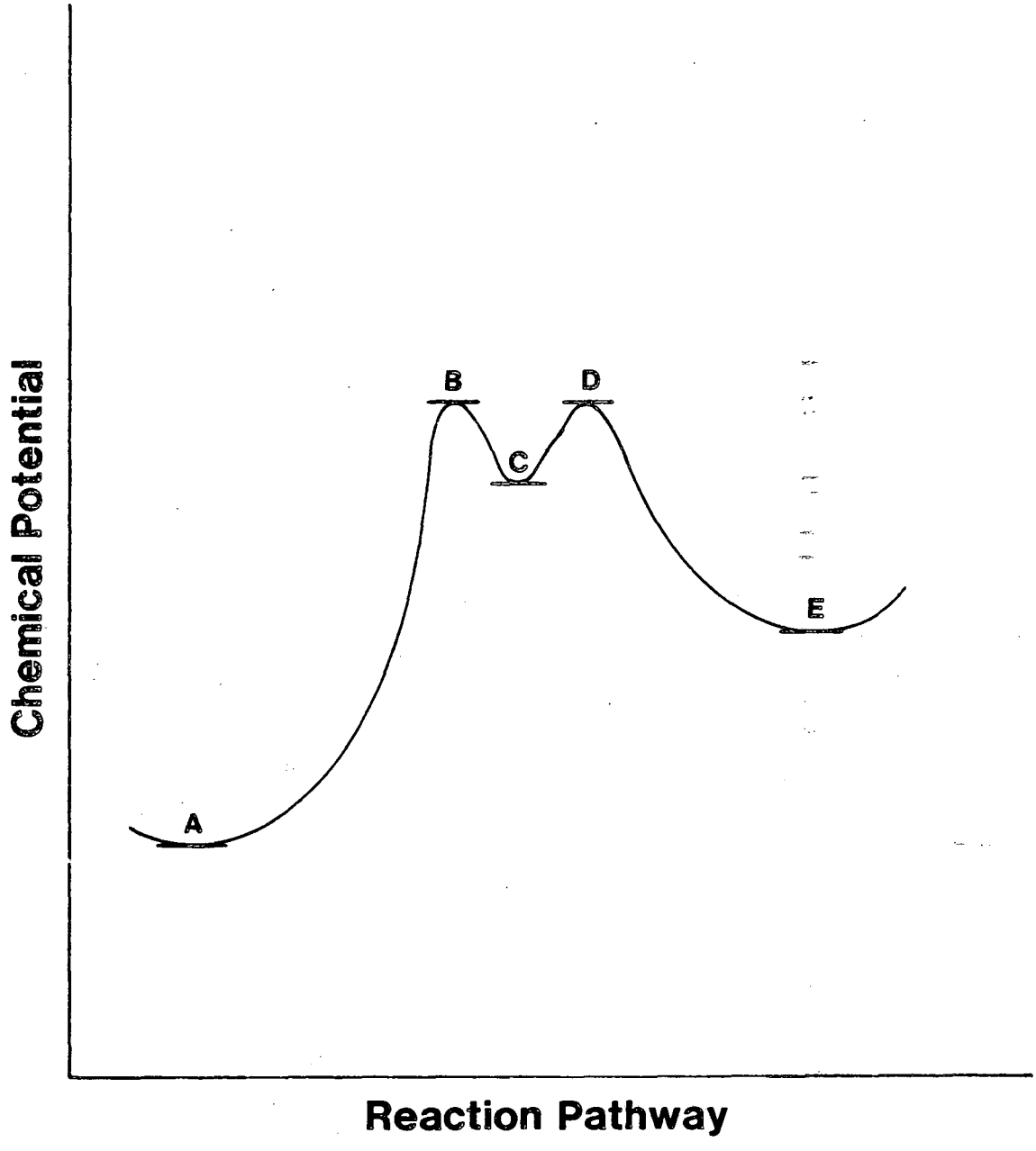

XBL 8512-5094

II EXPERIMENTAL

II.1 Thermal Desorption

Thermal desorption experiments were carried out in an ion pumped Varian vacuum system equipped with an off-axis manipulator, Varian Auger/LEED optics, a grazing incidence electron gun, an argon-ion sputter gun, and a Uthe Technology International (UTI) model 100C quadrupole mass spectrometer with programmable peak selector. The single crystal sample was heated in the early experiments by contact with a button heater and in the later experiments resistively. Sample cooling in the early experiments was done by contact to a liquid nitrogen cooled copper block, and in later experiments using a copper braid to a liquid nitrogen cooled copper cold finger. The mass spectrometer was modified when the heating method was changed. It was found when the crystal was electrically isolated that the mass spectrometer was delivering 300 microamperes to the crystal face. To ameliorate this condition and to improve the directional selectivity of the mass spectrometer an electrically isolated cage was fitted about the ionizer region (figure 2).

The rationale for this change is as follows: high efficiency mass spectrometer ionizers operate in the space charge limited regime; i.e., electrons from the ionizer filament are accelerated to the central region and then oscillate between the inner region and outer repeller grid until either the electron hits a grid or until it is lost to the outside. At low ionizer currents the first process predominates and the electron currents outside the ionizer can be small. At high ionizer currents (space charge limited operation) the electron density builds up in the inner region until the acceleration potential is inadequate to

inject electrons in the ionization region. In this case there is an electron gas in the inner region at a negative potential essentially equal to the acceleration potential (in our case 70 volts) which then leaks out the front of the ionizer. When a crystal is facing the ionizer we observe 70eV electrons at a flux of 1.9×10^{15}/second. This is adequate energy and flux to cause possible electron stimulated changes in the surface chemistry. The floating cage solves the problem by intercepting part of the electrons lost and charging up to a potential sufficient to repel any electron that escape the ionizer. The front plate serves as a collimator for the incident desorbed molecules. Two further modifications must be made. First, the charged cage proves to be more efficient at extracting ions from the inner region than the lenses into the quadrupole mass spectrometer: thus a second grid must be spot welded to the front of the inner region to isolate the ions from the field due to the floating cage. Second, this modification changes the balance of current lost from the filament to that intercepted by the inner cage, and the high pressure filament protection interlock must be inactivated. After this change was made the current to the crystal was less than one microampere, which also allows both the ion gauge and the Auger spectrometer to be operated with the mass spectrometer on. The present arrangement has the advantage that it requires minimal modification of the UTI mass spectrometer, but has the disadvantage that electron impact on the alumina ceramic tubes used to support the cage create electron stimulated desorption of oxygen atoms. This leads to a persistent mass 16 signal. The modification would be more convenient and permanent if the cage was attached by electrically isolated screws

into the quadrupole case.

The significance of these modifications shall be indicated in the discussion where the present results differ from those obtained earlier by the Muetterties group on the unmodified system.

After the crystal was mounted it was cleaned and the surface order was checked by LEED. Cleaning was by oxygen treatments at 770 K and 10^{-7}torr. Argon ion sputtering was used when necessary to remove contamination that was not removable by oxygen treatments.

The experimental protocol used for the thermal desorption experiments was to clean the crystal using oxygen treatments at 10^{-7}torr and 770 K followed by an anneal to 1200 K, and an Auger spectrum was taken. The crystal was then cooled to the dosing temperature and flashed to remove carbon monoxide, with the heater adjusted to give a heating rate of 25 K/second between 300 K and 500 K. When the crystal reached dosing temperature again, the adsorbate sample was introduced into the chamber though a needle doser. When the chamber pressure had dropped to a low value (generally $3x10^{-10}$torr) the crystal was rotated toward the mass spectrometer, the heater was turned on, and a mass spectrum was collected using a UTI programmable peak selector to simultaneously observe several peaks of interest. The temperature ramp and mass spectrometer program were terminated at 870 K and the data recorded on graph paper. After the experiment an Auger spectra was taken to determine the amount of decomposition.

Temperatures were measured using a chromel - alumel thermocouple spot welded to the crystal edge. The thermocouple signal was processed by an Omega thermocouple amplifier/cold junction and recorded using a Hewlett Packard x-y recorder. The accuracy of the temperature

measurement is limited by the uneven heating of the crystal - the estimated error is $\pm 5^{\circ}$. The relative intensity of the mass spectrometer signal is presented without any attempt to correct for the changing ionization efficiency and transmission of the mass spectrometer with changing species. The relative intensities of different peaks of the same mass are limited by the tailing of the earlier peaks due to limited pumping speed of the molecule - the error induced is very dependent on the molecule in question but should be on the order of ±15%. The identities indicated in the following thermal desorption spectra are derived from the mass data and in some case by analysis of the mass spectral cracking pattern. In some cases (H_2, HD, D_2, molecular ion) these assignments are unambiguous but in other cases the indicated identities are the most reasonable species consistent with the observed mass and the expected chemistry of the system.

Three methods of analysis will be used to treat the thermal desorption results. Molecules can desorb from the surface in either the desorption-limited or reaction limited-regimes. We have found that the temperature at which molecules such as hydrogen desorb from Pt(111) is perturbed by at most $\pm 30^{\circ}$ due to coadsorption of hydrocarbons or hydrocarbon fragments. Thus if desorption is observed at a temperature above that required for desorption (i.e. the desorption is reaction-limited), the appearance of the gas phase product indicates the onset of the production reaction.

Chemisorbed molecules can be displaced from the surface by other molecules in the gas phase. This allows the observation of reaction at temperatures below those needed for desorption. We have used

displacement reactions to indicate ordering of heats of chemisorption. One can also get trends of chemisorption heats from this kind of experiment: the displacement must be energetically favored to proceed. It is however important to note that displacement may not be seen for kinetic reasons. All of the displacement reactions that we observed supported the thermal desorption results.

Lastly, thermodynamic analysis such as that proposed by Redhead and others[9] allows the determination of the energy of activation toward desorption in well behaved cases. This kind of analysis requires that the desorption be uncomplicated by factors such as competitive reaction, anomalous heating and pumping rates, and intermolecular forces. We will use this form of analysis to detect trends in the activation energy of desorption (and, since these molecules have sticking coefficients near one, trends in heats of chemisorption) of families of similar molecules, where similar preexponential factors and desorption order are expected. This analysis will be used predominately at low coverages, to minimize the effect of intermolecular forces.

II.1.1 FIGURES

Figure 2

I is the unmodified UTI mass spectrometer ionizer. A is the inner (ionizing) region. B is the filament. C is the repeller grid. D is the acceleration grid/lens. E is the ion extraction and focusing lens.

II is the modified ionizer. F is the floating cage. G is the tantalum front plate. H is the supporting ceramic tubes. I is the ion region isolation grid.

I

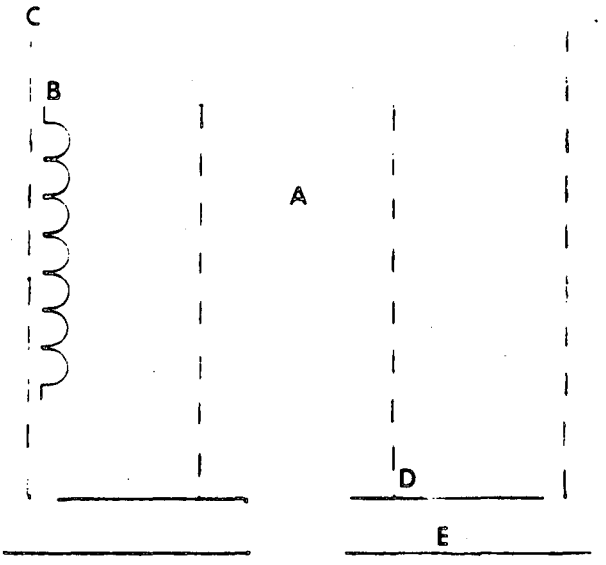

II

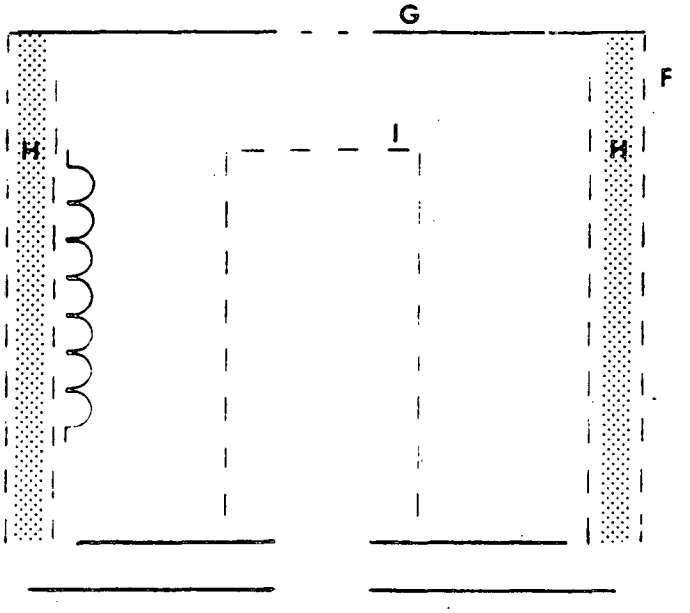

XBL 8512-5096

II.2 Near Edge X-ray Absorption Fine Structure (NEXAFS)

II.2.1. Theoretical Basis

NEXAFS is a spectroscopy that examines the energy and polarization dependence of the x-ray absorption coefficient in the region of the onset of absorption. It is associated with the excitation of electrons from the core levels of the absorbate to empty states localized in the region of the absorbate. Similar core level spectroscopies are XPS, ARPEFS, EXAFS, and XANES.

XPS (X-ray Photoelectron Spectrometry) uses fixed energy laboratory X-ray sources to investigate the binding energy of the core level electrons. It is an angle averaged method, and has been interpreted in terms of effective oxidation state and hybridization of the absorbing atom. XPS interpretation is complicated by the effects of screening of the core hole produced during photoemission by valence and other nearby polarizable electrons as well as by multielectron excitations.

ARPEFS (Angle Resolved Photoelectron Extended Fine Structure), on the other hand, uses variable energy X-ray sources (i.e. synchrotron radiation) and angle resolved electron detection to determine absorbate geometries. ARPEFS has been interpreted in terms of superposition of the direct and scattered photoelectron waves at the detector. ARPEFS is complicated by the same effects as for XPS as well as the presence of Auger electron emission peaks through which the photoemission peaks of interest sweep with changing photon energy.

EXAFS (Extended X-ray Absorption Fine Structure) is different from the preceding techniques. EXAFS investigates the behavior of the X-ray absorption coefficient in the extended fine structure region, where the structure is dominated by interference from the photoemitted electron

waves with the scattered photoelectron waves at the absorbing atom (figure 3). Thus if the detection method is invariant with photon energy (such as Auger detection) or isotropic then the detector placement does not affect the EXAFS signal. EXAFS suffers from weak signal, particularly with dilute absorbates. It is interesting to note that the near edge structure is generally obtained during EXAFS studies and discarded since the near edge structure cannot be interpreted by the single-scattering EXAFS picture.

XANES (X-ray Absorption Near Edge Structure) is in fact the same as NEXAFS (Near Edge X-ray Absorption Fine Structure). XANES is the acronym common used in investigations of the behavior of the x-ray absorption coefficient of weakly ordered bulk samples (such as alloys and biological materials)[10] in the region of the absorption edge. The NEXAFS acronym is commonly used in surface studies, and emphasizes the relation of NEXAFS with EXAFS and S(urface)EXAFS.

The core excitation for NEXAFS can be induced by photons or by high energy electrons. These excitations are dipole transitions and are characterized by small momentum transfer[11]. The classical momentum transfer for a given energy transition is $E_i/c-E_f/c$ for photons and $2(E_i/v-E_f/v) = (2m_eE_i)^{1/2}-(2m_eE_f)^{1/2}$ for electrons in forward scattering. Thus as the energy of the incident electron beam gets large with respect to the investigated energy loss the momentum transfer approximately equals $(m_e/4E_i)^{1/2}$ and the excitation cross section becomes dominated by the dipole term. Many molecules have been studied in the gas phase by inelastic electron forward scattering and we will use these results when available as gas phase standards for the present

work.

Figure 5 shows the extended x-ray absorption fine structure of molecular gas phase bromine compared with krypton. Characteristic features are the low level of absorption before the edge, due to excitation of valence electrons and higher core levels into continuum states. At the edge are strong features due to excitation of the 1s electrons into states localized on the atom or molecule, either continuum resonances (shape resonances), Rydberg transitions, or discrete states such as π^* states (figure 4). At higher energy the structures become weak and periodic, and are due to interference between the exiting photoelectron and the backscattered waves from adjacent atoms (EXAFS)(figure 3). The important points are that the near edge features are much stronger than the extended features and that the near edge features are due to empty states localized near the atom or molecule.

NEXAFS spectrometry can be divided into an excitation step followed by the relaxation and detection step. The polarization dependence and photon energy dependence of the near edge structure have been analysed in terms of the excitation step[13]. Prior work has focused on the interpretation of the near edge features (bound-state resonances and continuum resonances) of atomic species and diatomics. Bound-state resonances are straightforward in interpretation. They are generally due to empty atomic or molecular states that are bound either due to interaction with the core hole or because of correlation interaction. The continuum resonances are more complex. Continuum resonances are above the photoemission threshold, and can arise from a number of causes and have differing compositions. Atomic continuum resonances are due to

an interaction between the coulomb, correlation, and centrifugal potentials (particularly for high Z atoms) that create a barrier in the atomic potential for certain high angular momentum final states. These continuum resonances are characterized by a single, high angular momentum component in calculated final states[13a].

Most of our studies have involved excitation of 1s orbitals, which gives a particularly simple form to the transition probability. The excitation is a dipole transition and for 1s initial states the intensity of the transition is found by summing the p wave components of the final state projected to the initial state center.

Several levels of approximation are possible in the interpretation of polarization dependent NEXAFS spectra. At the lowest level of theory we assume that the final state is composed of a linear combination of atomic orbitals, with little participation by the substrate in the final state (i.e. oriented free molecule model). We further assume that the transition probability for orbitals located on centers other than the excited atom are small (since the 1s initial state is contracted by the high central field). In this case the transition is atomic-like in nature, i.e. the intensity is just proportional to the p orbital component of the antibonding final state. Polarization dependent spectra then indicate bond direction: when the electric field vector for linearly polarized light is along the p orbital direction the associated transition is at a maximum and is therefore either along or perpendicular to the bond direction at the absorbing atom, depending on the orbital type (π or σ). In general the intensity of the transition is proportional to $\cos^2\delta$ where δ is the angle between the electric field

vector and the p orbital axis.

The next higher level of theory allows for intensity due to transitions to final-state components localized on other centers. In this case the final state is still composed of the sum of atomic like orbitals but the transition is no longer only to atomic p orbital components: the dipole matrix element is nonzero for transitions from a 1s orbital to an s orbital on a different center if the electric field vector points towards the second center, for example. This means the important parts of the final state are no longer just the l=1 components. The useful quantity becomes the component of the angular momentum along the translation vector, which is preserved on translation. In the molecular case this is equivalent to investigating the behavior of the final state symmetry elements. If there is a reflection plane of symmetry in the final state that goes through the initial state center, then all projected components must preserved the reflection plane. Thus for example in benzene the π^* final state has a nodal plane through the bonds and so only a p_z component can appear in the π^* final state components projected to the initial center, and thus the transition has the same polarization dependence as would be predicted by the approximating the transition as being atomic in nature. Similarly if two or more nodal planes go through the initial state then the transition is not dipole allowed. In the general case the dipole transition intensity must be calculated in detail, which has been done for a few cases[16] and will be discussed later.

To describe the near edge structure in detail requires a theory that describes the final state well. The final state is highly excited and thus not handled well by methods that use the variational principle

to calculate the wavefunction. Additionally, the final states can be above the photoemission threshold and thus have traveling wave character i.e. they do not go to zero at large R. The canonical theories to describe these states are either scattering theories (which do not naturally describe the localized nature of the resonance) and orbital methods (which do not describe the large R behavior of the resonances well). In the multiple scattering methods it has been recently questioned to what degree multiple scattering must be included[12]. It may be sufficient to include only forward and backscattering in the calculations[12c]. Among the models used to determine molecular continuum resonance behavior are (primarily multiple scattering) Xα models, Stieltjes-Tchebycheff orbital models, and multichannel quantum defect theory. Multiple scattering Xα calculations have been carried out on N_2[13a,b,g,h], CO[13b,f,g], C_2H_4[13i], and C_6H_6[13j]. Both theoretical and experimental studies of N_2 find two resonances: one below the 1s photoemission threshold and one at ~0.8 Rydbergs above the photoemission threshold. The lower energy resonance is composed primarily of l=2 components and is a discrete transition to a π^* valence state, while the higher energy resonance is a shape resonance and is primarily composed of l=3 components. Similar resonances are seen for CO. We have calculated using MS Xα the expected NEXAFS spectra of C_6H_6 and the various forms of ethylene on the Pt(111) surface. We find that the spectra can be modeled quite well as oriented free molecules in the cases of benzene and as a metal cluster compound in the case of ethylene at 90 and 300 K (with the inclusion of an empirical broadening factor to deal with lifetime, vibrational broadening, and other effects), and that

the polarization dependence follows the expected trends. This treatment did not include multielectron effects and did not explicitly look for Rydberg states, thus we feel that in some cases the major features in the adsorption spectra may be interpreted in terms of discrete and continuum resonances, and if the molecule is not explicitly covalently bonded to the metal surface that the oriented free molecule model may be used. The situations where this is not supported will be indicated in the discussion of the results.

Stieltjes-Tchebycheff orbitals have been used by Langhoff et. al to describe continuum resonances for a number of molecules[14]. This is a molecular orbital approach, and uses the Stieltjes-Tchebycheff orbitals as approximate solutions of the Schrodinger equation. It has been shown that as the Stieltjes-Tchebycheff functions of arbitrarily high order are included in the molecular orbital the sum approaches the eigenfunctions of the Schrodinger equation. Further, if the Stieltjes-Tchebycheff excitation and ionization functions are defined as Radau type eigenstates then the energies of these states are the Radau quadrature points of the photoabsorption cross section and thus the photoabsorption cross section (i.e. EXAFS and NEXAFS) follows directly from the calculation[14]. They find final states that give electron density maps very similar to those expected for unoccupied molecular states: i.e. that the π^* final states are in fact π^* states (which is not surprising) and the continuum resonances look very much like σ^* states, which may be surprising considering the high angular momentum components found in the MS Xα calculations (suggestive of Rydberg-like components to the final states). The continuum resonances have to transform as the molecular potential transforms, thus the same symmetry

labels appropriate to molecular orbitals are (such as σ^*) appropriate for the continuum resonances regardless of the components of the final state. The high angular momentum components observed in the MS Xα may be due to the transformation from the atomic orbitals components (as used in molecular orbital approaches) to the body centered orbitals appropriate to scattering calculations.

Recently multichannel quantum defect theory has been applied to the problem of the near edge resonances[15]. This technique used a MS Xα calculation to determine the molecular potential and thus the quantum defect and phase shift for the continuum waves. Calculations for NO molecule indicate that the continuum resonances can be associated with Rydberg transitions, even for condensed phases. These continuum resonances have high angular momentum (l=3) and show bond length dependence on the energy position of the resonance. This is an interesting theory, but is unorthodox in its insistence that the Rydberg states are not perturbed by intermolecular interactions. Experimentally we observe that some of the resonances are perturbed by transition to condensed and surface adsorbed states while other resonances are not.

The relation of the energy position of the continuum resonances to bond length in molecules has been of recent interest[16]. This correlation follows conceptually from the particle in a box model - if the continuum resonance is localized to the region of the molecule then for diatomics and for resonances localized to a particular bond the longer the bond the lower the resonance energy. This correlation was predicted for vibrational states of molecules[13] and between families of similar molecules and was observed in the C_2H_n pseudo diatomics[16a,b].

We have subsequently applied the correlation to a number of gas phase, condensed phase, and surface species[16c-g]. The correlation has been fit to a linear relation between the position of the continuum resonance and the bond length. The correlation is of course only approximate and by its nature assumes that the major factor determining the energy of the resonance is to be found in the nature of a particular bond length: i.e. the resonance is localized in the region of the bond, trapped as it were between the atoms comprising the bond. Thus if there is evidence that the continuum resonance is delocalized over the entire molecule then a bond length correlation will not be found. In analogy with molecular orbital results for bonding and antibonding orbitals we find that the continuum resonances in highly symmetric molecules are in fact delocalized and thus the bond length can at this stage of the theory only be abstracted after a more tedious modeling analysis. I will use the bond length results only in a semi-quantitative sense in the following analysis.

To obtain a NEXAFS spectrum it is necessary to obtain the probability of X-ray absorption. X-ray absorption creates a core hole, thus the determination of the relative X-ray absorption coefficient is reduced to the determination of the relative population of core holes. The detection of the relative population of core holes depends on observation of effects related to filling of the core hole. The initial core hole relaxes by the transition of a valence electron to fill the core hole accompanied by either the emission of a photon (fluorescence) or the emission of a valence electron (Auger emission). The branching ratio for the different paths is determined by the atomic number of the absorbate atom: for atoms of the first row the fluorescence path is less

than 2%[17] and thus the Auger path has greater than 98% of the total signal. The Auger path may also cause the emission of an ion from the surface and detection of the ion current has been used to detect the surface EXAFS signal[18]. The low intensity of the fluorescence signal and the difficulties in the detection of X-rays in the first row element fluorescence X-ray energy range have made use of the Auger signal one of the most common means of the determination of the absorption coefficient.

Auger detection is not without its difficulties. The experimenter is concerned with the signal to noise ratio and the sources of artifactual structure. The available signal to noise ratio is limited by the sources of noise: for electron detection the primary sources of noise are inelastic processes that scatter electrons into the Auger window (from bulk valence emission for example) and at low signal strength counting noise. The largest signal to noise ratios we have observed for monolayer surface species and partial electron yield detection is on the order of 0.1.

A matter of primary concern is to identify and minimize the sources of structure in the NEXAFS spectra due to processes not associated with the formation of the core hole. Auger detection implicitly assumes that the Auger signal is independent of the details of the excitation process. In fact Auger shows angular dependence as well as excitation energy dependence, and thus this source of experimental artifacts must be considered in polarization-dependent NEXAFS studies. The angular dependence is due to diffraction from the substrate and electronic effects in the Auger fine structure. Diffraction effects give rise to

angular dependence that is slowly varying in electron energy[19a] whereas the electronics effects give sharp angular structure over a narrow energy range in the Auger envelope. We use partial electron yield detection and large solid angle detectors to minimize the effects of angle dependent Auger emission. Partial yield measurements collect all electrons with energies above a discriminator level, thus averaging out the Auger fine structure and diffraction features. The energy dependence is due to participation of the bound or pseudo bound core photoelectron in the Auger process[19c]. This participation is either indirect as seen in "spectator" effects (shifts in Auger decay energy due to screening of the Auger electron from the core hole field by the spectator bound electron) or direct as seen in the participation of the bound electron in the Auger process (autoionization or "participant Auger"). We have observed direct effects in the Auger decay of benzene (figures 6 and 7). In figure 6 we compare the electron energy distributions of benzene ice excited by 310eV photons (above the photoemission threshold) and by 285eV photons (at the π^* resonance energy). Note that there is a peak at 275eV in the electron energy distribution. This is not due to the π valence emission sweeping through the Auger window, since constant initial state spectra (spectra taken such that one observes electron of a constant binding energy as a function of photon energy) show that the resonance is associated with an occupied π^* final state. Figure 7 shows the effect on NEXAFS of using the electron emission at 260eV (standard Auger energy) and at 275eV (the "participant Auger" or autoionization energy) for detection. It is seen that detection at the 275eV peak increases the relative intensity of the π^* resonance relative to the σ resonances. In fact 30% of the core

holes produced at the π^* resonance decay by the autoionization path. Problems due to this effect are avoided by the use of partial yield detection: partial yield detection collects all electrons above a discriminator level, thus all of the Auger and "participant" or "spectator" Auger are collected.

There are other possible sources of spurious peaks having to do with interferences from substrate photoemission and these will be discussed in the next section.

II.2.1.1 FIGURES

Figure 3

Mechanism at work in EXAFS spectra. Photoelectrons from the absorbing center virtually scatter off neighboring atoms and interfere at the absorbing center to modulate the photoemission intensity.

Figure 4

Mechanism at work in NEXAFS spectra. Core electrons are excited to states in the region of the atom or molecule; i.e., bound states (such as partial filled valence orbitals or π^* states) and pseudo-bound states and scattering resonances in the continuum (shape resonances). The potential for atoms chemisorbed to a metal surface are indicated in I, the potential for molecules chemisorbed on metal surfaces is illustrated in II. Note that the centrifugal potential may be absent in the molecular case and continuum resonances may still be seen, due to local increase in wavefunction density in the region of the molecule due to the attractive part of the potential.

Figure 5

Part I is the X-ray absorption fine structure of bromine gas and krypton (from P. Eisenberger and B. M. Kincaid Science, 1978, 200, 1441). The krypton spectra is shifted in energy to coincide with the bromine spectra. Note the position and relative intensity of the near edge structure and the extended structure (NEXAFS and EXAFS, respectively) as indicated in part II.

Figure 6

Electron energy distributions near the carbon Auger energy of electrons emitted from a thick benzene ice condensed on a liquid nitrogen cooled tungsten surface. The spectra were collected with a PHI

double pass CMA at 181eV pass energy at the National Synchrotron Light Source (NSLS), Brookhaven National Laboratory. I is the emission with excitation above the photoemission threshold (by 310eV photons) and II is the emission at the π^* resonance (285eV). Note that no tungsten 4f photoemission is seen and the new peak at 275eV on the π^* resonance.

Figure 7

Constant final state (NEXAFS) scans of a multilayer benzene ice. A PHI double pass CMA at 181eV pass energy at NSLS was used to obtain the spectra. I is the NEXAFS spectra collected at 260eV (standard carbon Auger energy) and II is the NEXAFS spectra collected at 275eV (autoionization or "participant Auger" energy). These spectra are not corrected for the monochromator transmission function.

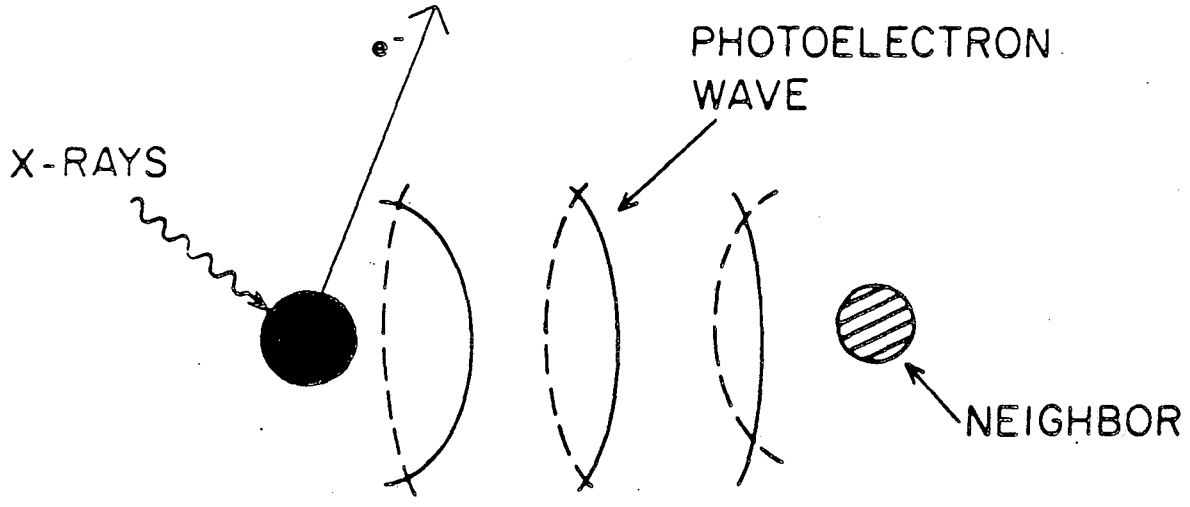

XBL 8512-5095

I

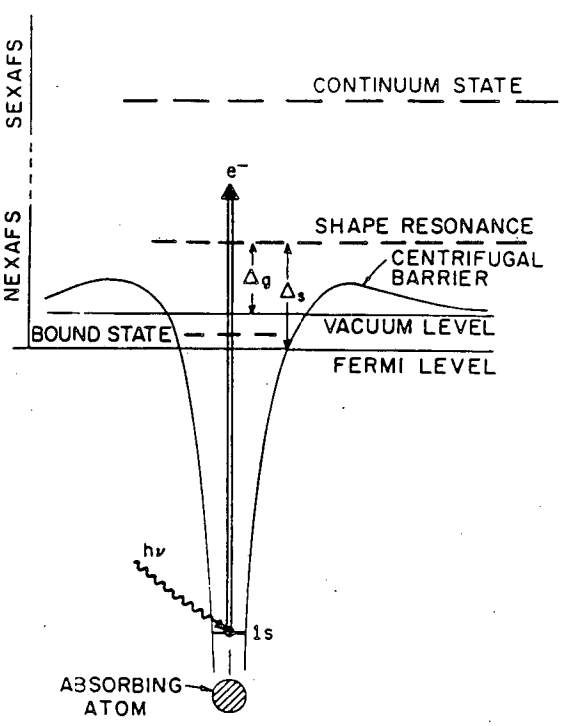

II

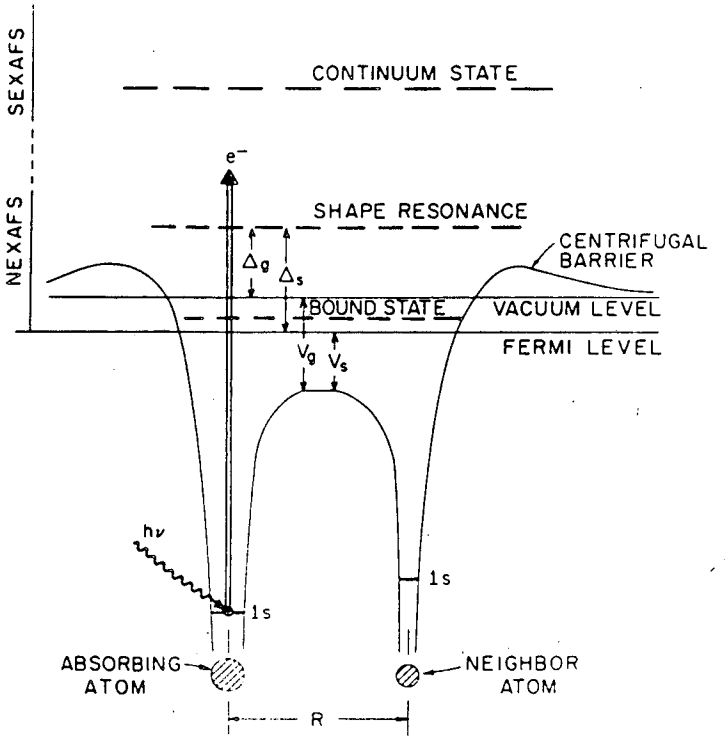

XBL 8512-5098

I

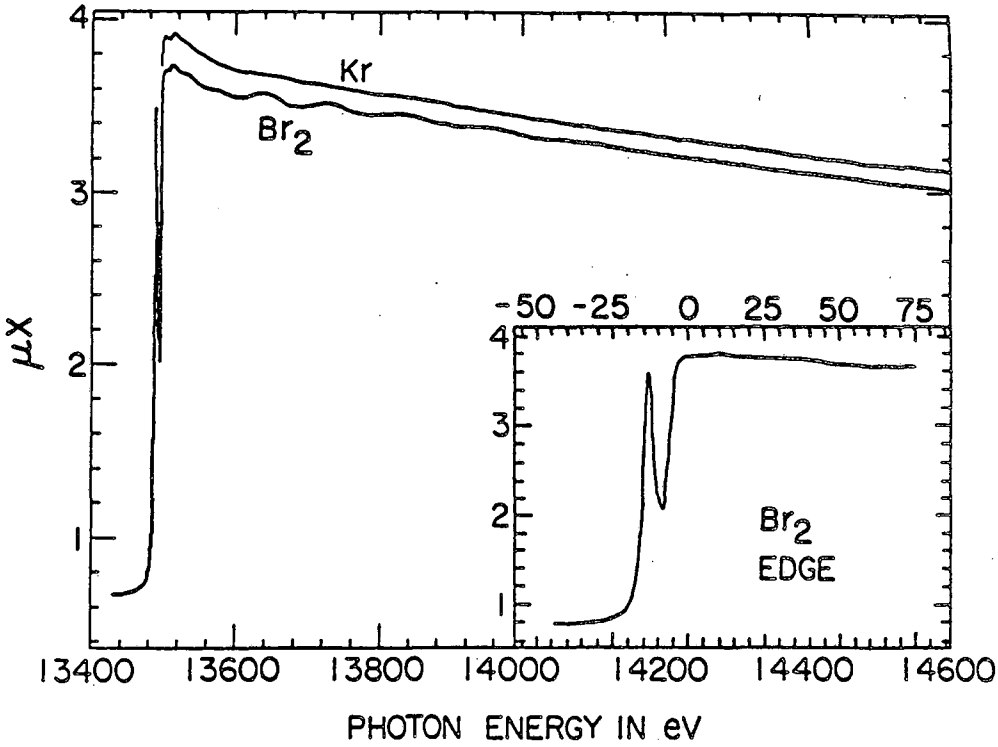

II

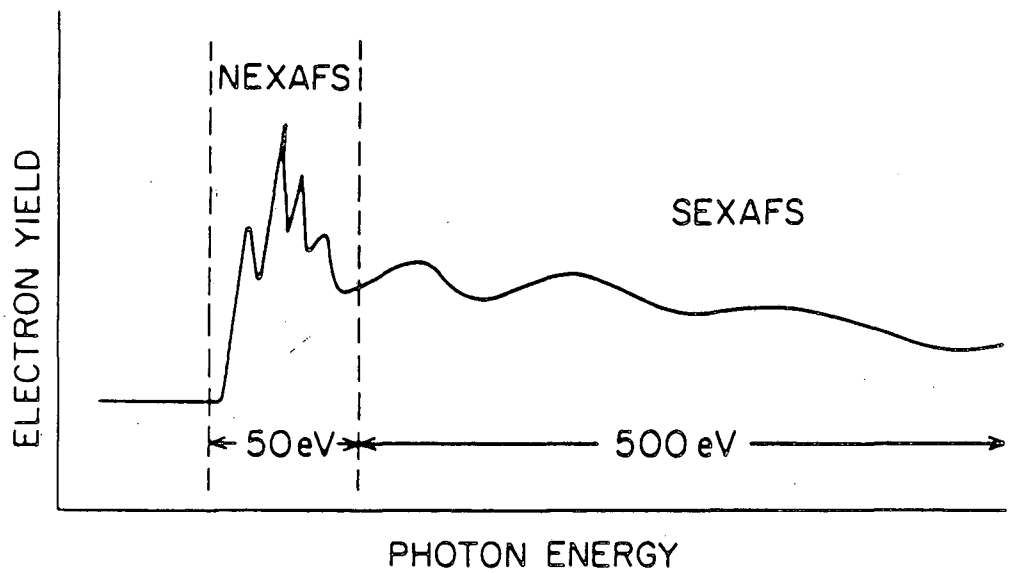

XBL 8512-5077

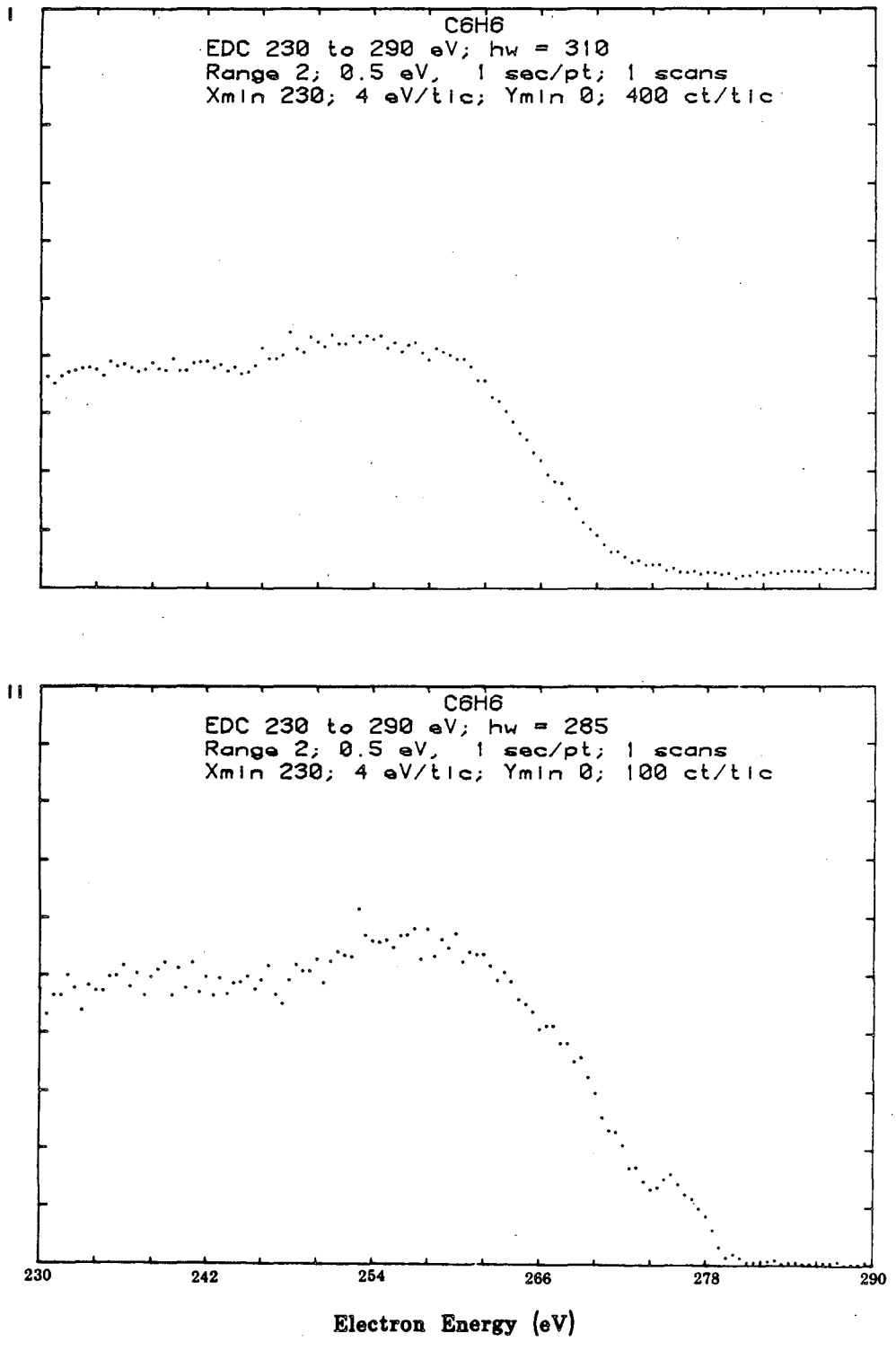

XBL. 8512-5101

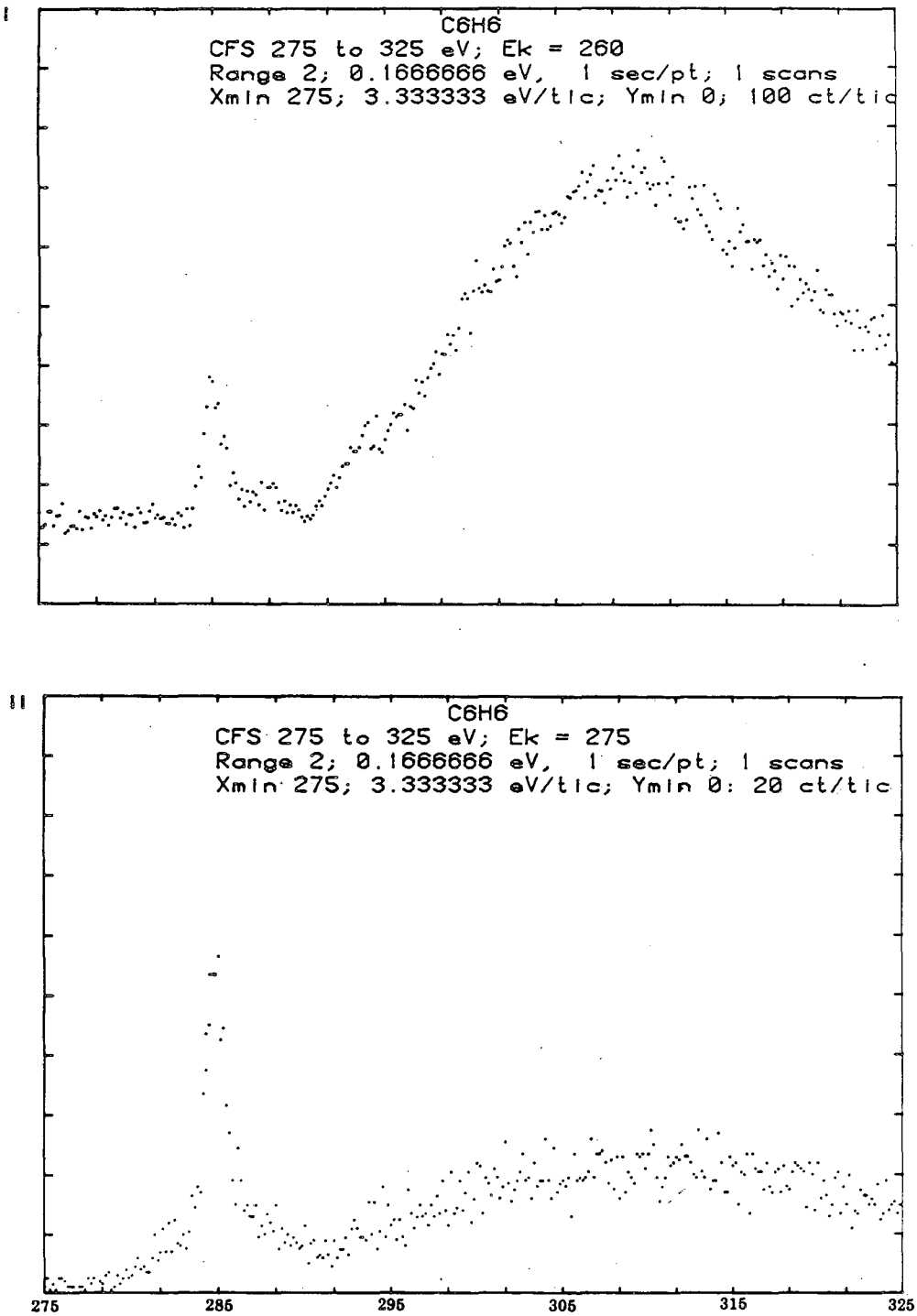

XBL 8512-5100

II.2.2 Experimental Apparatus, Previous Work, and Data Analysis

The experiment apparatus for the NEXAFS investigations was different than that used for the thermal desorption experiments and roughly follows the methods described elsewhere[20]. The experimental apparatus is indicated in figure 8. The synchrotron radiation entered from the left from beam line I-1 at the Stanford Synchrotron Radiation Laboratory after being energy selected by a grasshopper monochromator[21]. The available photon energy is from 40 eV to 1000eV and the photons are linearly polarized with the electric field vector in the horizontal plane. The beam is collimated by two pairs of opposing knife edges, one in the vertical and one in the horizontal direction, which serves to remove light scattered off the optics in a direction close to the monochromatic beam. The beam is passed through an intensity monitor where the photoemission from a metal (generally copper) grid detected by a channeltron is used to determine the relative beam intensity. The intensity monitor (which will be called the I_o monitor) is isolated from the rest of the vacuum chamber by straight through and gate valves at either end. An evaporator is located in the I_o section to allow the deposition of a fresh metal surface on the I_o grid. We generally did not use the evaporator - The change of the photoemission response with the deposition of background gases and their subsequent decomposition made this nonproductive. In fact, we found that the grid as found after the bakeout (i.e. covered by carbon) was more stable than a clean surface. The photon beam then passes into the main chamber, where it impinges on the sample. The sample chamber has a cylindrical mirror electron energy analyser (CMA), two partial yield detectors, low energy electron diffraction optics (LEED), and crystal cleaning and sample

preparation facilities. The two partial yield detectors have different characteristics: the detector based on a channeltron is located approximately 25° below the photon beam and perpendicular to the polarization direction and thus is on the photoemission node which maximizes the signal to noise, while the detector based on the channel plate is located perpendicular to the photon direction and along the polarization direction which maximizes the count rate and minimizes the Auger signal to photoemission background ratio. The partial yield detector based on the channel plate was placed with the front grid 1 inch from the sample and either along the electric field vector or tilted 20° below the electric field vector direction. The front grid subtends an angle of 53° and the channel plate (located ~1/2 inch behind the front grid) subtends 37°, giving a large angular acceptance and minimizing the effects of angular anisotropies of the NEXAFS. The CMA can also be used to collect NEXAFS spectra, as has been done in earlier work.

Resistive heating, which allows the heating of the sample during data collection, was used in the later experiments. Electron beam heating was always used for sample cleaning. Cooling was by contact with a liquid nitrogen cooled copper reservoir electrically isolated from the crystal mount by a sapphire gasket. Crystal cleaning was by oxygen treatments. Argon ion sputtering was used when necessary. Sample characterization was carried out using LEED, Auger, and TDS spectrometry. Sample temperature was measured with a chromel - alumel thermocouple spot welded to the crystal edge. The thermocouple signal was fed directly to a Hewlett Packard digital voltmeter for temperature

indication. The unevenness of the heating as well as the lack of a stabilized cold junction make the estimated error in the temperature on the order of $\pm 8^{o}$.

Experimental data collection and preliminary analysis utilized a PDP-11 computer that is part of the SSRL beam line I-1 instrumentation.

Previous work using NEXAFS (or XANES) by Dr. Stöhr focused on adatoms[20a] and diatomic chemisorbed molecules[20b,c] and formed the basis for the present work. Dr. Stöhr investigated the structure of N_2, NO, and CO adsorbed to Ni(100) and found spectra that established that all three species were oriented with the molecular bond vector along the surface normal. Figure 9 shows the NEXAFS spectra and data analysis for the carbon K edge of CO. The presented plots were obtained by normalizing the data by dividing by I_o to remove variation due to changes in the photon output of the light source and by subtraction of clean nickel spectra to remove features due to photoemission of the substrate. The signal was further normalized by setting the intensity far after the onset of molecular absorption to a constant with respect to polarization angle, thus removing the effects of the change in detection efficiency with changing detector to sample geometry.

Analysis of the polarization dependence of the NEXAFS spectra followed from the work of Wallace, Dehmer and Dill[12d,e] who showed that for cylindrically symmetric molecules the angular dependence of pure π or σ resonances was respectively the $\sin^2$ or the $\cos^2$ of the angle between the molecular axis and the electric field vector. The molecular axis was found to be within 10^{o} of parallel to the surface normal, in accord with the results of structural determinations involving LEED, angle resolved photoemission, ESDIAD, and HREELS, and is also what we

observe with CO on Pt(111)[22].

Partial yield detection necessitates some changes in the data analysis. We wish to remove feature from our data due to substrate Auger and photoemission as well as variations in the light flux available to us. The partial yield signal is composed of all electrons with energy above the discriminator level; i. e. valence photoemission, high energy substrate Auger emission, and the adsorbate Auger emission along with the inelastically scattered electrons that still have adequate energy to pass the discriminator. Thus the photon energy dependence of the signal is monotonically increasing relative to the same sample measured with Auger or total yield detection, due to the increased proportion of the inelastic yield that gets through the discriminator. The partial yield from the clean sample surface serves as the normalization factor in our experiments. This is justified if the only structures in the spectra are due to substrate emission and light flux variations. If no photoemission peaks enter the discriminator and no Auger lines in the detection window are turned on in the region of the photon scan then the partial yield signal is proportional to the photon output of the source (here being a combination of the basic spectral emissivity of the light source and the transmission function of the optics) multiplied by a monotonically increasing function that includes effects due to the higher proportion of sampled inelastic electrons and changes in sampling depth. Because all of the photoelectrons that are detected have at least an energy determined by the discriminator voltage (in our work generally greater than 200eV) the intrinsic structure in the valence photopeaks of the

sample are of the weak EXAFS variety and diffraction structure is averaged out since the detector (and electron flux from the surface) has an energy and angular width greater than the reciprocal lattice vector. As a practical matter Auger emission from the substrate is not generally significant in the following studies: for there to be an Auger line in the discriminator level (given that the discriminator level is set close to the Auger line of the adsorbate) there must be a core level with a binding energy near that of the studied adsorbate atom. This is not the case for platinum in the region of 275 to 315 eV, 375 to 450, 520 to 570eV, and 650 to 720 eV i.e. the regions of the carbon (284eV), nitrogen (399ev), oxygen (532eV) and fluorine (686eV) K edges. In our work therefore we shall use the partial yield from the clean surface to normalize our spectra to the photon flux and remove features due to substrate emission. Additionally, we shall set the signal before the onset of the core absorption to be constant with polarization angle to correct for the effects of changing sample - detector geometry.

The polarization dependence for the more complex molecules that we have studied require the approximations indicated earlier in this introduction. These approximations are that the transitions are dominated by the atomic part of the dipole element (or strictly equal to the atomic part where the symmetry of the molecule allows) and that unless otherwise indicated the molecule is weakly perturbed form the gas phase and thus the surface serves to orient the chemisorbed molecule (i.e. oriented free molecule model).

Here we examine the polarization dependence of the absorption coefficient. Figure 10 presents the coordinates utilized in the following discussion. We have indicated earlier that the elementary

dependence of the NEXAFS spectra for pure π and σ states is the $\cos^2$ of the angle between the electric field vector and the axis of the p orbital component of the final state. This dependence can be obtained by examining the spherical harmonic components centered on the initial state of the dipole matrix element integral. The initial state is a 1s orbital and thus has Y_o^o symmetry. The dipole operator has Y_1^m symmetry. Thus only final state components with Y_1^n symmetry will contribute to the absorption. If a node goes though the final state then only one Y_1^n is nonzero and thus the absorption coefficient goes as the $\cos^2$ of the angle between $\vec{E}$ and the normal to the nodal plane. The calculated NEXAFS spectra of benzene[7] using a full Xα treatment shows the expected polarization dependence.

Thus for transitions into bound π molecular states NEXAFS shows an absorption maximum when the electric field vector (and thus the initial p-wave of the excited 1s electron if this were a photoemission event) is directed along the atomic p orbital component (centered on the excited atom) of the final state molecular orbital.

We shall consider two types of unsaturated center. Many molecules with sp hybridization (e.g. carbon monoxide) have (local) $C_{\infty v}$ symmetry, and excitations into the π^* final states are equivalent in the plane perpendicular to the bond axis. The π^* orbitals of sp^2 hybridized molecules (e.g. benzene) by contrast, are made up of the atomic p orbitals perpendicular to the σ bonding plane (there are sp hybridized molecules with inequivalent π^* states [e.g. ketene H_2CCO] and the π^* resonances are treated independently similarly to sp^2 centers). Thus there are two type of expressions describing the observed polarization

dependence of the π^* transition that we will derive: that appropriate for π^* (or other) states of vector (sp^2) symmetry and those of plane (sp) symmetry.

Adsorbates chemisorbed on well defined crystal surfaces generally exist as domains that have the same rotational symmetry as the crystal substrate, i.e. for an fcc (111) surface there are 6 equivalent possible domains for the adsorbate. Therefore $\vec{M}$ in figure 10 will be found in 6 different directions, rotated by 60^o about the z axis. It can be shown for crystals with threefold symmetry or greater that the sum of $\cos^2\delta$ with $\vec{M}$ rotated into the equivalent directions is invariant under rotation of the crystal about the z axis (see appendix A at the end of this section).

Thus the sum over the domain directions can be replaced by an integral over ϕ and the expression describing the transition probability for 1s to π^* transitions is (using definitions from figure 10):

$$A\int_0^{2\pi}\sin^2(\delta)d\phi = A\int_0^{2\pi}(1-(\vec{E}\cdot\vec{M})^2)d\phi = A\pi(2-2\cos^2(\theta)\cos^2(\alpha)-\sin^2(\theta)\sin^2(\alpha)) \quad \text{Eq.1}$$

for sp hybridized molecules (e.g. CO) and

$$B\int_0^{2\pi}\cos^2(\delta)d\phi = B\int_0^{2\pi}(\vec{E}\cdot\vec{M})^2d\phi = B\pi(2\cos^2(\theta)\cos^2(\alpha)+\sin^2(\theta)\sin^2(\alpha)) \quad \text{Eq.2}$$

for sp^2 hybridized molecules (e.g. benzene or ethylene) where A and B are constants describing the absolute transition intensity.

For benzene we have found that the NEXAFS spectra of the adsorbed molecule are only weakly perturbed in the energy position of the peaks relative to the spectra of the condensed multilayer, and is indicative of the types of molecules where we will use the oriented free molecule model and the $\cos^2\delta$ relation of the π^* transition to determine the angle (α) of the π orbitals with respect to the surface i.e. in those cases where there is little evidence for strong adsorbate-surface interaction.

This involves integrating the π^* peak intensity at normal photon incidence and dividing by the integral of the π^* intensity at grazing (in our experiments 20^o) photon incidence. The spectra were normalized by dividing by clean Pt(111) spectra at the appropriate angle and the intensity before the onset of 1s excitation, i.e. the lowest scanned energy, was set to 1. The observed peak ratio is compared with the theoretical ratio presented in figure 11. The theoretical peak intensity ratio R for the π^* transitions for a photon angle θ_1 divided by that for a photon incidence angle θ_2 for sp^2 hybridized systems is given by:

$$R_v = \frac{\{2\cos^2(\theta_1)\cos^2(\alpha)+\sin^2(\theta_1)\sin^2(\alpha)\}}{\{2\cos^2(\theta_2)\cos^2(\alpha)+\sin^2(\theta_2)\sin^2(\alpha)\}} \qquad \text{Eq.3}$$

$$R_p = \frac{\{2-2\cos^2(\theta_1)\cos^2(\alpha)-\sin^2(\theta_1)\sin^2(\alpha)\}}{\{2-2\cos^2(\theta_2)\cos^2(\alpha)-\sin^2(\theta_2)\sin^2(\alpha)\}} \qquad \text{Eq.4}$$

For $\theta_1 = 90^o$ and $\theta_2 = 20^o$ we obtain:

$$R_v = \frac{(\sin^2(\alpha))}{(0.117+1.649\cos^2(\alpha))} \qquad \text{Eq.5}$$

for vector final states (sp^2 hybridized) and

$$R_p = \frac{\{2-\sin^2(\alpha)\}}{\{1.883-1.649\cos^2(\alpha)\}} \qquad \text{Eq.6}$$

for plane final states (sp hybridized). These relations are plotted in figure 11.

To summarize the data analysis, the data sweep(s) are summed and then divided by the appropriate clean spectra and corrections for the changing detector geometry made. To determine the relative angle of the molecule to the surface, a smooth background (similar to the background subtracted in reference 20c.) is subtracted from the region of the π^* resonance and the peak area ratio for two angles (in our studies 90^o and

20^{o}) is compared to the theoretical ratio. To estimate the error in the determination one must estimate the uncertainties in the angles of the crystal ($<2^{o}$), the polarization of the photon beam (from 85% to near 100%), the noise of the signal and error due to the background subtraction. The error in the peak area from these sources appears to be about 10% of the area of the most intense peak. To quantitate the error estimate in terms of angle, for final states of vector symmetry (i.e. sp^2 centers) for peak ratios near 8 (angles α near 90^{o}) the error in ratio is about 50% which lead to an uncertainty of about 15^{o}, at peak ratio of near 1 (angles α near 54^{o}) the error is about 15%, which leads to an uncertainty of about 7^{o}, and at ratios near 0 (angles near 0^{o}) the error in ratio is 0.1 and the associated uncertainty in angle is 23^{o}. Similar results are obtained for plane symmetry final states.

II.2.2.1 FIGURES

Figure 8

The experimental apparatus used to collect the NEXAFS spectra. Changes from the experimental apparatus of reference(s) 19 include the inclusion of the large area channel plate based detector and the use of resistive heating.

Figure 9

I is the NEXAFS spectra of CO chemisorbed to Ni(100). The photon incidence angle is indicated by θ. Note that the lower energy resonance (A) is maximized at normal photon incidence (electric field vector parallel to the surface) and is due to a π^* transition. Peak B is a above photoemission threshold and is a σ resonance and is maximized when the electric field is aligned with the bond direction. The arrows to the right of the spectra indicate the direction of the photon energy scan.

Part II is the analysis of the molecular orientation as determined by NEXAFS. The photon incidence angle is θ and is also the angle of the electric field vector with respect to the surface normal. The angle of the molecular bond vector to the surface normal is α. The angles α_1 and α_2 indicate the inclusion of thermal motion about the equilibrium bond angle. Best fit is found for α equal to 0^o, in accord with the results of LEED and other measurements. Similar results are seen both at the oxygen edge and for CO on Pt(111)[22].

Figure 10

Coordinate system used to derive the polarization dependence of the NEXAFS spectra. The molecular axis is along the bond vector for (local) sp hybridized centers and perpendicular to the bonding plane for (local)

sp^2 centers. The coordinate system is illustrated for benzene.

Figure 11

Theoretical peak area ratios for vector (sp^2) and plane (sp) symmetry final states, from the equations in the text. The angle α is defined in figure 10. These ratios when used with the experimental NEXAFS ratios yield the tilt of the molecular axis to the surface in the region of the absorbing atom.

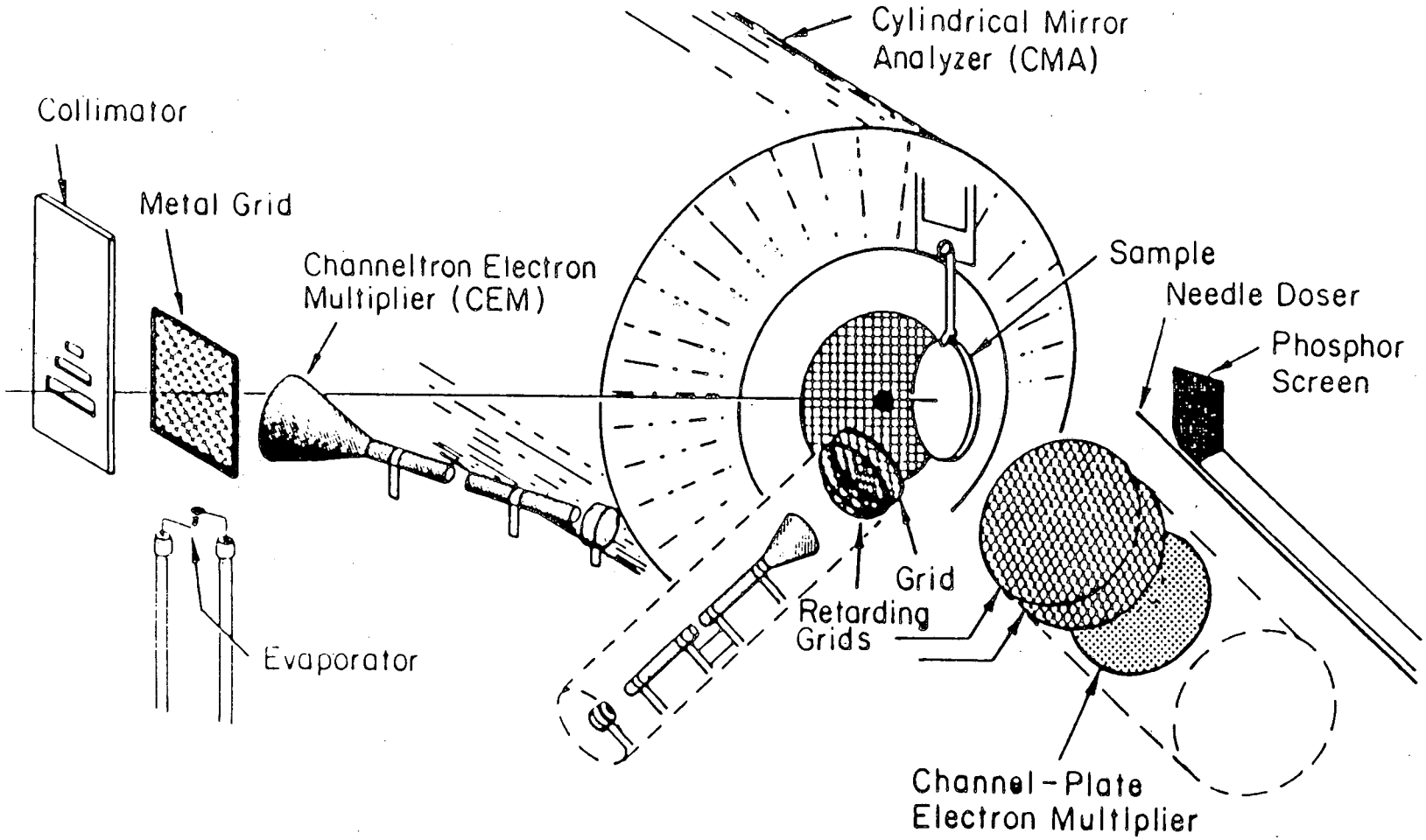

XBL 8512-5097

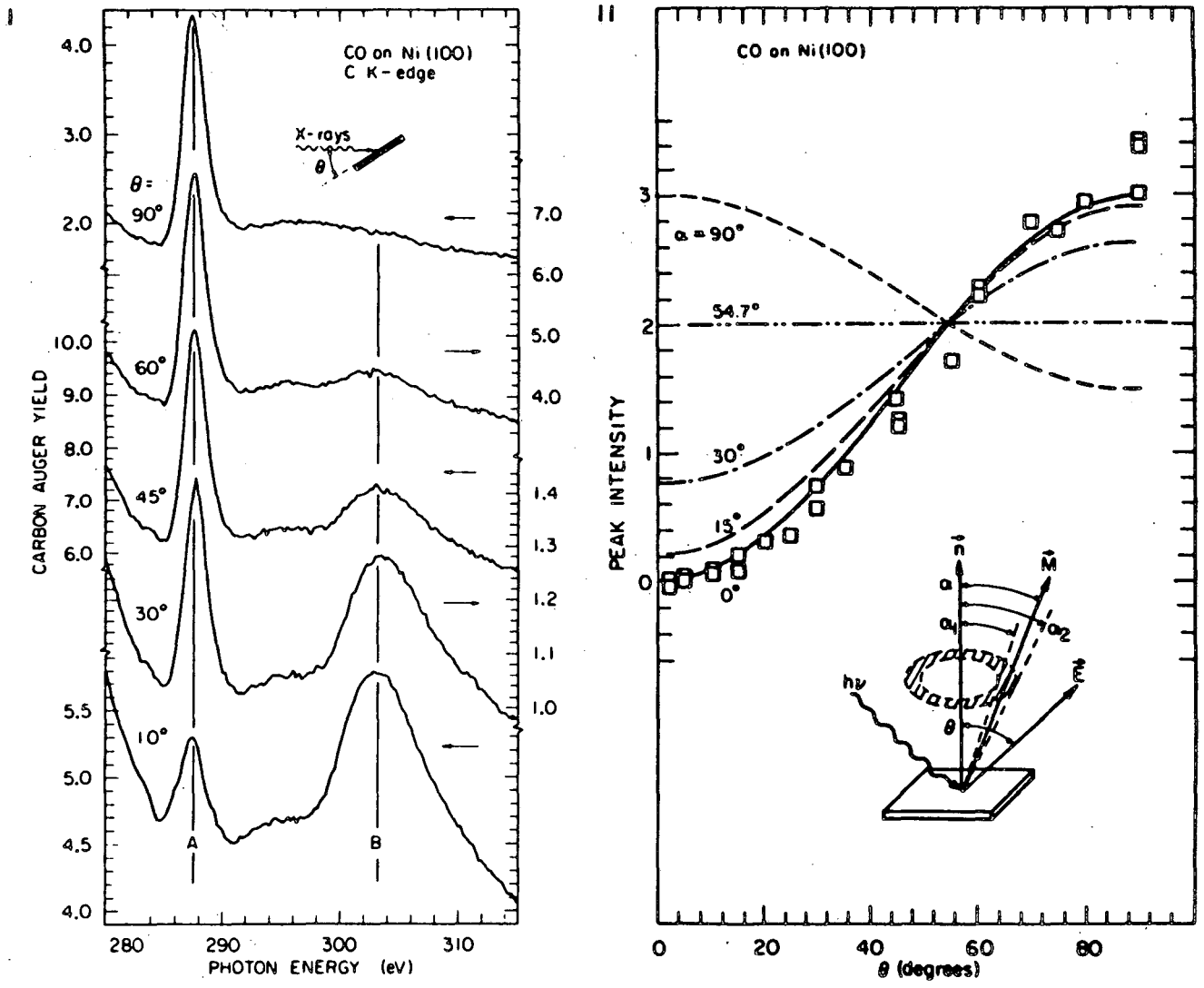

XBL 8512-5089

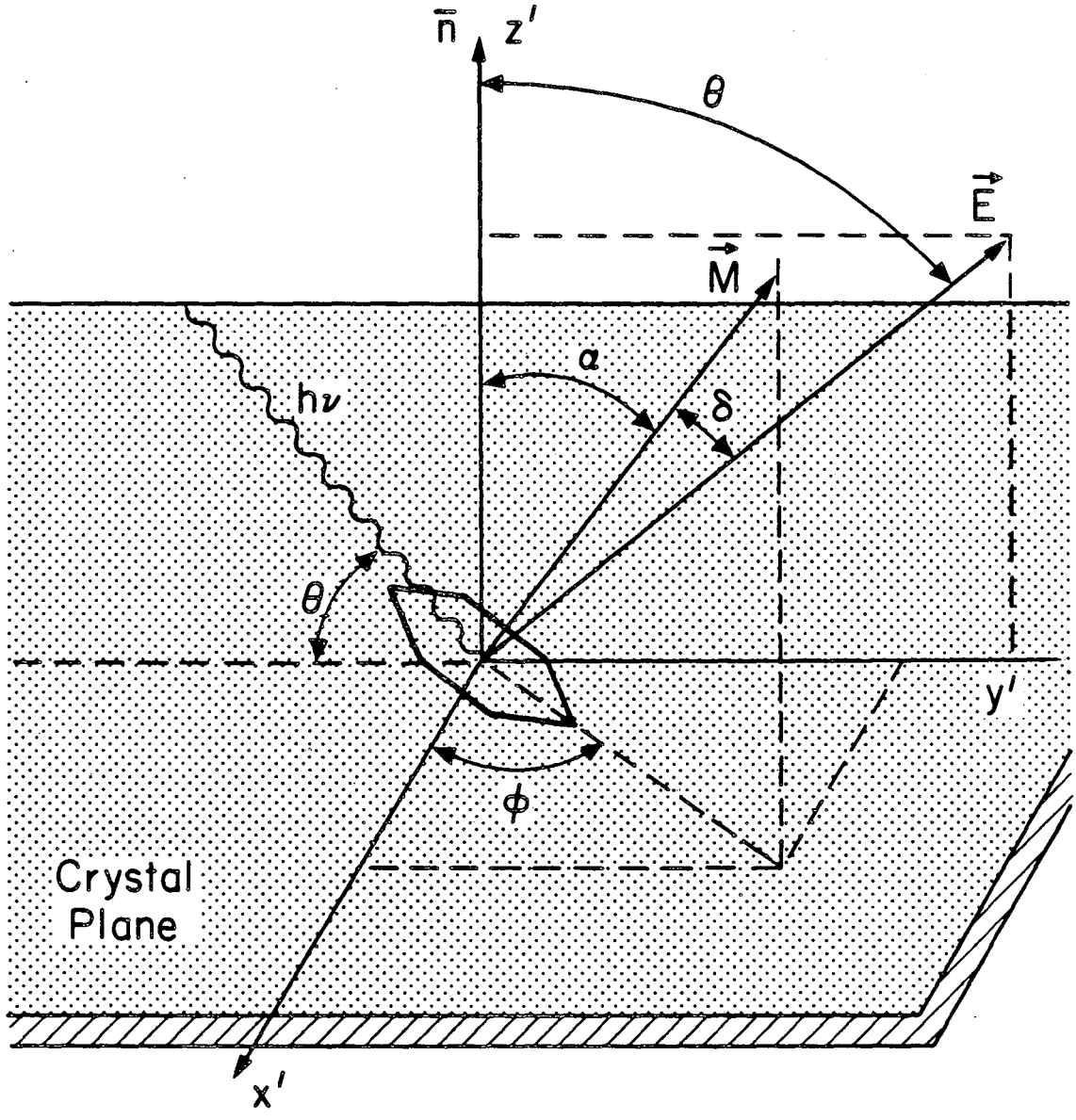

$\bar{n}$ Surface Normal

$\vec{M}$ Molecular Symmetry Axis

$\vec{E}$ Electric Field Vector

XBL 852-1102

Normal/Grazing NEXAFS Intensity Ratio

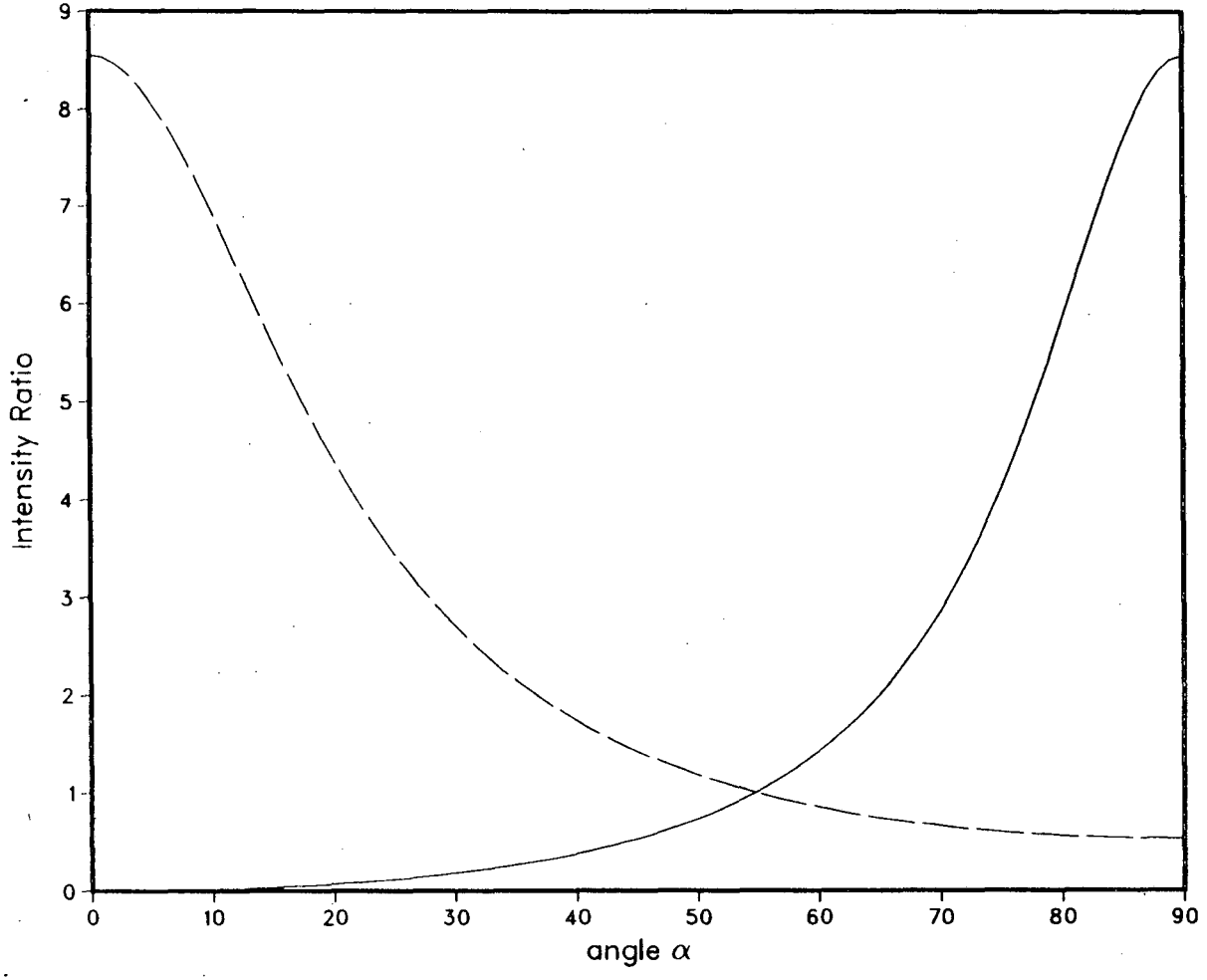

Legend

vector final state

plane final state

XBL 8512-5093

III RESULTS

III.1 Overview

This investigation is based on the examination of families of similar molecules to determine the systematic effects of the adsorbate on chemisorption. We have concentrated (as have our earlier studies[23]) on two classes of molecules: aromatic hydrocarbons and simple diatomic or pseudo diatomic carbon containing molecules.

The interaction of unsaturated carbon centers with metal surfaces is central to the understanding of the heterogeneous catalysis of organic reactions. The interaction of the π orbitals with the metal orbitals affords strong surface interactions and naturally leads to reactive chemisorption pathways.

A special subclassification of unsaturated systems are the aromatic systems. Aromatic molecules exhibit unusual stability and aromatic transition states are commonly suggested to rationalize and plan reaction schemes. Thus the characteristics of aromatic molecules chemisorbed on metal surfaces are of great importance. Additionally, aromatic molecules are expected to chemisorb with only small perturbations from the gas phase which simplifies the spectroscopic interpretation.

We will investigate benzenoid aromatic hydrocarbons with both exocyclic (i.e. the fluorobenzenes) and endocyclic substitution (e.g. pyridine). The aromatics with exocyclic substitution are studied to determine the basic nature of the aromatic surface chemical bond by inducing systematic shifts in the donor (HOMO) and acceptor (LUMO) levels. The studies of endocyclicly substituted benzenes address questions of the effect of heteroatoms on the bonding of aromatic

systems through the effect of lone pairs and/or labile bonds.

Diatomics and pseudo diatomics are the simplest of the strongly chemisorbed molecules (as differentiated from chemisorbed atoms which require direct σ bonding to the surface to satisfy valence requirements) which are amenable to investigation by NEXAFS and are the most capable of being modeled by in-depth theoretical treatments of situations where metal interactions must be explicitly considered to rationalize the observed chemical and spectroscopic behavior.

Amongst the simplest unsaturated hydrocarbons are ethylene and acetylene. There have been many experimental and theoretical studies of ethylene and acetylene chemisorbed to well characterized transition metal surfaces. Ethylene and acetylene chemisorb at low temperatures with their bond vectors parallel to transition metal surfaces and exhibit considerable rehybridization towards 1,2 di σ bonded species on reactive surfaces. CO, on the other hand, chemisorbs to Pt(111) with the bond vector perpendicular to the metal surface. This has been rationalized as due to the importance of the backbonding interaction of the π^* antibonding orbital, which is maximized by perpendicular bonding[24]. We will consider the adsorbate effects that lead to the selection of perpendicular verses parallel bonding.

Rehybridization in acetylene and ethylene suggests that cyclic unsaturated molecules on Pt(111) could have lost the π orbitals that can overlap and lead to aromaticity. Conversely, cyclic unsaturated hydrocarbons form many stable π coordinated complexes with metals. These complexes would lead one to expect that all of these hydrocarbons could exhibit flat, aromatic coordination states.

We will investigate the C_4 through C_8 cyclic polyenes to determine if the gas phase stabilities or the metal interactions dominate in carbocyclic surface states and, if metal interactions dominate, whether they enhance or suppress aromaticity. We will use thermal desorption spectroscopy (TDS) to determine the reactivity of the chemisorbed species and to indicate how to prepare intermediate states. Near edge x-ray absorption fine structure measurements (NEXAFS) will be used to determine electronic and structural parameters. We have found the interaction of these two techniques in a conjugate sense to be extremely useful in the elucidation of surface chemistry.

III.2 Benzene

Benzene chemisorption has been extensively investigated for the reasons suggested above and also because of the importance of benzene in the production of automotive fuels and as intermediates in the formation of carbon in the form of soot during combustion and coking in industrial catalysts.

Benzene chemisorbed to well characterized metal surfaces has been extensively studied by LEED[25], HREELS[26], photoemission[27], and NEXAFS[28]. A state with the benzene ring chemisorbed parallel to the metal surface is the generally accepted structure. This structure can be rationalized by the tendency to maximize the metal orbital - adsorbate π orbital overlap.

LEED studies on Pt(111) have in the past suggested both flat and inclined chemisorption states[25a,b,f,g]. Recently the importance of CO coadsorption in the preparation of ordered benzene has been indicated[26e] and the interpretation of the existing LEED spectra lead to the assignment of a chemisorption state with benzene π coordinated to the Pt(111) surface[25j].

HREELS studies of benzene on Pt(111)[26b] indicate two simultaneous chemisorption states (with atop and threefold hollow site coordination) with parallel π coordinated geometry and C_{3v} symmetry. Rehybridization of the benzene is not observed.

We have previously investigated benzene chemisorption on Pt(111) by thermal desorption spectrometry and chemical displacement reactions[23b]. For benzene chemisorption states formed at room temperature both molecular desorption (between 370 K and 490 K) and decomposition to form hydrogen and surface carbon (between 530 K and 650 K) were observed

(figure 12). A mixture of C_6H_6 and C_6D_6 exhibited no intermolecular deuterium scrambling at temperatures up to 390 K, establishing that there was no reversible hydrogen bond breaking before this temperature. All of the studies to date have indicated that benzene should chemisorb molecularly to Pt(111).

We will address four points in the following discussion of benzene chemisorption to Pt(111): the strong similarity between the multilayer ice spectra and the gas phase spectra for benzene, the theoretical basis for the interpretation of NEXAFS spectra, the structure of the benzene chemisorption state, and the conversion of that state to a carbonaceous overlayer with increasing temperature.

Figure 13 shows a comparison of the near edge structure obtained using photon excitation of a multilayer ice and monolayer at 100 K and electron excitation of a gas phase sample[7,29]. Note that the gas phase and multilayer ice spectra are identical (except for peak 2, probably due to a Rydberg state) and the peaks do not shift between the gas phase and the solid state, as expected[13h]. This similarity indicates that most of the final states of the excitation step (i.e. bound states and continuum resonances) are compact and not strongly perturbed by intermolecular effects. The exceptions to this generalization are the Rydberg states[30], which occur near the photoemission threshold and in general have low intensity in the NEXAFS spectra. We will therefore use the monolayer ice spectra when the gas phase spectra are not available to indicate the gas phase positions of the major resonances.

Comparison of the multilayer and monolayer spectra indicate the changes induced by chemisorption: peak 3 is subsumed into peak 1 and the

spectra show polarization dependence. This polarization dependence establishes the orientation of the adsorbed molecule as indicated later. The increase in width is due a combination of the decrease in lifetime of the final state and the mixing of empty metal orbitals into the final state orbitals of the adsorbate

Figure 14 shows a comparison of the experimental gas phase spectra and the theoretical spectra of benzene calculated using the MS Xα method and the oriented free molecule model[7]. The major features of the benzene spectra are assigned by the calculation as π^* and σ^* transitions. We find that the major peaks of the gas phase and multilayer ice spectra (peaks A, B, C, and D) are adequately modeled in their relative energy position and intensity. Comparison of the polarization dependent calculation (figure 15) with the monolayer spectra (figures 13 and 16) show a polarization dependence as would be expected for a benzene ring chemisorbed with the ring plane parallel to the metal surface. Comparison of the position of the σ resonances in the monolayer and multilayer spectra (figure 13) suggest that the bond lengths of the chemisorbed benzene are within 0.02Å of the gas phase molecule[7], in contrast to what has been recently observed on Rh(111)[25i,26e]. The ability to model the NEXAFS spectra of chemisorbed benzene by an oriented free molecule approach supports us in the use of similar models to analyse the polarization dependence of molecules that do not show evidence of direct metal orbital participation in bonding (i.e. adsorbate-metal σ bonding such as in ethylidyne[8]).

The monolayer of figure 13c,d was prepared by condensing a multilayer benzene ice (figure 13a) and subsequently evaporating off the multilayer at 200K. The spectra were taken at 100K. This experimental

protocol ensured that the sample was dosed to saturation coverage, gave the opportunity to obtain the spectra of the solid state, which is close to the spectra of the gas phase (undistorted) molecule. We found that unlike the spectra presented in figure 16, the monolayers were uncontaminated by CO coadsorption and were stable with respect to CO displacement during the course of the experiment for all the molecules examined.

The monolayer state prepared by room temperature chemisorption (figure 16) has coadsorbed CO and does not shows a residual π^* intensity at normal photon (grazing electric field vector) incidence. The apparent tilt in the molecules prepared from annealing the multilayer (figure 13) could be due to several factors: either an average tilt of the molecules of 35°, decomposition of a tilted component of the multilayer that had access to the surface (as is seen in cycloheptatriene, vide infra), partial rehybridization of the benzene toward sp^3 as is suggested for ethylene (vide infra), or an experimental problem (such as a tilt in the crystal along an axis perpendicular to the rotation axis of 32° or loss of polarization and spectra purity of the beam due to problem with the light source), or most likely a combination of all four causes.

Some early LEED work on benzene adsorbed on Pt(111)[25a,b] suggested that benzene may be tilted on Pt(111) at some coverages from work function, unit cell, and Auger evidence which in light of the present results are intriguing. However, subsequent analysis[25j] suggests that the apparent tilt is due to experimental difficulties from coadsorbed CO. Our spectra indicate that at room temperature a flat π coordinated

benzene is formed that has significant coadsorbed CO. The spectra of the benzene state formed from annealing a multilayer ice has no coadsorbed CO evident. The observed NEXAFS spectra is consistent with what has been seen with LEED with respect to the participation of CO coadsorption in the formation of a well behaved benzene monolayer. Latest LEED evidence suggest that the earlier suggestion of a tilted state was not supported by the data and rationalization of the observed apparent ring tilt in terms of a globally tilted species is therefore not suggested.

The observed apparent ring tilt may be due to disordering of the surface layer due to the low temperature at which it is formed: at liquid nitrogen temperature the multilayer forms with no apparent ordering (as indicated by the lack of polarization dependence of the NEXAFS spectra) and when the physisorbed layers are removed there is a component of the benzene coordinated to the surface by only a subset of the carbon atoms, yielding an apparent tilted surface species. The tilted molecules could go on to decomposition products (i.e. surface ethylidyne, methylidyne (CH), and other unsaturated hydrocarbon moieties) which would give π^* intensity at normal photon incidence. The normal incidence π^* intensity is 27% of the intensity at 20°, which means that ~27% of the carbon on the surface must be tilted or decomposed to explain the tilt by this means alone.

Rehybridization is not a convincing rationale for the π^* intensity at normal photon incidence both from the HREELS evidence[26b] and the lack of shift in the NEXAFS spectra between gas phase and monolayer spectra. In support of the rehybridization argument is the work indicating that for the case of ethylene, coadsorption of electron withdrawing groups

shifts the surface bonding towards π coordination[31]; and for CO and benzene, coadsorption of electron donating groups shifts the internal vibrational modes towards lower energies, consistent with rehybridization towards sp^3 carbons[32]. Our work is best rationalized in terms of only weak perturbation of the aromatic center by the surface and thus rehybridization is not suggested as the sole cause of the π^* intensity at normal photon incidence.

Figure 17 is a montage of NEXAFS spectra taken after the multilayer of figure 13 was annealed to successively higher temperatures. With increasing temperature the π^* component at normal photon incidence and the σ components at grazing incidence of the spectra monotonically increases. The peak area ratio indicates an apparent angle of the π system to the metal surface of 50 $\pm 10^{o}$, which is indicative of a surface state with the π orbitals nearly isotropic in orientation. No new resonances (in particular, no new σ resonances) appear at higher temperatures. The π^* intensity at normal photon incidence is indicative of the formation of π^*-like orbitals oriented parallel to the surface, such as one would expect for a surface ethylidyne or vinylidyne species. Indeed, C_2 fragments have been suggested as important intermediates in the formation of soot during combustion. Conversely, gas phase studies of the thermal decomposition of benzene have implicated direct condensation of aromatic fragments or phenyl radicals in the formation of soot[34].

There are three canonical models for the carbonaceous surface species - C_2 and similar fragments (generated by, for example, a retrotrimerization reaction), C_6 fragments, and surface graphite.

Figure 18 shows the NEXAFS spectra observed from an annealing set starting from an acetylene covered surface. Acetylene is a molecule which is expected to rehybridize significantly on chemisorption to the Pt(111) surface and thus requires modeling with techniques such as MS Xα to explain the observed spectra in detail. Even without detailed calculations some models and conclusions can be obtained and the spectra can be used as "fingerprints" to determine if two surface states are similar. These spectra do not look like the benzene spectra (figure 17): at high temperatures benzene shows strong σ resonances at normal photon incidence only while the acetylene derived carbonaceous layer shows strong σ resonances at both angles. The σ resonances at 345 K, grazing photon incidence, and at 287.4eV and 295eV (peaks B and D) that appear and then disappear (and are observed at 300 K for ethylene[8] i.e. are indicative of ethylidyne and other C_2 species with perpendicular orientation) are seen in acetylene and not in benzene. We therefore reject the model that proceeds though C_2 species.

Figure 19 shows the NEXAFS spectra of single crystal graphite[34]. Single crystal graphite is an extended valence bonded material and band structure calculations have been used to calculate the expected NEXAFS spectra[35]. At 30° photon incidence a π^* resonance is seen that disappears at normal photon incidence. They find σ resonances from 292eV to 318eV. The single crystal graphite NEXAFS spectra show a more extended σ structure and no π^* intensity at normal photon incidence, thus single crystal graphite alone is not an adequate model for the carbonaceous overlayer generated by pyrolysis of benzene on Pt(111) at temperatures up to 780 K. The normal incidence π^* intensity could be modeled by the inclusion of methylidyne-like species or by limiting the

size of the graphite islands: the edges of the islands would have orbitals similar to π^* orbitals. We believe this to be the correct model for the 780 K spectra (since after the loss of all of the hydrogen graphite is the obvious product), but the 556 K state has residual hydrogen and the π^* resonance shows almost no polarization dependence - the required island size would be 6 atoms and thus "graphite" would be a misnomer.

Figure 20 shows the NEXAFS spectra generated by fluorobenzene annealed to remove HF (vide infra), which we propose forms a surface C_6H_4 species i.e. a benzyne species with the ring plane parallel to the surface plane. We observe before the loss of HF a monolayer spectra essentially identical to benzene. After HF loss a strong, narrow π^* resonance at 285.7eV and normal photon incidence is observed, indicating a component with a π^* orbital oriented such that it does not mix with metal orbitals and close to parallel to the surface. This requirement is satisfied by benzyne. There is an alternative orientation for the benzyne state - a state with the ring plane perpendicular to the metal surface. This state was excluded on the grounds of the weak σ resonance at grazing photon incidence. The grazing incidence spectra should be compared with the spectra for α-pyridyl (vide infra). Figure 21 is closest to the annealed benzene NEXAFS spectra in the general features of the spectra. The benzene spectra does have broader π^* resonances at normal photon incidence and more σ resonance intensity at grazing photon incidence than the fluorobenzene spectra but this could be accounted for by contributions by a minority amount of decomposition to form ethylidyne and methylidyne moieties and perpendicularly bonded benzene

fragments.

To summarize, benzene chemisorbs with π coordination (with its ring plane essentially parallel to the surface) to Pt(111) at room temperature and below. The molecule is only weakly perturbed from the gas phase - multilayer spectra are essentially identical to gas phase spectra and the monolayer spectra exhibit the same major resonances as the gas phase. MS Xα calculations indicate that the major resonances can be explained as π^* and σ^* final states. We will therefore use the oriented free molecule model to analyse the energy position and polarization dependence of aromatic molecules in the subsequent discussions, unless there is evidence for direct metal-adsorbate σ bonding. Preparation of the benzene monolayer at 300K yielded a surface state with coadsorbed CO (similar to what has been reported on Rh(111)[26e]) and gave spectra indicative of a state with the benzene ring plane parallel to the metal surface, while preparation of the monolayer state by momentarily annealing a multilayer ice to 200 K yielded a state with an apparent ring tilt of 35° and no evidence for CO contamination. We suggest that the apparent ring tilt is primarily due to a kinetic disorder in the first layer of the ice prepared at 100 K that persists after the anneal to 200 K in either a tilted component to the benzene monolayer or decomposition to form metal-carbon bonded products, although we can not exclude some rehybridization of the surface benzene state without coadsorbed CO. At higher temperatures a carbonaceous overlayer forms. The NEXAFS spectra indicate that the benzene structure is by and large maintained but that the exclusively parallel π coordination of the surface species is lost on pyrolysis. We propose a benzyne-like state as the majority species at 556 K (after the first

hydrogen desorption peak) and a graphite-like species with small island size for the 780 K state.

III.2.1 FIGURES

Figure 12

This figure show the thermal desorption spectrum for ~1 monolayer of benzene chemisorbed on Pt(111) (note the start of multilayer desorption at ~200 K). The products observed include benzene, hydrogen, and surface carbon. At this coverage we observe ~0.2 monolayer of carbon on the surface after the experiment (which amount does not grow with increasing coverage) indicating ~22% decomposition. These results are similar to those we have obtained earlier[23b]. The ratio of the first hydrogen desorption peak to the second is dependent on coverage, but is approximately one to one.

Figure 13

Comparison of the gas phase electron energy loss (a), multilayer (b), and monolayer (c,d) NEXAFS spectra[7] of benzene. The gas and multilayer spectra are almost identical, indicating the compact nature of the final state orbitals and there is no shift of the σ resonances (C and D) between the multilayer (gas) and the monolayer spectra, suggesting that the benzene molecules in the monolayer are only weakly (<.02Å) perturbed from the gas phase. The gas phase spectrum was recorded using 2.8 keV electrons at a resolution of 1.0 eV FWHM. All of the spectra have had a background subtracted.

The multilayer spectrum showed no polarization dependence, indicating that the molecules comprising the ice grown at 100K are not preferentially oriented.

Note the weak π^* intensity in spectrum c, indicating an apparent residual ring tilt, as compared to figure 16, and the increase in the width of the π^* transition, due to escape of the excited π^* electron to

the metal, as compared to the σ resonances which do not change in width.

Figure 14

Experimental and calculated gas phase carbon edge spectra for benzene. The calculated spectra has been shifted so that the ionization threshold matches the experimental value determined by XPS.

Figure 15

Calculated carbon 1s NEXAFS spectra for monolayer benzene with the ring plane parallel to the surface using the MS Xα method and the oriented free molecule model. Note that the π^* transitions are strong when the electric field vector is normal to the surface (along the axis of the p orbital component on the excited atom of the final state) and that the σ resonances are strong when the electric field vector is directed along the bonding plane.

Figure 16

NEXAFS spectra for benzene dosed at 270 K and annealed for 1 minute to 300 K. The spectra were obtained at ambient temperature. Note the absence of peak A at normal photon incidence (indicating that the ring plane is strictly parallel to the metal surface) and peak B, due to coadsorbed CO.

Figure 17

Benzene annealed to successively higher temperatures. (a) is the benzene monolayer presented earlier, prepared from a multilayer ice by annealing to 200 K. (b) is the surface state of a. annealed to 556 K (i.e. after the first major hydrogen desorption peak). (c) is the surface state of (b) annealed to 780 K (after the last hydrogen desorption peak). Peak A is the π^* resonance and peaks B and C are

the σ resonances. The appropriate intensity scale is indicated by the scale the plot terminates on. Note the lack of new σ resonances and the increasing width and lack of polarization dependence of the π^* resonance at 556 K.

Figure 18

Acetylene annealing set. (a) is a monolayer prepared by dosing to saturation at 90 K. (b) is the state of (a) annealed to 345 K. (c) is the state of (b) annealed to 520 K. Note the similarity of (b) to features in the published NEXAFS spectra of ethylene prepared under similar circumstances[8] and figure 4.

Figure 19

(a) is the single crystal graphite NEXAFS spectra[34]. Note the disappearance of the π^* transition at normal photon incidence and the extended σ features. The angle α here is the angle between the surface normal and the photon propagation vector - our convention here is 90-α. Features due to π states are indicated by dashed lines and σ states by solid in the peak assignments. (b) is a fit of peak A (the lowest π state, similar to our π^* states) intensity to a $\sin^2\alpha$ relation. (c) is the calculated band structure of graphite. The peak positions and assignments are indicated on the right.

Figure 20

Fluorobenzene (C_6H_5F) annealed to 470 K (just after the HF desorption, before the onset of H_2 desorption). We propose this as the NEXAFS spectra for a 1,2 eliminated benzene. We propose a benzyne-like edge coordinated 1,2 di σ bound benzene species. The π^* intensity grazing photon incidence is in this case due to both the projection of the ring π^* resonance onto the grazing incidence spectra and the metal-

carbon orbitals (note the narrower resonance at normal incidence).

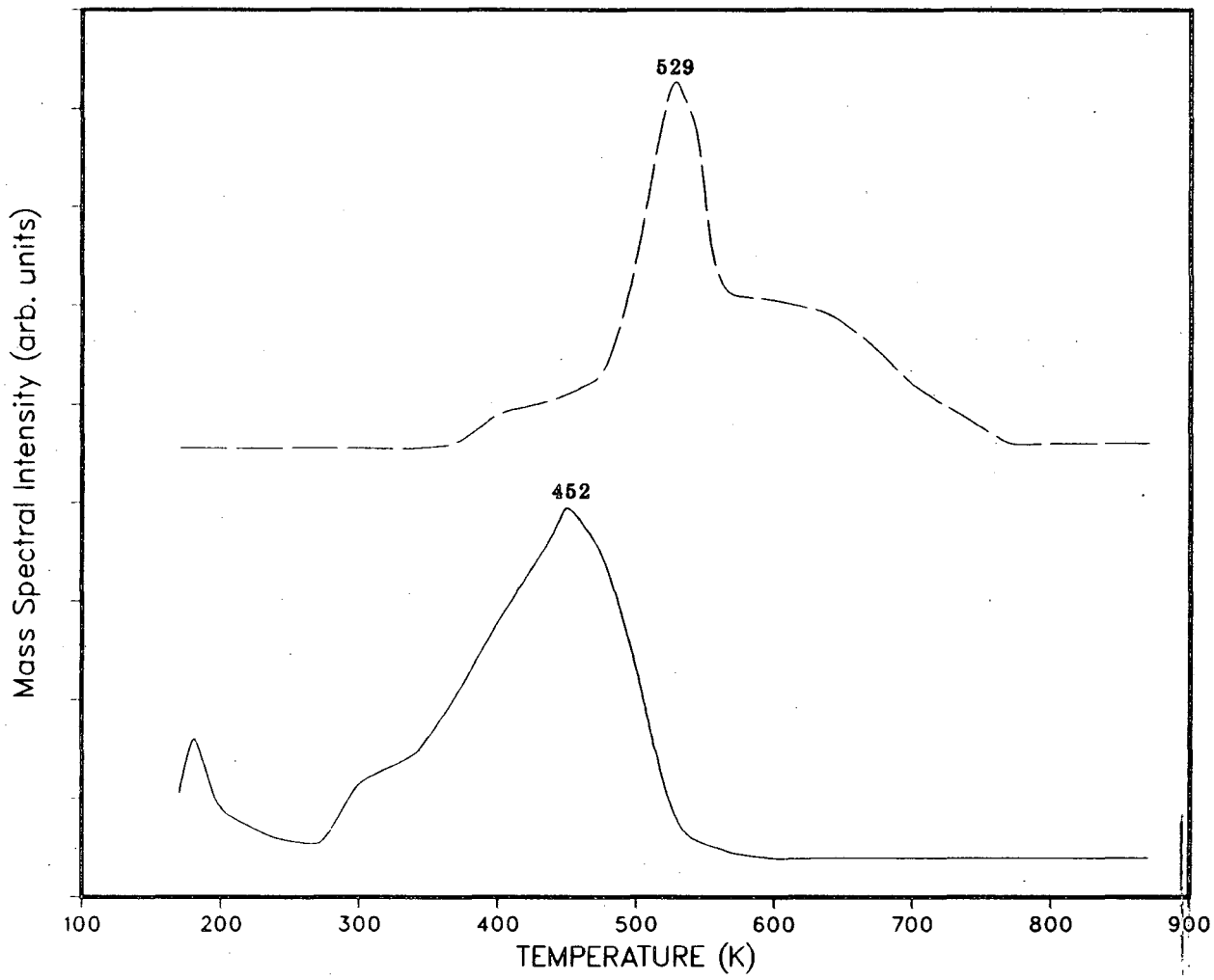

XBL 8512-5106

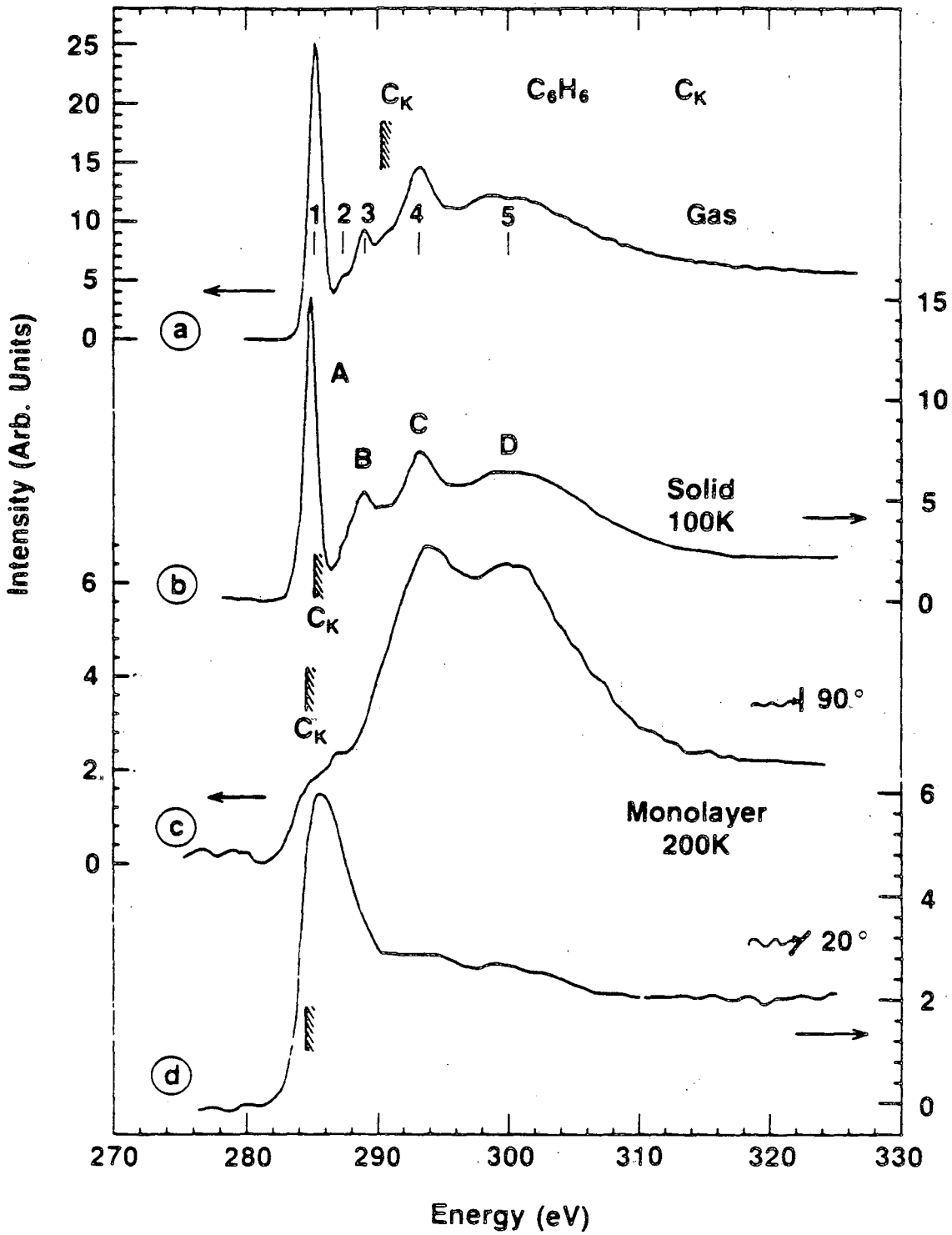

XBL 8512-5088

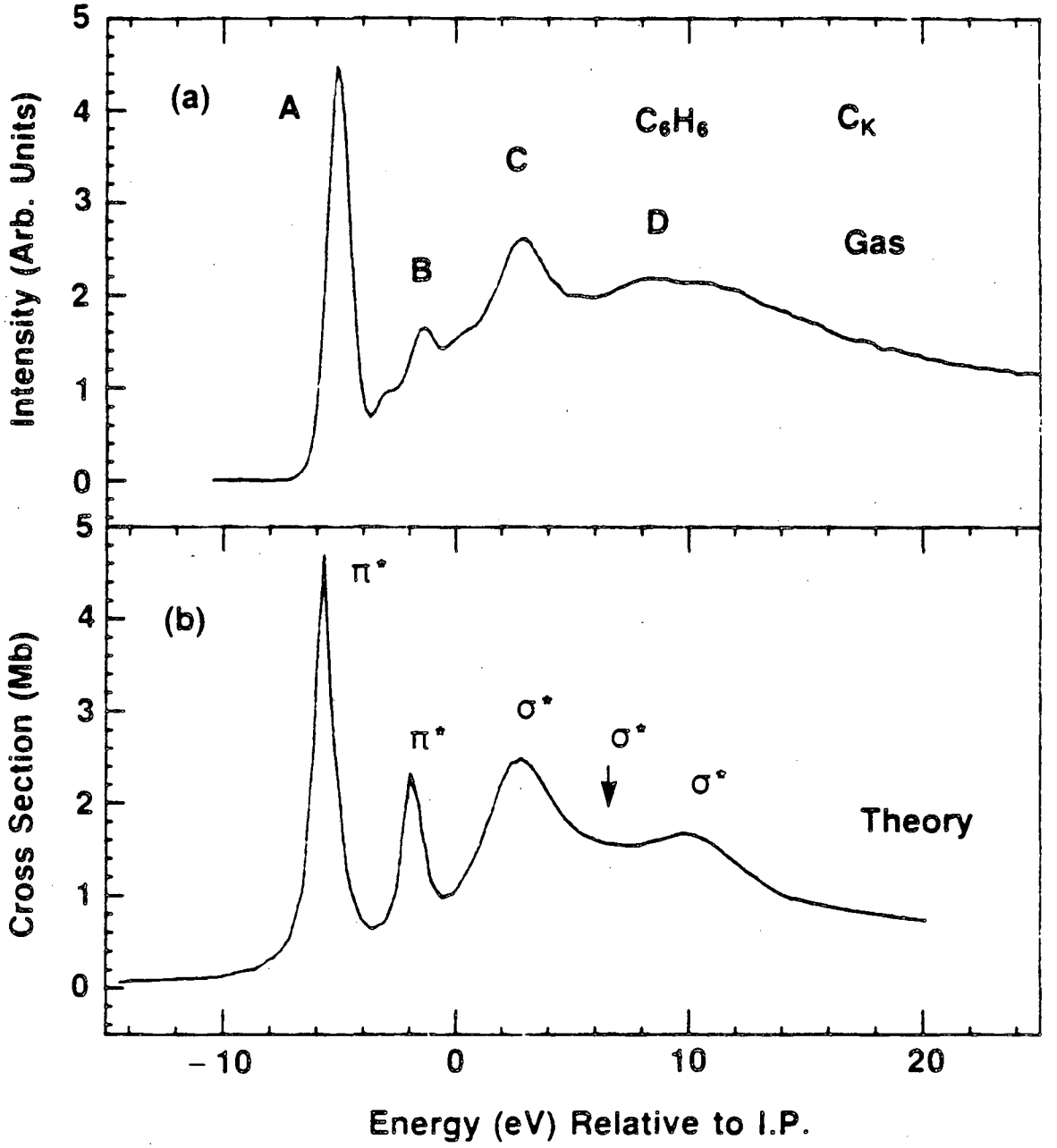

XBL 8512-5087

C_6H_6 monolayer - theoretical NEXAFS

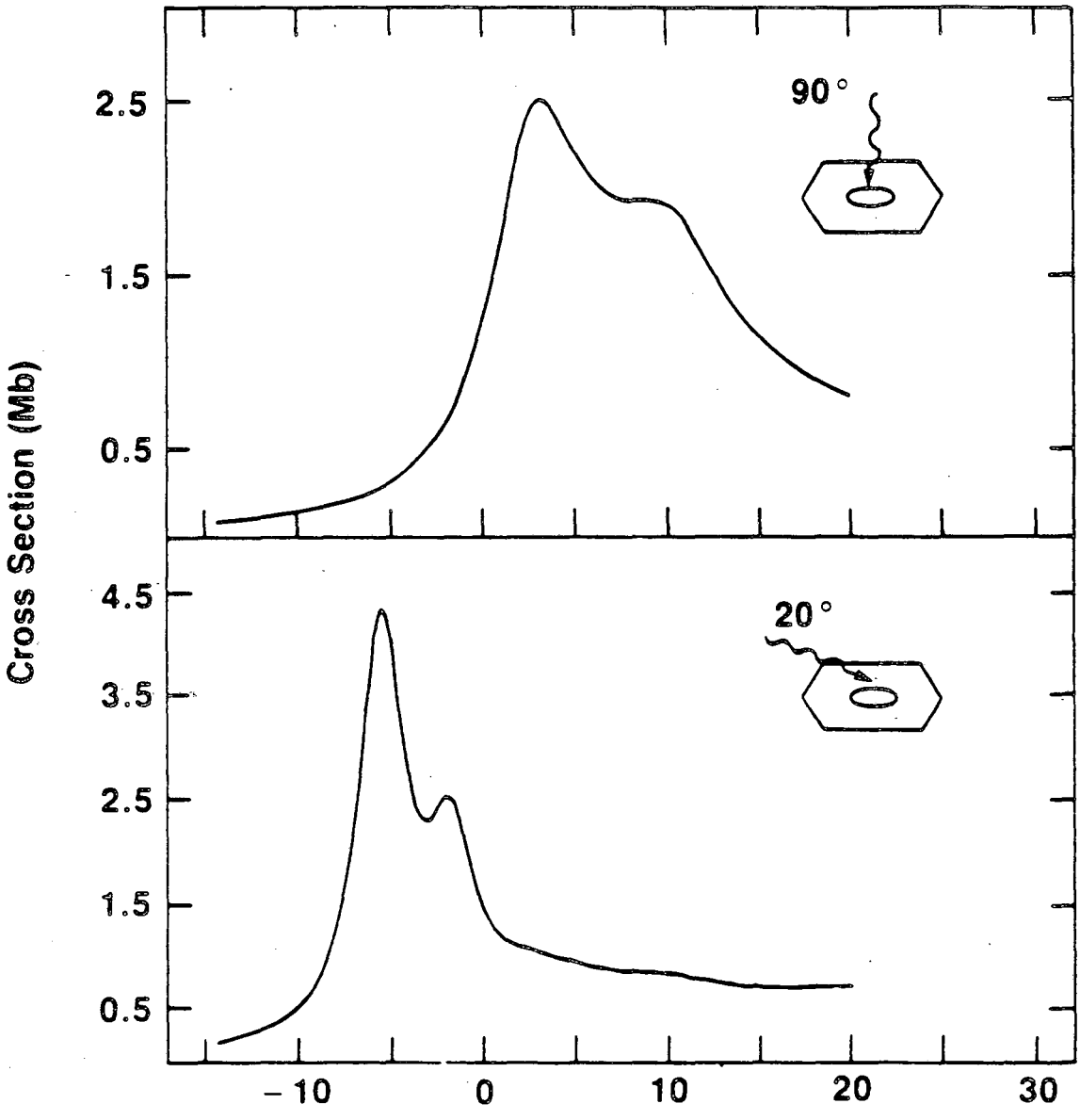

XBL 8512-5086

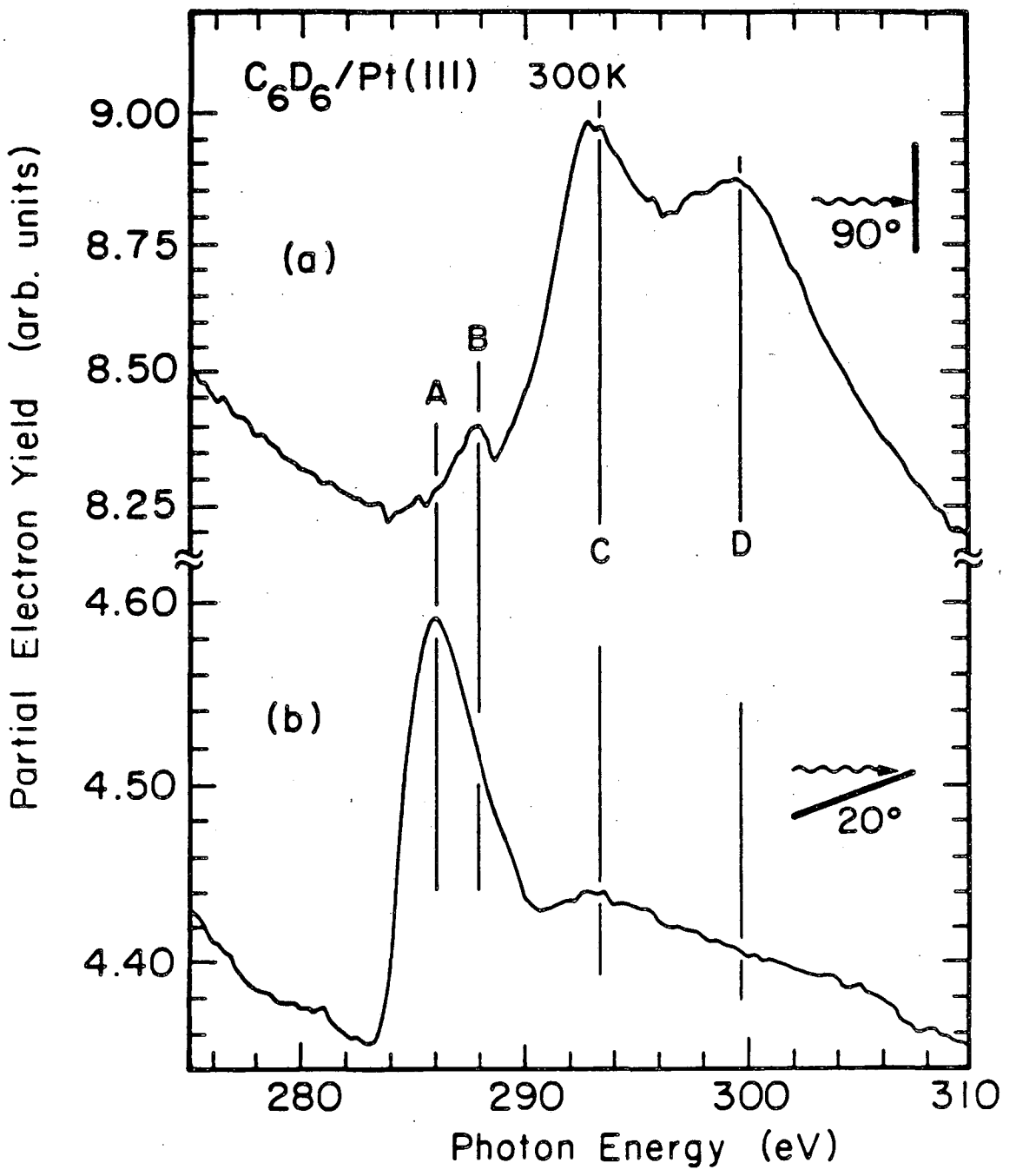

XBL 8512-5092

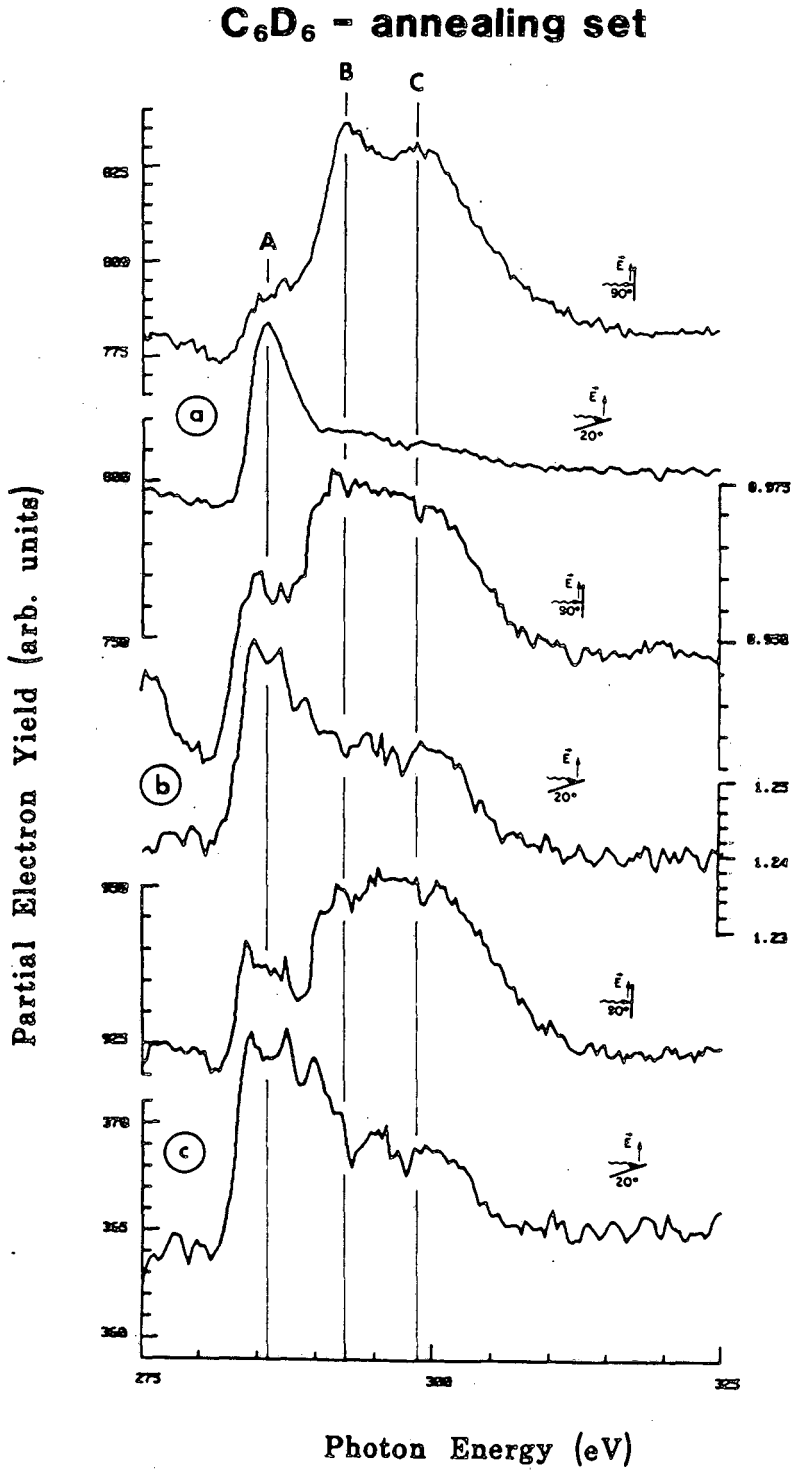

XBL 8512-5083

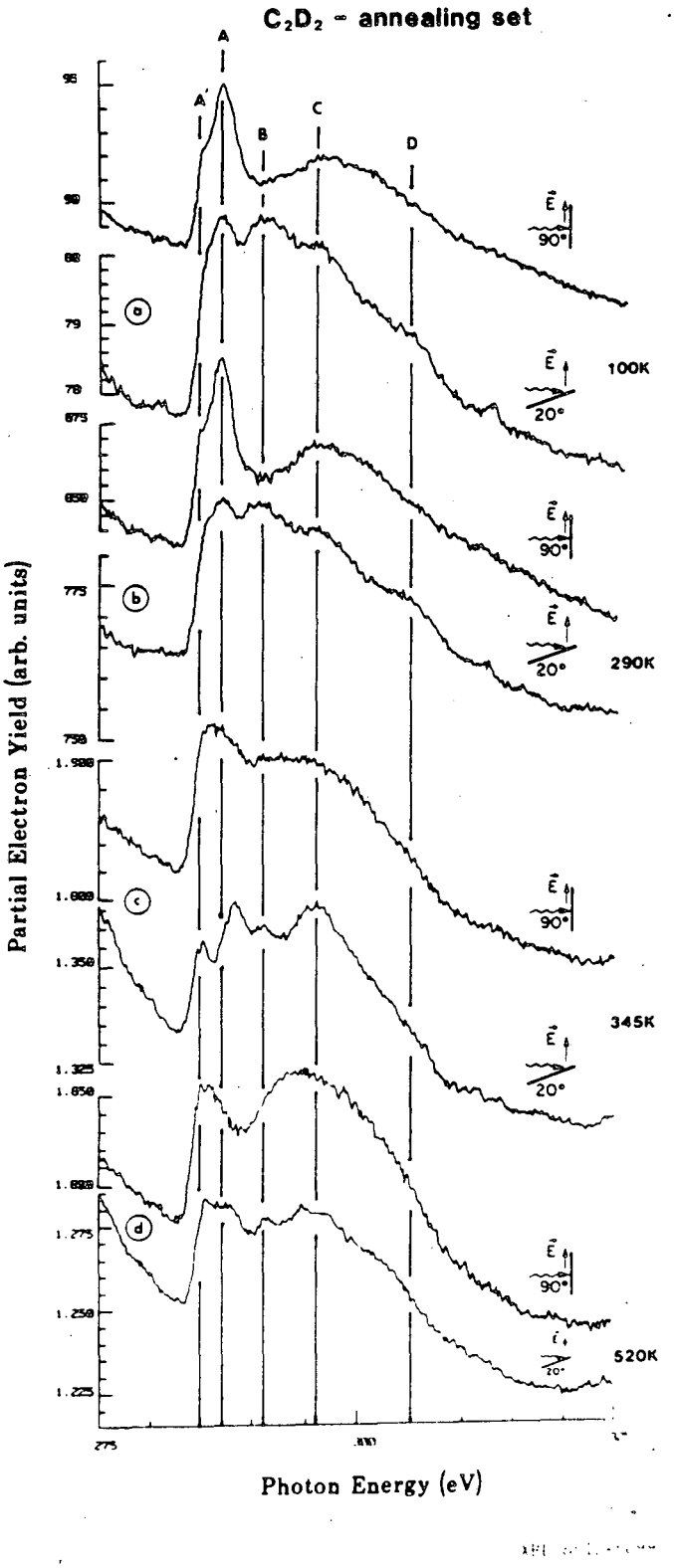
C_2D_2 - annealing set
A
A'
B
C
D
E
90°
20°
100K
290K
345K
520K
a
b
c
d
Partial Electron Yield (arb. units)
Photon Energy (eV)

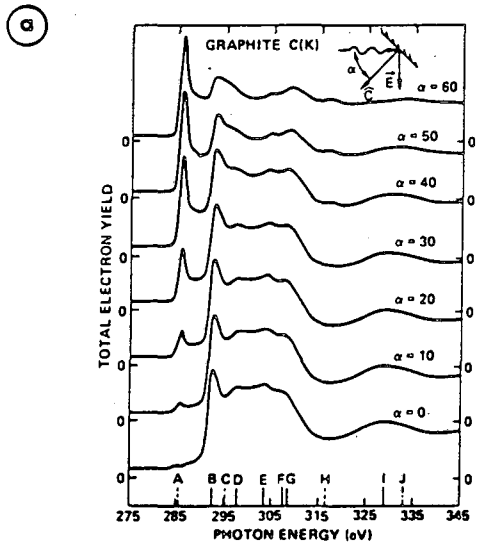

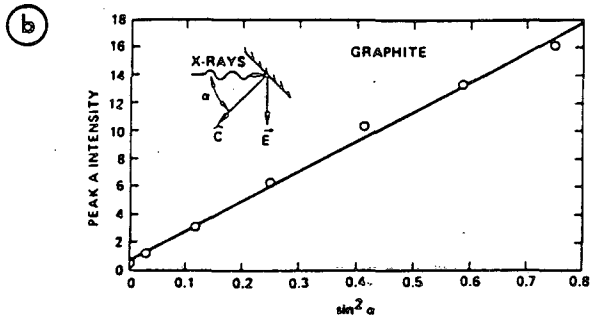

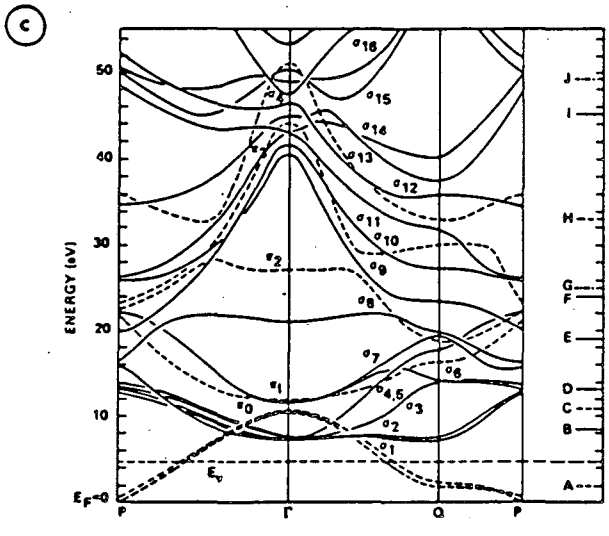

XBL 8512-5084

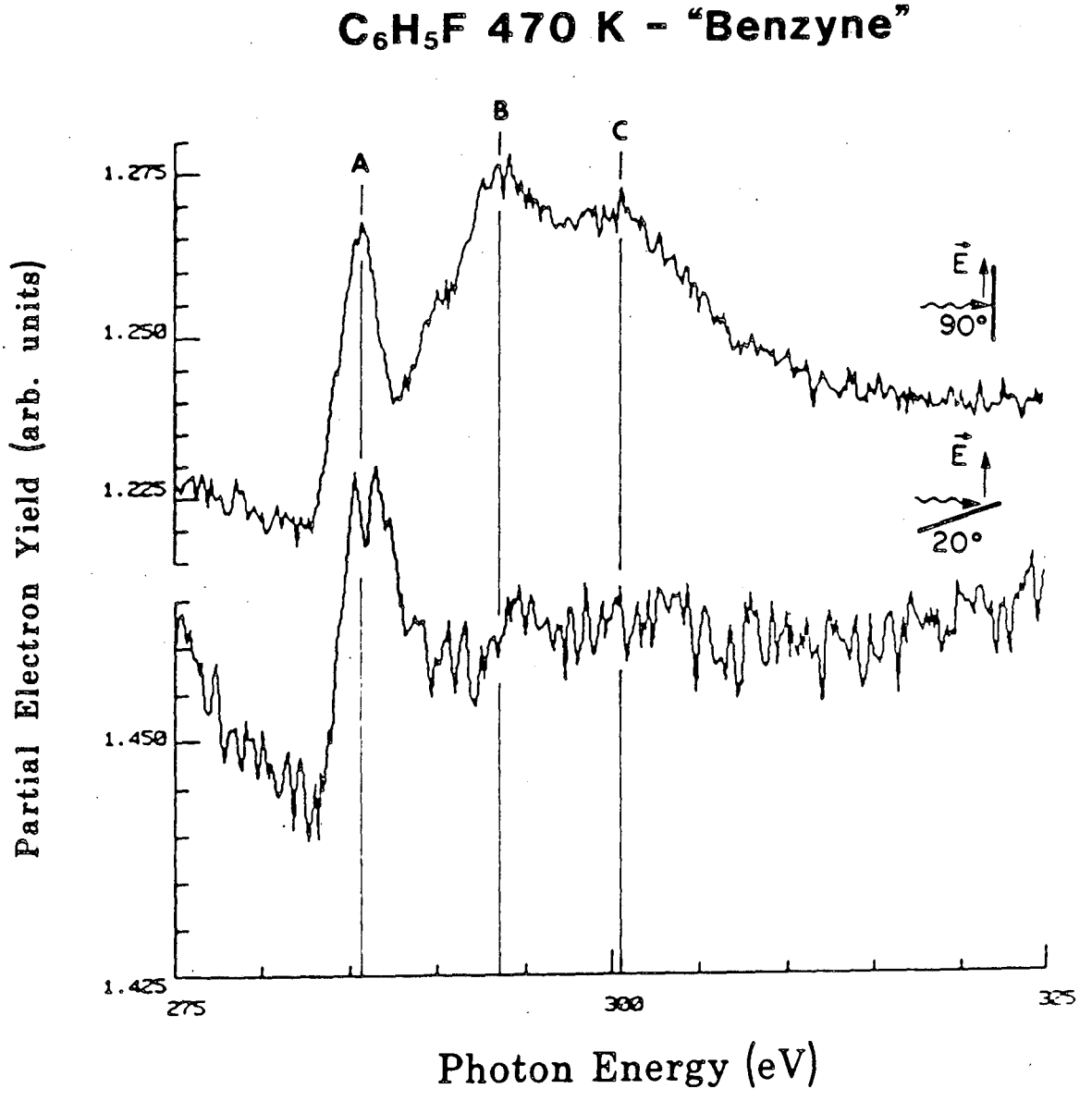

XBL 8512-5085

III.3 Fluorinated Benzenes

The investigation of the fluorinated benzenes was initiated to determine the principal parameters determining the chemisorption energy of aromatic molecules. The coordination of closed shell molecules to metal centers has been explicated in terms of donor/acceptor interactions. Closed shell molecules can have both relatively high lying occupied states (π states and lone pairs) that can mix with empty metal orbitals (donor interactions) as well as low lying empty states (π^* and σ^* states) that can mix with occupied metal orbitals (acceptor interactions) and lead to bonding. The fluorinated benzenes allow investigations of the relative importance of donor vs. acceptor interaction using systematic shifts of the energies of the HOMO and LUMO levels. There have been extensive studies of fluorinated benzenes that have determined the HOMO and LUMO levels both experimentally and theoretically. Additionally, fluorine has a Van der Waals radius of 1.35 Å which is close to the Van der Waals radius of hydrogen (1.2 Å). The geometry of benzene chemisorption (ring parallel to the surface) suggests that the influence of direct metal - fluorine interactions on the overall surface chemical bond should be minimized. Lastly, Redhead analysis of the thermal desorption spectra upon determination of the preexponential factor yields the activation energy of desorption. If there is no special activation energy for desorption (equivalently, if the adsorption is molecular [not reactive] and the sticking coefficient is one, as is the case for benzene) then the activation energy is just the chemisorption energy. The fluorinated benzenes, if they chemisorb similarly to benzene (π coordinated, not dissociative) can be assumed to have similar preexponential factors to desorption and thus the trends

in chemisorption energy may be obtained utilizing less stringent initial assumptions.

The use of the fluorinated benzenes in this study is predicated on the assumption that they are molecularly adsorbed. A photoemission study of chlorobenzene indicated that the molecule was molecularly adsorbed at room temperature[36]. A comparison of the bond strength of C-F verses C-Cl bonds (127 verses 97 kcal./mole, compared with 112 kcal./mole for C-H bonds) in the monosubstituted benzenes suggests that the fluoro compound should be more stable. While the determination of the chemisorption energy of fluorine on Pt(111) is complicated by the formation of volatile platinum fluorides, a value of 52.6 kcal./mole has been found[37] (compare to 57 kcal./mole for hydrogen[38] and 47.6 kcal./mole for Cl[39] adsorption to Pt(111)), suggesting that the fluorobenzenes should be more stable than chlorobenzene. Lastly, the large body of work with the simple fluorinated alkanes and alkenes[40] indicate that for these molecules on platinum the initial chemisorption is dissociative and at higher coverages (greater than .25 monolayer) the chemisorption is associative. We shall investigate the thermal desorption of the fluorobenzenes and determine the extent and mechanisms of decomposition.

Prior work with fluorine and fluorinated hydrocarbons interacting with metals has investigated both coordination and surface complexes.

Very illuminating was the characterization of $(C_5H_7O_2)Rh(C_2H_4)(C_2F_4)$[41a] and $(C_5H_5)Rh(C_2H_2)(C_2F_4)$[41b] using X-ray diffraction. The Rh-C lengths for the ethylene and tetrafluoroethylene ligands indicate that the tetrafluoroethylene is closer to the rhodium

(and thus more strongly bound) than the ethylene is, due to the increased backbonding (acceptor interactions) for tetrafluoroethylene. Rhodium in these compounds is in the +1 formal oxidation state, so the tendency towards acceptor interactions should be greater for unoxidized and surface metal centers.

Conversely, the fluorinated benzenes have been used to synthesize analogs of the $M(Ar)_2$ sandwich compounds. In particular, the chromium compounds of the form ArCrAr' have been synthesized by metal vapor reactions. The stability of these compounds have been studied by NMR and vibrational spectroscopies and the structures determined for the $C_6H_6Cr(C_6F_5PPh_2)$ analog using X-ray diffraction[42]. X-ray diffraction indicates that the fluorinated ring is closer (Cr-C distances 2.083 - 2.104 Å) to the chromium than the benzene ring (2.142 - 2.164 Å)[42h]. An analysis of the vibrational spectroscopy of the mixed ring system shows the symmetric stretch between the rings and the chromium atom occurs at 227 cm^{-1} for $Cr(C_6H_6)_2$ and 340 cm^{-1} in $(C_6H_6)Cr(C_6F_6)$[42g], indicating stronger bonding for the fluorinated molecule. This is to be contrasted with the decreased shift in the in-plane vibrations of the fluorinated arene with electronegative substitution, suggesting decreased backbonding and weaker bonds[43]. Studies indicate that the stability of the symmetric fluorinated arene is lower than the mixed benzene fluoroarene complex, due to the inadequate ability of the metal center to supply electrons to the electronegative fluorinated arene[42c,e]. This rather complex state of affairs suggests that the correlation of fluorination (and thus donor verses acceptor ability) with bonding may be difficult, although we might hope that a metal surface would be more capable of supplying electron density to the adsorbate than an isolated

metal atom.

Electrochemical studies of the fluorinated benzenes on polycrystalline platinum electrodes have been carried out to determine surface coverage and stability towards electrochemical oxidation and reduction[44]. The surface coverage (prepared by adsorption from dilute aqueous solution followed by a wash with pure electrolyte) decreased with fluorine substitution and the stability of the adlayer was invariant with fluorine substitution.

Theoretically the donor verses acceptor problem can be addressed from two perspectives - the electronegativity of the adsorbate can be shifted or the Fermi level of the surface can be shifted. Anderson et. al.[45] proposed that the bonding of benzene to Pt(111) is dominated by donor interactions and small Kekule' distortions of 0.04 Å will be found. Further, they suggest that the C-H bonds will bent 19° away from the surface and that coadsorption of potassium should decrease the binding energy of benzene on Pt(111), as is observed[46], based on a model where the effect of the potassium is to shift the valence band energy. However, if the valence band is shifted by greater amounts cathodic (figure 8 in reference 8) then the chemisorption energy will increase again as acceptor interactions begin to predominate. Other treatments[47] suggest that the metal surface should in general be electron donating, and the acceptor effect should be seen at all times.

We will address three points: the reactivity changes induced by fluorination, the structures determined by NEXAFS for the fluorobenzene chemisorption states, and the trends in chemisorption energies of the fluorobenzenes, including the correlation of these trends with HOMO and

LUMO levels.

The thermal desorption spectra of monofluorobenzene is shown in figure 21. We observe hydrogen, hydrogen fluoride, and a small amount of benzene along with molecular desorption. After the experiment we see residual carbon, from 60% decomposition at ~.25 monolayer to 20% decomposition at ~1 monolayer. The important features are the fact that HF production precedes hydrogen desorption and that benzene production is essentially simultaneous with hydrogen desorption. Comparison with benzene TDS (figure 12) indicates that the molecular desorption has been shifted down in energy and that the first hydrogen peak has been split up into the HF peak and smaller hydrogen peaks. The benzene production is presumably due to the hydrogenation of the species produced by HF loss - which we have earlier suggested as a π coordinated "benzyne" species. Attempts to intercept the active hydrogen in such a hydrogenation have failed - coadsorbing D_2 or C_6D_6 and normal monofluorobenzene yielded only normal benzene, but deuterium incorporation was noted in the HF product. Mixtures of C_6D_6 and C_6H_5F yielded no C_6D_5F, thus reversible C-F bond breaking with facile deuterium exchange is precluded.

The other members of the fluorinated benzenes gave even simpler chemistry. 1,4 difluorobenzene gave only hydrogen, HF and molecular desorption, 1,3,5 trifluorobenzene gave molecular desorption, HF and small amounts of hydrogen. 1,2,4,5 tetrafluorobenzene, and pentafluorobenzene gave only molecular desorption and HF. Hexafluorobenzene gave only molecular desorption and left no residual carbon after the experiment. No evidence for the loss of fluorine to form F_{n-1} products were observed for any molecule other than

monofluorobenzene. The species investigated were chosen to have the lowest dipole moments of their level of fluorination, in an attempt to minimize the effects of dipole - dipole interactions in the molecular desorption.

The most insightful experiment was to run a mixture of C_6D_6, C_6H_5F, and C_6F_6 (figure 22). Both HF and DF are formed - HF at 199° C and DF at 275° C. The DF must arise from intermolecular reaction and is in fact almost simultaneous with D_2 evolution. The HF is produced both intermolecularly (as seen by the early initiation of the HF desorption) and intramolecularly (as seen by the features in the HF curve that follow the H_2 desorption). H_2 evolution is seen to precede D_2 evolution by a small amount, but whether this is due to activation by the fluorine substitution or isotope effect is not show by these experiments. Experiments with a mixture of C_6H_6, C_6D_5F, and C_6F_6 would address this point.

Figure 23 is the NEXAFS spectra of monofluorobenzene at 90 K (a multilayer ice) and at 250 K (a monolayer). The monolayer shows polarization dependence as would be expected from a flat, π coordinated ring, similar to benzene. The shift in the π^* resonance is unusual for the aromatic molecules we have examined, and may indicate some C-F bond cleavage or more likely rehybridization towards a poly σ bonded species (see the shift in the π^* resonance in cyclopentene dehydrogenation, vide infra). Similar spectra of C_6F_6 indicate that it too is flat and π coordinated. It is interesting to note that there was evidence of CO displacement of the C_6F_6 during the course of the experiment, in marked contrast to C_6D_6. Figure 24 shows the NEXAFS spectra of the sample of

figure 23 annealed to 470 K. Note the appearance of π^* intensity at normal photon incidence, indicating π orbitals oriented parallel to the metal surface. Note also the narrower width of the normal photon incidence π^* resonance, also suggestive of a π system that does not interact with the metal surface. Comparison with the 300 K pyridine spectra (vide infra) shows similar resonance behavior at the π^* region but not at the σ^* region - for pyridine there is significant σ intensity at grazing incidence while at grazing incidence for the 470 K monofluorobenzene spectra there is no evident σ intensity. For this reason we propose a structure where the benzene has lost HF to form C_6H_4 and the molecule is still parallel to the surface i.e. π coordinated benzyne.

Table 1 lists the temperatures of the thermal desorption maxima, the ionization potentials (i.e. HOMO energies), the first electronic excitation energies (i.e. the HOMO - LUMO gaps), and the derived relative thermal desorption energies for the fluorobenzenes studied. As fluorination increases the ionization potential (generally) increases and since the HOMO - LUMO gap is approximately constant the molecules are generally better acceptors and worse donors with increasing fluorination. The determination of the thermal desorption maxima is complicated by the effects of multiple desorption states, possible electron damage, and coverage effects but the general trend is that the thermal desorption energy decreases with increasing fluorination until trifluorobenzene and then increases until one reaches hexafluorobenzene. This trend is not explained by either strictly donor or acceptor behavior. This behavior may be explained in several ways. After Anderson et al. we could be going from a regime where the primary effect

is a donor effect to one where the primary effect is an acceptor interaction. Again from figure 8 of reference 8 the expected variation of binding energy is about .2 eV, or 4.6 Kcal./mole, which is close to the observed variation. Another rationale is that there is direct metal - fluorine repulsive interactions. The fluorine has had its valency requirements filled and is a close shell, as far as the metal is concerned. The obvious model for the steric interaction of fluorine with the surface is neon. The bonding distance for neon is between 3 and 4 Å from theoretical calculations for Pt(111)[48a] and comparison with neon on graphite[48b]. The bonding distance for the benzene - Rh(111) system[25i] is 2.15 Å. If we assume similar bonding distance for benzene - Pt(111) the average ring - surface distance must increase from benzene to 1,3,5 trifluorobenzene. Higher fluorination has little effect on bonding distance and thus the acceptor effect takes over. Supportive of this model are preliminary results we have obtained with C_6H_6, C_6H_5F, and C_6F_6 on Cu(111). Cu(111) has a work function of 4.9 eV and Pt(111) has a work function of 5.93 eV. The thermal desorption maxima should increase from C_6H_6 to C_6F_6 on Cu(111) if we are in the region of transferal to acceptor behavior in Pt(111), since Cu(111) is about 1 volt more cathodic. In fact the observed trend in T_{max} is $C_6H_6 > C_6H_5F > C_6F_6$. If the steric model is appropriate then the implicit assumption of no metal - hydrogen interaction in the interpretation of shifts in vibrational frequencies for chemisorbed molecules must be examined for possible effects due to multicenter interactions i.e. the shifts to lower frequencies may be due to multicentered interactions "softening" the C-H bond rather than due to rehybridization. If, however, the

proposed[45] rehybridization of the carbon to swing the C-H vectors towards the surface normal is in fact correct then steric arguments are probably invalid.

In summary then we find that the fluorinated benzenes chemisorb with varying amounts of decomposition, but that molecular desorption is seen in all cases. The primary products of decomposition are hydrogen and HF, with the relative amounts of each determined by the stoichiometry of the adsorbate. The fluorine is an efficient scavenger of hydrogen. No fluorine desorption was seen - in those cases where there is no molecular or surface hydrogen no decomposition was seen. Mono and hexa fluorobenzene chemisorb at 300 K to give flat, π coordinated surface states. Monofluorobenzene loses HF to give what we propose to be "benzyne", a 1,2 eliminated benzene which is also flat and π coordinated. The heat of chemisorption decreased with fluorination until trifluorobenzene, whereupon it started to increase. All of the fluorobenzenes desorbed at temperatures below that required for (the high temperature state of) benzene. This trend may be explained by either a shift from donor to acceptor in the course of the fluorination or by metal - fluorine interactions that increase the ring surface distance for steric reasons.

Table 1

Adsorbate	T_{max} (K)	I.P.	Ex. E.	Chemisorption Energy
C_6H_6	452-490[a]	9.24	3.90	28.0-30.4
C_6H_5F	418±15	9.19	3.90	25.7±.9
1,4 $C_6H_4F_2$	351-437[b]	9.33		21.7-27.1
1,3,5 $C_6H_3F_3$	399	9.64	3.95	24.7
1,2,4,5 $C_6H_2F_4$	400			24.8
C_6HF_5	411±4	10.1	3.90	25.5±.2
C_6F_6	420±13	9.93	3.86	26.0±.8

I. P.s are the vertical I. P.s from "Handbook of Spectroscopy", J. W. Robinson ed., CRC Press, Cleveland, Ohio, 1974, and are accurate to ± 0.05 volt. The excitation energies are from R. P. Frueholz, W. M. Flicker, O. A. Mosher, A. Kuppermann Chem. Phys. Lett., 52, 1977, 86 and are accurate to ± 0.05 eV. The chemisorption energies are in kcals/mole, and are estimated using the Redhead[9a] method and approximation function E = T(K)*.062 and with b = 25°/sec. v = 10^{13}.

a. aggregate of my results and the low coverage results of M.-C. Tsai, E. L. Muetterties J. Am. Chem. Soc., 104, 1982, 2534

b. double peak

III.3.1 FIGURES

Figure 21

Thermal desorption curves for monofluorobenzene. The sample was dosed at 170 K and the heating rate was 25°/sec. Note the HF production which precedes hydrogen loss and the small amount of benzene product.

Figure 22

Thermal desorption of a mixture of C_6D_6, C_6H_5F, and C_6F_6. Not shown is the molecular desorptions, which do not change significantly from the pure adsorption case. This sample was dosed at 270 K and the heating rate was 25°/sec. Note that the HF production precedes the DF production, and that the H_2 production precedes the D_2 production. The DF must arise from an intermolecular reaction.

Figure 23

NEXAFS spectra of monofluorobenzene. a is the multilayer ice at 90 K and b is the monolayer formed after an anneal to 250 K. Note the polarization dependence of the monolayer, indicative of a π coordinated ring and peak B, perhaps due to a C-F σ resonance. The shift in the energy of the π^* resonance is unusual.

Figure 24

NEXAFS spectra of monofluorobenzene annealed to 470 K. Note the π^* intensity at normal photon incidence and the weak σ intensity at grazing incidence, which indicates a π coordinated "benzyne" - like species, as contrasted to α-pyridyl (vide infra).

MONOFLUOROBENZENE

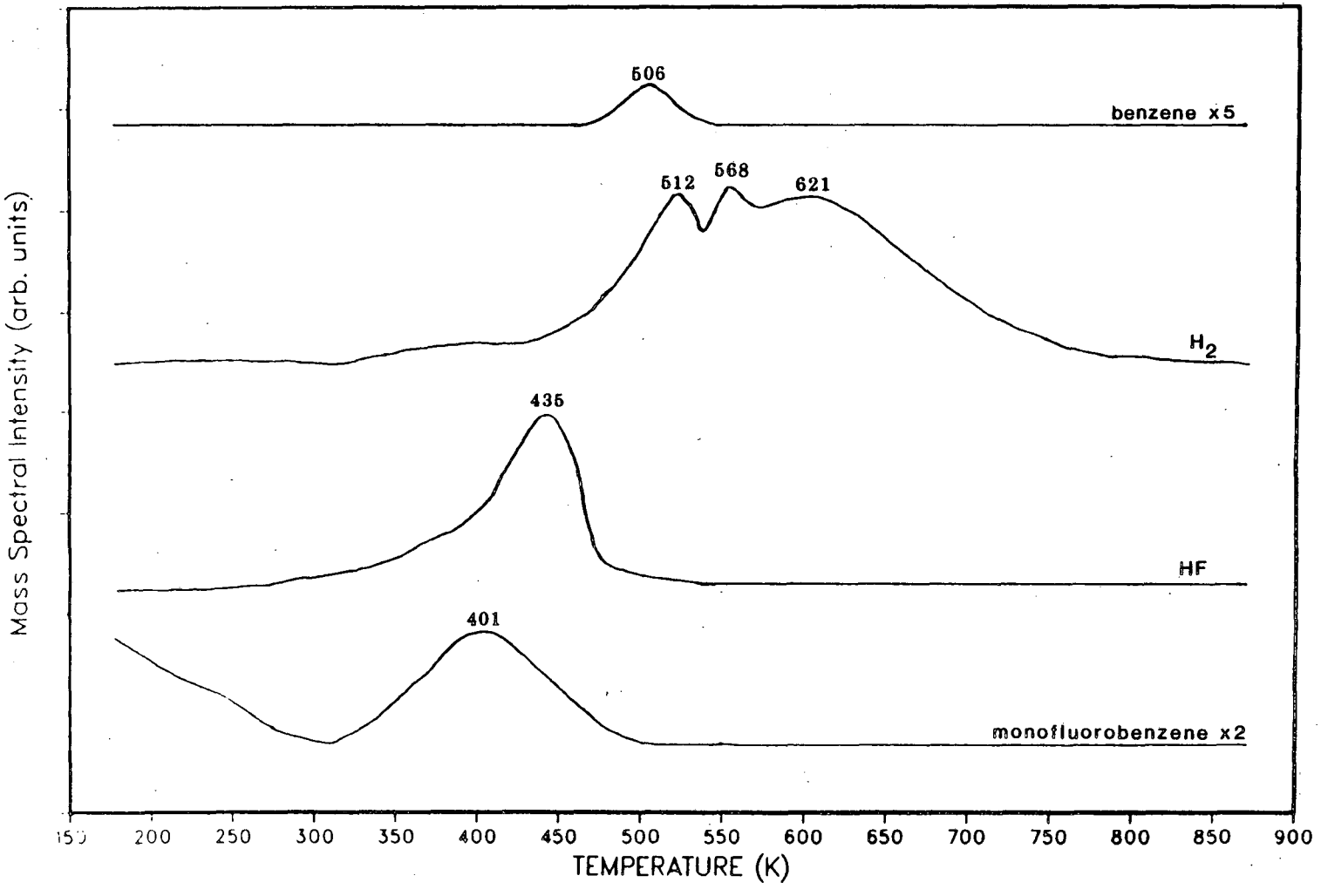

XBL 8512-5139

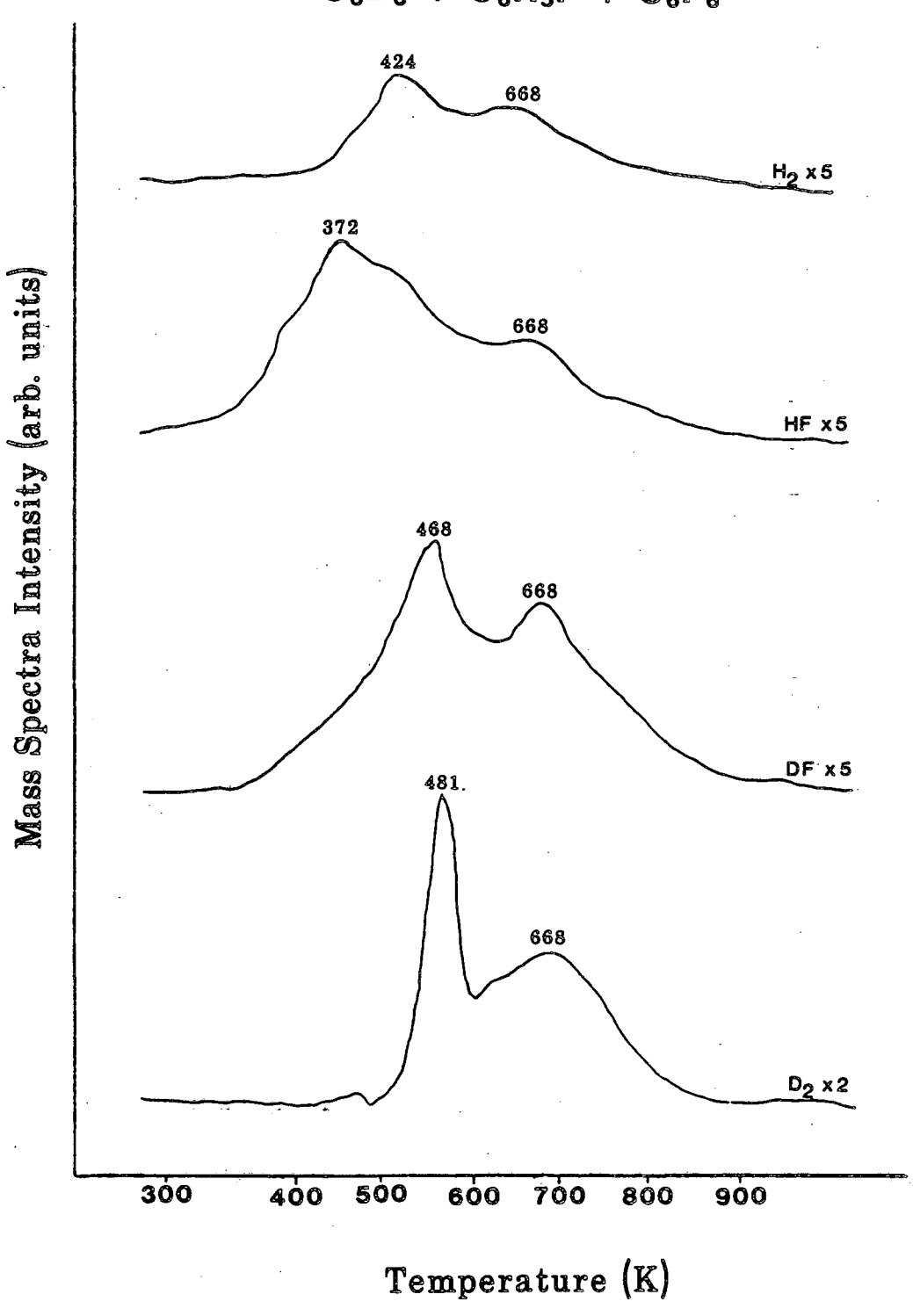
$C_6D_6 + C_6H_5F + C_6F_6$
424
668
H_2 x5
372
668
HF x5
468
668
DF x5
481.
668
D_2 x2
Mass Spectra Intensity (arb. units)
300
400
500
600
700
800
900
Temperature (K)

XBL 861-11

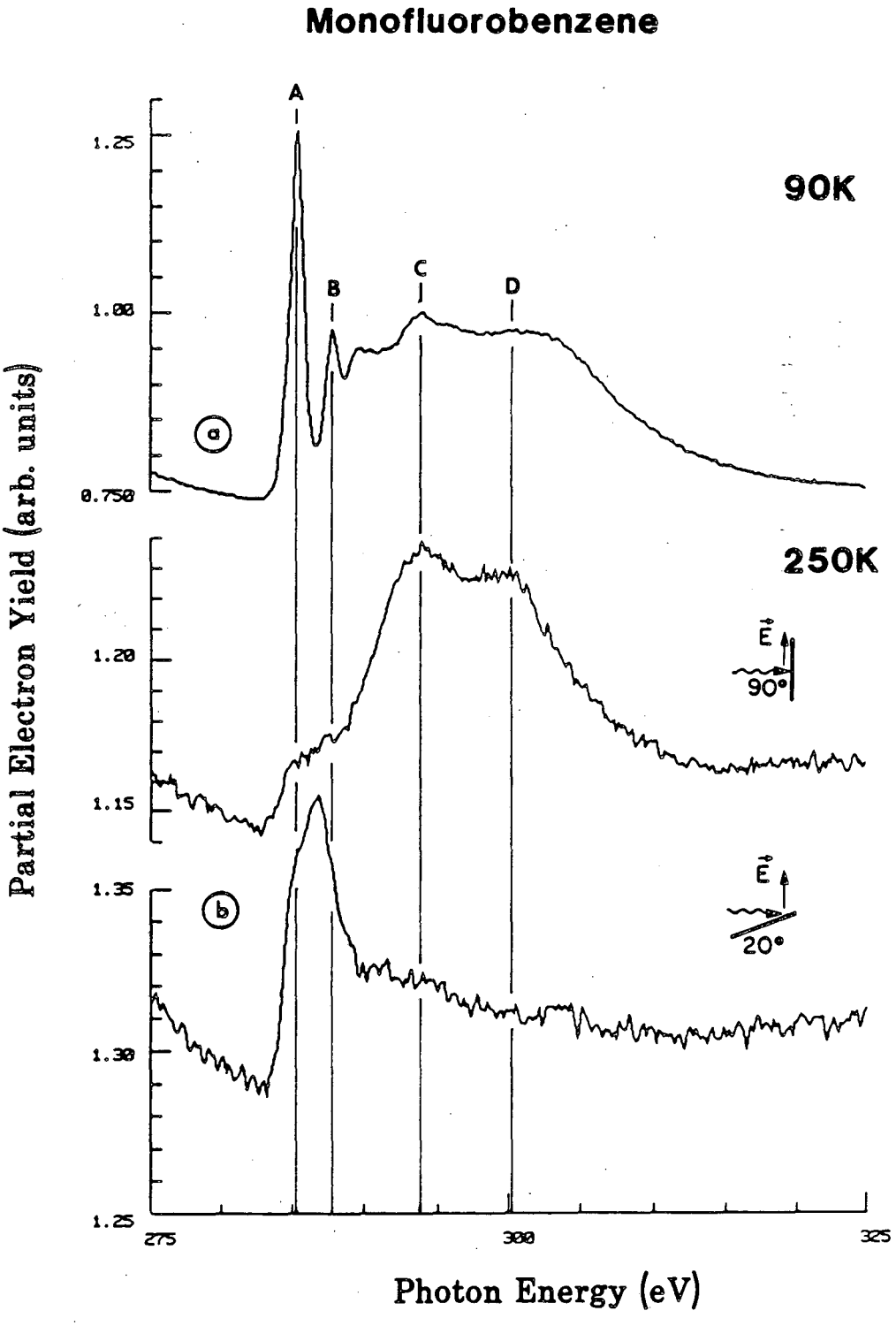

XBL 8512-5147

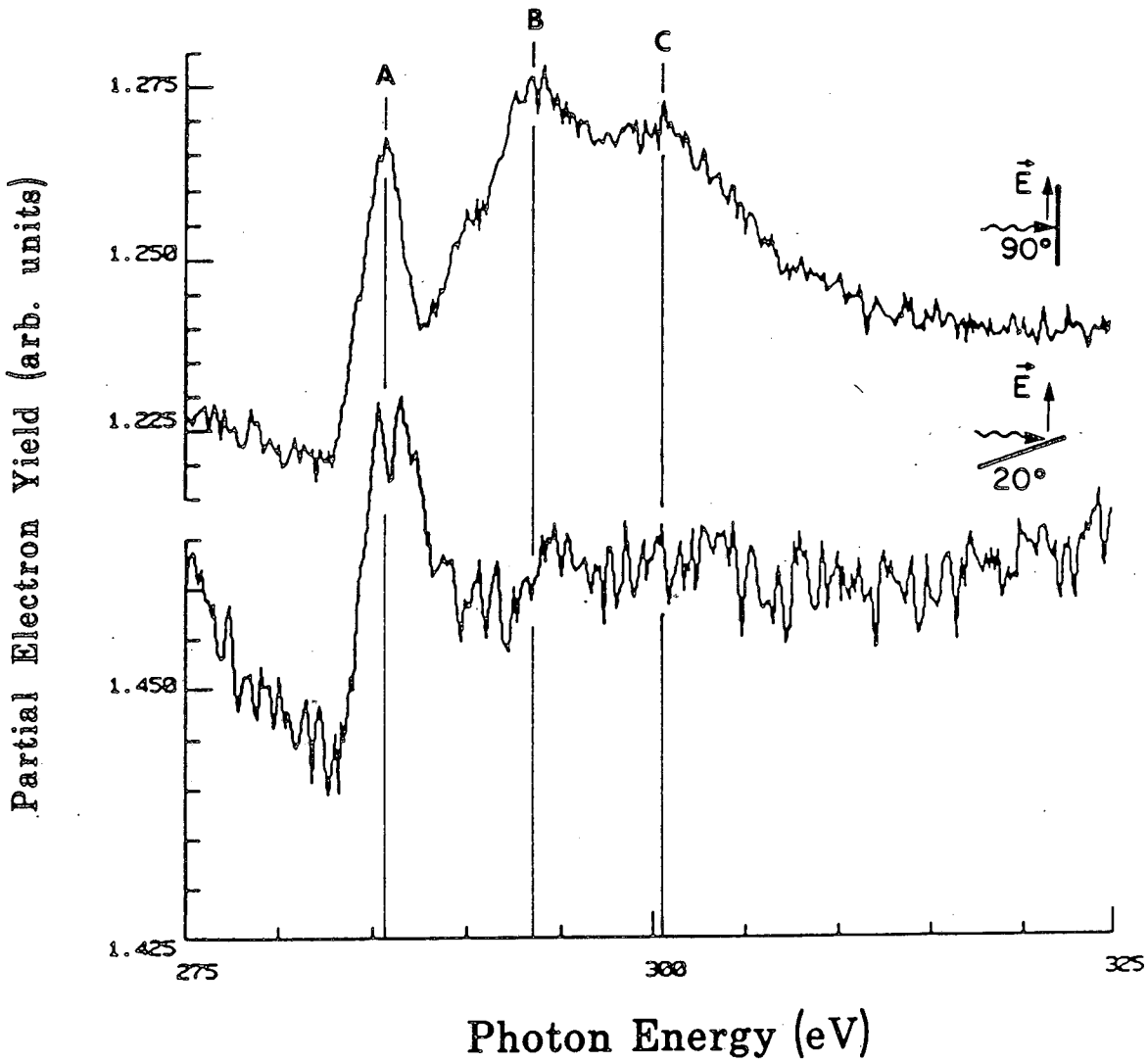

XBL 8512-5085

III.4 Heterocyclic Benzeniod Aromatics: Pyridine

We have investigated pyridine chemisorption to determine the importance of heteronuclear substitution on the surface chemistry of aromatic molecules. In the coordination compounds containing pyridine bonding through the lone pair of the nitrogen predominates, except when the pyridine is substituted to sterically inhibit nitrogen coordination (i. e. 2,6 dimethyl pyridine, which coordinates through the π system). Labeling studies of pyridine chemisorption on nickel indicated a geometry with the ring plane perpendicular to the metal surface, similar to the coordination compound analogs[49]. Lately parallel coordinated pyridine has been proposed[50-64]. Determination of the pyridine chemisorption geometry tests the relative importance of lone pair verses π coordination on metal surfaces and investigates the extent of the correlation of surface chemistry to coordination chemistry. Heteronuclear substitution also labilizes the a C-H bonds and induces interesting chemistry. Pyridine chemisorption is also of general interest to determine the cause of the strong surface enhanced Raman spectra it generates.

There have been many recent investigations of pyridine chemisorption on well defined surfaces of group 8 metals[50-64]. The literature includes studies of pyridine chemisorption on well characterized surfaces of nickel[50-53], copper[54-55], rhodium[56], palladium[57-58], silver[59-60], iridium[61], and platinum[62-64].

Previous studies of pyridine chemisorption have revealed a dependence of the angle between the pyridine ring plane and the metal surface with both coverage and temperature. On both Ag(111)[60] and Ni(100)[53] surfaces temperature and coverage dependent orientations have

been found: parallel to the surface for low temperatures and coverages but tilted with respect to the surface at higher temperatures or coverages. Tilted or perpendicular pyridine chemisorption states have in fact been suggested for all the surfaces studied. However, for the methods utilizing electronic transitions the structural assignments have been generally based on the observation of quenching of electronic transitions (such as π-π^* excitations), valence level shifts, or symmetry arguments and as such are approximate or ambiguous i.e. they generally indicate whether the observed state is in a high symmetry state or (perhaps slightly) perturbed from a symmetric state. The technique that has been used up to now to give quantitative geometric information is the analysis of HREELS intensities[52,53,56,59,60]. It has been recently noted that the determination of angle is dependent on the assumption that the coverage and angular dependence of the intrinsic intensity of the (two or more) analyzed transitions are the same[53]. In contrast, for the angles and energies utilized here the reflectivity of the substrate to X-ray radiation is less than 0.5%[65] (At 20 degrees and 280 eV, lower at higher energies and incidence angles) thus allowing the determination of the dependence of a single transition (such as a 1s to π^* transition) to electric field vector direction. Thus for unsaturated molecules weakly perturbed by chemisorption the analysis of the polarization dependence of NEXAFS transitions of π symmetry allow the determination of the relative angle of the unsaturated system in a straightforward manner.

For aromatic molecules we have found that the NEXAFS spectra of the adsorbed molecule are only weakly perturbed in the energy position of

the peaks relative to the spectra of the condensed multilayer (Figs. 4 and 6). We therefore will use the oriented free molecule model and the $\cos^2 D$ relation of the π^* transition to determine the angle α of the ring with respect to the surface.

In accord with previous work and in agreement with what is found for pyridine coordination complexes we will consider only those possible pyridine geometries with the nitrogen atom coordinated to the metal surface. It is interesting to note that we observe a shift in the position of the π^* resonance at the nitrogen edge of +2 eV when the pyridine is annealed to the high temperature state. This can be rationalized by invoking a repulsive dipole - dipole interaction between the molecular dipole (formed by the nitrogen core hole and the electron in the π^* orbital) and the surface dipole (formed from the electron density in space above the metal surface) or with a 1s core level shift (such as is seen for $C_5H_5NFe(CO)_4$), which is consistent with the nitrogen down geometry.

The thermal desorption curves of perdeuterated pyridine are shown in figure 25. Three deuterium desorption peaks were observed with area ratios of approximately 1:2:2, similar to that reported for Ni(100)[51]. Pyridine multilayer desorption occurred at ~200K with a tail on the pyridine desorption peak extending to 370K. The thermal desorption curves of perdeuterated pyridine rather than normal pyridine are presented to obviate the concern over background hydrogen contamination. We have found for pyridine that the hydrogen peaks shift by no more than 12 degrees on deuteration. These results will be discussed with the associated NEXAFS spectra.

The multilayer NEXAFS spectra for pyridine are shown in figure 26.

Both carbon K edge and nitrogen K edge spectra were recorded. The sample was prepared by condensing $6*10^{-6}$ torr-seconds (6 Langmuir or 6L) on the Pt(111) surface held at 90K. The spectra show almost no polarization dependence, suggesting that the orientation of the pyridine molecules in the ice is isotropic. Peaks A and B are π^* transitions, and the peaks C and D are σ transitions. The π resonances are sharper than those for the subsequent monolayer states and are examples of the effect of the longer lifetime and small overlap with the metal states of the resonances for molecules in the multilayer matrix.

Annealing the multilayer (6L) sample shown in figure 26 to 240K momentarily and cooling to 90K yields the spectra shown in figure 27. This case shows a π^* resonance that predominates at grazing photon incidence ($\vec{E}$ near normal). Analysis of the π^* region gives a ratio of I_{90}/I_{20} of 0.57 for the carbon edge and 0.83 for the nitrogen edge. A smooth background was subtracted to generate the peak areas. This and the uncertainty in the degree of polarization of the photon beam (effective polarization from 85% along the plane of the synchrotron ring[66] and up) gives an uncertainty of 20% (±0.11 for the carbon edge, ± 0.15 for the nitrogen edge) in the ratio and an apparent tilt angle α of 52±6 degrees (averaged over multiple determinations of angle). Previously, several geometries have been suggested for pyridine chemisorbed on group 8 metals. On Ag(111) a low temperature, high coverage, state with a tilt angle α of approximately 55^{o} to the surface has been proposed[59,60]. However, we have investigated a number of different annealing schemes and find that the conversion from the tilted to the perpendicular state occurs as low as 240K (albeit slowly). Thus

the spectra at 240K may show some degree of conversion to the perpendicular state so the actual tilt angle α of the ring for the low temperature form may be smaller than 52 ± 6^{o}. If the chemisorption state of figure 27 were not mixed then one would expect that the π^* transition would have the same width at all electric field vector directions. The observed greater width of the resonance with grazing photon incidence suggests a mixed state, but the possible overlap of peak B with peak A precludes further analysis. Note that 240K is in the region of the desorption tail of molecular pyridine from Pt(111) and thus there may be some contribution due to coverage in the observed ring tilt.

Figure 28 shows spectra from pyridine dosed at room temperature to saturation (~24L) , followed by a momentary anneal to 320K, with the spectra taken at room temperature. The large π^* resonance at normal photon incidence ($\vec{E}$ parallel to the surface) and large σ resonance at grazing incidence ($\vec{E}$ near normal to the surface) are consistent with a perpendicular orientation for the ring. Analysis of the π^* resonance gives a ratio of 6.0±30% (±1.8) for the carbon edge and 9.3±50% (±4.7) for the nitrogen edge giving an angle α of 85±10 degrees.

Figure 29 shows the sample of figure 27 after annealing to 410K (past the first hydrogen desorption) and cooling to 90K. A state very similar to figure 28 is observed, i.e. a perpendicular coordination state. Analysis gives a ratio of 3.0±30% (±0.9) for the carbon edge and 2.5±30% (±0.8) for the nitrogen edge which indicates an angle α of 74±10 degrees (averaged over multiple determinations of angle).

The question of the reversibility of the transformation from the tilted to the perpendicular state has been of interest[52,53]. When spectra were taken at elevated temperatures (for example, figure 28)

they systematically indicate a ring angle closer to perpendicular. This increase in apparent angle would be produced by a reversible conversion of about 10% of the perpendicular form to a tilted form at 90K, which is at the limit of the reliability of the measurement and data analysis.

The thermal desorption of pyridine shows the loss of one hydrogen equivalent at 370K. The desorption temperature of hydrogen adsorbed on clean Pt(111) is 350-370K. We infer that the observed low temperature hydrogen peak is desorption limited and thus the C-H cleavage that generates it occurs at or below room temperature. This leads to the assignment of the high temperature pyridine chemisorption state shown in figures 28 and 29 to the previously suggested[62] α-pyridyl form. Thus we propose that the conversion to the perpendicular form at higher temperatures is motivated by the formation of a metal carbon bond. Figure 30 shows the angles obtained for all the states investigated by this study.

In figure 31 we present a dynamic picture of pyridine chemisorption on Pt(111) as a function of temperature. Pyridine forms a disordered multilayer on chemisorption at 90K. On annealing the multilayer to progressively higher temperatures the multilayer evaporates and a monolayer with a tilted ($\alpha \leq 52^{o}$) pyridine ring is formed. Slowly at 240K and more rapidly at higher temperatures the α C-H bond is cleaved and the pyridine is converted to an α-pyridyl state characterized by the ring becoming perpendicular to the surface. This transformation may be reversible to an extent of approximately 10%. It is interesting to note that for high coverages a pyridine desorption is evident at higher temperatures (~470K) and thus disproportionation of the pyridine might

be invoked to provide for a small degree of reversibility of the formation of the α-pyridyl. More detailed thermal desorption studies and EELS results will be presented by V. Grassian and E. L. Muetterties (in preparation).

In summary, substitution of nitrogen into the benzene ring does not induce lone pair only coordination, although π symmetry overlap with d orbitals can not be excluded. This is in marked contrast to what is observed for mononuclear platinum pyridine coordination complexes, suggesting that the adsorbate donor interaction is less important relative to the π orbital interaction for platinum surfaces as contrasted to platinum atoms. Nitrogen substitution does activate the α C-H bond, leading to the formation of a perpendicular ring on the surface, in contrast to what is observed with benzene.

TABLE 2

Point	Anneal Temp.	NEXAFS Temp.	Edge	Ratio	Angle	Sample #
A	240K	90K	C	0.57	45	1
B	240K	90K	N	0.83	51	1
C	240K	90K	C	1.2	58	2
D	255K	90K	C	1.02	55	2
E	270K	270K	C	7.85	85	2
F	320K	290K	C	6.0	80	3
G	320K	290K	N	9.3	90	3
H	410K	90K	C	3.0	71	1
I	410K	90K	N	2.5	68	1
J	410K	90K	C	5.86	80	2

Experimental conditions used to prepare the points indicated in figure 30. Samples 1 and 2 were prepared by annealing an ice to consecutive higher temperatures with spectra between anneals, at the indicated temperatures. Sample 3 was dosed to saturation at 290K and the indicated anneal and cooling followed. The K edge investigated is shown and an angle α is derived.

III.4.1 FIGURES

Figure 25.

Thermal desorption spectra (or equivalently the temperature programmed reaction spectra) of perdeutero-pyridine. Pyridine was dosed at 170K and $0.33*10^{-6}$ torr-second (0.33 Langmuir or 0.33L) background pressure with a needle doser and thus the coverage is approximately half of saturation. Mass spectrometric (UTI model 100C) detection of the gas phase products was employed. The molecular ion intensity is plotted verses surface temperature for the gas phase products. The temperatures chosen for NEXAFS investigation are indicated.

Figure 26.

The NEXAFS spectra for an approximately 6 layer multilayer of pyridine on Pt(111) (assuming sticking coefficient of 1). Section I is the carbon K edge and section II is the nitrogen K edge. Peaks A and B are π^* transitions, and the peaks C and D are σ transitions. The gas phase 1s binding energy relative to the vacuum level of carbon in pyridine is between 285.5 and 286.3 eV[67a] and the nitrogen 1s binding energy in pyridine is 404.9eV[67b]. Resonances below the binding energy are bound state resonances. For chemisorption states the onset of absorption corresponds to excitation to the Fermi level of the metal. Thus the region from the onset of absorption to the onset plus the work function are resonances below the photoemission threshold and correspond to the bound molecular resonances. The work function of pyridine covered Pt(111) for saturation coverage at 278K is approximately 3 volts[62]. These spectra were taken with normal incidence photons.

Figure 27.

NEXAFS spectra of pyridine chemisorbed on Pt(111). The sample was

prepared from the multilayer of figure 26 by momentarily heating to the indicated temperature. Note the strong π^* transition at grazing photon incidence (near normal electric vector) and strong σ transitions at normal photon incidence (parallel electric vector) for both carbon and nitrogen K edges, consistent with a pyridine tilt angle α of 52±6 with respect to the surface.

Figure 28.

The NEXAFS spectra of 24L of pyridine deposited on Pt(111) at room temperature and momentarily annealed to the indicated temperature. Note the strong π^* transition at normal photon incidence (parallel electric vector) and the strong σ transitions at grazing photon incidence (electric vector near normal), consistent with a pyridine ring perpendicular to the surface.

Figure 29.

NEXAFS spectra of pyridine chemisorbed on Pt(111). Preparation was as for figure 27, with an added anneal to 410K. Note the similarity with figure 28.

Figure 30

The theoretical peak ratio of the intensity of the π^* transitions for normal and 20° photon incidence for sp^2 hybridized systems. We indicate the observed peak ratios for three different pyridine samples. See Table 2 for the experimental parameters of the indicated points.

Figure 31

Proposed chemisorption states for pyridine on Pt(111). The diagrams on the left show the electric field direction that yield the NEXAFS spectra presented earlier. State I corresponds to figure 26.

State II corresponds to figure 27 (assuming an unmixed state). State III corresponds to figures 28 and 29.

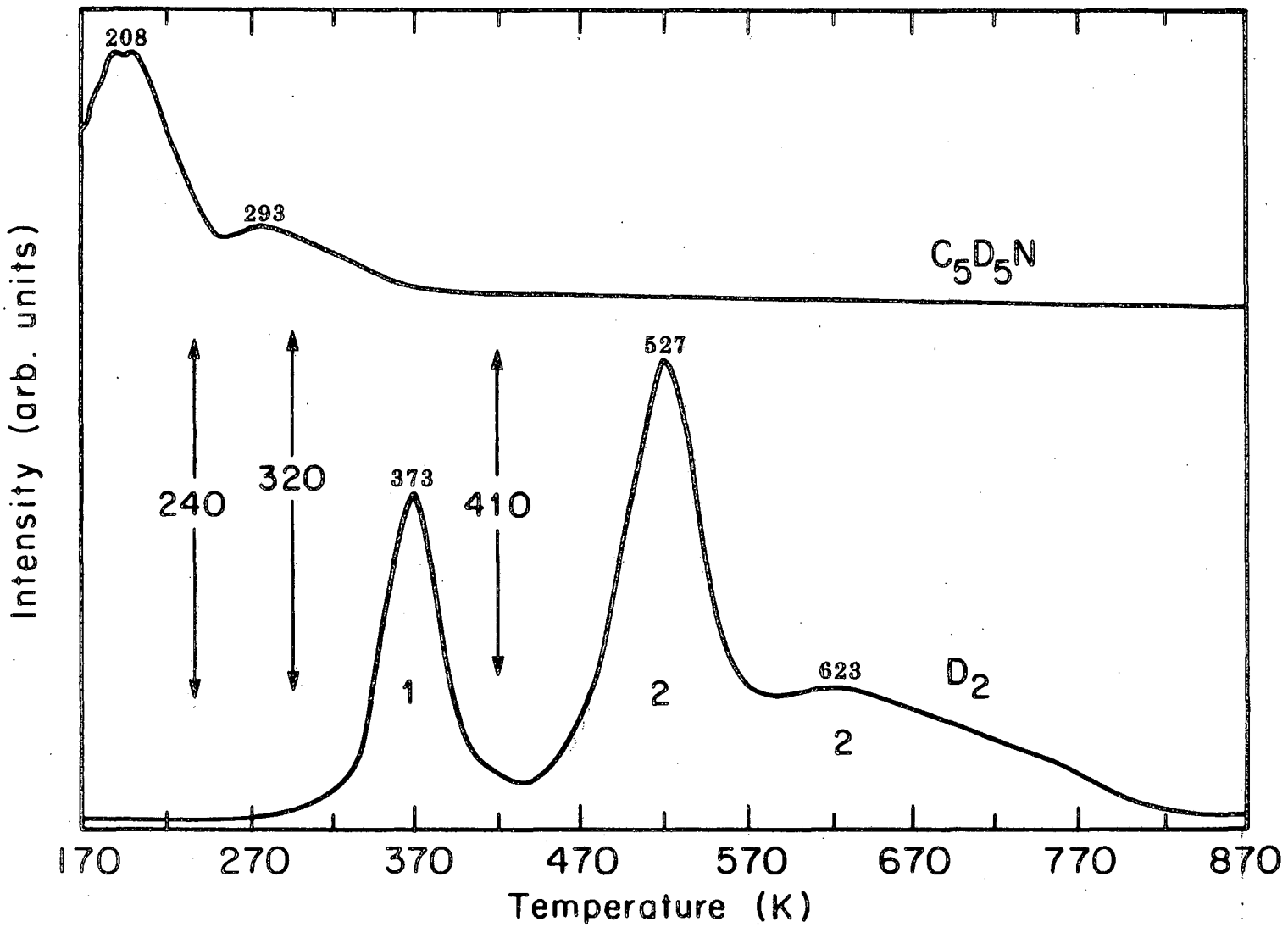

XBL 852-1096 A

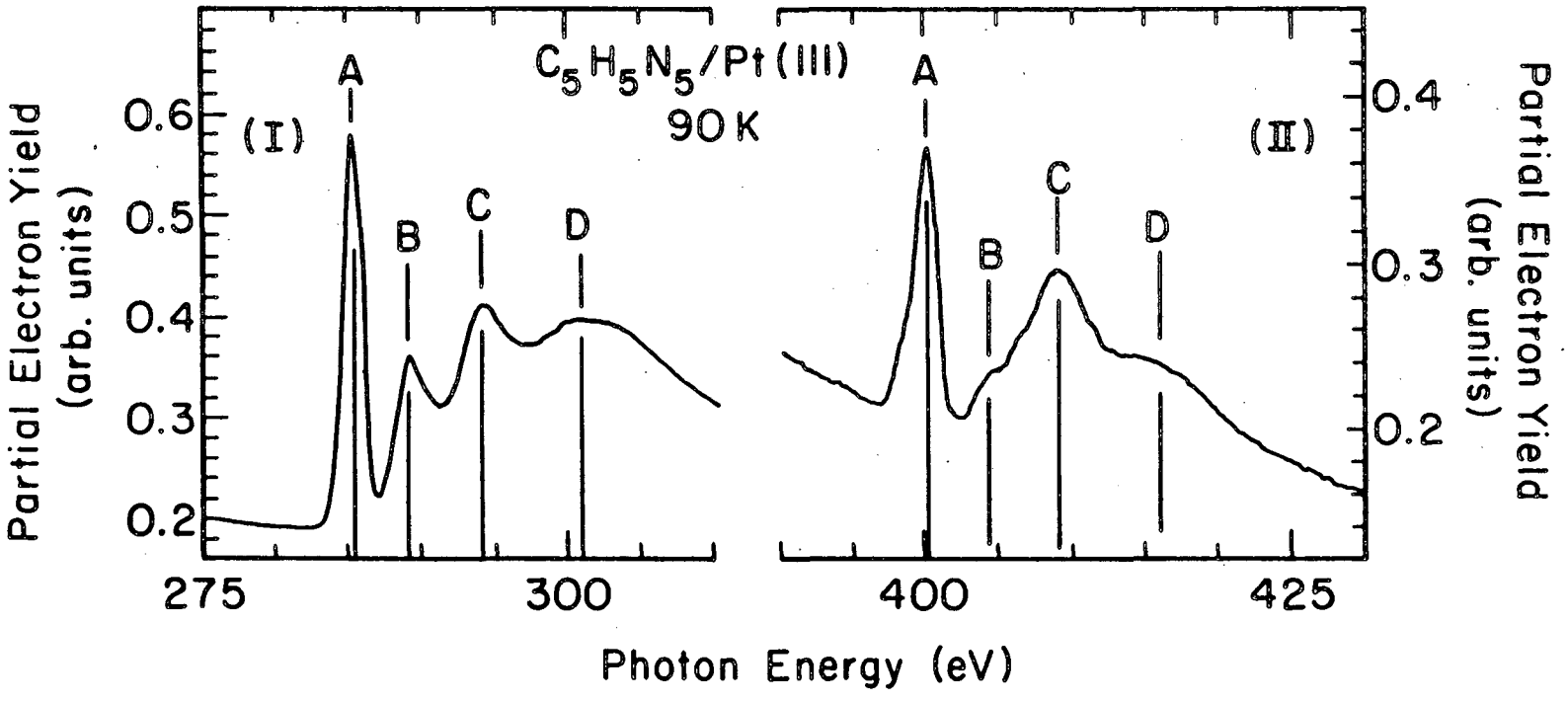
$C_5H_5N_5$/Pt(III)
90 K
(I)
(II)
A
B
C
D
Partial Electron Yield
(arb. units)
0.6
0.5
0.4
0.3
0.2
0.4
0.3
0.2
275
300
400
425
Photon Energy (eV)

XBL 852-1095

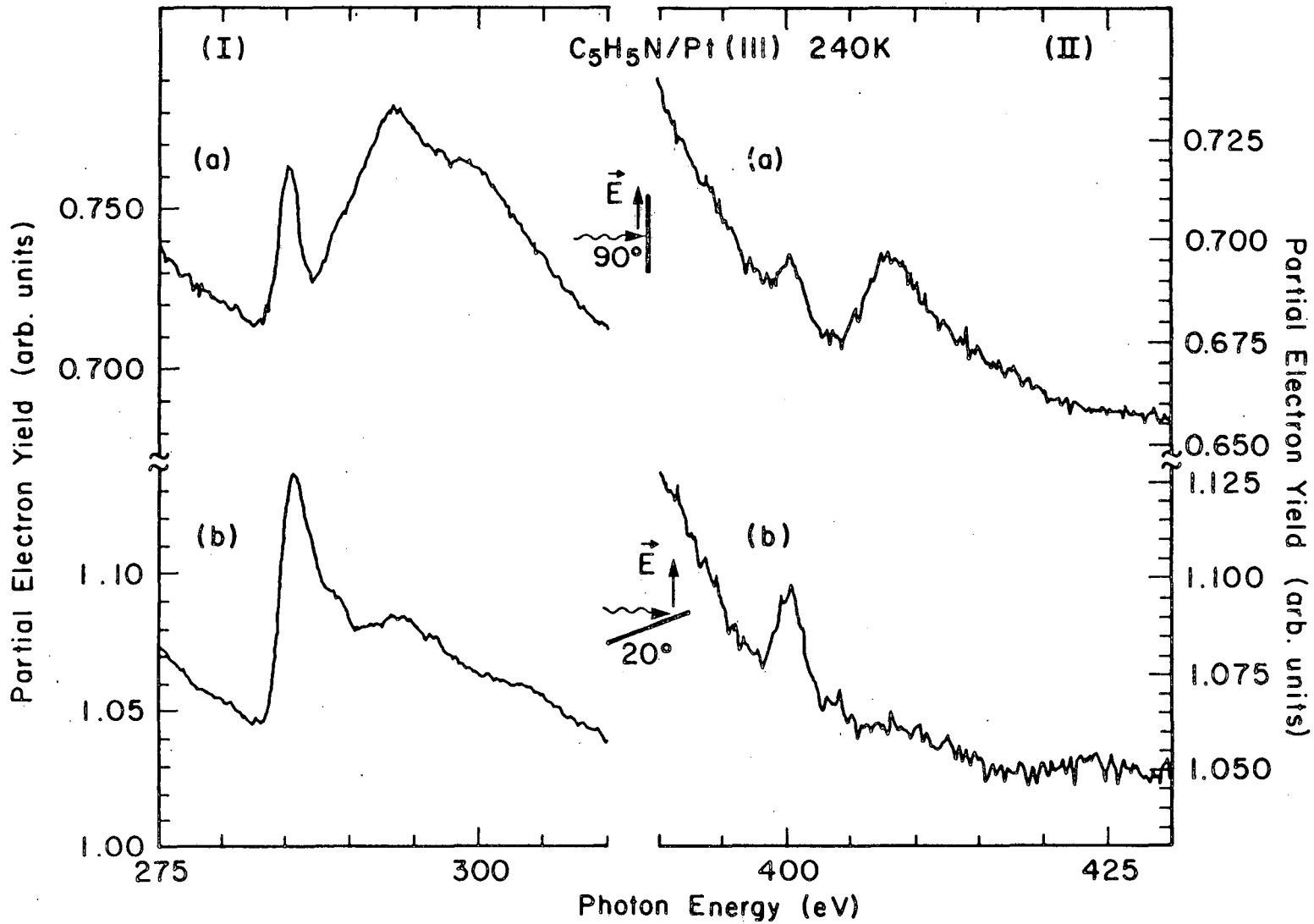
(I)
$C_5H_5N/Pt(III)$ 240K
(II)
(a)
(b)
E
90°
20°
0.750
0.700
1.10
1.05
1.00
0.725
0.700
0.675
0.650
1.125
1.100
1.075
1.050
275
300
400
425
Photon Energy (eV)
Partial Electron Yield (arb. units)
Partial Electron Yield (arb. units)

XBL 852-1097

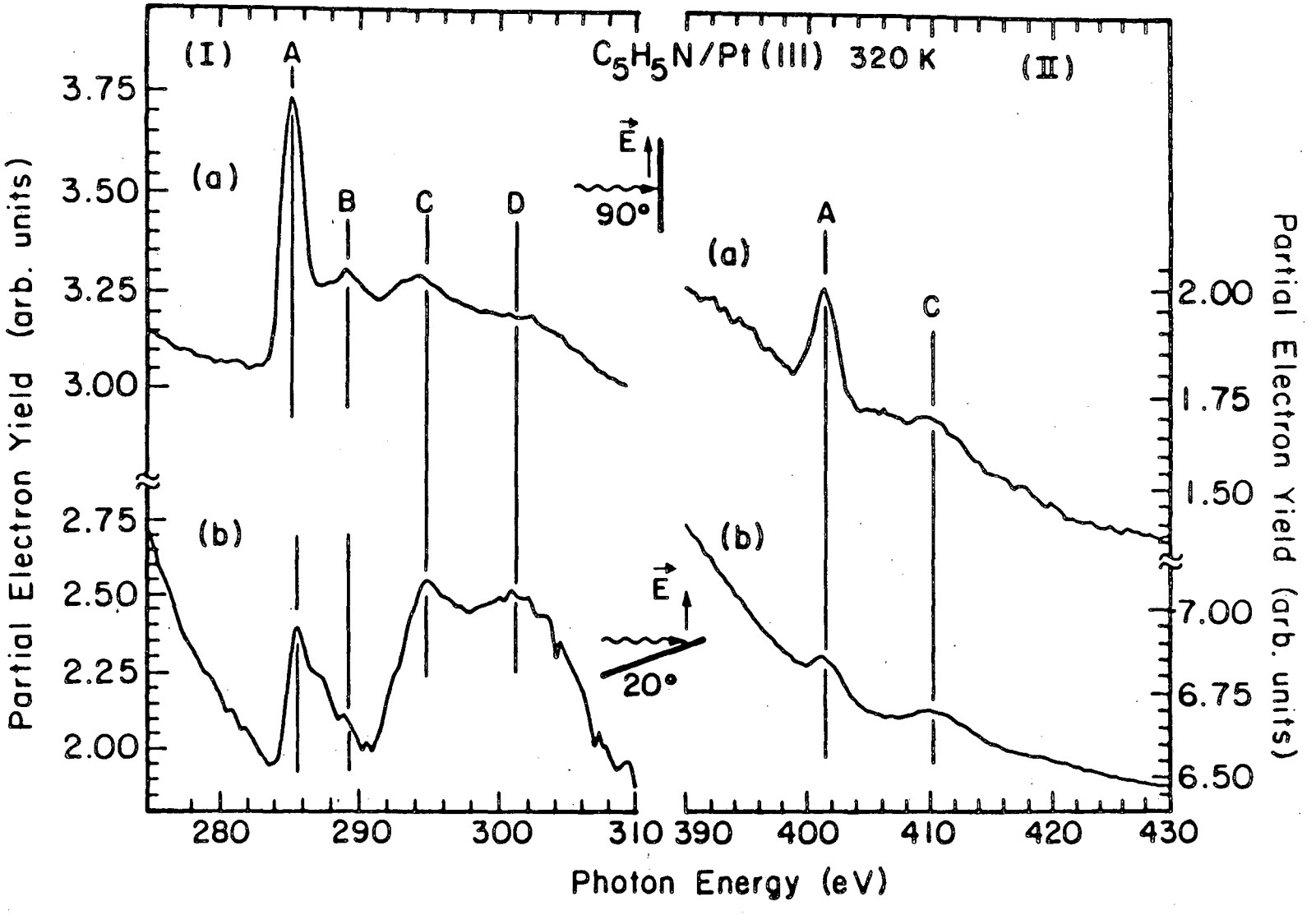
(I)
A
B
C
D
$C_5H_5N/Pt(III)$ 320 K
(II)
(a)
(b)
$\vec{E}$
90°
20°
3.75
3.50
3.25
3.00
2.75
2.50
2.25
2.00
2.00
1.75
1.50
7.00
6.75
6.50
280
290
300
310
390
400
410
420
430
Partial Electron Yield (arb. units)
Photon Energy (eV)

XBL 852-1098

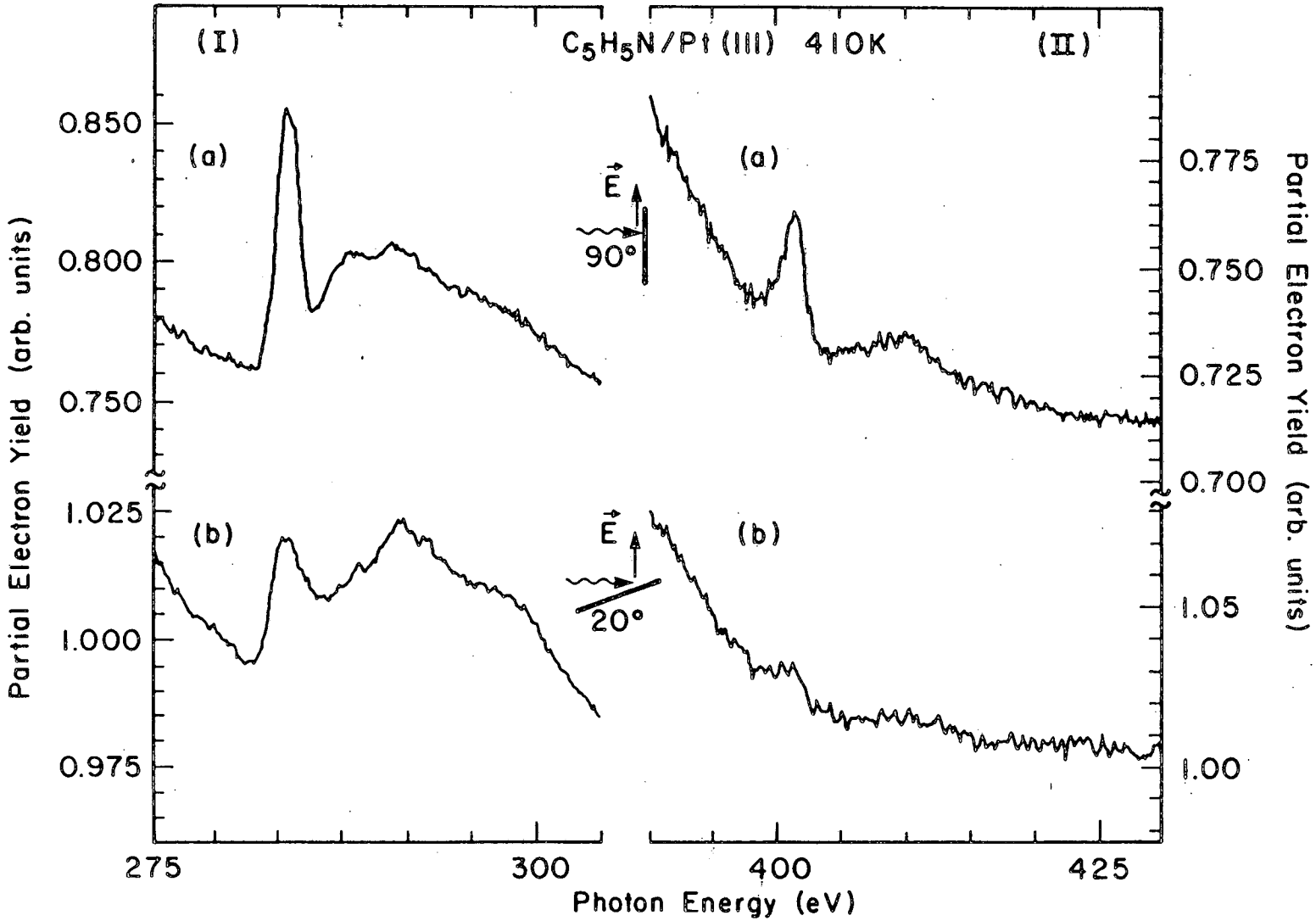
(I)
C_5H_5N/Pt(111) 410K
(II)
(a)
(b)
$\vec{E}$
90°
20°
0.850
0.800
0.750
1.025
1.000
0.975
0.775
0.750
0.725
0.700
1.05
1.00
275
300
400
425
Photon Energy (eV)
Partial Electron Yield (arb. units)
Partial Electron Yield (arb. units)

XBL 852-1099

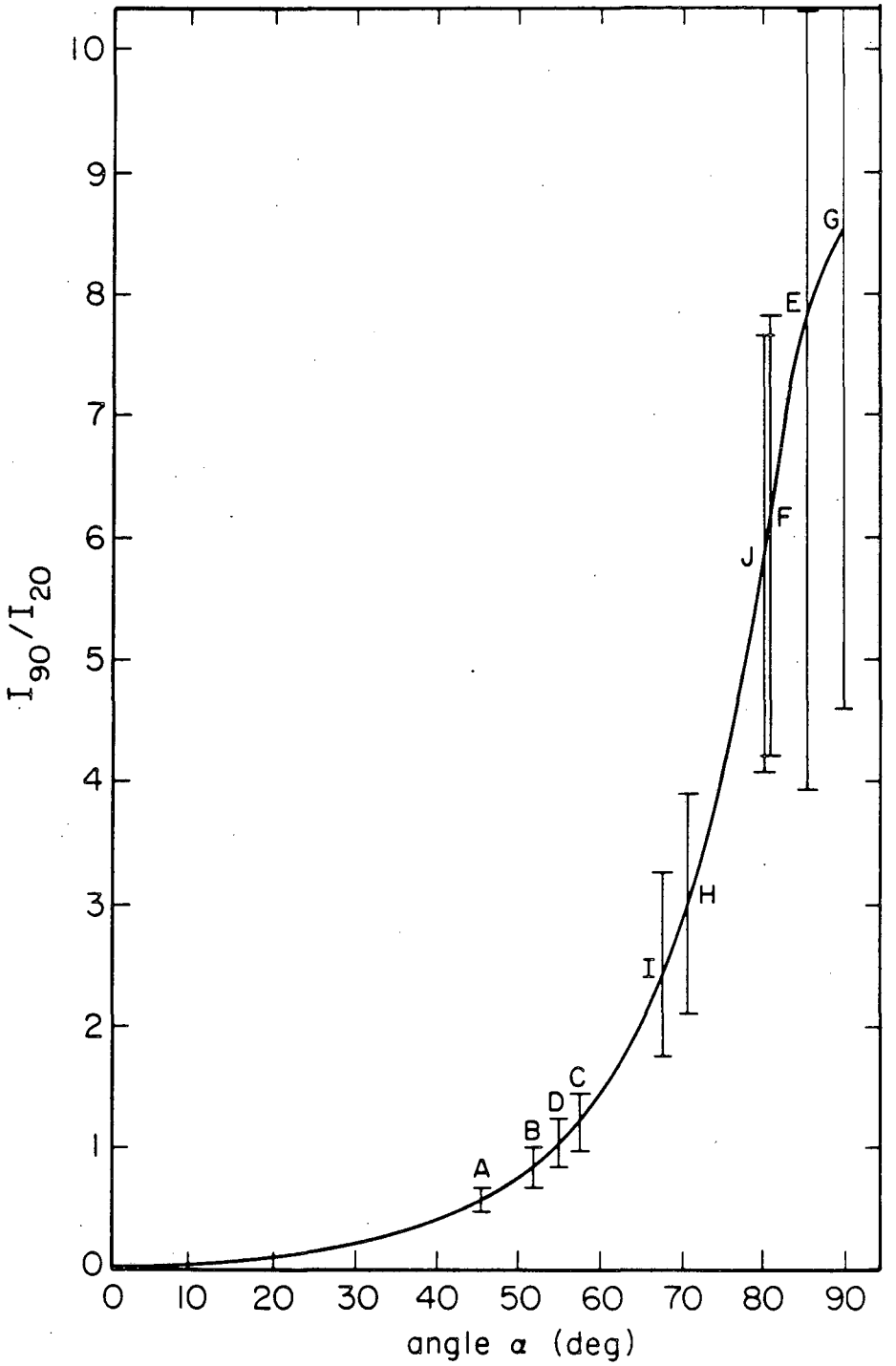
I_{90}/I_{20}
angle α (deg)
0
10
20
30
40
50
60
70
80
90
1
2
3
4
5
6
7
8
9
10
A
B
C
D
E
F
G
H
I
J

XBL 855-2332

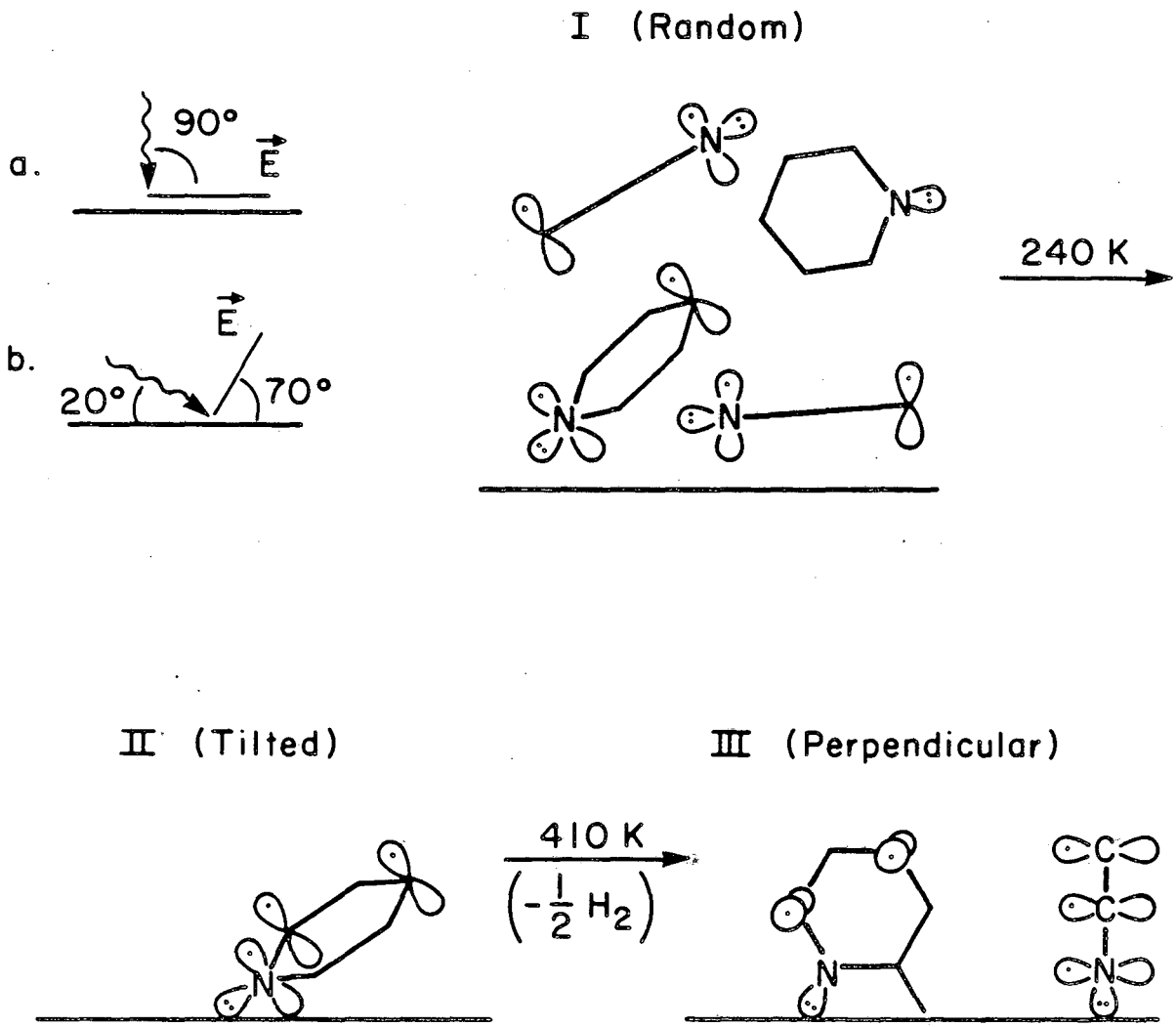
I (Random)
a.
90°
E
b.
E
20°
70°
N
N
N
N
240 K
II (Tilted)
III (Perpendicular)
410 K
(-½ H2)
N
N
C
C
N

XBL 852-1100

III.5 Heterocyclic Nonbenzeniod Aromatics: Thiophene

Thiophene has been the center of much attention primarily because it is a model compound for the hydrodesulfurization reaction. We find it of interest also because it is an aromatic molecule where the heteroatom is not formally involved in the π system - the molecule is aromatic because of the overlap of the lone pair electrons into the carbon π system. From such systems we expect that the extrusion of the heteroatom is an important part of the surface chemistry. As part of a larger investigation of the surface chemistry of thiophene on the nickel group metals[68] I investigated the structure and reactivity of thiophene and some substituted thiophenes on Pt(111). The general trends are that sulfur extrusion was an early step in the decomposition and at low coverage thiophene chemisorbs irreversibly. Surface sulfur, either from decomposition or coadsorption, inhibits reaction and allows the observation of gas phase hydrocarbon products for all except the most reactive surfaces (i.e. Ru(001) and Os(001)). Regiospecific C-H bond cleavage was observed for Ni(100), Ru(001), and Os(001).

The questions to be addressed are: what are the modes of bonding of thiophene, what are the products and reaction path, and what are the effects of surface sulfur and surface structure on reactivity?

Thermal desorption studies of thiophene at high ($>\sim$.5 monolayer) coverage on Pt(111) (Figure 32) gave hydrogen, a small amount of molecular desorption, butadiene, and surface carbon and sulfur. There was no evidence for acetylene or other C_2 species other than from mass spectrometer ionizer fragmentation, indicating that the carbon framework stays intact. If the sample was heated to the vicinity of 1200 K, masses indicative of CS and CS_2 were observed. There is some ambiguity

in assignment of the CS peak since CS has the same mass as CO_2.

At low thiophene coverage (Figure 33) the only products in the thermal desorption are hydrogen and surface carbon and sulfur. Thermal desorption results identical to those observed at high coverage can be obtained by predosing the crystal with 1/4 monolayer of sulfur (prepared by annealing a H_2S monolayer to 800 K. The coverage was determined by Auger spectrometry[69]) and dosing identically to figure 33. It can be inferred from these results that the C-S bond is cleaved before the reactions leading to gas phase products.

To probe for regiospecific C-H bond cleavage similar to what was seen on Ni(100) we undertook thermal desorption investigations of 2,5 dideuterothiophene which at low coverage (figure 34) gave D_2 in only the low temperature (354 K) peak. HD and H_2 showed up in both hydrogen peaks. At high thiophene coverage or with sulfur coadsorption, no specificity in the hydrogen desorption was observed.

2,5 dimethyl thiophene at low coverage gave a large enhancement of the low temperature hydrogen peak and a decrease in the high temperature hydrogen peak with respect to thiophene. Thermal desorption experiments with low coverage 3 methyl thiophene enhance the high temperature hydrogen desorption. These results are consistent with the thiophene ring being tilted with respect to the surface when C-H bond cleavage occurs. At high coverage (figure 35) we observe mass 78 (which we assign as benzene) and mass 82 (which we assign as dimethyl butadiene). The mass 78 product is very interesting - if it is indeed benzene then the surface state that generates it must isomerize the double bonds in the thiophene. In benzene the multiple bonds are all isomerically cis,

whereas in 2,5 dimethyl thiophene the multiple bonds are all trans.

To summarize the thermal desorption results on Pt(111), we find a strong coverage dependence in the chemistry of thiophene on Pt(111): at low coverage the only gas phase product was H_2 while at high coverage butadiene and thiophene were also found. Methyl and deuterium labeled thiophenes at low coverages gave results consistent with the interpretation that the thiophene was tilted with respect to the surface when C-H bond cleavage was taking place. The deuterium labeling experiments did not indicate total specificity in C-H bond cleavage, but the chemistry may be complicated by rehydrogenation of the surface intermediates, leading to hydrogen-deuterium scrambling before hydrogen desorption.

The structure consistent with the above results is a vinyl bridged diethylidyne - both the α carbons are bonded to the metal (rationalizing the partial specificity of C-H bond cleavage and the methyl thiophene results: the 3 methyl thiophene is enhanced in the high temperature hydrogen peak and the 2,5 dimethyl thiophene is enhanced in the low temperature peak and the double bonds are now singly bonds, allowing the isomerization to form benzene (see the last structure of figure 41).

We initiated NEXAFS investigations to answer two questions: when does C-S bond cleavage occur, and what is the structure of the chemisorbed thiophene. We expected that the thiophene would adsorbed tilted to the surface and that there would be molecular resonances at the sulfur edge that would disappear, indicating C-S bond scission. The NEXAFS spectra of a multilayer (a) ice and a submonolayer (b) dose (0.6 L) of thiophene at 90 K are presented in figure 36. We observe that the π^* resonance (peak A) is seen only at grazing photon incidence in

the submonolayer, characteristic of a ring parallel to the surface. Peak B we assign to the C-S δ resonance. Note that at the sulfur L edge we observe what appears to be a doublet of doublets in the ice that are resolved in the submonolayer into two doublets. Since the L edge is a p state the polarization selection rules are not as clear as for the K shell and polarization dependence analysis will not be attempted here. We assign the resonances roughly as π^* and C-S δ similarly to the carbon edge. The submonolayer was in fact prepared first, and the ice was made by dosing ~6 L at 90 K.

Annealing the ice of figure 36 to 180 K yields the state of figure 37. Here we see a spectra similar to that obtained by dosing to a submonolayer at 90 K. A further anneal to 290 K give the state of figure 38. Note that the carbon π^* peak (peak A as in figure 36) now shows intensity at normal photon incidence, indicating π orbitals oriented parallel to the surface. The sulfur edge also shows and marked decrease in the intensity of the molecular features at ~165 eV, indicating C-S bond scission. By 470 K the sulfur edge molecular features have disappeared (figure 39) and a resonance at 170 eV, characteristic of surface sulfur appears. At the carbon edge the π^* resonance (peak A) is continuing to grow in while the C-S δ resonance is decreasing. The C-S δ resonance at the carbon edge is totally absent by 500 K (figure 40).

We propose the reaction pathway shown in figure 41. At low temperatures the thiophene is π coordinated with its ring plane parallel to the metal surface. At higher temperature (500K > T > 180K) the sulfur atom is extruded and the molecule become the previously mentioned

vinyl bridged diethylidyne.

There are several supporting results for this proposed reaction scheme. The temperature at which C-S bond cleavage occurs on the clean surface is probably below 290 K - the decrease in the 165 eV features is nearly completed by this temperature. The residual signal is probably due to the self poisoning of the surface by the sulfur. The π coordination of the low temperature state and the early extrusion of sulfur is supported by work done by our collaborators[70] - the HREELS evidence indicates that the ring is π bound and that at 350 K a vibration assigned to a M-S vibration appears. XPS of the sulfur 2s level indicates sulfur extrusion between 235 K and 350 K. Additionally, HREELS of C_4 molecules on Pt(111) derived from thiophene and unsaturated butanes give spectra consistent with the vinyl bridged diethylidyne[71] state.

An implication of this work is if sulfur can be removed and the hydrocarbon products hydrogenated off efficiently from the platinum surface, then the hydrodesulfurization reaction could be made to proceed at near room temperature on clean metal surfaces.

III.5.1 FIGURES

Figure 32

Thermal desorption of a high coverage (1.2 L) of thiophene on Pt(111). The crystal was dosed at 170 K and the heating rate was 25°/sec.

Figure 33

Thermal desorption of a low coverage (0.06 L) of thiophene on Pt(111). The crystal was dosed at 170 K and the heating rate was 25°/sec.

Figure 34

Thermal desorption of a low coverage (0.06 L) of 2,5 dideuterothiophene on Pt(111). The crystal was dosed at 170 K and the heating rate was 25°/sec.

Figure 35

Thermal desorption of 2,5 dimethyl thiophene on Pt(111). The crystal was dosed at 170 K with 1.2 L of 2,5 dimethyl thiophene.

Figure 36

NEXAFS spectra of thiophene at 90 K. (a) is the multilayer prepared by dosing the state of (b) with 6 L of thiophene. In all of the following spectra (I) are the carbon K edge spectra and (II) are the sulfur L edge spectra. Note the high intensity and narrow width of the resonances, typical of multilayer spectra. (b) is the monolayer prepared by dosing 0.6 L of thiophene at 90 K. Note the polarization dependence, which is similar to that of benzene.

Figure 37

NEXAFS spectra of thiophene annealed to 180 K. This sample was prepared by annealing the sample of figure 36 (a) to 180 K. Note the

similarity to figure 36 (b).

Figure 38

NEXAFS spectra of thiophene annealed to 290 K. The sulfur molecular resonances are sharply diminished in intensity and the π^* resonance at the carbon edge is growing in at normal photon incidence.

Figure 39

NEXAFS spectra of thiophene annealed to 470 K. Here we note that the sulfur edge has only the 170 eV peak and the carbon C-S δ resonance is almost gone.

Figure 40

NEXAFS spectra of thiophene annealed to 500 K. The carbon edge C-S δ resonances at normal photon incidence have disappeared. The carbon edge π^* resonances are intense at both photon angles.

Figure 41

Proposed reaction path for thiophene adsorbed to Pt(111). The thiophene is π coordinated at low temperature and becomes normal to the surface at higher temperature. The intermediate in the formation of hydrocarbon product is a vinyl bridged diethylidyne.

THIOPHENE high coverage

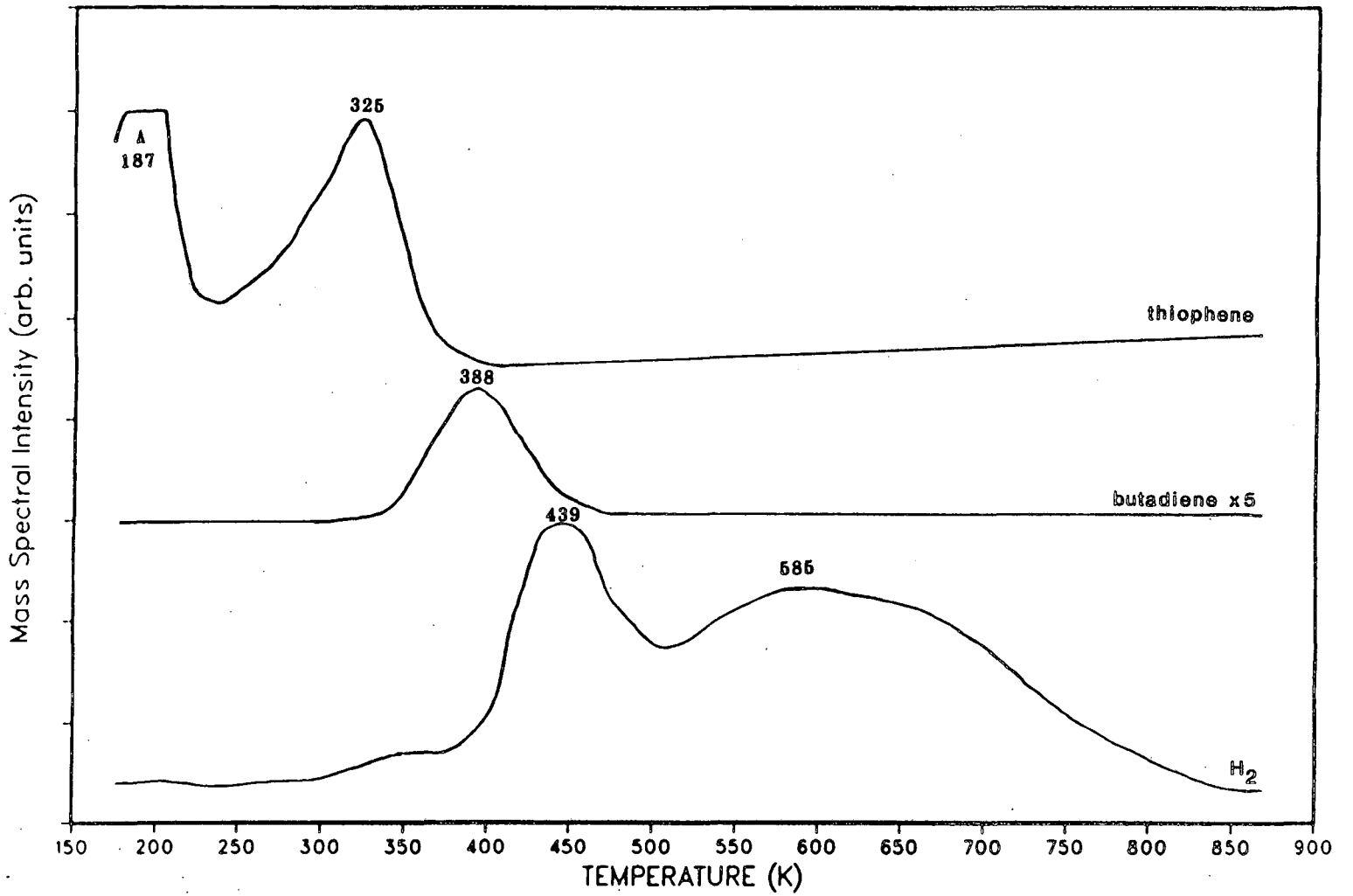

XBL 8512-5140

THIOPHENE low coverage

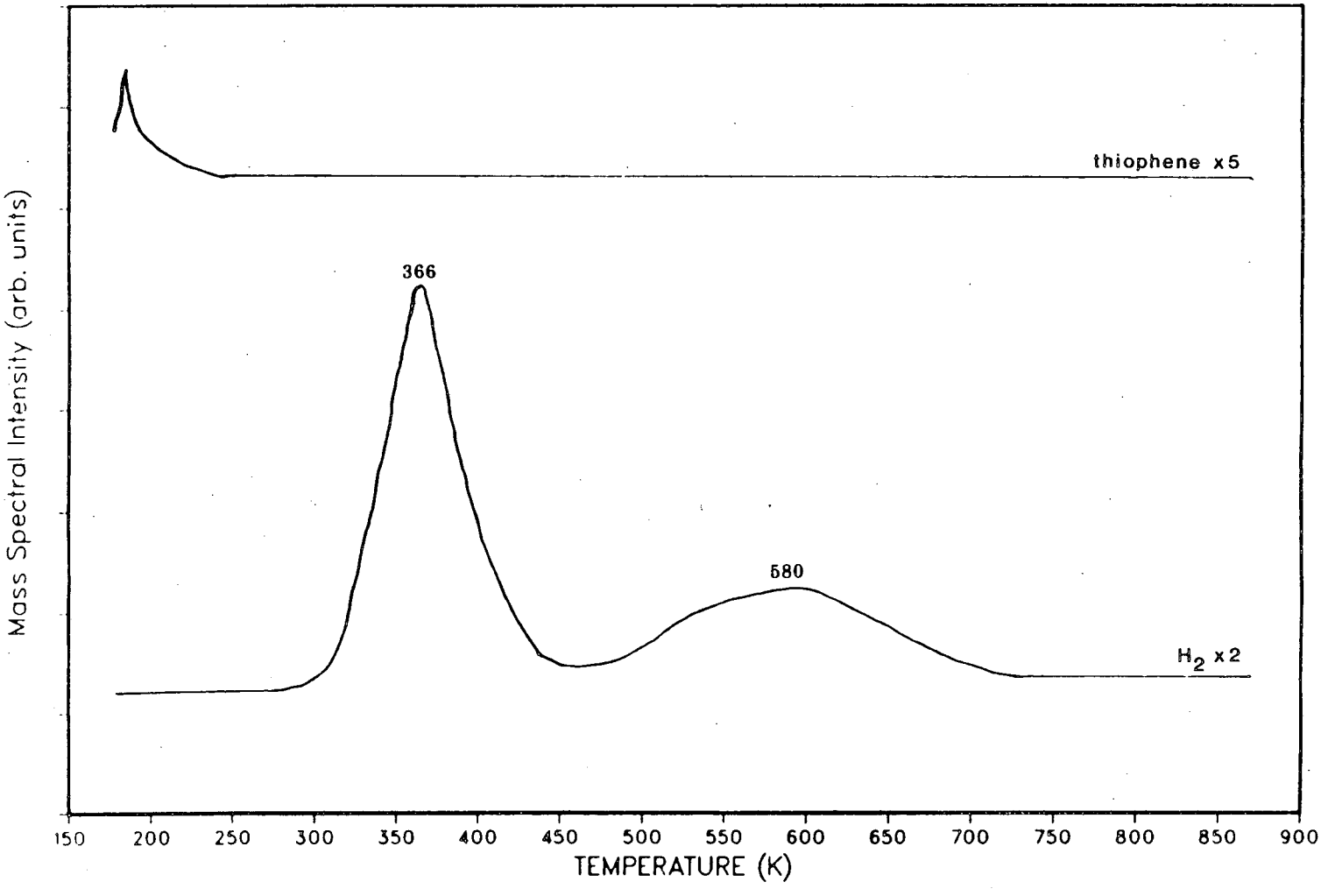

XBL 8512-5142

2,5 d_2 - THIOPHENE

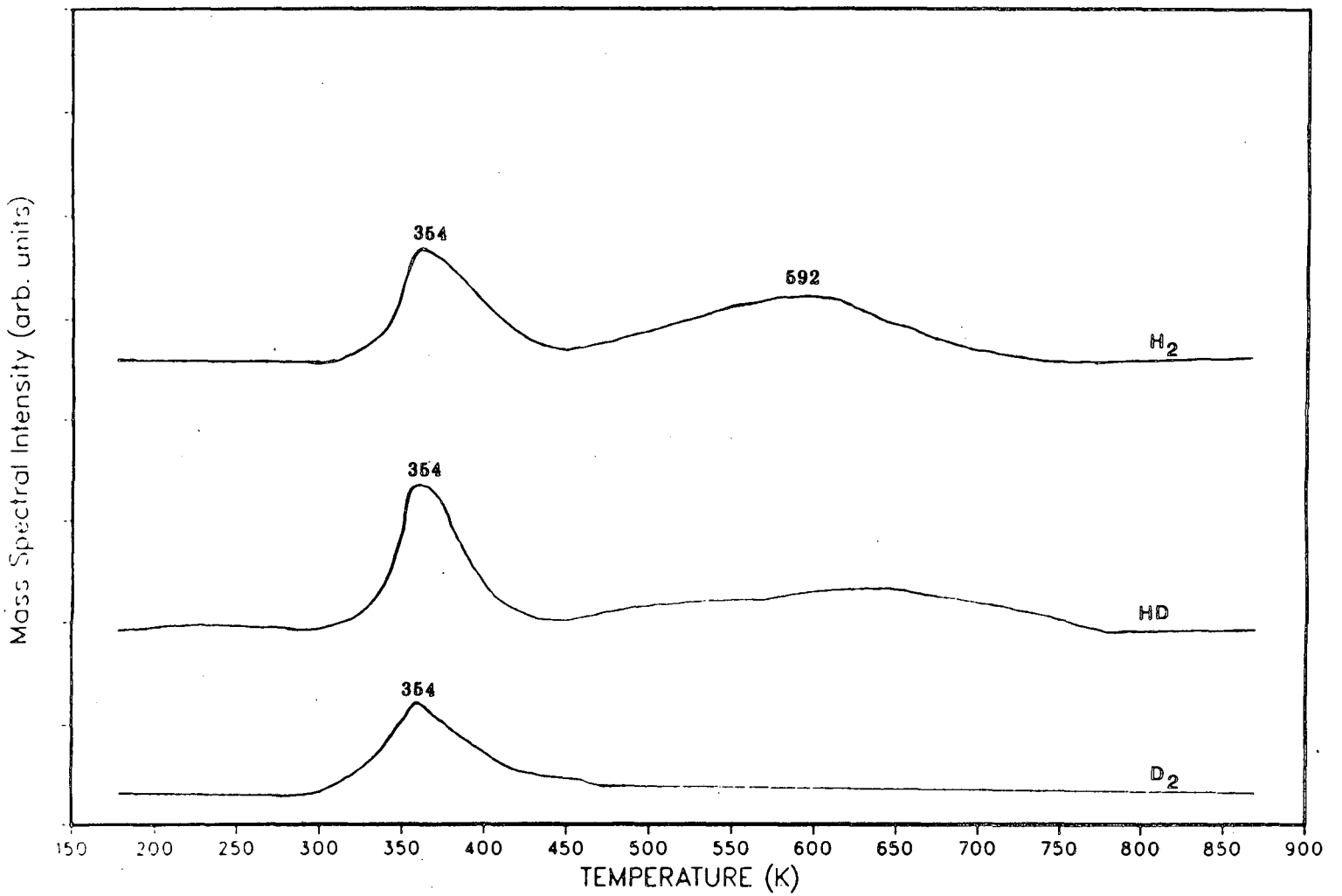

XBL 8512-5141

2,5 DIMETHYL THIOPHENE

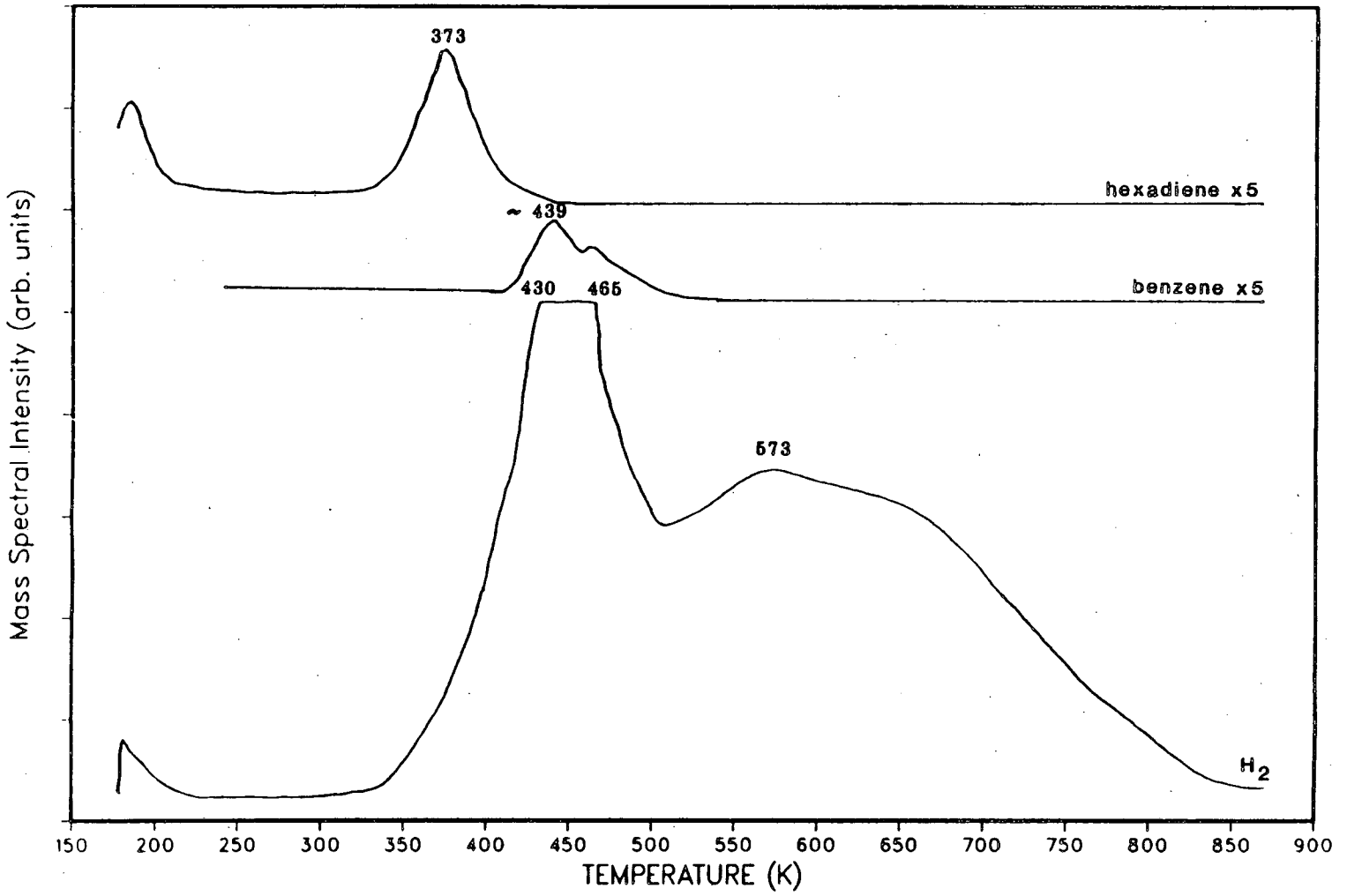

XBL 8512-5143

Thiophene - C_4H_4S

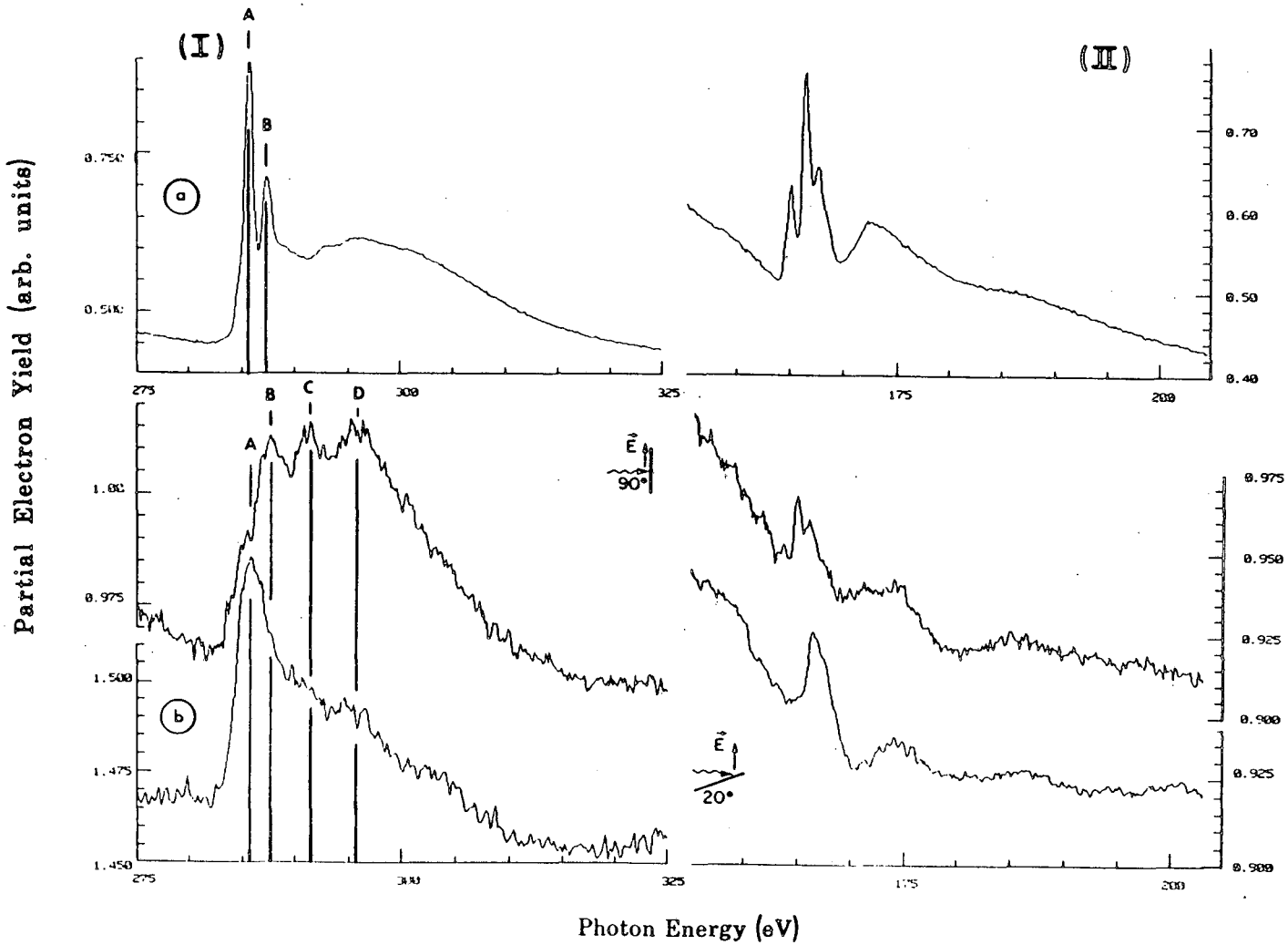

-- XBL 8512-5078

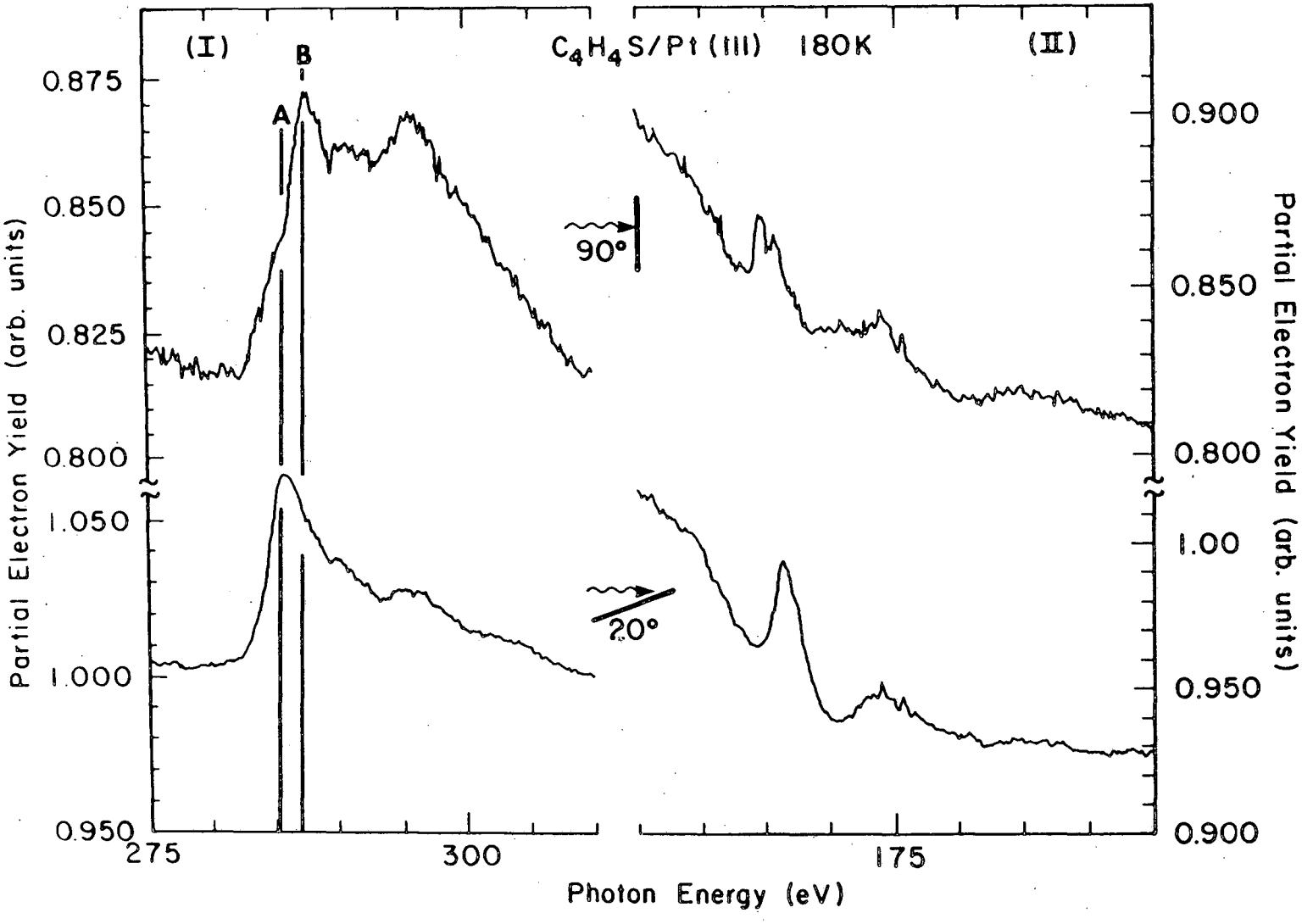

XBL 8512-5081

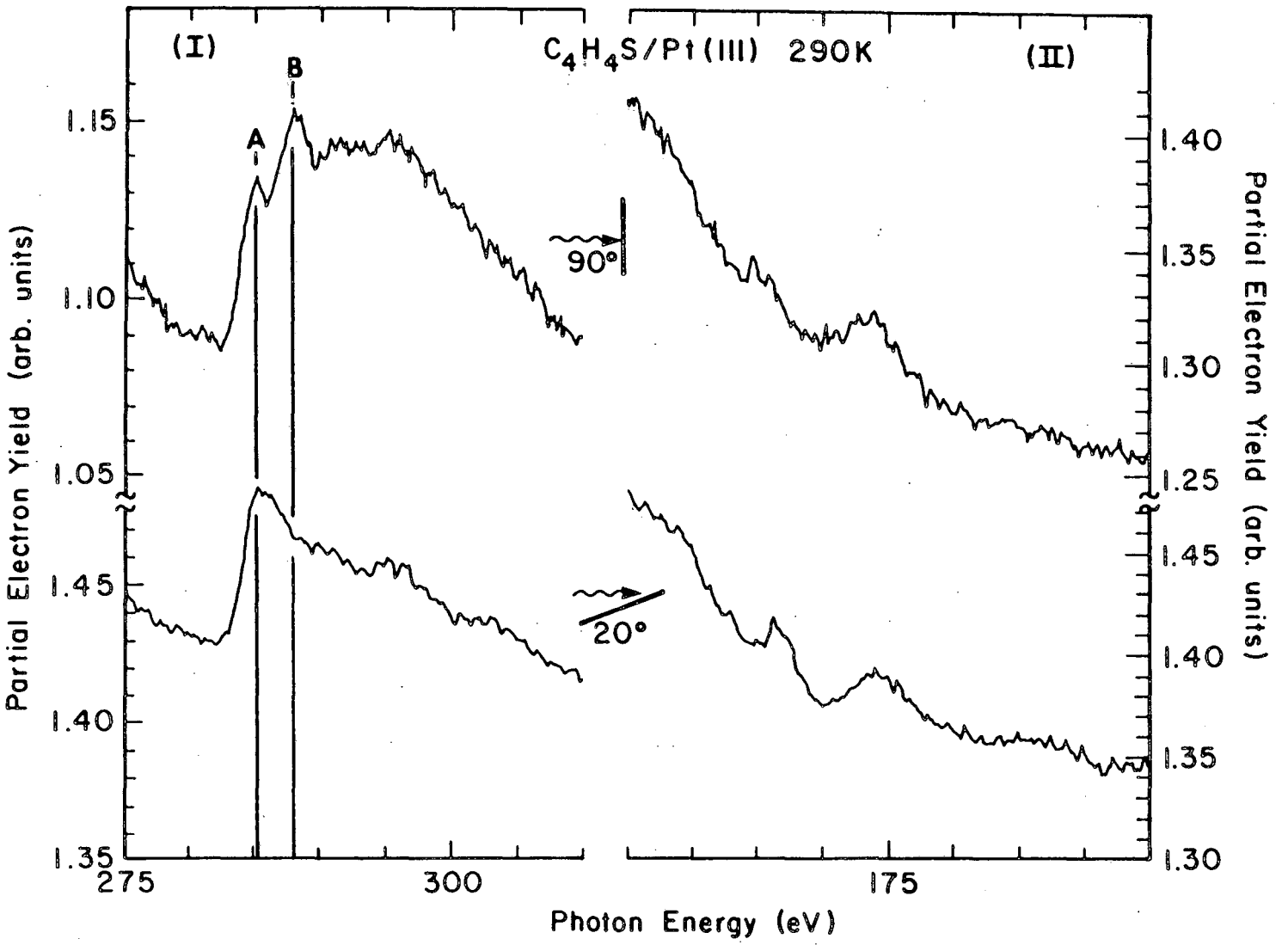

XBL 8512-5080

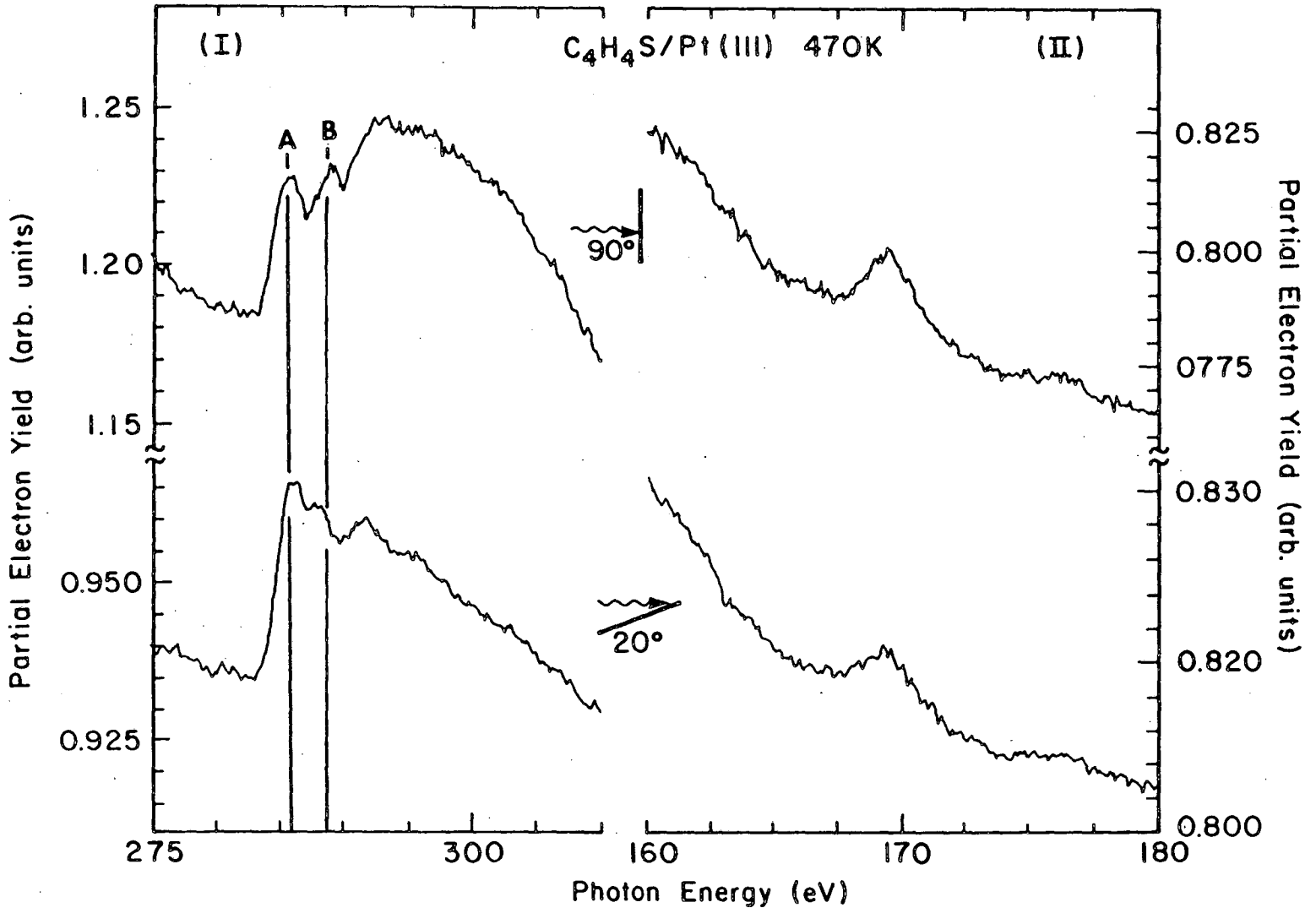

XBL 8512-5082

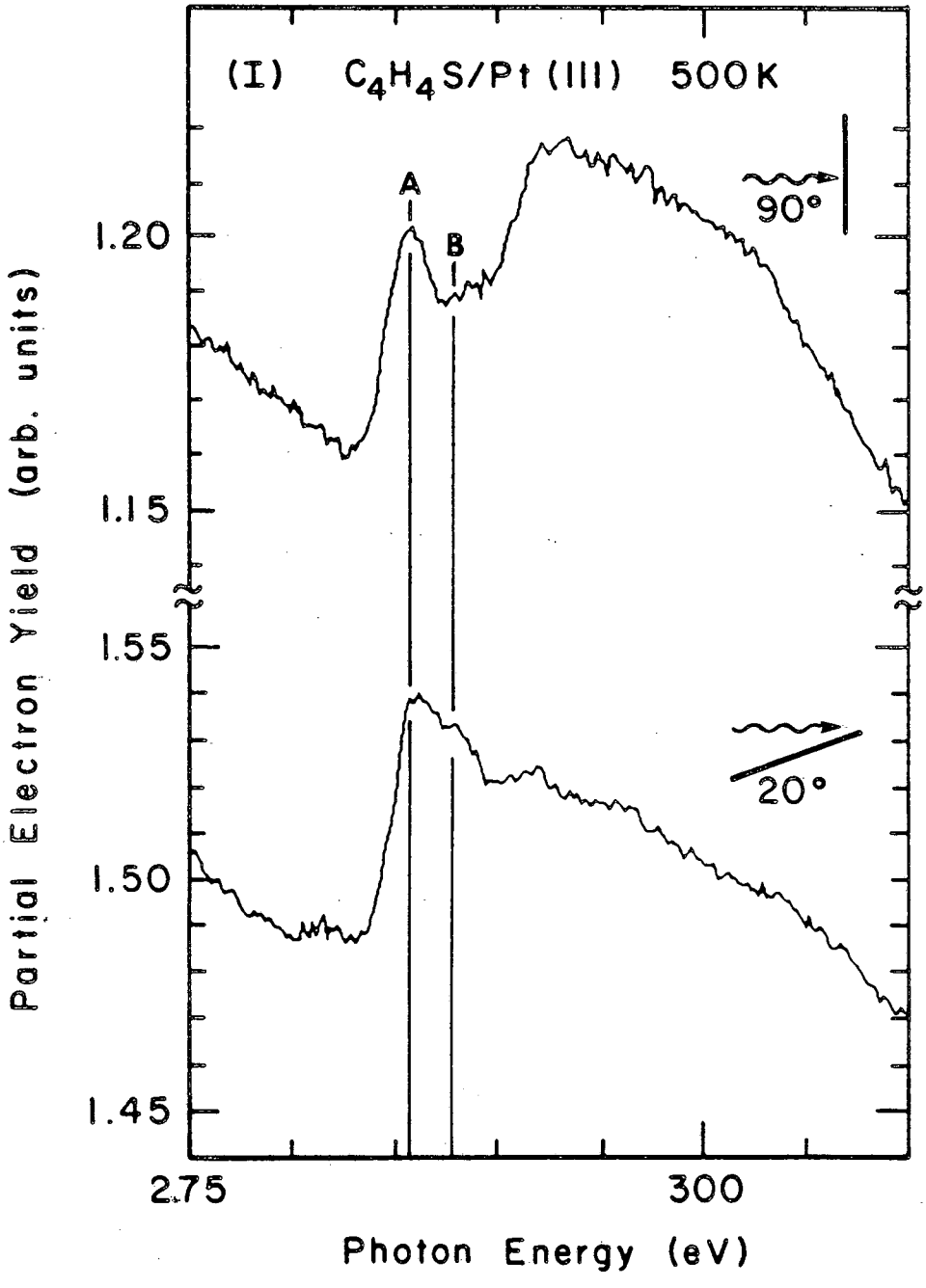

XBL 8512-5107

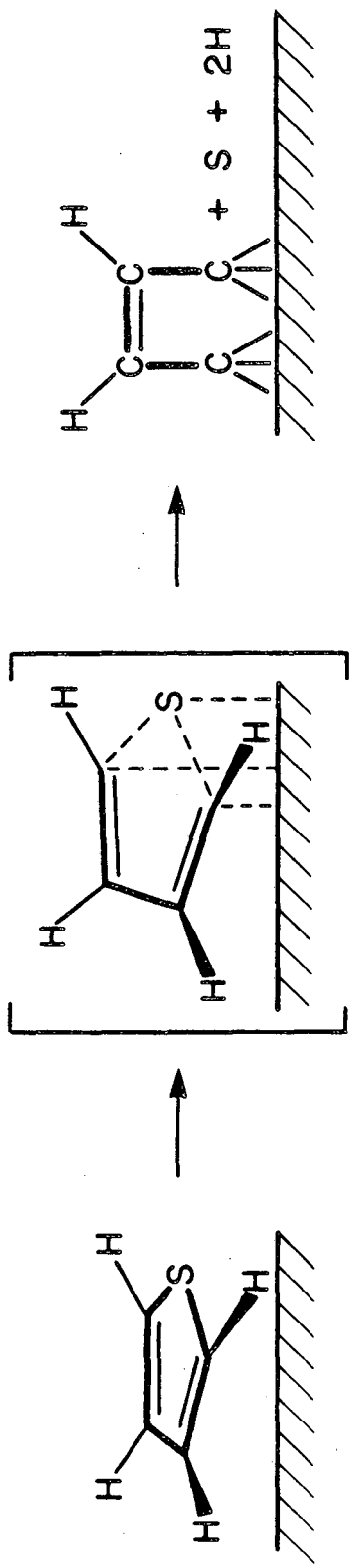

XBL 8512-5091

III.6 Carbocyclic Nonbenzeniod Cyclic Polyenes

III.6.1 Overview

This section describes NEXAFS and thermal desorption investigations on benzene and other cyclic polyenes chemisorbed on the Pt(111) surface carried out to obtain information with respect to the importance of aromaticity in surface species and to complement our earlier studies[23].

Amongst the simplest unsaturated hydrocarbons are ethylene and acetylene. There have been many experimental and theoretical studies of ethylene and acetylene chemisorbed to well characterized transition metal surfaces. Ethylene and acetylene chemisorb at low temperatures with their bond vectors parallel to transition metal surfaces and exhibit considerable rehybridization towards 1,2 diσ bonded species on reactive surfaces (in particular, the platinum surfaces). Similar rehybridization for cyclic unsaturated molecules on Pt(111) would result in the loss of the π orbitals that can overlap and lead to aromaticity.

Alternatively, cyclic unsaturated hydrocarbons form many stable π coordinated complexes with metals: i.e. benzene forms $(C_6H_6)_2Cr$ as well as mono benzene complexes[72], cyclopentadienyl (C_5H_5) forms $(C_5H_5)_2Fe$ as well as many singly singly coordinated compounds. The other cyclic polyenes are more rarely found: cycloheptatrienyl (C_7H_7) as $(C_5H_5)V(C_7H_7)$ and $[C_7H_7Mo(CO)_3]^+BF_4^-$ [73], cyclooctatetrene (C_8H_8) as $(C_8H_8)_2U$ and $C_8H_8ZrCl_2 \cdot THF$[74] and cyclobutadiene (C_4H_4) as, for example, $C_4H_4Fe(CO)_3$[75,76]. These complexes would lead one to expect that all of these hydrocarbons could exhibit flat, aromatic coordination states.

Previous work involving the chemisorption of cyclic polyenes on well characterized metal surfaces have investigated benzene and cyclopentene and derived species.

Benzene chemisorbed to well characterized metal surfaces has been extensively studied. A state with the benzene ring chemisorbed parallel to the metal surface is generally found. This structure can be rationalized by the tendency to maximize the metal orbital - adsorbate π orbital overlap.

Cyclopentene and derived species on Pt(111) have been studied by Avery et. al[77] using thermal desorption spectrometry and HREELS. He finds that cyclopentene can be dehydrogenated (with loss of 3 mole equivalents of hydrogen atom) to form a species with only one C-H stretch and suggests a surface cyclopentadienyl state.

III.6.2 Cyclopentene

Figure 42 presents the thermal desorption spectra for cyclopentene on Pt(111). The only desorption observed other than multilayer desorption is hydrogen desorption in two regions: a low temperature desorption limited peak at 324K and a high temperature peak at 639K with a shoulder to higher temperatures. The peaks have an area ratio of 3:5 as reported by Avery et. al[77].

The NEXAFS spectra for the cyclopentene ice (figure 43) shows a weak π^* resonance at 284.7eV , a very weak resonance at 288eV, and σ resonances at 290.5 and 295.4eV. On annealing to 170K (figure 44a) a monolayer state with the π^* at 284.2eV and σ resonances at 290.4 and 295.2eV are found, with a polarization dependence suggestive of orientation of the π system perpendicular to the surface and with the σ framework of the molecule to be found preferentially parallel to the surface. The resonance energies are only weakly perturbed from their solid phase values. Annealing to 300K momentarily and recooling

to 90K gave no difference in the NEXAFS spectra - annealing to 300K and holding the temperature there during the data collection (repeating the conditions used previously[77]) yields the cyclopentadienyl state (figure 44b). This state is characterized by an intense π^* resonance at 286eV and σ resonances at 291.7eV and 297.5eV. The π^* resonance is now at the same energy as for benzene and the σ resonances have increased by 1.3 and 2.3 volts, suggesting a bond length decrease of .03 and .05Å, although as with benzene[7] the correct value of the shift must be calculated using MS Xα calculations. The polarization dependence of the π^* and σ resonances mimic that of benzene i.e. the π^* resonance is seen at grazing photon incidence and the σ framework is seen at normal photon incidence; indicating a flat, unsaturated molecule chemisorbed parallel to the surface. Further anneals to 410K (past the first hydrogen desorption) leads to a surface state indistinguishable from the 300K state that is in addition stable to cooling to 90K.

In summary then we observe the formation of a cyclopentadienyl fragment in the dehydrogenation of cyclopentene. The dehydrogenation seems to be either slow or reversible at 300K. This is in accord with previous results[77], which were based on HREELS analysis - at 300K the hydrogen stretches collapsed into a single peak, suggesting a single type of hydrogen in the chemisorbed species.

III.6.3 Cycloheptatriene

Figure 45 presents the thermal desorption spectra of cycloheptatriene. At low coverages only hydrogen desorption in three peaks at 415K, 485K, and 647K. At high coverages (~2L) hydrogen is observed at 366K, 485K, and 648K. Mass 78 (which we shall hence forth call benzene - benzene is the most stable of the isomers of C_6H_6 and is

the most probable product) is also observed at 298K with a weak peak at 485K. This benzene production is remarkable, since the temperature of benzene desorption from clean and carbon contaminated (from benzene decomposition) Pt(111) is on the order of 373K to 473K. Benzene production is only seen at coverages sufficient to deposit a multilayer of cycloheptatriene.

The NEXAFS of cycloheptatriene ice is shown in figure 46. A strong π^* resonance is seen at 284.6eV with weaker peaks at 286.5eV, 288.1eV, 292.6eV, and 300eV. The monolayer spectra of cycloheptatriene are shown in figure 47a. A strong π^* resonance is seen at 285.2eV with a shoulder at 287.4ev. Sigma resonances are seen at 292.5eV and 300.5eV. Annealing to 0^oC (just before the onset of benzene desorption) yields spectra (figure 47b.) similar to the monolayer spectra, but with the π^* peak at 285.2eV and 90^o less intense, suggesting that the π system is "flatter", i.e. that the molecule looks more like a flat conjugated system.

Our past studies of cyclic polyenes on platinum and nickel[23] were carried out with dosing at room temperature - thus, chemistry that occurs below room temperature or proceeding from a multilayer was not observed. The anomalously low temperature production of benzene was not observed. The structure for chemisorbed C_7H_8 (figure 48) we presented earlier is in accord with the observed NEXAFS results: primarily π coordination (with torsion of the π orbitals next to the methylene carbon) and the methylene carbon tilted away from the surface (and thus σ^* intensity at grazing incidence for longer {closer to threshold resonances} bonds).

HREELS spectra (provide by V. Grassian of the University of California, Berkeley) of cycloheptatriene ice and ice annealed to 240K (figure 49, inset) show multiple peaks in the C-H stretch region. Spectra of cycloheptatriene dosed and taken at room temperature show a single C-H stretch (figure 49, main figure), again suggestive of a C_7H_7 species.

The question of the coordination state of the annealed cycloheptatriene surface species is complicated by the observed benzene production. Benzene yields a state with a parallel ring plane and thus has a π^* transition that is greatest at grazing photon incidence. The amount of benzene produced is small, however: less than 10% of a monolayer estimated from thermal desorption peak areas of benzene thermal desorption (The peak area of the desorbed benzene/ peak area of desorption of saturation coverage of benzene = 4.7/72.2 = 6.5%. Saturation coverage of benzene on Pt(111) has residual decomposed carbon = .2 C/Pt thus the benzene peak area may be low by about 20% and so a better estimate of amount of benzene production would be 5%.) and Auger spectrometry of the carbon overlayer after the anneal (Residual carbon left on the Pt(111) after anneal to 870K was 1.01±.05 C/Pt (determined from a radiochemical Auger calibration of aromatic carbon on Pt(111) {S. M. Davis, Ph.D. thesis, University of California, Berkeley, 1981}) thus the carbon lost as hydrocarbon was less than that necessary to induce observable depletion of the residual carbon. We estimate the threshold of observable carbon loss to be 10%.), and thus the majority species at 270K is not likely to be benzene, but rather flat, parallel coordinated C_7H_7. The source of the benzene is not unequivocally determined by the present study, but the low benzene desorption temperature and high

coverage of cycloheptatriene requirement suggest a model where a second layer cycloheptatriene, coordinated in a low coordination fashion (figure 50) could extrude one coordinated carbon and yield a benzene ring on top of the cycloheptatriene overlayer - which would desorb at low temperature. If this model is correct then the observed benzene production signals C-C bond cleavage since the desorption would be reaction limited.

Thus we give evidence for a coordinated C_7H_8 species as suggested in our earlier work and give more suggestive evidence for a C_7H_7 surface state which is coordinated with the ring planar and parallel to the metal surface.

III.6.4 Cyclooctatetrene

Cyclooctatetrene thermal desorption, taken from reference 23b, exhibits above room temperature a C_8H_8 desorption at 423K (~30%) and hydrogen desorptions at 393K, 598K and 653K. No hydrocarbon other than cyclooctatetrene was observed.

NEXAFS spectra for solid (figure 51a.) and monolayer (figure 51b.) states of cyclooctatetrene show significant differences. The π^* resonance at 284.9eV in the monolayer is very weakly perturbed in energy position and of similar width (at normal photon incidence) compared to the multilayer and shows polarization dependence that indicates a state where the pi orbitals are tilted at 45 ± 3^{o} with respect to the surface normal. The peak at 286.7eV in the multilayer is much weaker than the peak at 284.9eV, while in the monolayer the peaks are of equal intensity at grazing photon incidence and of unequal intensity at normal photon incidence. This polarization dependence can be rationalized by invoking

rehybridization of the coordinated carbons. If the carbons are rehybridized towards sp^3 (similar to what is seen for ethylene on Pt(111)) then the peak near 286.7eV comes from different phenomena - the peak in the multilayer is likely due to a π^*(8e) final state[78] while the peak in the monolayer can not be due to the same state - the polarization dependence of all the π^* states are the same. A rehybridization toward sp^3 would swing the final state toward the surface normal and raise the final state energy, as observed. In summary then, we propose a state with the cyclooctatetrene coordinated in the 1,2,5,6 positions, similar to that seen for 1,5 cyclooctadiene (see figure 52). The observed polarization dependence of the 284.9eV peak is consistent with this geometry.

III.6.5 Cyclobutene

The thermal desorption spectra for cyclobutene adsorbed at room temperature shows only hydrogen desorption at 370K and 510K[23b]. Chemisorption at 90K gave NEXAFS spectra as indicated in figure 53. A π^* transition at 285eV is observed, with a broad σ resonance near 291.3eV. Annealing to 180K yield the monolayer spectra (figure 54a.), characterized by a π^* resonance at 284.7eV and σ resonances at 291eV and 299.2eV. The polarization dependence is suggestive of a tilt to the π^*, as might be expected due to metal hydrogen interactions in cyclobutene forcing the C_4 ring away from parallel to the surface. Annealing to 420K (past the first hydrogen desorption) yields a spectra (figure 54b.) totally different from the starting material. This spectra is characteristic of decomposed hydrocarbon on Pt(111). It is very similar to spectra obtained by heating C_2D_2 chemisorbed to Pt(111) (figure 18) to similar temperatures (i.e. 345K to 520K). While the spectra can not

be interpreted in terms of detailed structure without considerable calculational effort, it is clear that cyclobutene, in contrast to cyclopentene, has not dehydrogenated to form a flat, π coordinated surface state.

III.6.6 Summary

Cyclopentene, benzene, and cycloheptatriene all form flat, π coordinated species near room temperature on Pt(111), in contrast to cyclooctatetrene and cyclobutene which form bent and fragmented surface states at elevated temperature. This implies that gas phase aromaticity arguments predict the observed structures and the extent of rehybridization in systems that can fill the π molecular orbitals (i.e. aromatic molecules) is small enough to allow significant π orbital overlap, in agreement with what is suggest by uv photoemission studies of benzene[48] and in contrast with the implications of the HREELS studies of C_2 hydrocarbons on Pt(111) (vide infra). We see low temperature states of the cyclopentene, cycloheptatriene, and cyclobutene that can be rationalized by the tendency to form parallel π complexes of unsaturated compounds, altered by any steric perturbations induced by other molecular features.

In conclusion then we see facile dehydrogenation in C-5 and C-7 rings to form the corresponding aromatic system, similar to the previously well known dehydrogenation of C-6 rings to give benzene[23c], a behavior that is not shared by the C-4 and C-8 ring systems.

III.6.7 FIGURES

Figure 42

Thermal desorption spectra of cyclopentene. The temperature of adsorption was 170K and the heating rate was 25°/second. The only molecules desorbing were cyclopentene from the multilayer and hydrogen.

Figure 43

NEXAFS spectra of cyclopentene ice. The photon incidence angle was 90°.

Figure 44

NEXAFS spectra of cyclopentene monolayer (a.) and annealed (b.) to 300K to form cyclopentadienyl adsorbed to the surface. Note shifts of the σ and π resonances.

Figure 45

Thermal desorption spectra for high coverages of cycloheptatriene. Thermal desorption spectra for low coverages are similar in the hydrogen trace and the other masses are not seen. Conditions were as for cyclopentene. The peak at 190K in the benzene trace is due to fragmentation of the desorbing cycloheptatriene.

Figure 46

NEXAFS spectra of cycloheptatriene ice. Notice the slight dependence on photon incidence angle (greatest of all these molecules) which maybe be due to crystallinity of the multilayer ice.

Figure 47

NEXAFS spectra of monolayer (a.) and annealed (b.) cycloheptatriene.

Figure 48

Proposed structure of C_7H_8 at 240K (from 23b).

Figure 49

HREELS spectra of cycloheptatriene on Pt(111) with the C-H stretch region for the several temperatures shown. The arrows indicate the half height of the elastic peak - the peak width at half height is 75 cm^{-1}. Note the multiple peak in the C-H stretch region (300 - 400 meV) for 120K and 225K (the ice and monolayer respectively) and the single peak for the C-H stretch for the 300K spectra.

Figure 50

Suggested reaction pathway for the anomalously low temperature production of benzene from cycloheptatriene.

Figure 51

NEXAFS spectra of cyclooctatetrene ice (a.) and monolayer (b.). the photon incidence angle for the ice was 90^{o}. Note the different polarization dependence of peak A and B and the lack of shift in energy position of peak A from the ice to the monolayer.

Figure 52

Proposed structure for cyclooctatetrene adsorbed on Pt(111) at 210K. The position of the platinum atoms was not determined, they are included only to suggest a reasonable registry to the surface. The angle was determined by analysis of the polarization dependence of peak A of figure 51b. Hydrogens are not indicated.

Figure 53

NEXAFS spectra of cyclobutene ice. Photon incidence angle was 90^{o}.

Figure 54

NEXAFS spectra of monolayer (a.) and annealed (b.) cyclobutene. The residual π^{*} intensity at normal photon incidence can be rationalized

by tilting of the molecule induced by metal-hydrogen interactions.

CYCLOPENTENE

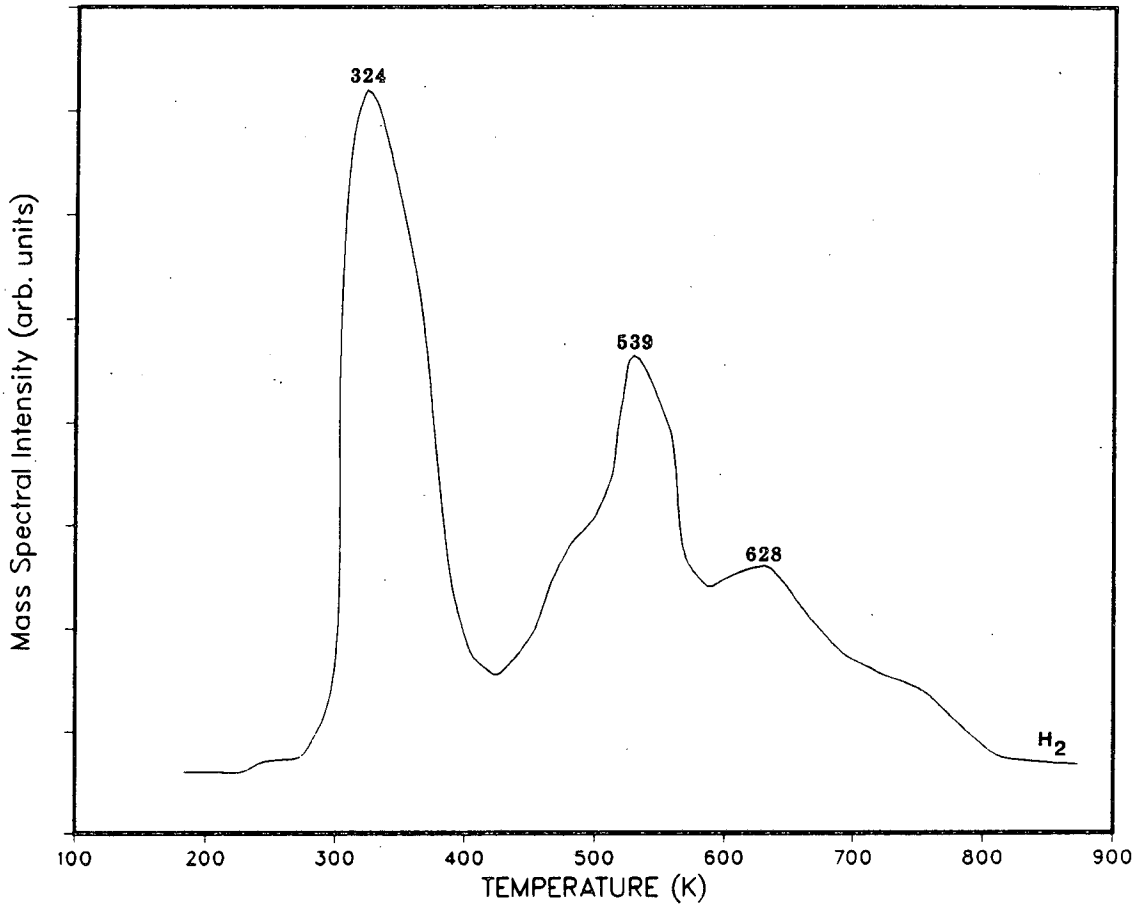

XBL 861-9

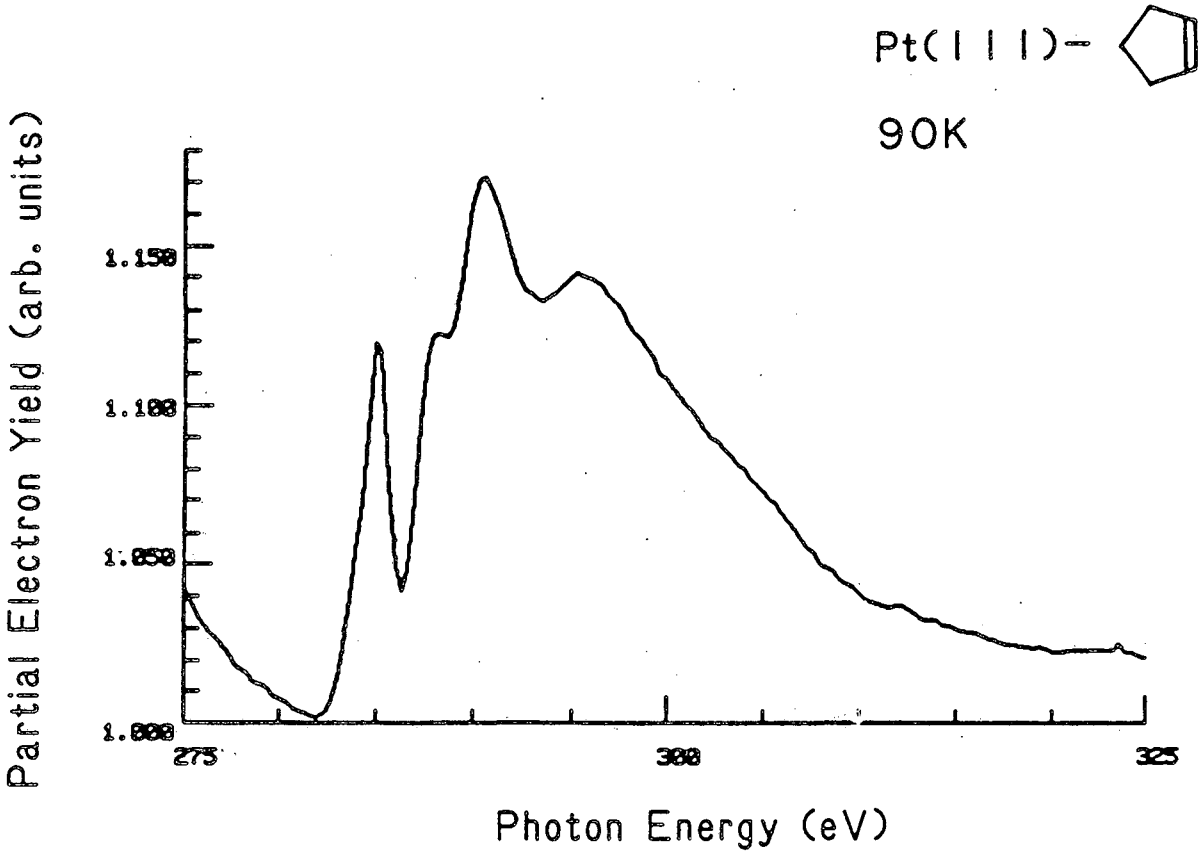

XBL 8512-5109

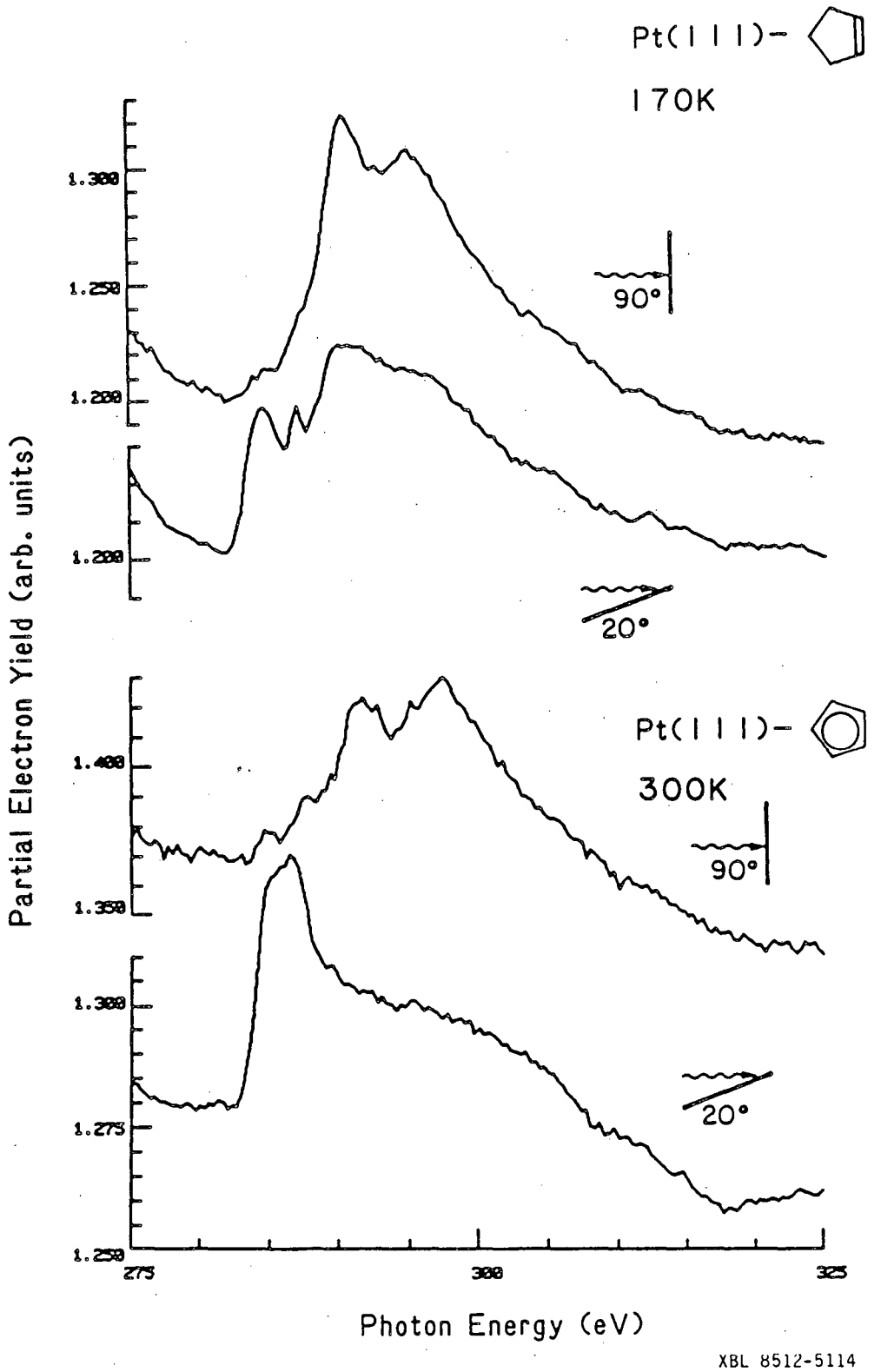

XBL 8512-5114

CYCLOHEPTATRIENE

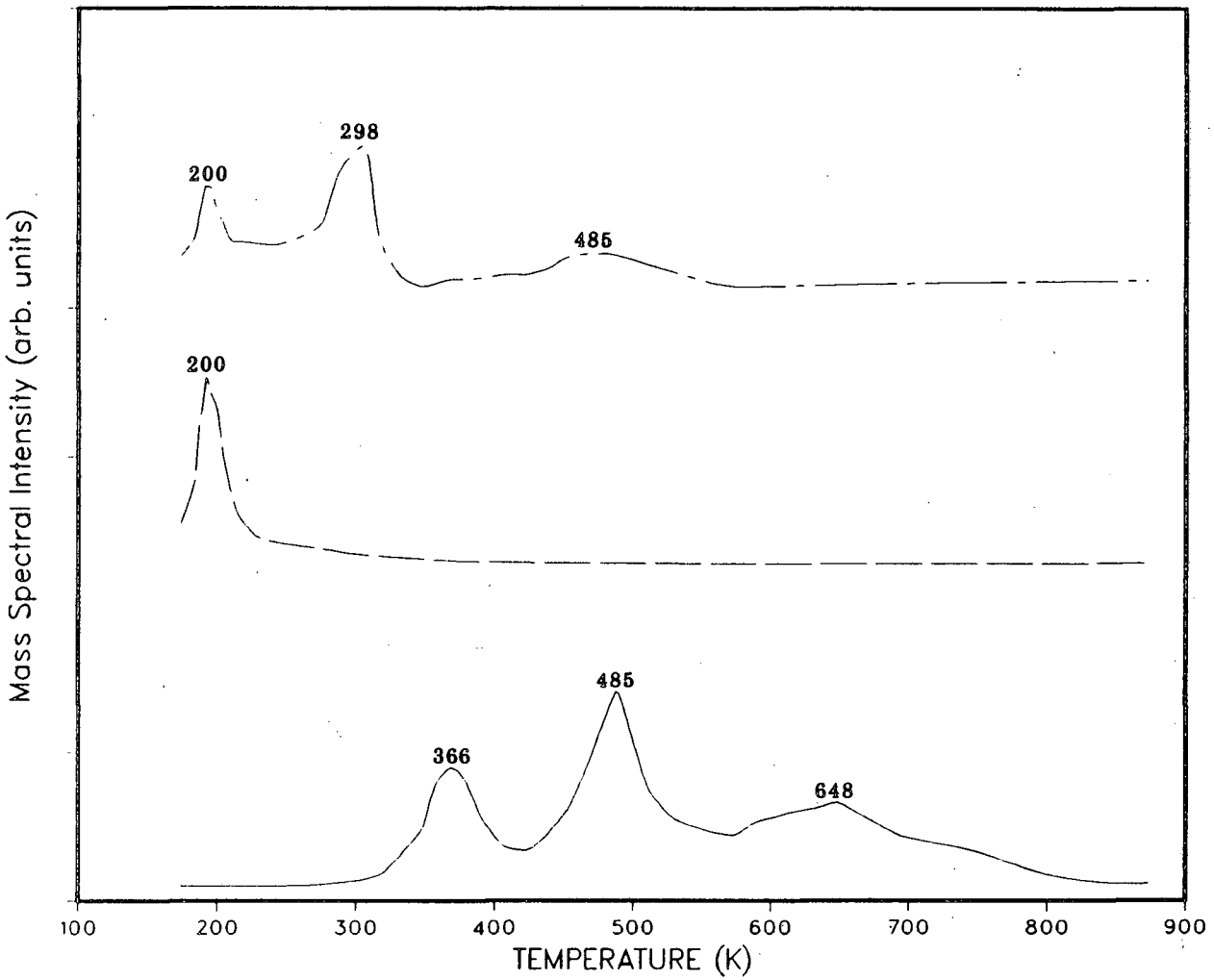

Legend

H_2

cycloheptatriene x7

benzene x35

XBL 861-10

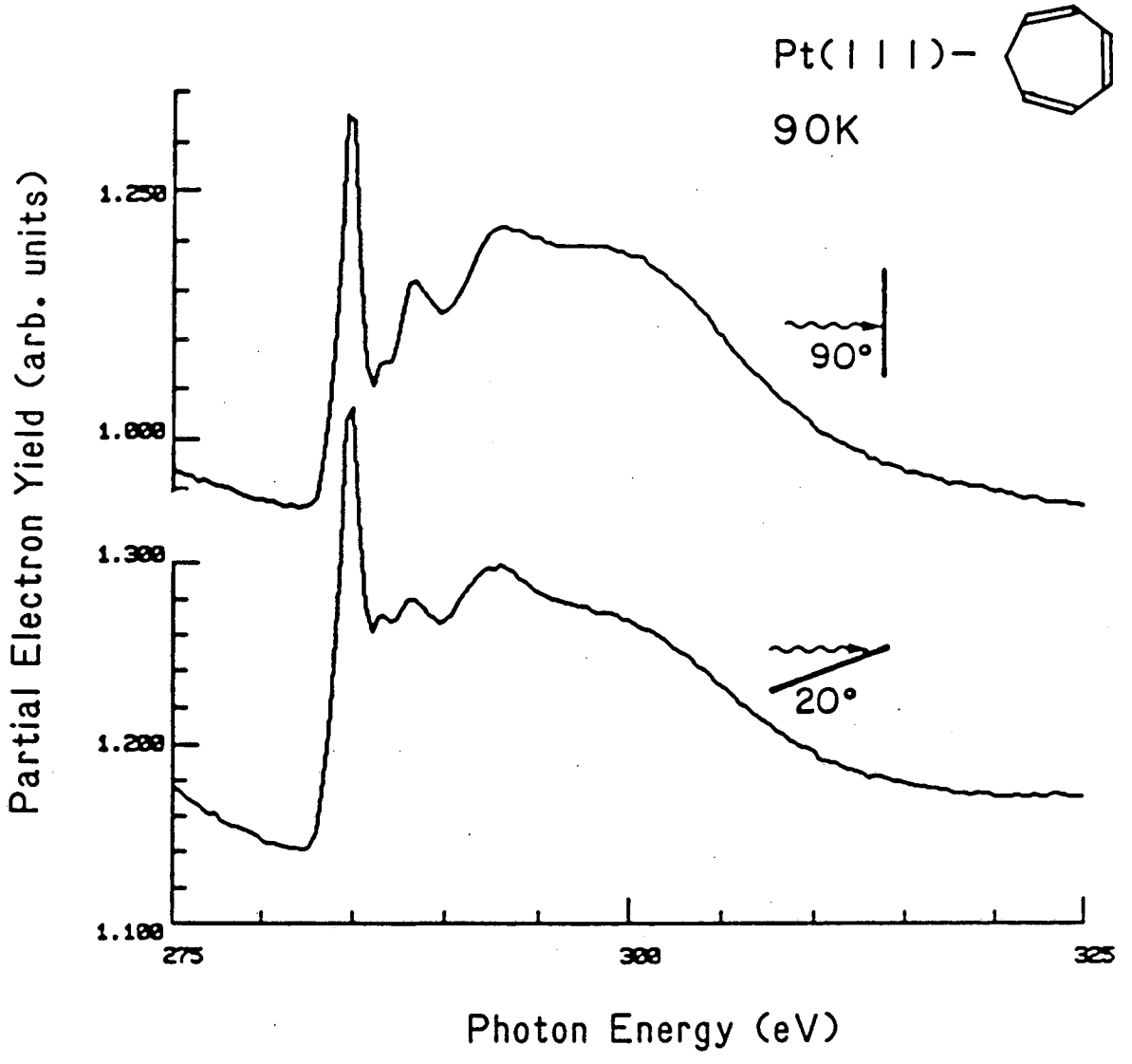

XBL 8512-5110

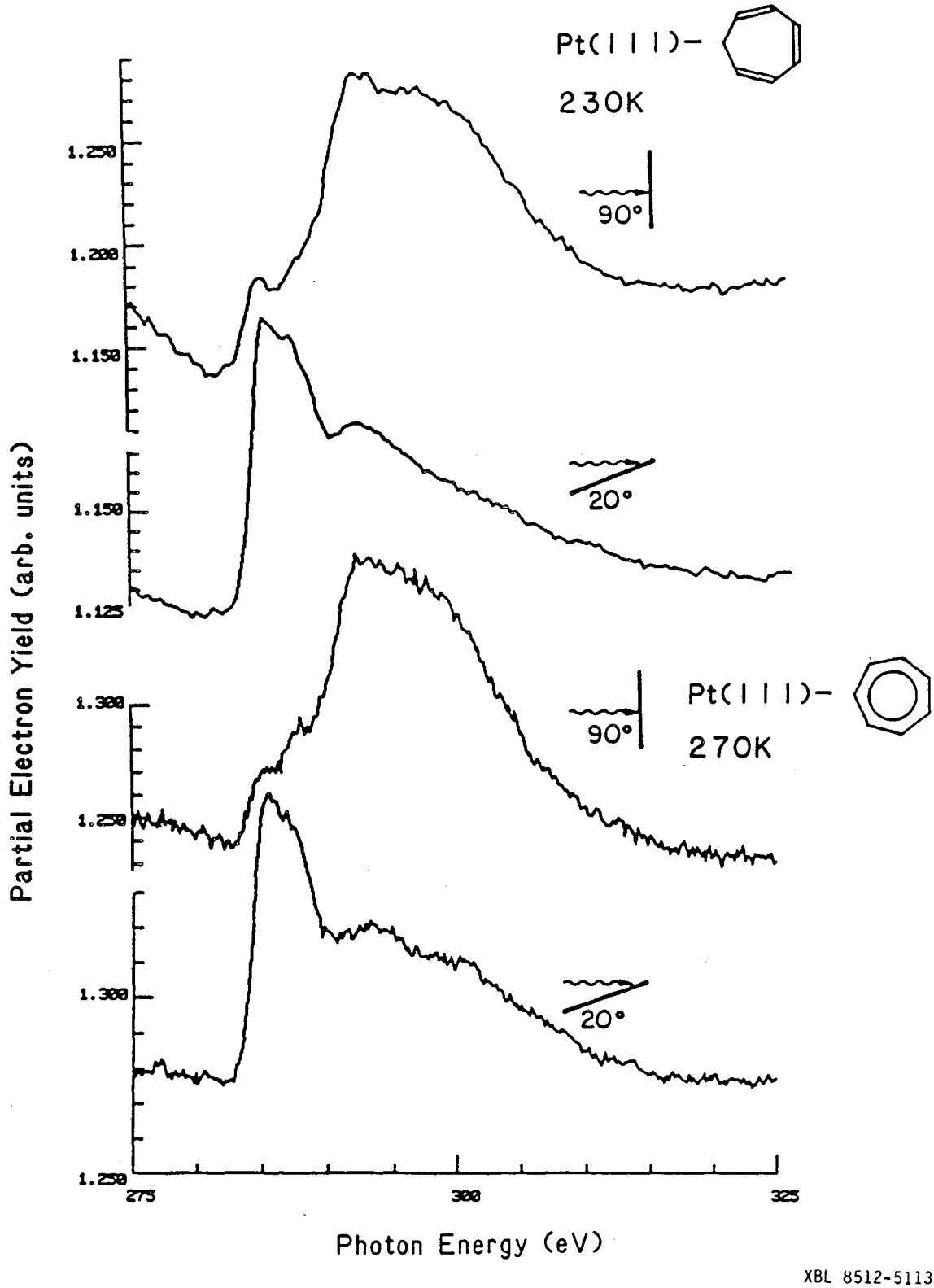

XBL 8512-5113

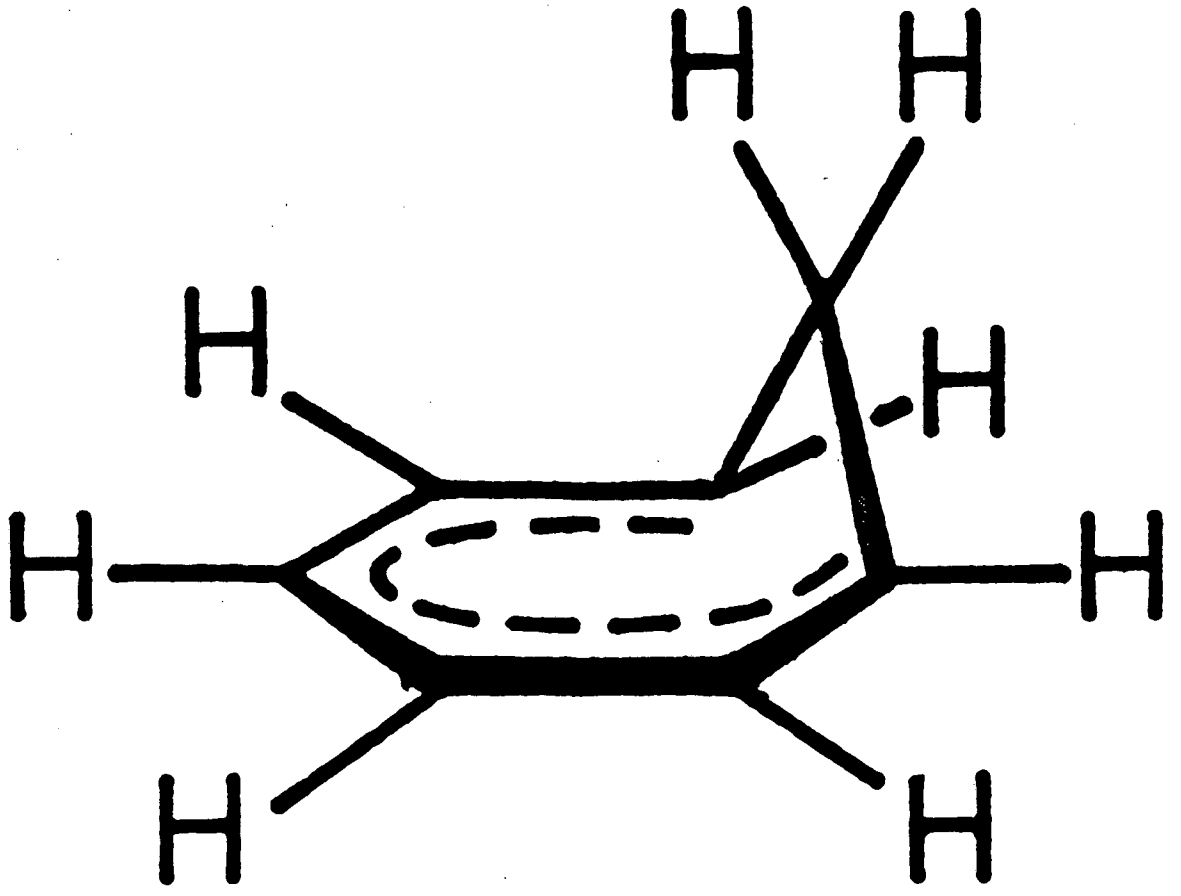

XBL 825-10263

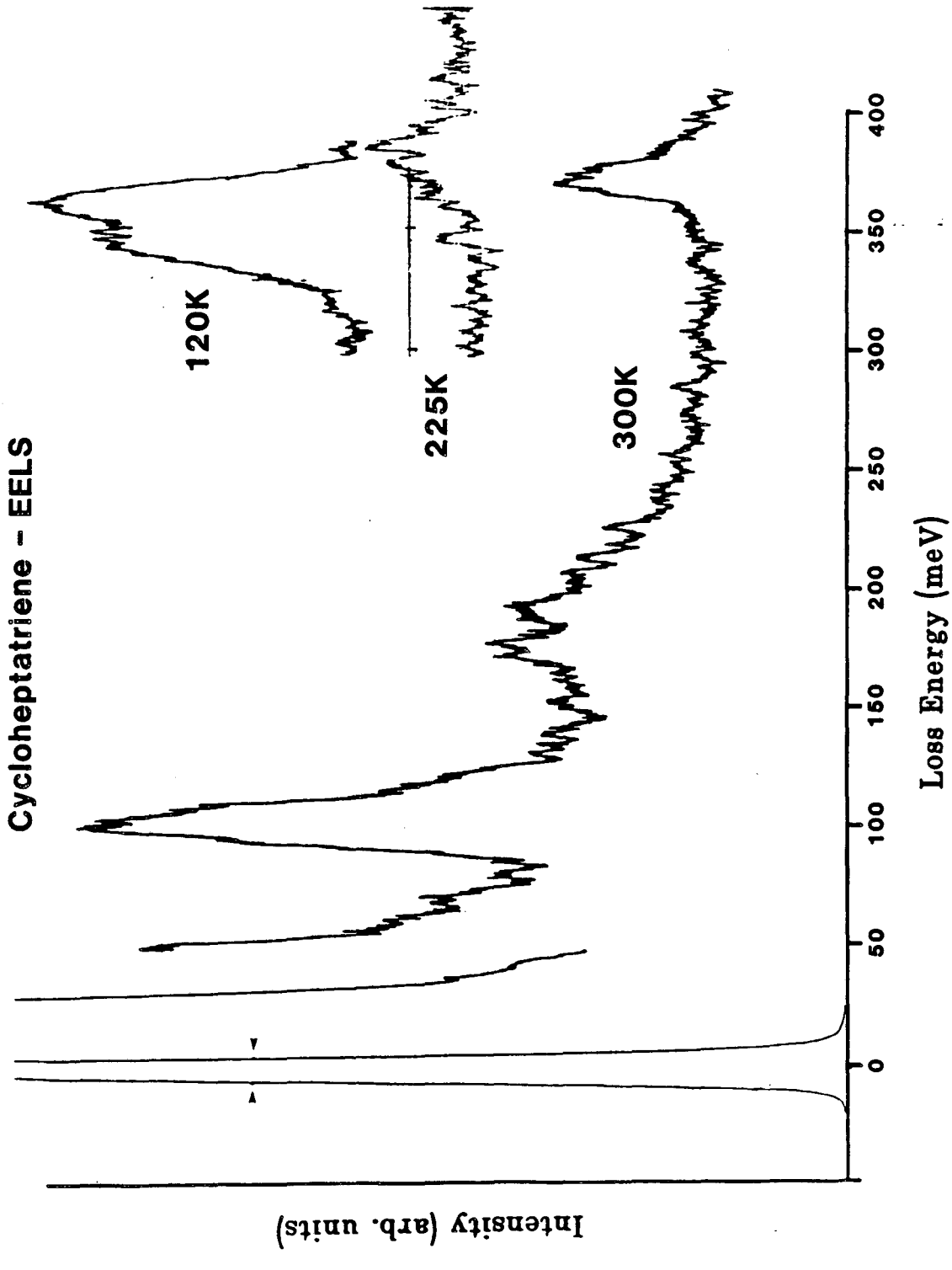
Cycloheptatriene - EELS
120K
225K
300K
Intensity (arb. units)
0
50
100
150
200
250
300
350
400
Loss Energy (meV)

XBL 861-8

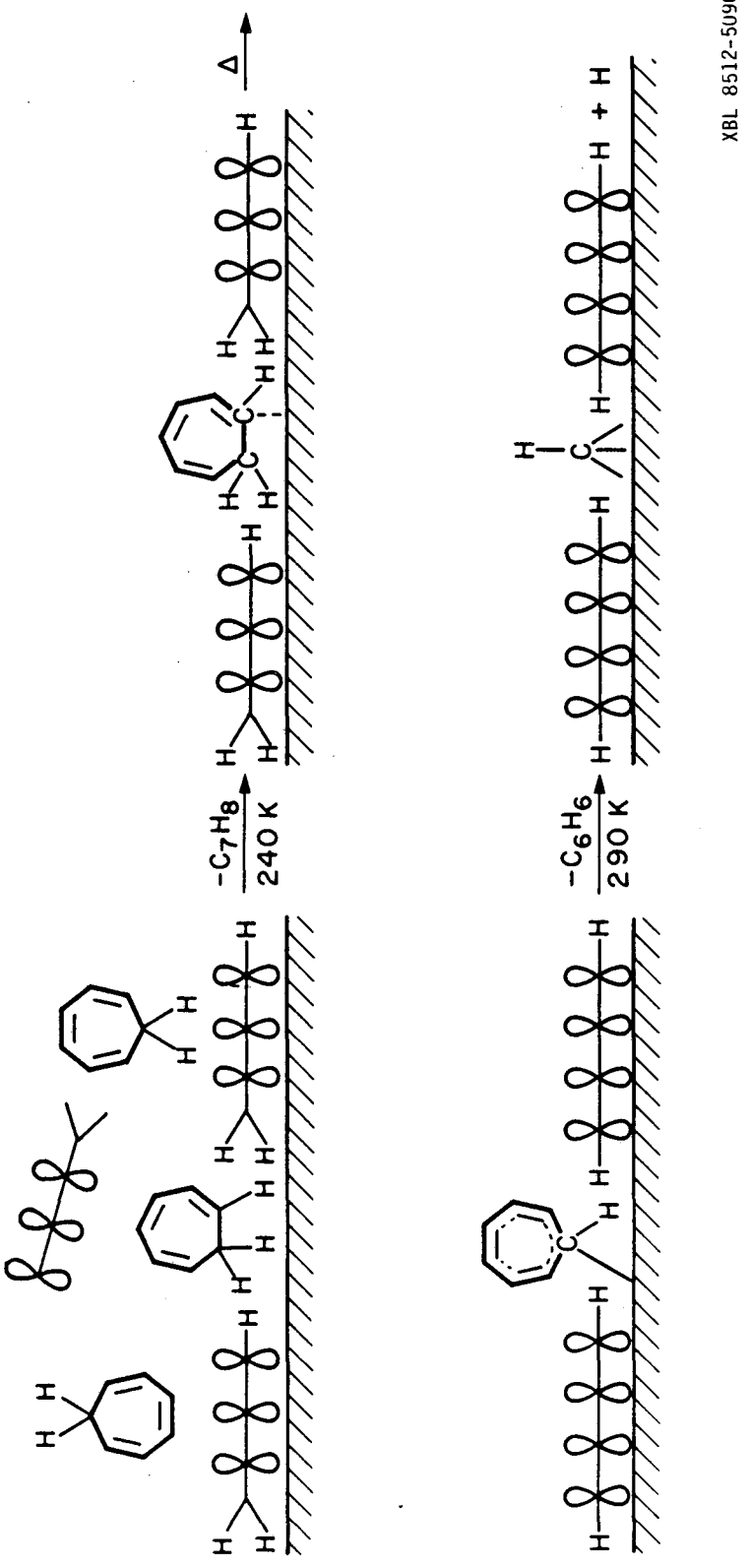

XBL 8512-5090

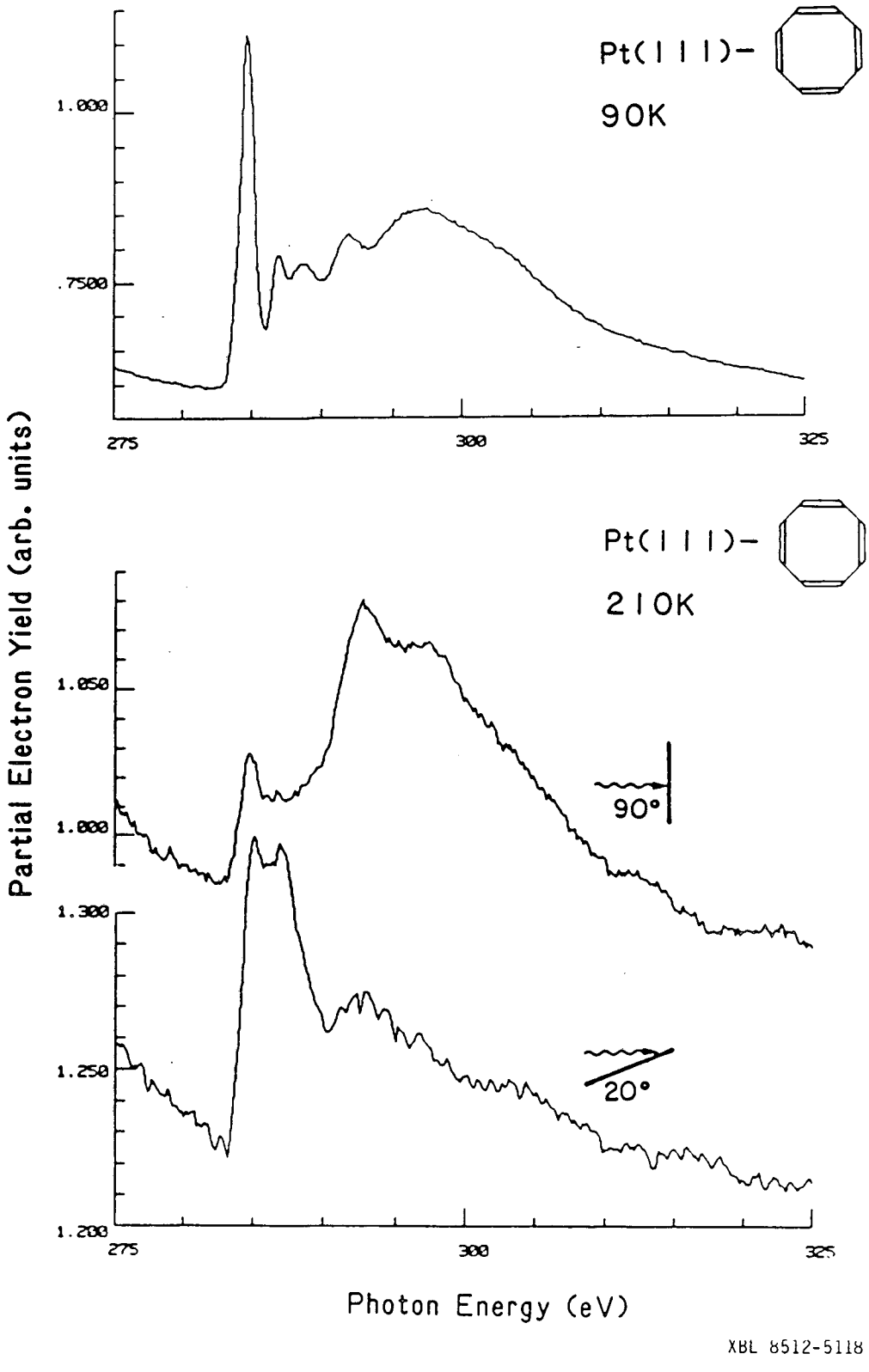

XBL 8512-5118

Structure of Cyclooctatetrene on Pt(111)

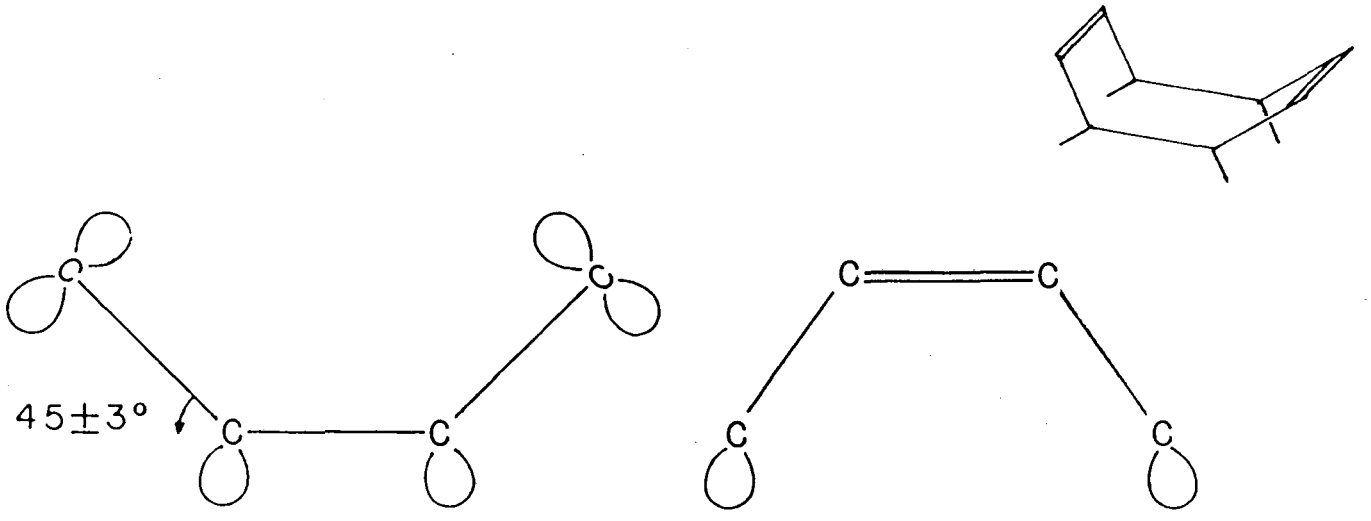

XBL 8512-5117

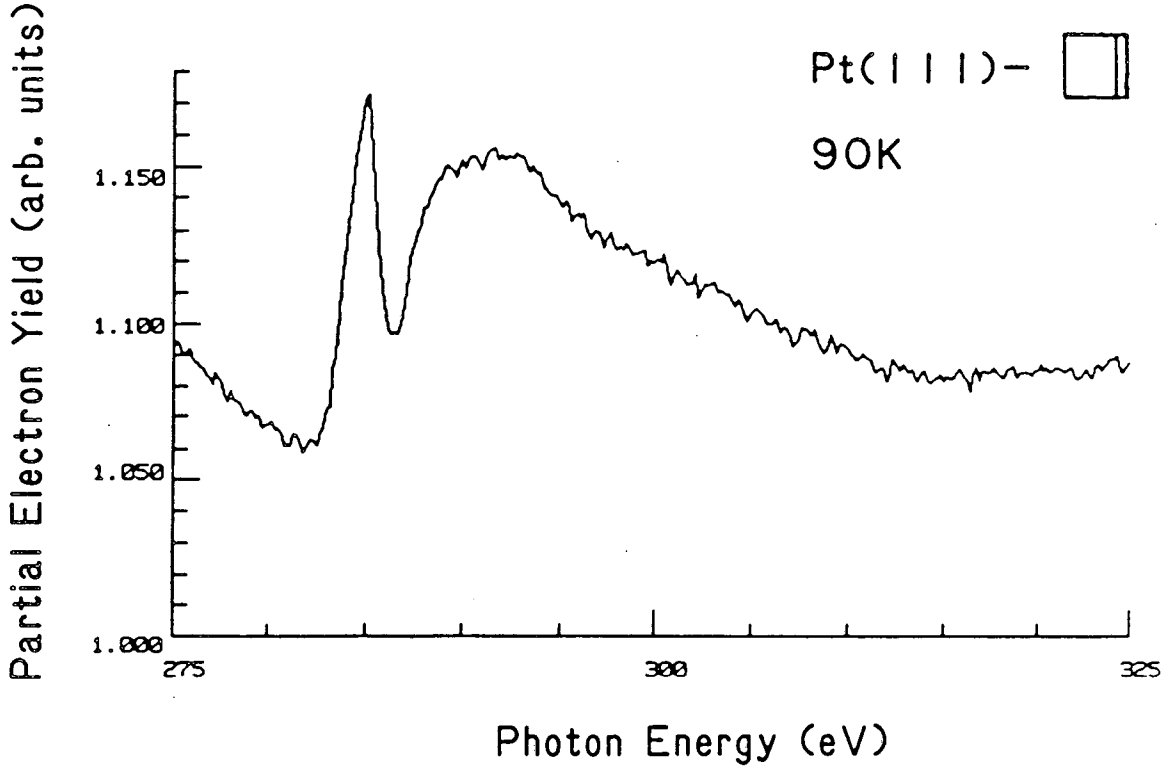

XBL 8512-5108

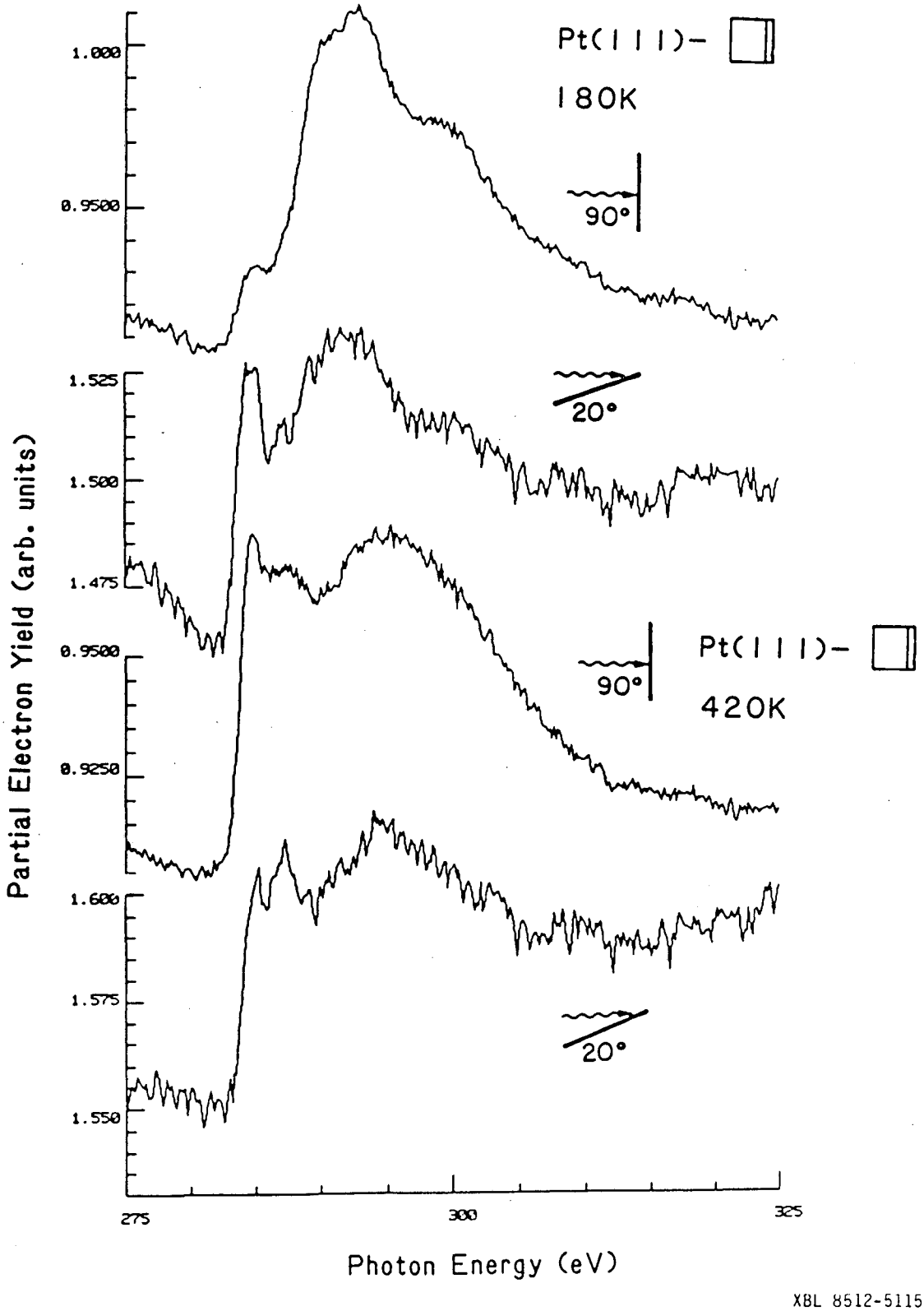

XBL 8512-5115

III.7 Small Molecules: CO, Ethylene, Acetylene, and Acetonitrile

III.7.1 Carbon Monoxide

We have presented results from earlier studies of CO chemisorption by NEXAFS in the introduction (see figure 9). In industrial practice, alkali metal promoters are used to change the reactivity of transition metal catalysts. There has been much recent work using HREELS, UPS, TDS, ESDIAD, and other techniques to determine the effects of alkali metal co-adsorption on the chemisorption geometry of CO[80]. NEXAFS, in common with other core level spectroscopies, allows one to observe the effects of co-adsorption without interference from emission from heteroatomic co-adsorbates in the spectra of the species of interest. We have therefor investigated the effects of Na co-adsorption on the chemisorption geometry of CO on Pt(111)[16g].

The NEXAFS spectra of CO (at saturation coverage) on clean and Na predosed (to 0.2 monolayer) Pt(111) at normal photon incidence are shown in figure 55. At this photon incidence the π^* transition predominates. There are three changes in the π^* transition of CO on the sodium modified surface: the π^* transition decreases in amplitude by 30%, the transition becomes broader (from 1.7 to 2.5 eV FWHM), and the transition shifts to lower photon energy by 0.6 eV in comparison to CO on clean Pt(111). Analysis of the polarization dependence of the π^* transition indicates that the CO molecular vector is within $\pm 15^{\circ}$ of the surface normal for CO on the clean surface and is $10^{\circ} \pm 15^{\circ}$ from the surface normal for the Na modified surface. The NEXAFS spectra at grazing incidence are shown in figure 56. At grazing photon incidence the σ resonances predominate. At both the carbon K edge (a) and the oxygen K edge (b) we observe a shift in the position of the σ resonance toward

lower photon energy with Na predose. This shift to lower photon energy is consistent with a bond lengthening of 0.12 ±0.03 Å [16g].

These results may be rationalized by invoking the previously suggested[80a-d] enhanced backbonding of the CO induced by an increase in the donor ability of the metal caused by alkali metal co-adsorption. The lack of any significant tilt suggests that models that propose direct interactions between the Na and the oxygen end of the CO are not likely in this case. Increased backbonding would increase the interaction between the metal filled states and the adsorbate empty states, leading to a decrease in the intensity of the π^* transition due to a decrease in the availability of empty states because of charge transfer to the CO, and the π^* width would increase due to increased admixture of metal orbitals into the final state. The energy shift of the π^* resonance can be explained by a combination of C 1s binding energy shift and possible rehybridization shift of the π^* state[16g].

The change in bond length may also be explained by increased backbonding decreasing the bond order of the CO. The estimated shift of 0.12 Å is larger than any seen in molecular clusters and may indicate some rehybridization of the CO accompanying backbonding.

III.7.2 C_2 Molecules

Amongst the simplest unsaturated hydrocarbons are ethylene and acetylene. There have been many experimental and theoretical studies of ethylene and acetylene chemisorbed to well characterized transition metal surfaces. Ethylene and acetylene chemisorb at low temperatures with their bond vectors parallel to transition metal surfaces and exhibit considerable rehybridization towards 1,2 diσ bonded species on

reactive surfaces (in particular, the platinum surfaces). Ethylene transforms at 300 K to a state where the C-C bond vector is normal to the surface (generally accepted as being ethylidyne). These states have been investigated experimentally determined by Auger[81], UPS[82], XPS[83], HREELS[84], LEED[85], and NEXAFS[86], and as well as being treated theoretically[87]. Interpretation of NEXAFS spectra of these states are complicated by the effects of the metal - carbon σ bonding, requiring explicit inclusion of the metal orbitals in the final state.

Figures 57 and 58 show ethylene chemisorbed at 90 K and 300 K respectively to Pt(111). The low temperature state (figure 57) shows the expected π^* intensity at grazing photon incidence and σ intensity at normal photon incidence, indicating a C-C bond vector parallel to the surface. The high temperature state no longer has a well separated low energy resonance - the π^* type state is washed out by interactions with the metal surface. At grazing photon incidence a σ resonance (peak D) is seen indicating a normal C-C bond vector, consistent with the ethylidyne structure. MS Xα calculations have been carried out to model the NEXAFS spectra of ethylene at 90 K and 300 K[8]. Model spectra are shown in reference 8b, figures 4,7, and 9 for diσ parallel bonded ethylene, π parallel bonded ethylene, and ethylidyne, respectively. The important features are that the diσ and π forms of parallel bonded ethylene give very similar spectra and thus are not explicitly distinguishable using NEXAFS and the modeled ethylidyne structure shows the expected σ resonance (peak D in figure 58) but the detailed features of the π^* region and the background are not well modeled.

In summary the ethylene NEXAFS can be modeled in its overall structure by MS Xα techniques, which indicate that the low temperature,

parallel bonded state could be either π or σ coordinated. The ethylidyne structure for the high temperature form is supported, with the σ resonance indicating a perpendicular bond vector.

Acetylene was investigated as an archetypical parallel bound sp hybridized molecule. We expect that acetylene is also strongly σ bound to the metal surface. We have earlier referred to the acetylene NEXAFS spectra as a model of C_2 generated carbonaceous overlayers. Figure 59, a repeat of figure 18, is presented for our discussion here. We observe at 90 K that the π^* transitions (peaks A and A') are strongest and best separated from the σ resonances for normal photon incidence (electric field vector parallel to the surface), consistent with the expectation of a rehybridized parallel coordinated acetylene state: the strong noninteracting π^* and σ final state shows clearly while at grazing photon incidence a complex spectra similar to the kind of spectra seen for ethylidyne, i.e. involving metal - carbon orbitals[86], is observed. A number of interesting resonances at grazing incidence can be seen, in particular a σ resonance at 304.1eV (peak E), which is what would be expected for a bond length of ~1.3Å, suggestive of a minority species with a perpendicular C-C bond vector that is only 0.10Å longer than the gas phase value of the C-C bond distance in acetylene and is close to the gas phase bond length for ethylene (1.34Å) i.e. a surface state consistent with vinylidyne is observed. At higher temperatures the σ intensity at grazing photon incidence (indicating C-C bonds perpendicular to the surface) grows and at still higher temperatures decreases. The π^* resonances at higher temperature shifts to lower energies and loses polarization dependence. This loss of polarization

dependence could be explained by the formation of methylidyne in a high coordination site. Figure 60 shows the model we suggest - mixed parallel and perpendicular acetylenic species that at higher temperatures show contributions from ethylidyne and then methylidyne (CH) species.

III.7.3 Acetonitrile

We have previously investigated nitriles on the nickel group metals by TDS and isotope labeling experiments[68a,88]. An orientation with the C-N bond vector nearly normal (analogous to what is seen in coordination chemistry for acetonitrile coordination) for acetonitrile and a parallel C-N bond vector methyl isocyanide was proposed on the basis of the observed chemistry. Later, HREELS evidence suggested a parallel orientation for acetonitrile and a normal orientation for methyl isocyanide at low coverage[88b,89]. The thermal desorption of acetonitrile from Pt(111) was in early work complicated by a small and poorly reproducible amount of decomposition. After the modification of the ionizer of the mass spectrometer (described in the experimental section) no decomposition was observed - acetonitrile desorbed totally reversibly. It was possible to create unusual products (e.g. mass 52 - cyanogen) by intentionally exposing the sample to electron flux. We initiated investigation of acetonitrile coordination to Pt(111) by NEXAFS to address the question of the chemisorption geometry.

Figure 61 is the NEXAFS spectra of acetonitrile ice (a) and monolayer at 180 K. The monolayer spectra shows interesting behavior at the nitrogen edge - the π^* resonance shifts in energy with polarization direction and the σ resonances (particularly peak C) are more intense at normal photon incidence. The σ behavior is consistent with a parallel

chemisorption geometry: the higher photon energy resonance (peak C) should be primarily due to the shorter bond i.e. the C-N bond. This bond is parallel to the surface. The other bond (the C-C) is at an angle to the surface and is more ambiguous in its polarization dependence. The shift in the energy of the π^* transition indicate two different π states on nitrogen. This is in contrast to the carbon edge where we see a sharp, non-interacting π^* resonance at normal photon incidence and a broad but unshifted resonance at grazing photon incidence. The interpretation of this is complicated by the 300 K behavior of acetonitrile.

Figure 62 is the carbon edge NEXAFS spectra for acetonitrile dosed to saturation at 300 K. The nitrogen edge shows no adsorption features, indicating a total loss of nitrogen from the surface. Figure 62 should be compared with figure 58 - a remarkable similarity can be seen. To summarize the observations, acetonitrile in the environment of the NEXAFS experiment (~1 - 2 hours, photon flux of $\sim 10^{10}$ ~300 eV photons/second and the attendant electron flux) at 90 K is stable, while to some extent at 180 K and completely at 300 K is unstable and at 300 K forms ethylidyne. This reaction probably requires the electron flux - the TDS and HREELS experiments saw no evidence for decomposition. The conversion of a acetonitrile to nitrogen and ethylidyne has precedence in the organometallic literature in the metathesis reaction.

Metathesis is the process by which substituted multiple bonds may be induced to exchange substitutents e.g. RCCR + R'CCR' -> 2RCCR'. This process is catalyzed by homogeneous tungsten, molybdenum, tantalum, and niobium complexes or heterogeneously using the tungsten, molybdenum, or

rhenium oxides. The reaction rate is increased by aluminium salts as co-catalysts[90]. A similar reaction with acetonitrile would yield N_2 and MeCCMe (2 butyne). An investigation of the accepted mechanisms for metathesis show that ethylidyne would be the expected fate of the carbonaceous fragment.

Figure 63a shows the two proposed mechanisms for olefin metathesis. Mechanism 1 proceeds through a dimer, which then cleaves to form the products. There is precedence for polymers from nitriles on platinum[91], but these polymers have been of the $(CN)_x$ type. This mechanism is not the presently accepted one - it does not explain the statistical distribution of the products. The other mechanism proceeds through a metallacyclobutane intermediate (2). These intermediates can be prepared independently and are active in metathesis.

Figure 63b shows the similar mechanisms for the surface case. Here the carbonaceous intermediate is intercepted to form the more stable ethylidyne intermediate before it can form the alkyne. The required insertion of a metal into the C-N triple bond has precedence in the literature[94], in which $W_2(OCMe_3)_6$ reacts with the cyanide group and splits up to give a tungsten nitride and a tungsten alkylidyne. The subsequent reaction of the surface nitride to give N_2 and more ethylidyne requires that the surface be warm enough to allow surface migration of the acetonitrile. This mechanism is the one we prefer - the surface cyclobutadiene - like intermediate of mechanism 1 has been earlier shown in this thesis to be not particularly stable. The nitride intermediate has precedent in nitrile chemistry[91b], and is stable to 600 K[93], and thus the mechanism allows the nitride some significant residence time and thus relaxes the entropic requirements of the first

mechanism, which requires the dimer and the activating electron to be in the interaction region all at the same time.

We propose then a reaction of acetonitrile in the presence of electron flux that produces N_2 and ethylidyne. N_2 on the surface should desorb at around 200 K - 300 K[93], leaving only the ethylidyne to be observed by NEXAFS. Now the interpretation of the shift of the nitrogen π^* transition becomes possible - it is due to the intermediate (either surface nitride or possibly the acetonitrile dimer) that has been frozen out by the cessation of the migration of acetonitrile after the momentary anneal.

In conclusion our data is consistent with the proposed[89] parallel chemisorption of acetonitrile on Pt(111). We investigated a number of nitriles to determine if normal coordination (similar to CO) could be found for any case. We operated on two models: that the parallel chemisorption was due to steric effects of the methyl group on the carbon (and thus we examined methyl isocyanide and hydrogen cyanide) or the carbon was too electropositive to allow nitrogen coordination (similar to the coordination complex case) due to inadequate antibonding orbital density at the carbon. We studied trifluoroacetonitrile in an attempt to increase the electronegativity of the carbon. The spectra are presented in appendix B for completeness and as a guide to other NEXAFS investigations - parallel coordination seems to predominate, with the possible exception of the high temperature hydrogen cyanide and methyl isocyanide state.

III.7.4 FIGURES

Figure 55

NEXAFS spectra at normal photon incidence for saturation coverage of CO on clean (a) and Na predosed (to 0.2 monolayer) (b) Pt(111)[16g]. Peak A is the π^* transition. (c) shows (a) and (b) superimposed after the dotted background had been subtracted and (a) was shifted by 0.6 eV so as to put the π^* transition maximum at the same energy. Note the decrease in the intensity of (b). XPS denotes the C 1s binding energies.

Figure 56

NEXAFS spectra at grazing photon incidence for CO on clean and Na predosed Pt(111)[16g]. (a) is the carbon K edge spectra and (b) is the oxygen K edge spectra. Peak A is the π^* transition and peak B is the σ transition. Note the strong shift of the σ resonance towards lower photon energy at both edges.

Figure 57

NEXAFS spectra of ethylene dosed to saturation at 90 K. Note the polarization dependence in the π^* region and the σ resonance at normal photon incidence, indicating parallel coordination.

Figure 58

NEXAFS spectra of ethylene dosed to saturation at 300 K. Note the lack of polarization dependence in the π^* region and the strong σ resonance at grazing photon incidence (peak D), indicating a bond vector normal to the surface.

Figure 59

Acetylene annealing set. (a) is a monolayer prepared by dosing to saturation at 90 K. (b) is the state of (a) annealed to 345 K. (c) is

the state of (b) annealed to 520 K. Note the similarity of (b) to features in the published NEXAFS spectra of ethylene prepared under similar circumstances[8] and figure 58.

Figure 60

Proposed surface species for the thermal evolution of an acetylene overlayer on Pt(111). (a) is the low temperature (i.e. 90 K) situation: primarily parallel bound acetylene with some possible vinylidyne. (b) is the room temperature situation: primarily ethylidyne with methylidyne. (c) is the high temperature state (520 K): primarily methylidyne with some residual parallel and normal diatomic species.

Figure 61

NEXAFS spectra of acetonitrile ice (a) and monolayer (b). The monolayer was obtained by annealing the ice momentarily to 180 K and cooling to 90 K. Note the shift of the π^* transition at the nitrogen edge and not at the carbon edge, suggesting two different π states at the nitrogen.

Figure 62

Carbon edge NEXAFS spectra for acetonitrile dosed to saturation at 300 K. The spectra were taken at 300 K. There was no adsorption at the nitrogen edge. Note the strong similarity to figure 58.

Figure 63

Proposed mechanisms for olefin metathesis on homogeneous metal centers (a) and on surfaces (b). Mechanism (1) is the cyclobutadiene mechanism (which is not the favored mechanism) and (2) is the generally accepted metallacyclobutane mechanism. For acetonitrile X is CMe and Y is N.

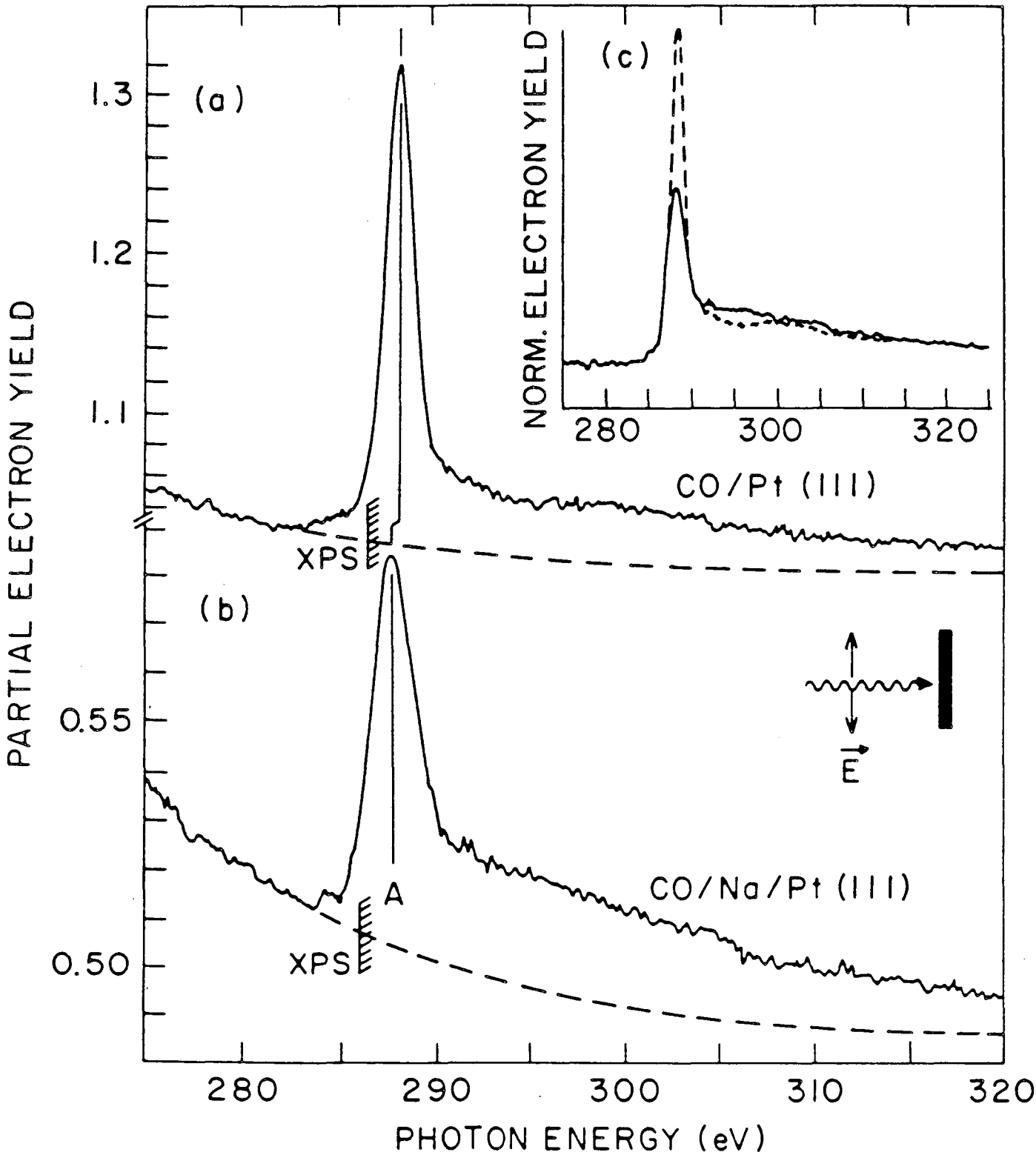
(a)
(b)
(c)
1.3
1.2
1.1
0.55
0.50
PARTIAL ELECTRON YIELD
NORM. ELECTRON YIELD
280
300
320
CO/Pt (111)
CO/Na/Pt (111)
XPS
XPS
A
E
280
290
300
310
320
PHOTON ENERGY (eV)

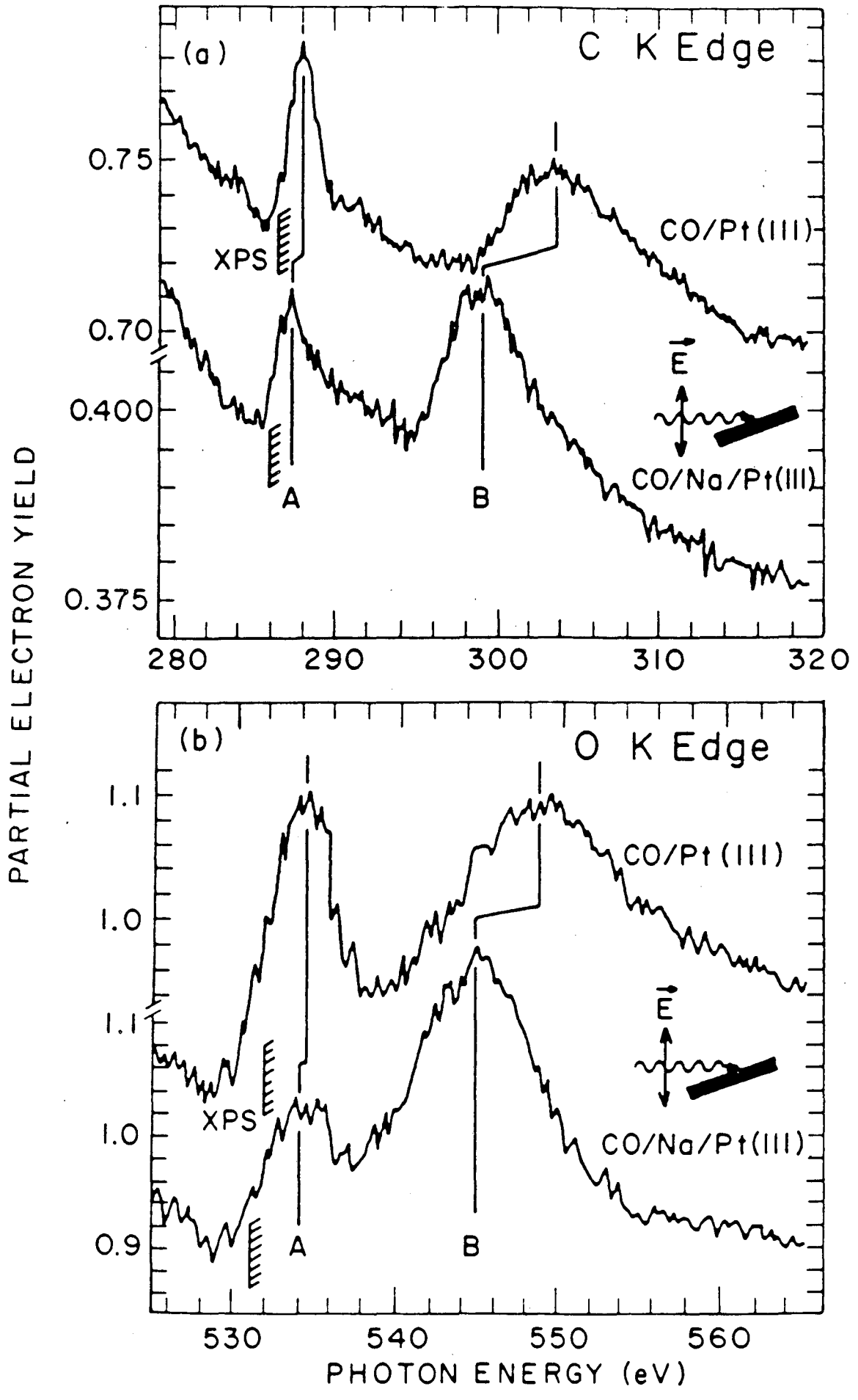
(a)
C K Edge
0.75
0.70
0.400
0.375
XPS
A
B
CO/Pt(111)
CO/Na/Pt(111)
E
280
290
300
310
320
(b)
O K Edge
1.1
1.0
1.1
1.0
0.9
XPS
A
B
CO/Pt(111)
CO/Na/Pt(111)
E
530
540
550
560
PHOTON ENERGY (eV)
PARTIAL ELECTRON YIELD

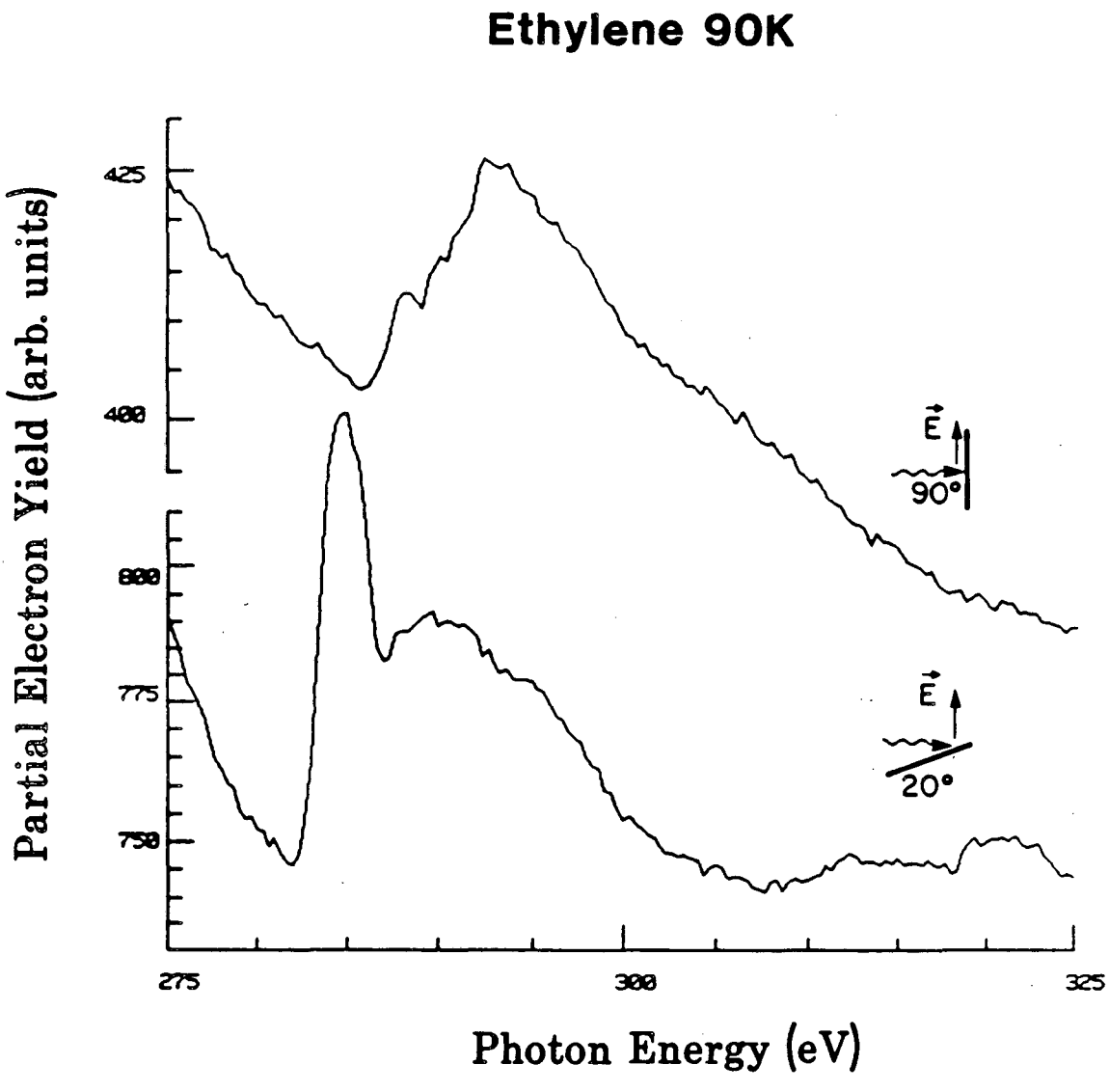

XBL 8512-5146

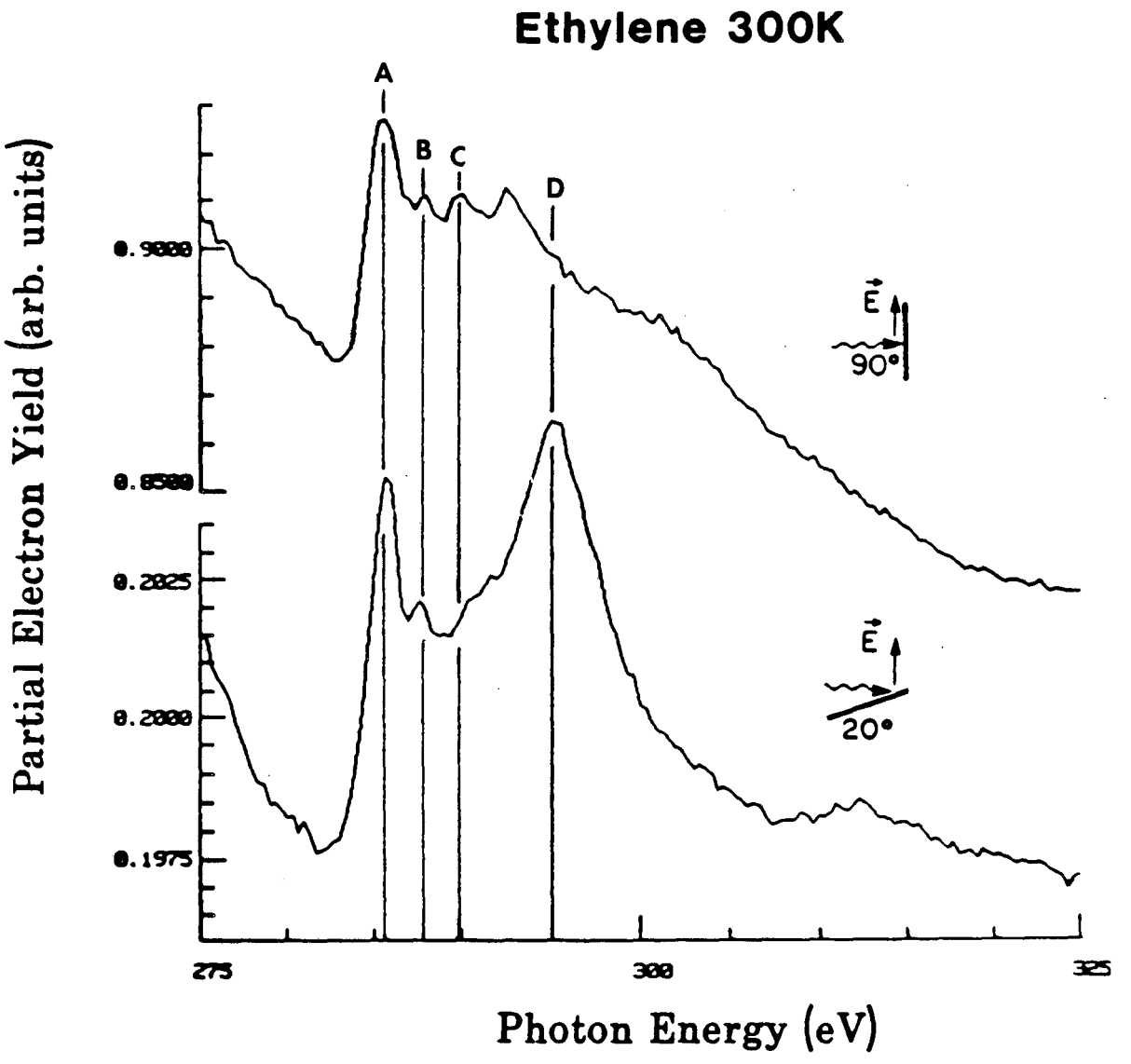

XBL 8512-5144

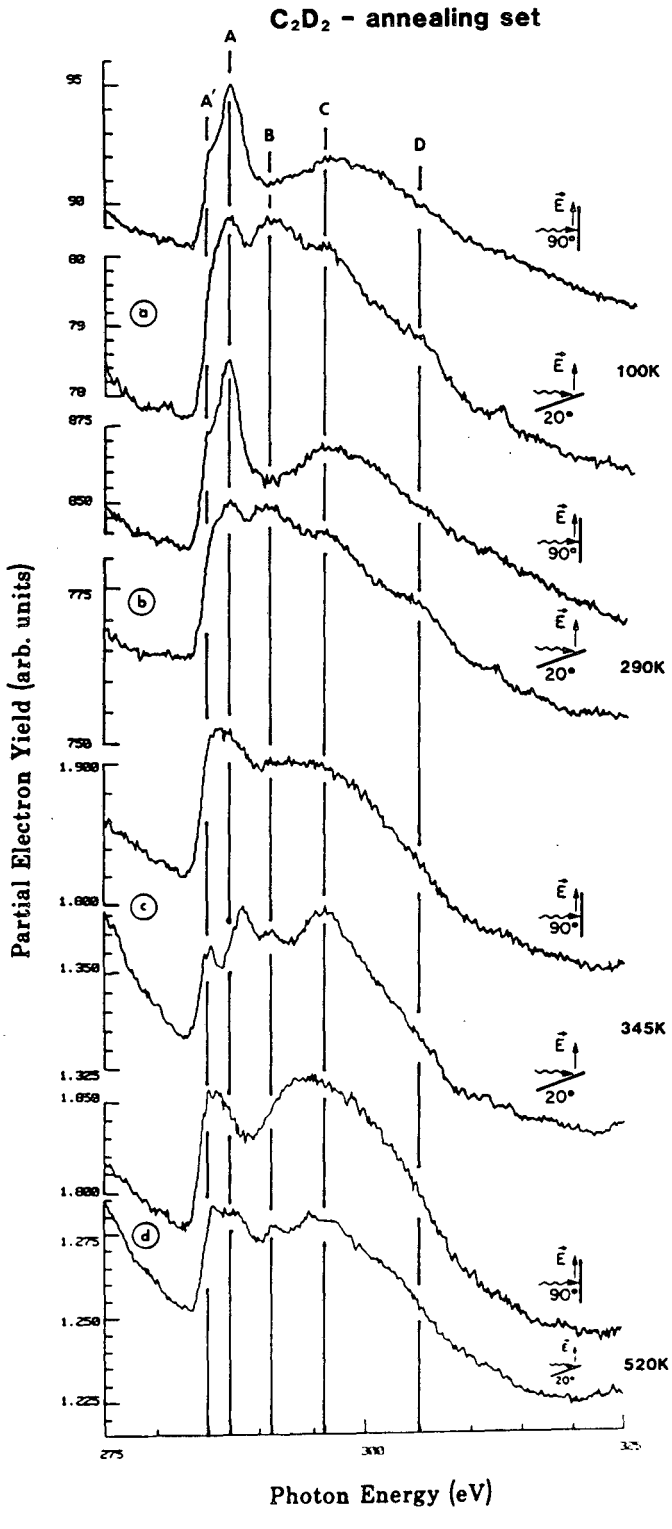

XBL 8512-5099

C_2H_2 proposed structures

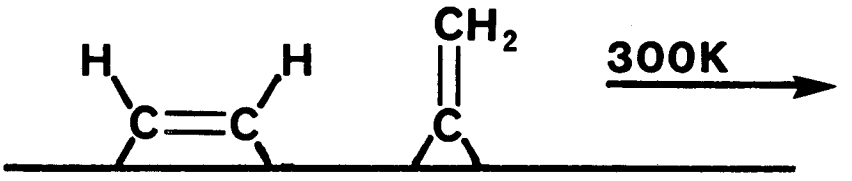

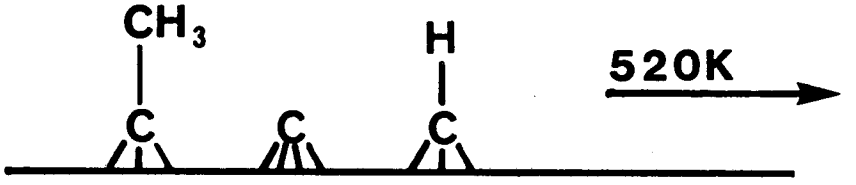

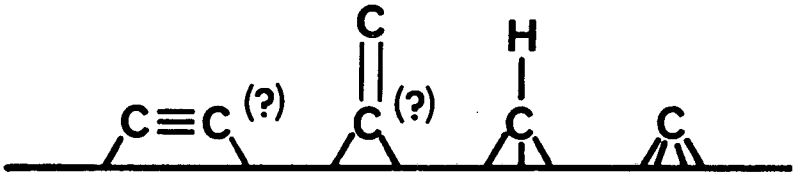

XBL 861-7

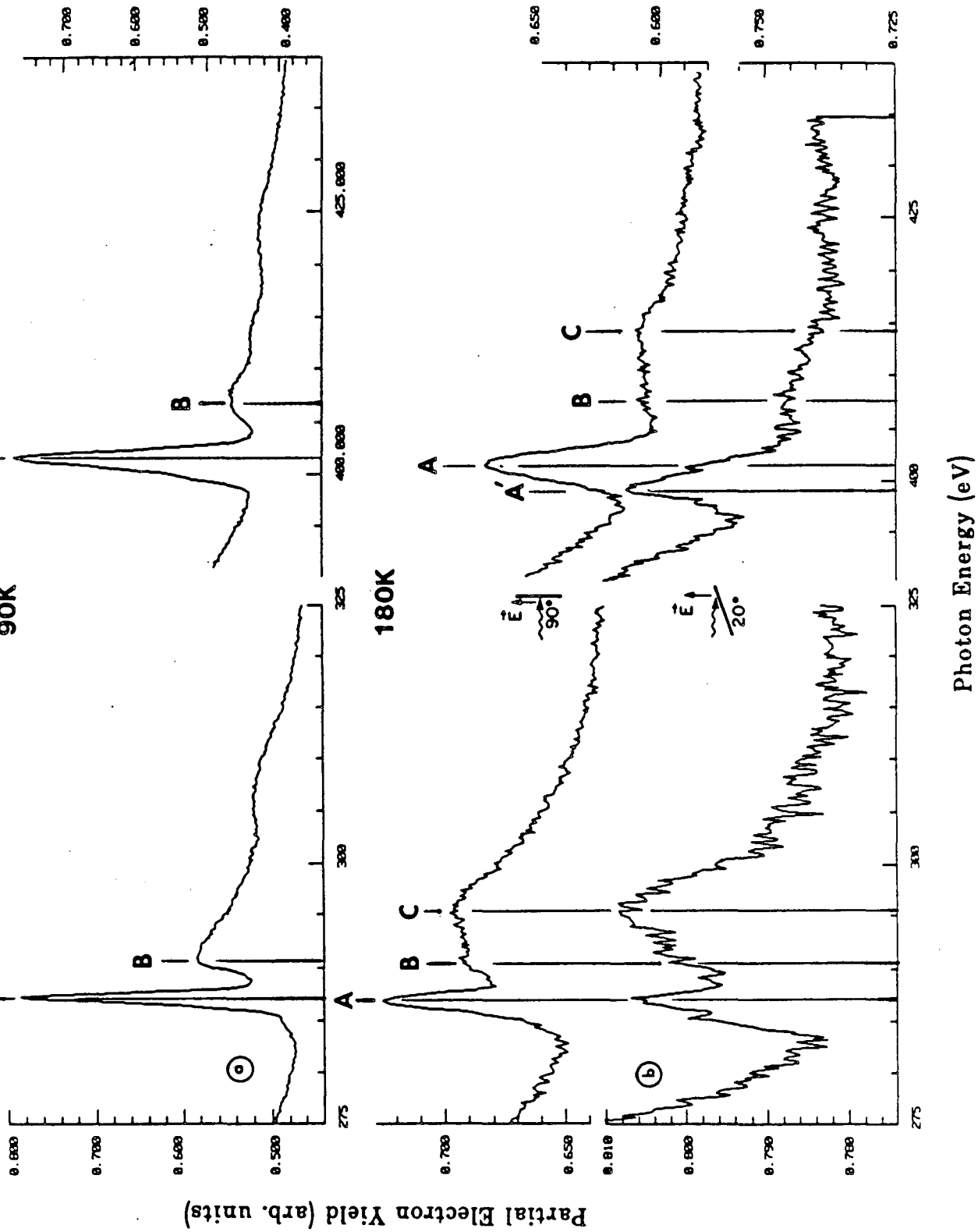
Acetonitrile
90K
180K
A
B
C
A'
(a)
(b)
Partial Electron Yield (arb. units)
Photon Energy (eV)

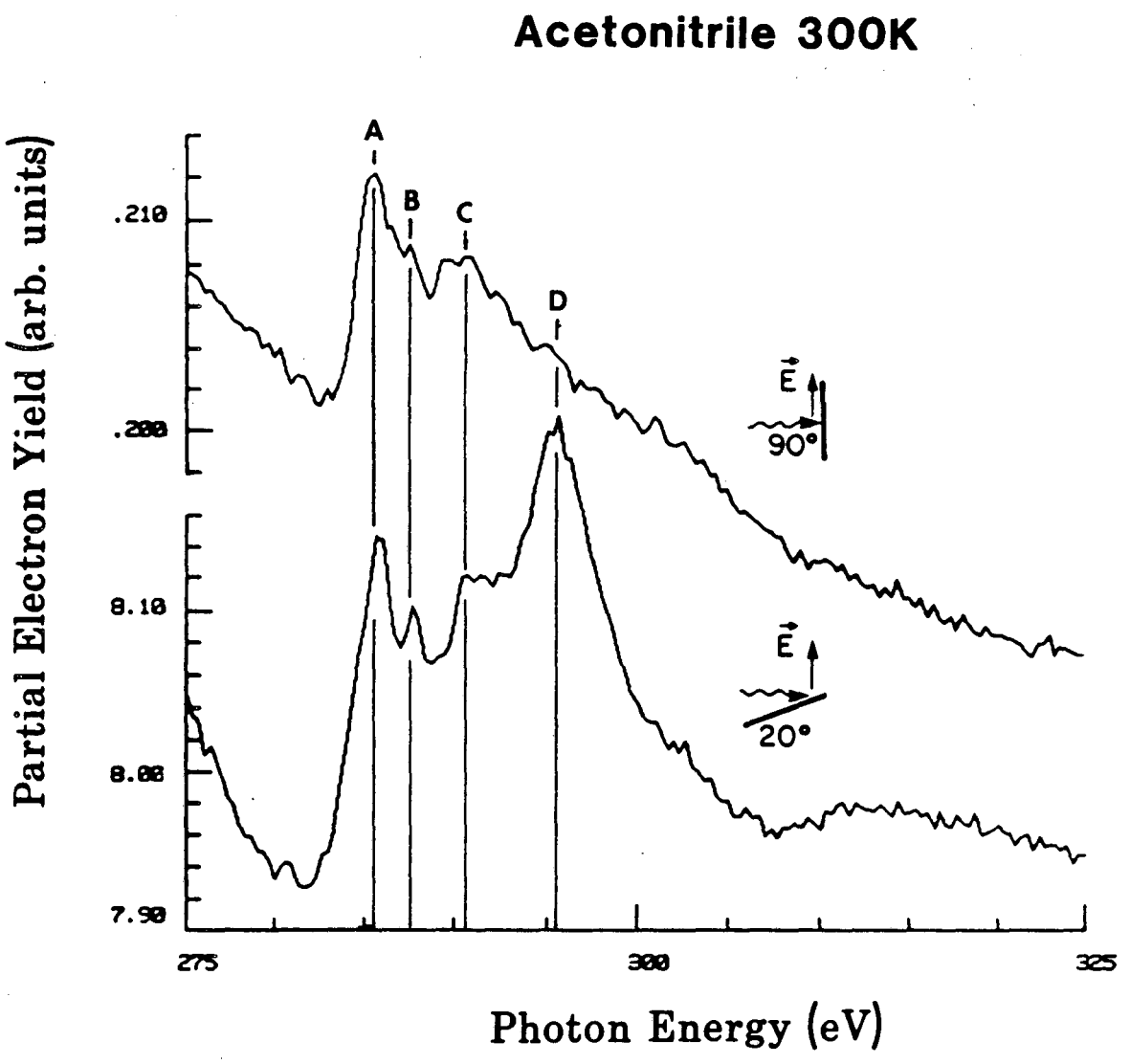

XBL 8512-5145

Metathesis

a.

1. $M + X \equiv Y \longrightarrow \overset{X \equiv Y}{\underset{M}{|}} + X \equiv Y \longrightarrow$

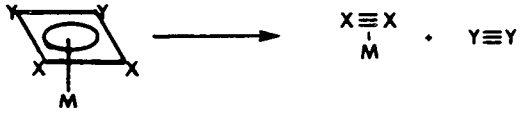

2. $2M + X \equiv Y \longrightarrow\!\!\longrightarrow M \equiv X + M \equiv Y$

$M \equiv Y + X \equiv Y \longrightarrow \overset{X \equiv Y}{\underset{M \equiv Y}{|}} \longrightarrow$

b.

1. $\xrightarrow{e^-\ ?}$

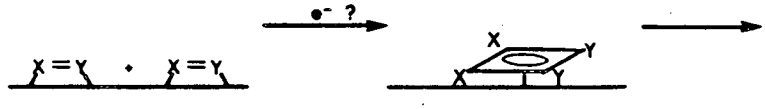

$\longrightarrow$

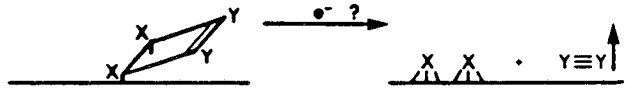

$\xrightarrow{e^-\ ?}$

2. $\xrightarrow{e^-\ ?}$

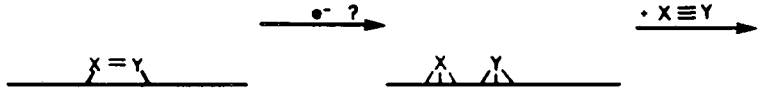

$\xrightarrow{+ X \equiv Y}$

$\xrightarrow{e^-\ ?}$

IV SUMMARY

We have investigated a number of aromatic and pseudo diatomic systems and in the process demonstrated some of the utilities and failings of NEXAFS.

Benzene is the archetypical aromatic system. We found it to be π coordinated at temperatures below that required for decomposition. At higher temperatures we studied the NEXAFS spectra for information on the structure of the decomposed benzene and found that the σ bonds seemed to remain parallel to the surface, while π^* intensity indicative of π orbitals parallel to the surface appeared. We proposed a benzyne-like species.

The fluorinated benzenes allowed the systematic variation of HOMO and LUMO levels to determine the relative effects of donor verses acceptor interactions in aromatic π coordiation. We found that the effect was not simple: the temperature of the desorption dropped until trifluorobenzene and then increased. We suggested the possible competing effects of steric interactions between the fluorines and the surface and the donor/ acceptor effects of the metal surface and further suggested that they might be important for hydrogen.

Pyridine was a system where quantitative estimates of relative angle between the π system and the surface. We found that there was a temperature dependent change in the ring tilt and attribute it to the formation of a metal - carbon bonded α-pyridyl.

Thiophene showed how NEXAFS can determine bond cleavages that do not lead to volatile products by the variation of the molecular resonances. Thiophene is π coordinated at low temperature and forms a vinyl bridged diethylidyne after sulfur loss.

Similarly, the cyclic polyenes showed how the appearance of molecular features can indicate chemical change, in this case by the growth of the π^* transitions. The C_4 and C_8 polyenes did not form flat surface states, whereas the C_5, C_6, ande C_7 rings did, suggesting that the degree of interaction was not sufficient to invalidate gas phase aromaticity rules.

The insensitivity of NEXAFS to co-adsorbates lead to the investigation of CO on a Na modified Pt(111) surface. We found that the CO maintained its perpendicular orientation and that the bond length of the CO increased, in accord to the electronic effect model. The other diatomics chemisorbed parallel to the surface at low temperature. An unusual decomposition of acetonitrile was noted and a mechanism proposed. The observation of decomposition due to electron flux suggests that there are limits in some cases to the photon flux that can be used to study the system.

NEXAFS has shown itself to be a powerful technique for the determination of structural parameters of partially ordered systems, such as on might find in a reacting system. The present limitations have to do with the detection method - electron detection is only compatible with high vacuum or better and is plagued by inelastic components to the spectra. Recent work with fluorescence detection have promised improvements in the ability to reliably normalize the spectra and use the technique in higher pressures.

This work should be expanded in several directions. More time should be spent with submonolayer coverages, rather than investigating saturation coverages exclusively. Also, the effects of π verses σ

coordination should be extended to both more and less reactive metals. The proposed mechanisms should be tested, by for example for the acetonitrile decomposition, independent generation of the proposed intermediates and the study of them in isolation and in the reacting environment.

V BIBLIOGRAPHY

1. "The Compact Edition of the Oxford English Dictionary", J. Murray, et. al. eds., Oxford University Press, New York, 1971

2.a. L. D. Marks Surf. Sci. 1984, 139, 281

b. R. S. Becker, J. A. Golovchenko, B. S. Swartzentruber Phys. Rev. Lett. 1985, 54, 2678

c. H.H. Farrell, M. Levinson Phys. Rev. B 1985, 31, 3593

3. T. E. Madey, D. E. Ramaker, and R. Stockbauer Ann. Rev. Phys. Chem. 1984, 35, 215

4.a. S. Lehwald, H. Ibach, J. E. Demuth Surf. Sci. 1978, 78, 577

b. N. V. Richardson Surf. Sci. 1979, 87, 622

c. J. C. Bertolini, J. Rousseau Surf. Sci. 1979, 89, 467

d. G. D. Waddill, L. L. Kesmodel , preprint of "Benzene chemisorption on palladium surfaces"

5. J. E. Demuth Surf. Sci. Lett. 1980, 93, L82

6.a. J. E. Demuth, K. Christmann, P. N. Sanda Chem. Phys. Lett. 1980 76, 201

b. Ph. Avouris, J. E. Demuth J. Chem. Phys. 1981, 75, 4783

c. Ph. Avouris, N. J. DiNardo, J. E. Demuth J. Chem. Phys. 1984, 80, 491

d. N. J. DiNardo, Ph. Avouris, J. E. Demuth J. Chem. Phys. 1984, 81, 2169

7. J. A. Horsley, J. Stöhr, A. P. Hitchcock, D. C. Newbury, A. L. Johnson, F. Sette J. Chem. Phys. submitted

8.a. R. J. Koestner, J. Stöhr, J. L. Gland, J. A. Horsley Chem. Phys. Lett. 1984, 105, 332

b. J. A. Horsley, J. Stöhr, R. J. Koestner J. Chem. Phys., 83, 1985,

3146

9.a. P. A. Redhead Trans. Farad. Soc. 1961, 62, 8

b. P. A. Redhead Vacuum 1962, 12, 203

c. G. Carter Vacuum 1962, 12, 245

d. D. A. King Surf. Sci. 1975, 47, 384

e. J. L. Falconer, R. J. Madix J. Catal. 1977, 48, 262

f. J. L. Taylor, W. H. Weinberg Surf. Sci. 1978, 78, 259

g. C.-M. Chan, R. Aris, W. H. Weinberg Appl. Surf. Sci. 1978, 1, 360

h. C.-M. Chan, W. H. Weinberg Appl. Surf. Sci. 1978, 1, 377

i. A. Redondo, Y. Zeiri, W. A. Goddard, III Phys. Rev. Lett. 1982, 49 1847

j. J. M. Soler, N. Garcia Surf. Sci. 1983, 124, 563

10.a. A. Bianconi, S. Doniach, D. Lublin Chem. Phys. Lett. 1978, 59, 121

b. M. Belli, A. Scafati, A. Bianconi, S. Mobilio, L. Palladino, A. Reale Solid State Commun. 1980, 35, 355

c. much of part III and some of part VII in "EXAFS and Near Edge Structure", A. Bianconi, L. Incoccia, S. Stipcich eds. Springer Series in Chemical Physics 27, Springer-Verlag, New York

11. M. Inokuti Rev. Mod. Phys. 1971, 43, 297

12.a. J. E. Müller, W. L. Schaich Phys. Rev. B, 1983, 27, 6489

b. D. Normal, J. Stöhr, R. Jaeger, P. J. Durham, J. B. Pendry Phys. rev. Lett., 1983, 51, 2052

c. G. Bunker, E. A. Stern Phys. Rev. Lett., 1984, 52, 1990

d. D. D. Vvedensky, D. K. Saldin, J. B. Pendry "Multiple Scattering Effects in Near-Edge X-ray Absorption Spectra" presented at the 1st

International Conference on the Structure of Surfaces, Berkeley, California, USA, 13-16 August, 1984

13.a. J. L. Dehmer, D. Dill Phys. Rev. Lett. 1975, 35, 213

b. J. W. Davenport Phys. Rev. Lett. 1976, 36, 945

c. J. W. Davenport J. Vac. Sci. Technol. 1978, 15, 433

d. S. Wallace, D. Dill Phys. Rev. B 1978, 17, 1692

e. S. Wallace, D. Dill, J. L. Dehmer Phys. Rev. B 1978, 17, 2004

f. T. Gustafsson Surf. Sci. 1980, 94, 593

g. D. Dill, J. R. Swanson, S. Wallace, J. L. Dehmer Phys. Rev. Lett. 1980, 45, 1393

h. J. L. Dehmer, D. Dill, A. C. Parr "Photoionization of Small Molecules" in Photophysics and Photochemistry in the Vacuum Ultraviolet, 1985, D. Reidel Publishing Co., 341

i. ref. 8a.

j. ref. 7.

14.a. M. R. Hermann, R. W. Langhoff Chem. Phys. Lett., 1981, 82, 242

b. M. R. Hermann, P. W. Langhoff Phys. Rev. A, 1983, 28, 1957

c. M. R. Hermann, S. R. Langhoff, P. W. Langhoff Chem. Phys. Lett., 1984, 109, 150

d. M. R. Hermann, G. H. F. Diercksen, B. Fatyga, P. W. Langhoff to be published

15. L. Xiao-Ling, P. Xiao-Chuan, L. Jia-Ming, C. M. Lee Chinese Phys. Lett. submitted

16a. C. R. Natoli in ref 10c, page 43

b. A. Bianconi, M. Dell'Ariccia, A. Gargano, and C. R. Natoli in ref 10c, page 57

c. A. P. Hitchcock, S. Beaulieu, T. Steel. J. Stöhr, F. Sette J. Chem.

Phys., 1984, 80, 3927

d. F. Sette, J. Stöhr, A. P. Hitchcock Chem. Phys. Lett., 1984, 110, 517

e. J. Stöhr, F. Sette, A. L. Johnson Phys. Rev. Lett., 1984, 53, 1684

f. F. Sette, J. Stöhr, A. P. Hitchcock J. Chem. Phys., 1984, 81, 4906

g. F. Sette, J. Stöhr, E. B. Kollin, D. J. Dwyer, J. L. Gland, J. L. Robbins, A. L. Johnson Phys. Rev. Lett., 1985, 54, 935

17. J. Stöhr "Everything You Always Wanted to Know About SEXAFS but Were Afraid to Ask" in Principles, Applications, and Techniques of EXAFS, SEXAFS, and XANES to be published by Johm Wiley and Sons, NY, R. Prins and D. C. Konigsberger, eds.

18.a. R. Jaeger, J. Feldhaus, J. Haase, J. Stöhr, Z. Hussain, D. Menzel, D. Norman Phys. Rev. Lett., 1980, 45, 1870

b. R. Jaeger, J. Stöhr, J. Feldhaus, S. Brennan, D. Menzel Phys. Rev. B, 1981, 23, 2102

c. R. Jaeger, J. Stöhr, R. Treichler, K. Baberschke Phys. Rev. Lett., 1981, 47, 1300

d. J. Stöhr, R. Jaeger, S. Brennan Surf. Sci., 1982, 117, 503

e. R. Jaeger, R. Treichler, J. Stöhr Surf. Sci., 1982, 117, 533

19.a. R. Baudoing, E. Blanc, C. Gaubert, Y. Gauthier, N. Gnuchev surf. Sci., 1983, 128, 22

b. E. Umbach, Z. Hussain Phys. Rev. Lett., 1984, 52, 457

c. L. Ungier, T. D. Thomas J. Chem. Phys., 1985, 82, 3146

d. J. W Gadzuk Surf. Sci., 60, 1976, 76

20.a. D. Norman, P. J. Durham, J. B. Pendry, J. Stöhr, R. Jeager in ref. 10c, 146

b. J. Stöhr, K. Baberschke, R. Jeager, R. Treichler, S. Brennan Phys. Rev. Lett., 1981, 47, 381

c. J. Stöhr, R. Jaeger Phys. Rev. B, 1982, 26, 4111

21. J. Stöhr Characterization of the Grasshopper Monochromator, part of the SSRL beam line I-1 documentation

22. F. Sette, J. Stöhr, E. Kollin, D. J. Dwyer, J. L. Gland, J. L. Robbins, A. L. Johnson Phys. Rev. Lett., 1985, 54, 935

23.a. M.-C. Tsai, J. Stein, C. M. Friend, and E. L. Muetterties J. Am. Chem. Soc. 1982, 104, 3533

b. M.-C. Tsai, Ph.D. thesis, University of California, Berkeley, 1982

c. M.-C. Tsai, C. M. Friend, and E. L. Muetterties J. Am. Chem. Soc. 104, 2539 (1982)

24. E. Shusterovich, R. C. Baetzold, E. L. Mutterties J. Phys. Chem., 1983, 87, 1100

25.a. J. L. Gland and G. A. Somorjai Surf. Sci., 1973, 38, 157

b. P. C. Stair, G. A. Somorjai J. Chem. Phys., 67, 1977, 4361

c. B. E. Nieuwenhuys, D. J. Hagen, G. Rovida, and G. A. Somorjai Surf. Sci., 1976, 59, 155

d. T. E. Fisher, S. R. Kelemen, and H. P. Bonzel Surf. Sci., 1977, 64, 157

e. B. E. Nieuwenhuys and G. A. Somorjai Surf. Sci., 1978, 72, 8

f. P. C. Stair, Ph.D. thesis, university of Calfornia 19

g. R. J. Koestner, Ph.D. thesis, University of California 1982

h. G. Broden, T. Rhodin, and W. Capehart Surf. Sci., 1976, 61, 143

i. M. A. Van Hove, R. F. Lin, G. A. Somorjai Phys. Rev. Lett., 51, 1983, 778

j. M. A. Van Hove private communication

26.a. J. C. Bertolini, G. Dalmai-Imelik, and J. Rousseau Surf. Sci., 1977, 67, 478

b. S. Lehwald, H. Ibach, and J. E. Demuth Surf. Sci., 1978, 78, 577

c. J. C. Bertolini and J. Rousseau Surf. Sci., 1979, 89, 467

d. F. P. Netzer, E. Bertel, and J. A. D. Matthew Surf. Sci., 1980, 92, 43

e. B. E. Koel, J. E. Crowell, C. M. Mate, and G. A. Somorjai J. Phys. Chem., 1984, 88, 1988

f. M. Abron, J. C. Bertolini, J. Billy, J. Massardier, B. Tardy Surf. Sci., 162, 1985, 395

27.a. J. E Demuth and D. E. Eastman Phys. Rev. B, 1976, 13, 1523

b. D. R. Lloyd, C. M. Quinn, and N. V. Richardson Solid St. Comm., 1977, 23, 141

c. G. L. Nyberg and N. V. Richardson Surf. Sci., 1979, 85, 335

d. S. R. Kelemen and T. E. Fisher Surf. Sci., 1981, 102, 45

e. P. Hofmann, K. Horn, and A. M Bradshaw Surf. Sci., 1981, 1260,

f. N. V. Richardson and N. R. Palmer Surf. Sci., 1982, 114, L1

28. A. L. Johnson, E. L. Muetterties, and J. Stöhr, J. Am. Chem. Soc., 1983, 105, 7183

29. A. P. Hitchcock and C. E. Brion J. Electron Spectrom. and Rel. Phenom. 10, 317 (1977)

30.a. H. Friedrich, B. Pittel, P. Rabe, W. H. E. Schwartz, B. Sonntag J. Phys. B: Atom. Molec. Phys., 13, 1980, 25

b. M. B. Robin "Higher Excited States of Polyatomic Molecules", Academic Press, New York, 1974

31. H. Steininger, H. Ibach, S. Lehwald Surf. Sci., 117, 1982, 685

32.a. E. L. Garfunkel, J. J. Mai, J. C. Frost, M. H. Farias, G. A. Somorjai J. Phys. Chem., 87, 1983, 3629

b. J. E. Crowell Ph.D. thesis, University of California, Berkeley, 1984

33.a. R. D. Smith, A. L. Johnson Combustion and Flame, 51, 1983, 1

b. S. H. Bauer, C. F. Aten Chem. Phys., 39, 1963, 1253

34. R. A. Rosenberg, P. J. Love, V. Rehn "EXAFS and Near Edge Structure III", K. O. Hodson, B. Hedman, J. E. Penner-Hahn eds., Springer Proc. in Phys. 2, Springer-Verlag, Berlin 1984

35. R. F. Willis, B. Fitton, G. S. Painter Phys. Rev. B, 9, 1974, 1926

36. N. V. Richardson, N. R. Palmer Surf. Sci., 114, 1982, L1

37. E. Bechtold Appl. Surf. Sci., 7, 1981, 231

38. E. L. Muetterties, R. M. Wexler Surv. Prog. Chem., 10, 1983, 61

39. W. Erley Surf. Sci., 94, 1980, 281

40.a. T. A. Clarke, R. Mason, M. Tescari Proc. R. Soc. Lond. A., 331, 1972, 321

b. T. A. Clarke, I. D. Gay, R. Mason Chem. Phys. Lett., 27, 1974, 562

c. T. A. Clarke, I. D. Gay, R. Mason J. Chem. Soc. Chem. Comm., 1974, 331

d. T. A. Clarke, I. D. Gay, B. Law, R. Mason Fara. Disc. Chem. Soc., 60, 1975, 119

e. R. Mason, M. Textor, Y. Iwasawa, I. D. Gay Proc. R. Soc. Lond. A., 354, 1977, 171

41.a. J. A. Evans, D. R. Russell Chem. Comm., 1971, 197

b. L. J. Guggenburger, R. Cramer J. Am. Chem. Soc., 94, 1972, 3779

42.a. M. J. McGlinchey, T.-S. Tan Can. J. Chem., 52, 1974, 2439

b. T.-S. Tan, M. J. McGlinchey J. Chem. Soc. Chem. Comm., 1976, 155

c. M. J. McGlinchey, T.-S. Tan J. Am. Chem. Soc., 98, 1976, 2271

d. A. Agarwal, M. C. McGlinchey, T.-S. Tan J. Organomet. Chem., 141, 1977, 85

e. N. Hao, M. C. McGlinchey J. Organomet. Chem., 161, 1978, 381

f. N. Hao, M. C. McGlinchey J. Organomet. Chem., 165, 1979, 225

g. J. D. Laposa, N. Hao, B. G. Sayer, M. C. McGlinchey J. Organomet. Chem., 195, 1980, 193

h. R. Faggiani, N. Hao, C. J. L. Lock, B. G. Sayer, M. J. McGlinchey Organometalics, 2, 1983, 96

43. K. J. Klabunde, H. F. Efner Inorg. Chem., 14, 1975, 789

44. J. L. Stickney, M. P. Soriaga, A. T. Hubbard, S. E. Anderson J. Electroanal. Chem., 125, 1981, 73

45. A. B. Anderson, M. R. McDevitt, F. L. Urbach Surf. Sci., 146, 1984, 80

46. E. L. Garfunkel, J. J. Mai, J. C. Frost, M. H. Farias, G. A. Somojai J. Phys. Chem., 87, 1983, 3629

47. E. Shusterovich, R. C. Baetzold, E. L. Muetterties J. Phys. Chem., 87, 1983, 1100

48.a. A. Van der Avoird Surf. Sci., 18, 1969

b. L. W. Bruch, J. M. Phillips, X.-Z. Ni Surf. Sci., 136, 1984, 361

49. R. M. Wexler, PhD thesis, University of California, Berkeley 1983

50. R. M. Wexler, M.-C. Tsai,C. M. Friend, E. L. Muetterties J. Am. Chem. Soc., 104, 1982, 2034

51. H. J. Robota, P. M. Whitmore, C. B. Harris J. Chem. Phys., 76(4), 1982, 1692

52. Ph. Avouris, N. J. DiNardo, J. E. Demuth J. Chem. Phys., 80(1), 1984, 491

53. N. J. DiNardo, Ph. Avouris, J. E. Demuth J. Chem. Phys., 81(4), 1984, 2169

54. B. J. Bandy, D. R. Lloyd, N. V. Richardson Surf. Sci., 89, 1979, 344

55. G. L. Nyberg Surf. Sci., 95, 1980, L273

56. M. Mate, G. A. Somorjai Proceedings First Internat. Conf. on the Structure of Surfaces (ICSOS I) August 1984, Berkeley CA. Springer Series in Chemical Physics (to be published)

57. F. P. Netzer, P. Mack Chem. Phys. Lett., 95(6), 1983, 492

58. F. P. Netzer, P. Mack J. Chem. Phys., 79(2), 1983, 1017

59. J. E. Demuth, K. Christmann, P. N. Sanda Chem. Phys. Lett., 76(2), 1980, 201

60. Ph. Avouris, J. E. Demuth J. Chem. Phys., 75(10), 1981, 4783

61. F. P. Netzer, E. Bertel, J. A. D. Mathew Surf. Sci., 92, 1980, 43

62. J. L. Gland, G. A. Somorjai Surf. Sci., 38, 1973, 157

63. A. L. Johnson, E. L. Muetterties, J. Stohr J. Am. Chem. Soc., 105, 1983, 7183

64. N. V. Richardson Proceedings First Internat. Conf. on the Structure of Surfaces (ICSOS I) August 1984, Berkeley CA. Springer Series in Chemical Physics (to be published)

65. B. L. Henke, P. Lee, T. J. Tanaka, R. L. Shimabukuro, B. K. Fujikawa Atomic Data and Nuclear Data Tables 27, 1982, 1

66. J. Stohr, R. Jaeger Phys. Rev. B, 26, 1982, 4111

67.a. "Handbook of Spectroscopy", J. W. Robinson ed., CRC Press, Cleveland, Ohio 1974

b. R. S. Brown, A. Tse, J. C. Vederas, J. Am. Chem. Soc., 102, 1980, 1174 ; R. S. Brown, A. Tse Can. J. Chem., 58, 1980 694

68.a. R. M. Wexler, Ph.D. thesis, University of California, Berkeley 1983

b. K. L. Shanahan, Ph.D. thesis, University of California, Berkeley 1984

c. T. M. Gentle, Ph.D. thesis, University of California, Berkeley 1984

d. E. L. Muetterties, R. M. Wexler, T. M. Gentle, K. L. Shanahan, D. G. Klarup, A. L. Johnson, V. H. Grassian, K. B. Lewis, T. G. Rucker, R. Lum unpublished manuscript.

69. W. Heegemann, K. H. Meister, E. Bechtold, K. Hayek Surf. Sci., 49, 1975, 161

70. J. Stöhr, J. L. Gland, E. B. Kolin, R. J. Koestner, A. L. Johnson, E. L. Muetterties, F. Sette Phys. Rev. Lett., 53, 1984, 2161

71. N. Avery, private communication

72. E. L. Muetterties, J. R. Bleeke, E. J. Wucherer, T. A. Albright Chem. Rev., 1982, 82, 499

73. E. F. Ashworth et. al. J. C. S. Dalton 1693 (1977), M. Green et. al. J. C. S. Dalton, 1977, 1755

74.a. J. A. Butcher et. al. J. Am. Chem. Soc., 1978, 100, 1012

b. C. A. Harmon et. al. Inorg. Chem., 1977, 16, 2143

c. K. D. Warren Struct. Bonding, 1977, 33, 97

d. D. J. Brauer, C. Kruger Inorg. Chem., 1975, 14, 3053

75. R. H. Grubbs, T. A. Pancoast Synth. React. Inorg. Metal. Org. Chem., 1978, 8, 1

76. A review of the IR spectra of coordination complexes of π bound organo-transition metal complexes may be found in G. Davidson, Organometal. Chem. Rev. A, 1972, 8, 303

77. N. R. Avery Surf. Sci., 1984, 146, 363

78. D. C. Newbury, A. P. Hitchcock, J. Stöhr, A. L. Johnson in preparation

79. (this reference intensionally left blank)

80.a. E. L. Garfunkel, J. E. Crowell, G. A. Somorjai J. Phys. Chem., 86, 1982, 310

b. J. E. Crowell, G. A. Somorjai J. Vac. Sci. Technol. A, 2, 1984, 881

c. E. L. Garfunkel, M. H. Farias, G. A. Somorjai J. Am. Chem. Soc., 107, 1985

d. M. Kudo, E. L. Garfunkel, G. A. Somorjai J. Phys. Chem., 89, 1985, 3207

e. F. P. Netzer, D. L. Doering, T. E. Madey Surf. Sci., 143, L363

81.a. N. D. S. Canning, M. D. Baker, and M. A. Chesters Surf. Sci. 1981, 111, 441

b. S. D. Foulias, K. J. Rawlings, and B. J. Hopkins Surf. Sci. 1982, 114, 1

c. S. D. Foulias, K. J. Rawlings, G. G. Price, and B. J. Hopkins Surf. Sci., 1982, 118, 47

d. S. D. Foulias, K. J. Rawlings, and B. J. Hopkins Surf. Sci., 1983, 133, 377

82.a. ref. 25 h.

b. J. E. Demuth and D. E. Eastman Phys. Rev. B, 1976, 13, 1523

c. J. E. Demuth Chem. Phys. Lett., 1977, 45,1, 12

d. J. E. Demuth Surf. Sci., 1979, 80, 367

e. J. E. Demuth Surf. Sci., 1979, 84, 315

f. M. R. Albert, L. G. Sneddon, W. Eberhardt, F. Greuter, T. Gustafsson, and E. W. Plummer Surf. Sci., 1982, 120, 19

g. W. T. Tysoe, G. L. Nyberg, and R. M. Lambert Surf. Sci., 1983, 135,

128

h. W. Sesselmann, B. Woratschek, G. Ertl, J. Küppers, and H. Haberland Surf. Sci., 1983, 130, 245

83.a. N. Freyer, G. Pirug, and H. P. Bonzel Surf. Sci., 1983, 125, 327

b. N. Freyer, G. Pirug, and H. P. Bonzel Surf. Sci., 1983, 126, 487

c. ref. 2f.

84.a. H. Ibach, H. Hopster, and B. Sexton Appl. Surf. Sci. 1977, 1, 1

b. H. Ibach and S. Lehwald J. Vac. Sci. Technol. 1978, 15, 407

c. C. Backx and R. F. Willis Chem. Phys. Lett. 1978, 53, 471

d. J. C. Bertolini, J. Massardier, and G. Dalmai-Imelik J. Chem. Soc. Far. I 1978, 74, 1720

e. L. H. Dubois, D. G. Castner, and G. A. Somorjai J. Chem. Phys. 1980, 72, 5234

f. A. M. Baro and H. Ibach J. Chem. Phys. 1981, 74, 4194

g. H. Ibach and S. Lehwald J. Vac. Sci. Technol. 1981, 18, 625

h. J. A. Gates and L. L. Kesmodel Surf. Sci., 1982, 120, L461

i. W. Erley, A. M. Baro, and H. Ibach Surf. Sci. 1982, 120, 273

j. J. A. Gates and L. L. Kesmodel J. Chem. Phys. 1982, 76, 4281

k. E. M. Stuve, R. J. Madix, and B. A. Sexton Surf. Sci. 1982, 123, 491

l. C. Nyberg, C. G. Tenstål, S. Andersson, and M. W. Holmes Chem. Phys. Lett. 1982, 87, 87

m. C. E. Anson, B. J. Bandy, M. A. Chesters, B. Kieller, I. A. Oxton, and N. Sheppard J. Electron Spectrom. and Rel. Phenom. 1983, 29, 315

n. L. L. Kesmodel and J. A. Gates J. Electron Spectrom. and Rel. Phenom. 1983, 29, 307

o. J. A. Gates and L. L. Kesmodel Surf. Sci. 1983, 124, 68

p. L. L. Kesmodel J. Chem. Phys. 1983, 79, 4646

q. U. Seip, M.-C. Tsai, J. Küppers, and G. Ertl Surf. Sci. 1984, 147, 65

r. J. A. Stroscio, S. R. Bare, and W. Ho Surf. Sci. 1984, 148, 499

s. L. L. Kesmodel, G. D. Waddil, and J. A. Gates Surf. Sci. 1984, 138, 464

t. B. J. Bandy, M. A. Chesters, M. E. Pemble, G. S. McDougall, and N. Sheppard Surf. Sci. 1984, 139, 87

u. E. M. Stuve and R. J. Madix J. Phys. Chem. 1985, 89, 105

v. E. M. Stuve, R. J. Madix, and C. R. Brundle Surf. Sci. 1985, 152, 532

85.a. ref. 84e.

b. ref. 82g.

c. ref. 84r.

d. L. L. Kesmodel, P. C. Stair, R. C. Baetzold, and G. A. Somorjai Phys. Rev. Lett., 1976, 36, 1316

e. C. Casalone, M. G. Cattania, and M. Simonetta Surf. Sci., 1981, 103, L121

f. C. Casalone, M. G. Cattania, F. Merati, and M. Simonetta Surf. Sci., 1982, 120, 171

g. ref. 81c.

86.a. R. G. Carr, T. K. Sham, and W. E. Eberhardt Chem. Phys. Lett., 1985, 113, 63

b. ref. 8

87.a. A. Gravezzoti and M. Simonetta Surf. Sci., 1980, 99, 453

b. A. B. Anderson and A. T. Hubbard Surf. Sci., 1980, 99, 384

c. P. Geurts and A. Van der Avoird Surf. Sci., 1981, 102, 185

d. P. Geurts and A. Van der Avoird Surf. Sci., 1981, 103, 416

e. P. Geurts and A. Van der Avoird Surf. Sci., 1981, 103, 431

f. T. E. Felter and W. H. Weinberg Surf. Sci., 1981, 103, 265

g. I. A. Howard and G. Dresselhaus Surf. Sci., 1984, 136, 229

h. S. S. Hiett, F. Flores, P. J. Grout, N. H. March, A. Martin-Rodero, and G. Senatore Surf. Sci., 1984, 140, 400

88.a. C. M. Friend, J. Stein, E. L. Muetterties J. Am. Chem. Soc., 103, 1981, 767

b. C. M. Friend, Ph.D. thesis, University of California, Berkeley 1980

89.a. B. A. Sexton, N. R. Avery Surf. Sci., 129, 1983, 21

b. N. R. Avery, T. W. Matheson Surf. Sci., 143, 1984, 110

90.a. J. P. Collman, L. S. Hegedus "Principles and Applications of Organotransition Metal Chemistry", University Science Books, Mill Valley, California, 1980

b. G. Wilkinson, F. G. A. Stone, E. W. Abel eds. "Comprehensive Organometallic Chemistry", Pergamon Press, Oxford, 1982

91.a. M. E. Bridge, R. A. Marbrow, R. M. Lambert Surf. Sci., 57, 1976, 415

b. J. R. Kingsley, D. Dahlgren, J. C. Hemminger Surf. Sci., 139, 1984, 417

92. M. L. Listerman, R. Schrock Organometallics, 4, 1985, 74

93.a. B. E. Nieuwenhuys, W. M. H. Sachtler Surf. Sci., 34, 1973, 317

b. M. Wilf, P. T. Dawson Surf. Sci., 60, 1976, 561

c. R. A. Shigeish, D. A. King Surf. Sci., 62, 1977, 329

VI.1 APPENDIX A

We wish to show that the sum over ϕ of $\cos^2((\delta)$ [$\phi = \varepsilon+2\pi j/n$ ($j = 0$ to $n-1$)] is independent of ε for n greater than 2.

LEMMA:

Proof of the sum of $\cos(2\pi j/n+\varepsilon)$ or $\sin(2\pi j/n+\varepsilon)$ ($j = 0$ to $n-1$) is zero: Let n_j be the jth nth root of 1. Then $n_j = \exp(2\pi ij/n)$. $n^n = 1$. Therefore:

$n^n - 1 = 0 = (n_1 - 1)(n^{n-1} + n^{n-2} + \ldots + 1) = (n_{j-1} + \ldots + 1)$

Since, for n greater than 1, $n_1 - 1$ does not equal zero;

$(n_{j-1} + \ldots + 1) = 0$. Thus $\exp(2\pi i[j-1]/n) + \ldots + 1 =$

$\cos(2\pi[j-1]/n)+i\sin(2\pi[j-1]/n) + \ldots + 1+i =$

$\{\cos(2\pi[j-1]/n) + \ldots + 1\} + i\{\sin(2\pi[j-1]/n) + \ldots +1\} = 0$

Thus $\cos(2\pi[j-1]/n) + \ldots + 1 = 0$ and

$\sin(2\pi[j-1]/n) + \ldots + 1 = 0$

Similarily, $(\exp[\varepsilon i])*(\exp[2\pi i\{j-1\}/n] + \ldots + 1) = (\exp[\varepsilon i])*0 = 0 =$

$\{\cos(2\pi[j-1]/n +\varepsilon) + \ldots + \cos(\varepsilon)\} + i\{\sin(2\pi[j-1]/n +\varepsilon) + \ldots + \sin(\varepsilon)\}$

Thus $(\cos[2\pi\{j-1\}/n +\varepsilon] + \ldots + \cos[\varepsilon]) = 0$ and

$(\sin[2\pi\{j-1\}/n +\varepsilon] + \ldots + \sin[\varepsilon]) = 0$

END OF LEMMA

Using the definitions from figure 8,

$\cos^2((\delta) = (E\cdot M)^2 = ([0,\sin\theta,\cos\theta]\cdot[\sin\alpha*\cos\phi,\sin\alpha*\sin\phi,\cos\alpha])^2 =$

$(\sin\theta*\sin\alpha*\sin\phi + \cos\theta*\cos\alpha)^2 =$

$\sin^2\phi(\sin^2\alpha*\sin^2\theta) + 2\sin\phi(\sin\alpha*\sin\theta*\cos\theta*\cos\alpha) + \cos^2\alpha*\cos^2\theta$

We want to look at the sum for $\phi = 2\pi j/n + \varepsilon$ for $j = 0$ to $n-1$.

By the lemma the second term goes to zero, and the third term is independent of ϕ, thus we need only examine the first term, in fact we need only show that the sum of $\sin^2\phi$ for $\phi = 2\pi j/n + \varepsilon$ for $j = 1$ to $n-1$

is independent of ε.
So:

$\sin^2\phi = 1 + (1/2)\sin(2\phi)$

If n = 1 then by inspection the assertion is not true.

If n = 2 then the assertion is not true, because the sum becomes

$2 + (1/2)\{\sin 2\varepsilon + \sin(2\varepsilon + 2\pi)\} = 2 + \sin 2\varepsilon$

If n is even and greater than 2 then let m = n/2 then

$1+(1/2)\sin 2\varepsilon + 1+(1/2)\sin(4\pi/n + 2\varepsilon) + \ldots + 1+(1/2)\sin(4\pi[n-1]/n + 2\varepsilon) =$

$2\{1+[1/2]\sin 2\varepsilon + 1+(1/2)\sin(2\pi/m + 2\varepsilon) + \ldots + 1+(1/2)\sin(2\pi[m-1]/m + 2\varepsilon)\} =$

n + 0 (by the lemma) which is independent of ε.

If n is greater than 2 and odd, then let m = (n-1)/2

$1+(1/2)\sin 2\varepsilon + 1+(1/2)\sin(2\pi/n + \ldots + 1+(1/2)\sin(4\pi[n-1]/n + 2\varepsilon) =$

the sum of $\{(1 + (1/2)\sin 2\phi)$ for j = 1 to m$\}$ +

the sum of $\{(1 + (1/2)\sin 2\phi)$ for j = m+1 to n$\}$

The first sum is a sum over all ϕ of the form $2\pi j/n + \varepsilon$ for j even

and the second sum is over all ϕ of the form $2\pi j/n + \varepsilon$ for j odd

(for example, $4\pi[m+1]/n = 2\pi 2[m+1]/n = 2\pi[n+1]/n = 2\pi/n$)

which, by the lemma = n + 0, independent of ε

Thus the sum of $\cos^2\delta$ or $\sin^2\delta$ is independent of rotation about the surface normal for domains with 3 fold or higher symmetry.

APPENDIX B

Here we present without interpretation NEXAFS spectra of various cyano and isocyano compounds.

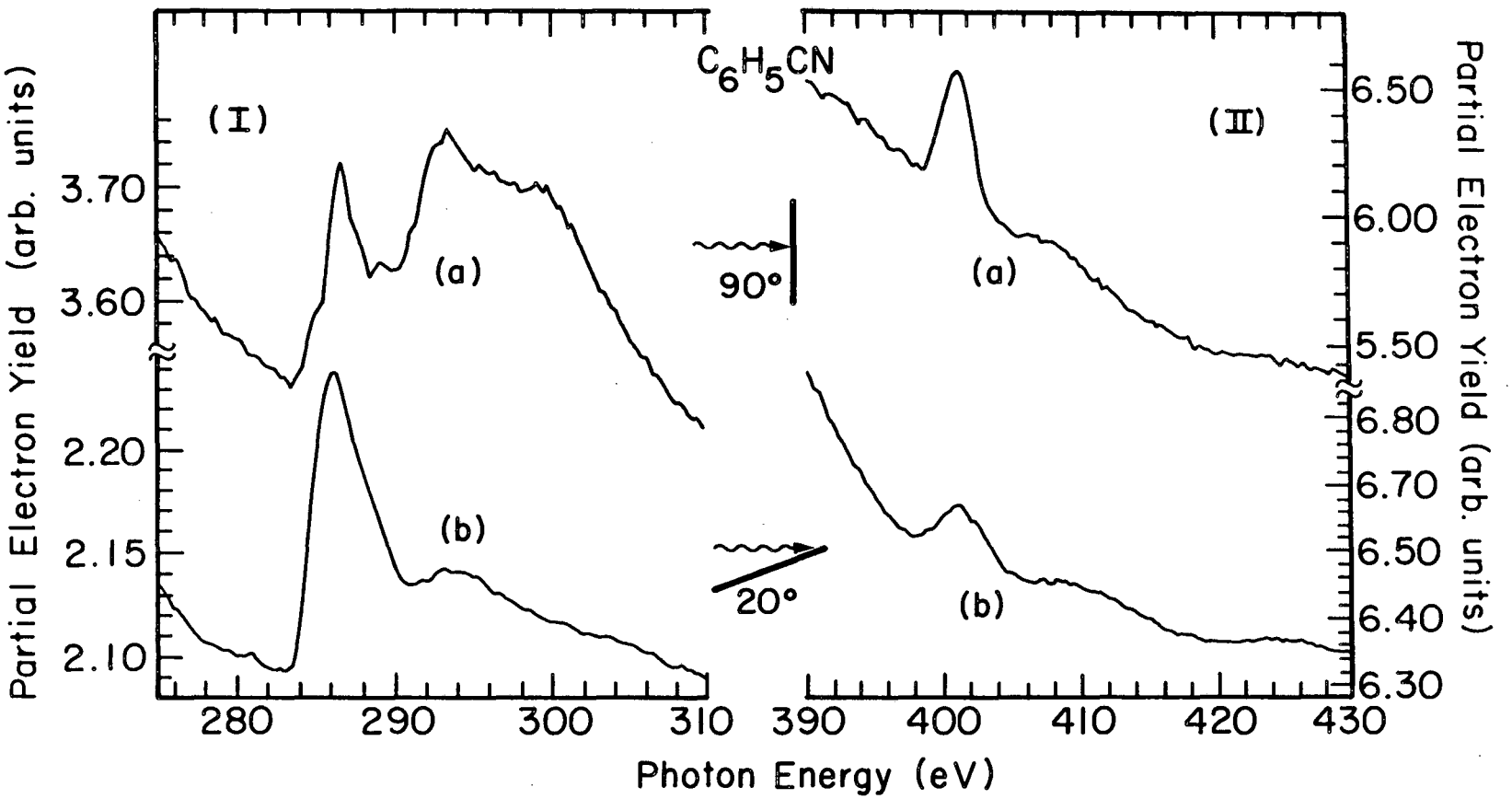

XBL 8512-5138

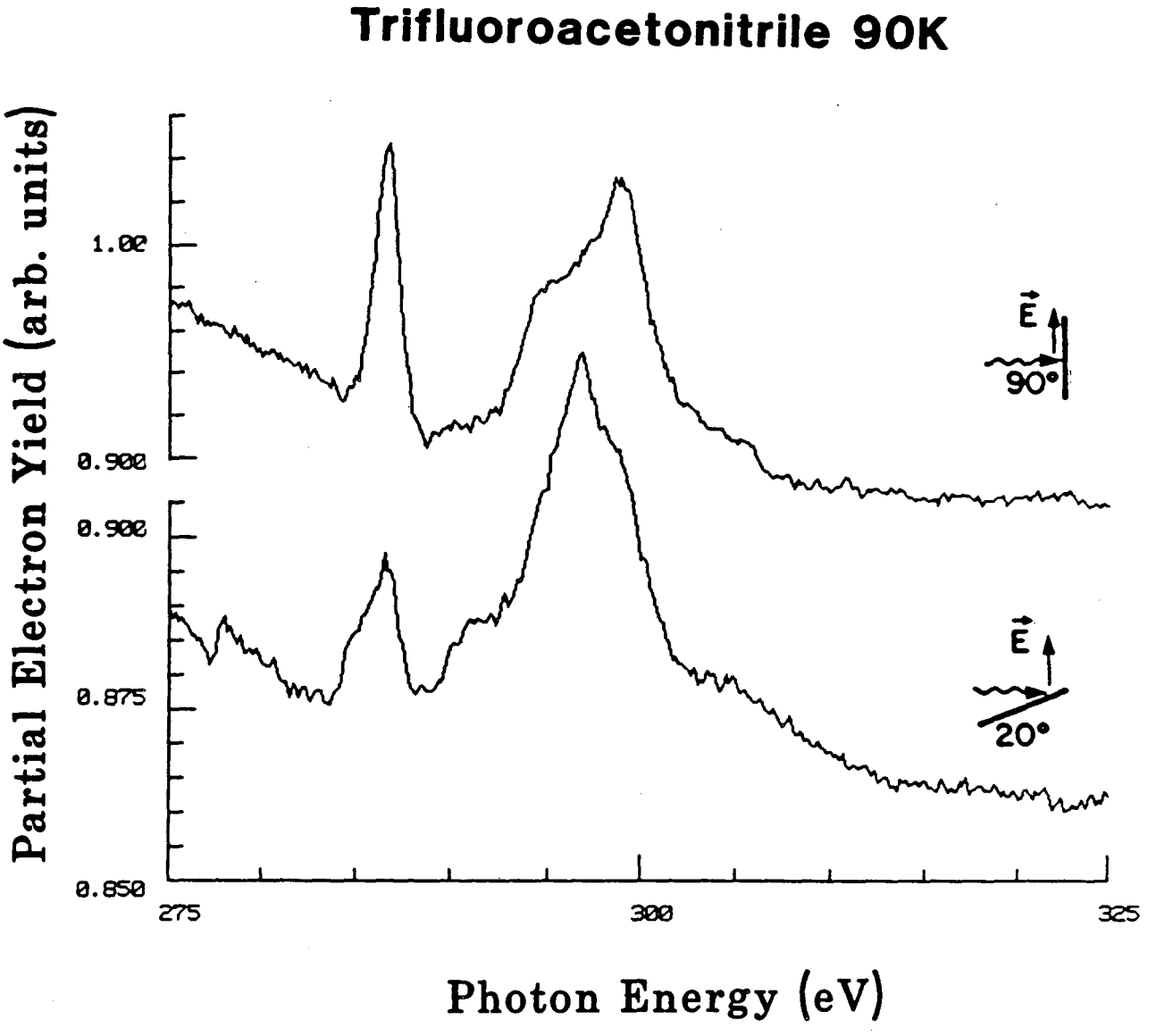
Trifluoroacetonitrile 90K
Partial Electron Yield (arb. units)
1.00
0.900
0.900
0.875
0.850
275
300
325
Photon Energy (eV)
E
90°
E
20°

Trifluoroacetonitrile 90K

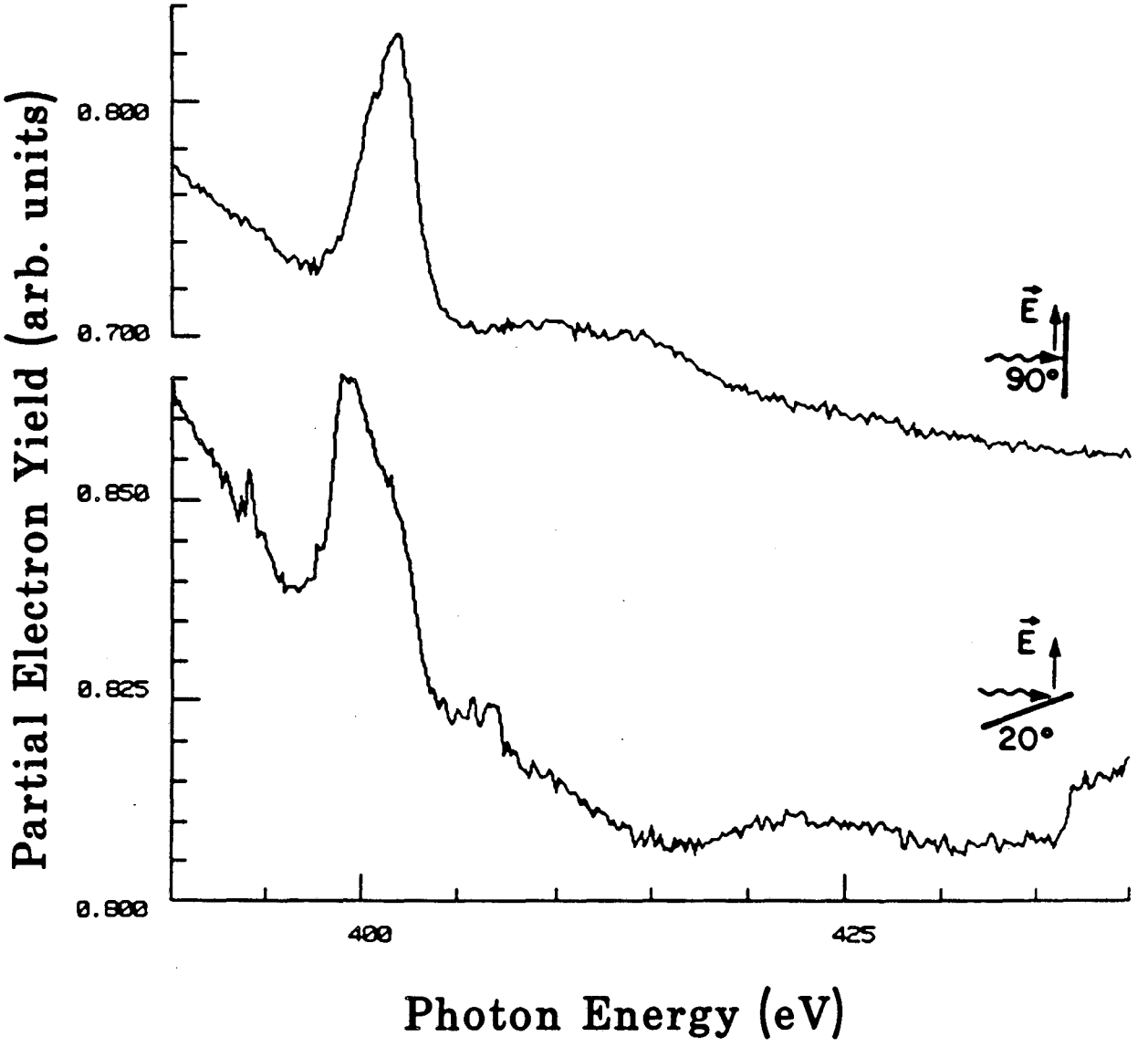

Trifluoroacetonitrile 140K

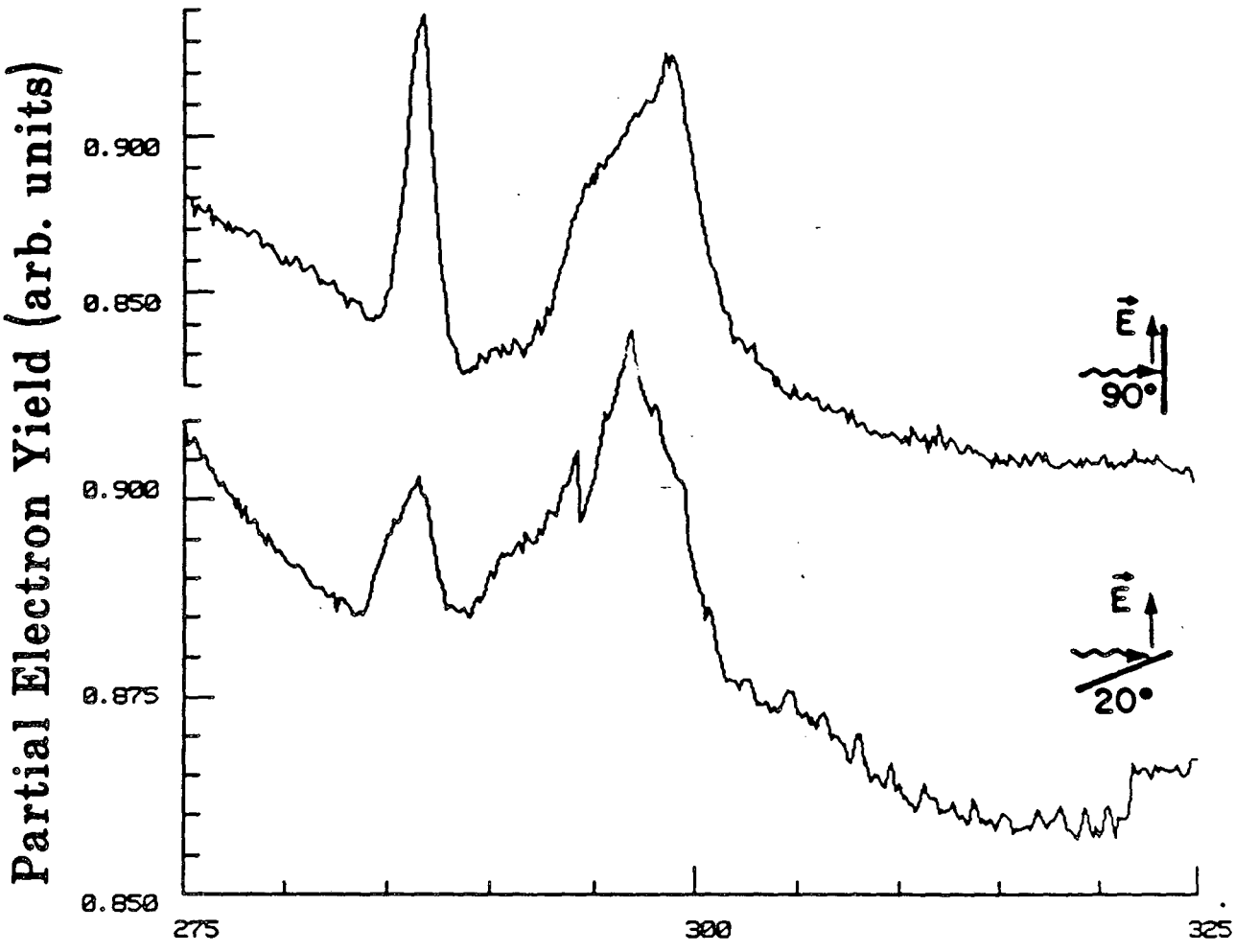

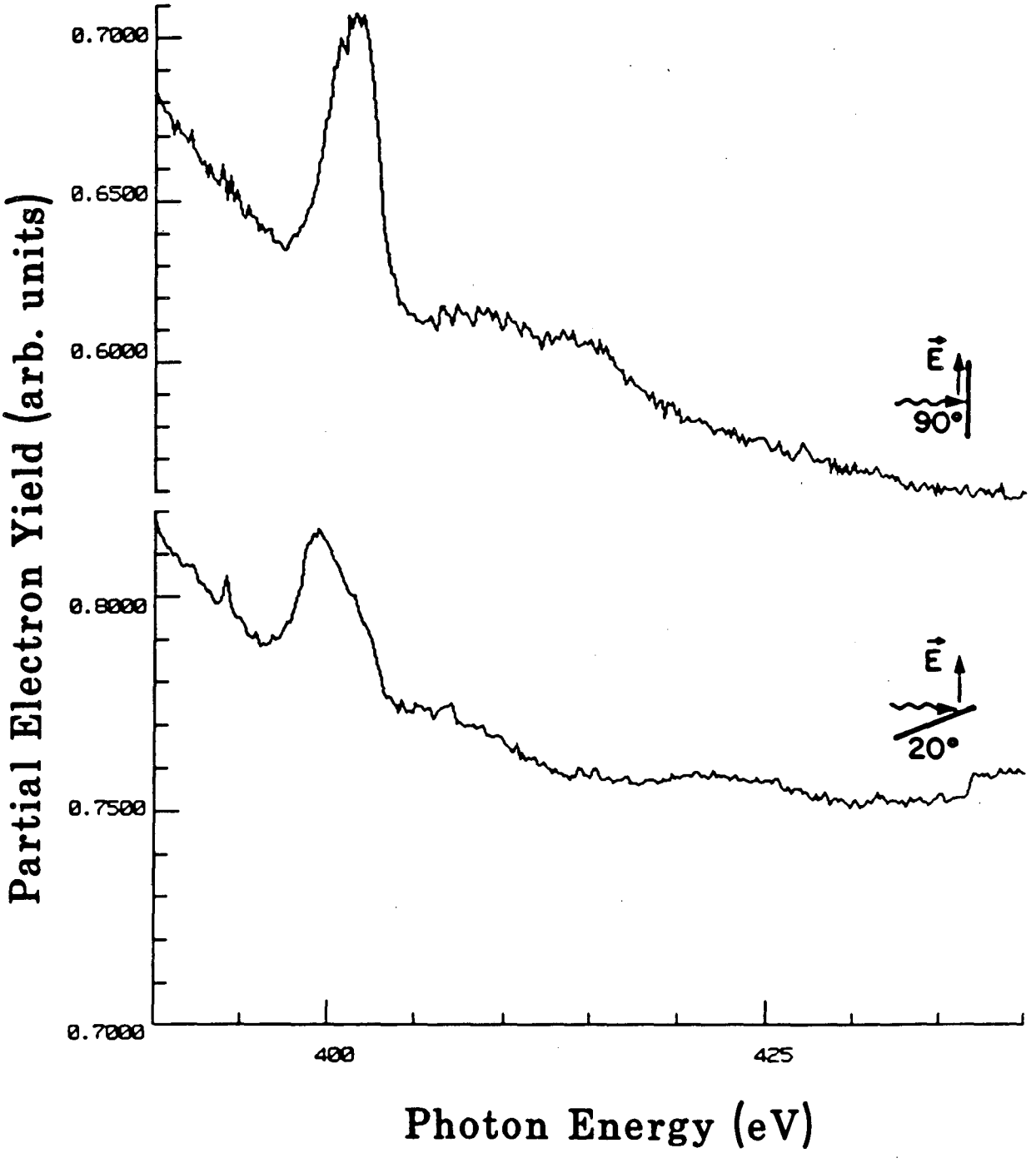
Trifluoroacetonitrile 140K
Partial Electron Yield (arb. units)
0.7000
0.6500
0.6000
0.8000
0.7500
0.7000
400
425
Photon Energy (eV)
E
90°
E
20°

HCN 310K

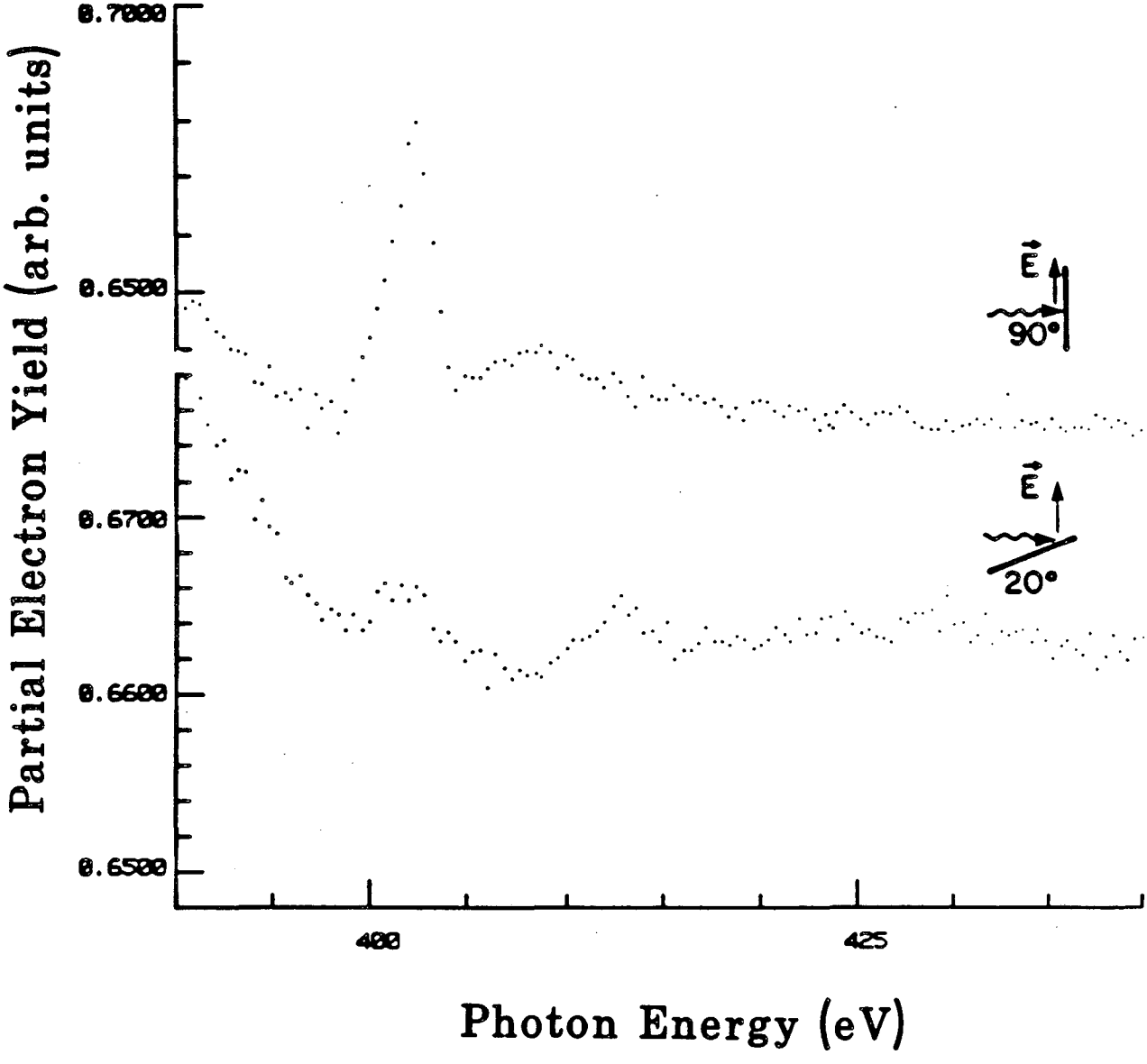
Partial Electron Yield (arb. units)
0.7000
0.6500
0.6700
0.6600
0.6500
400
425
Photon Energy (eV)
E
90°
E
20°

Trifluoroacetonitrile 250K

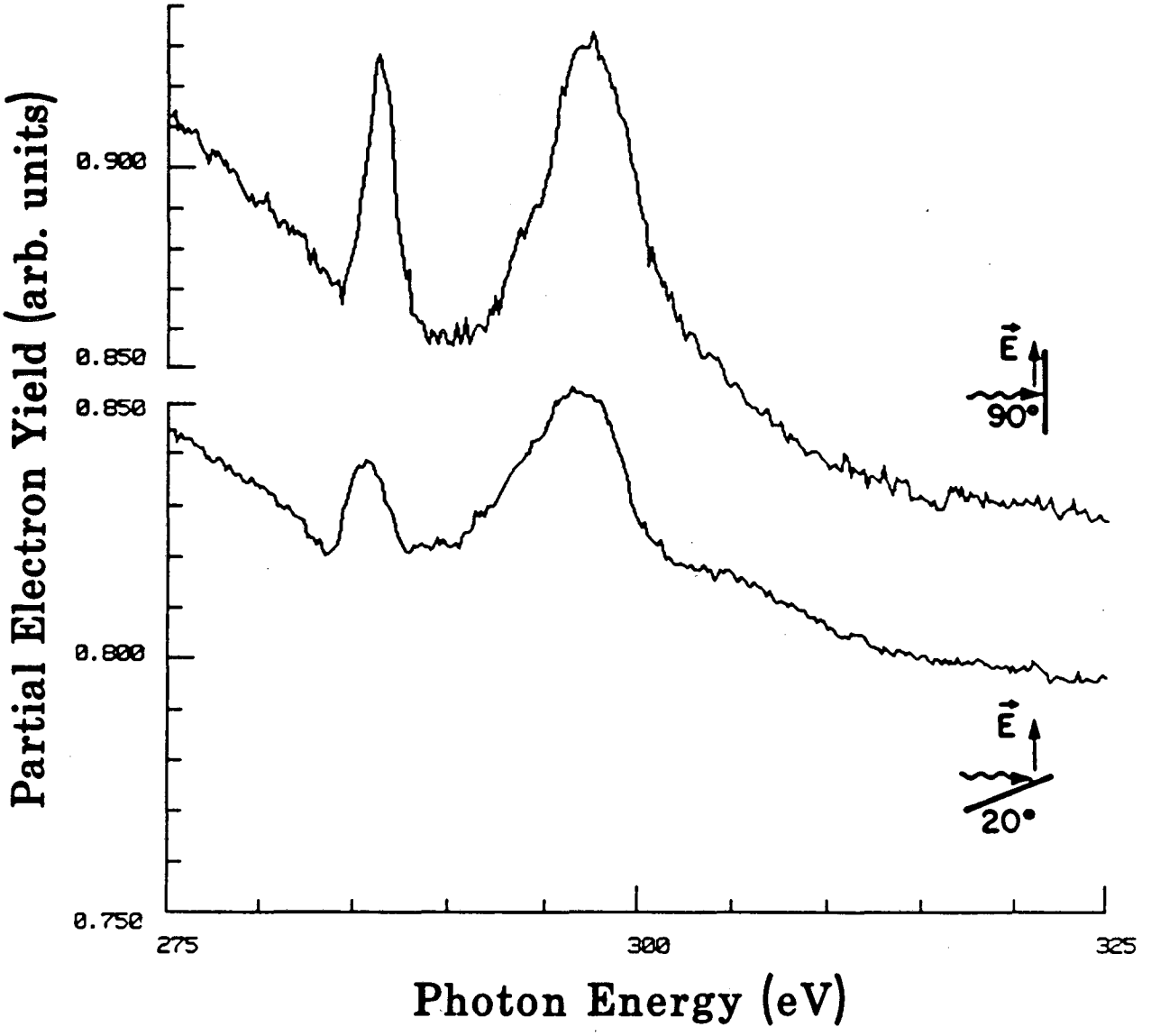

Trifluoroacetonitrile 250K

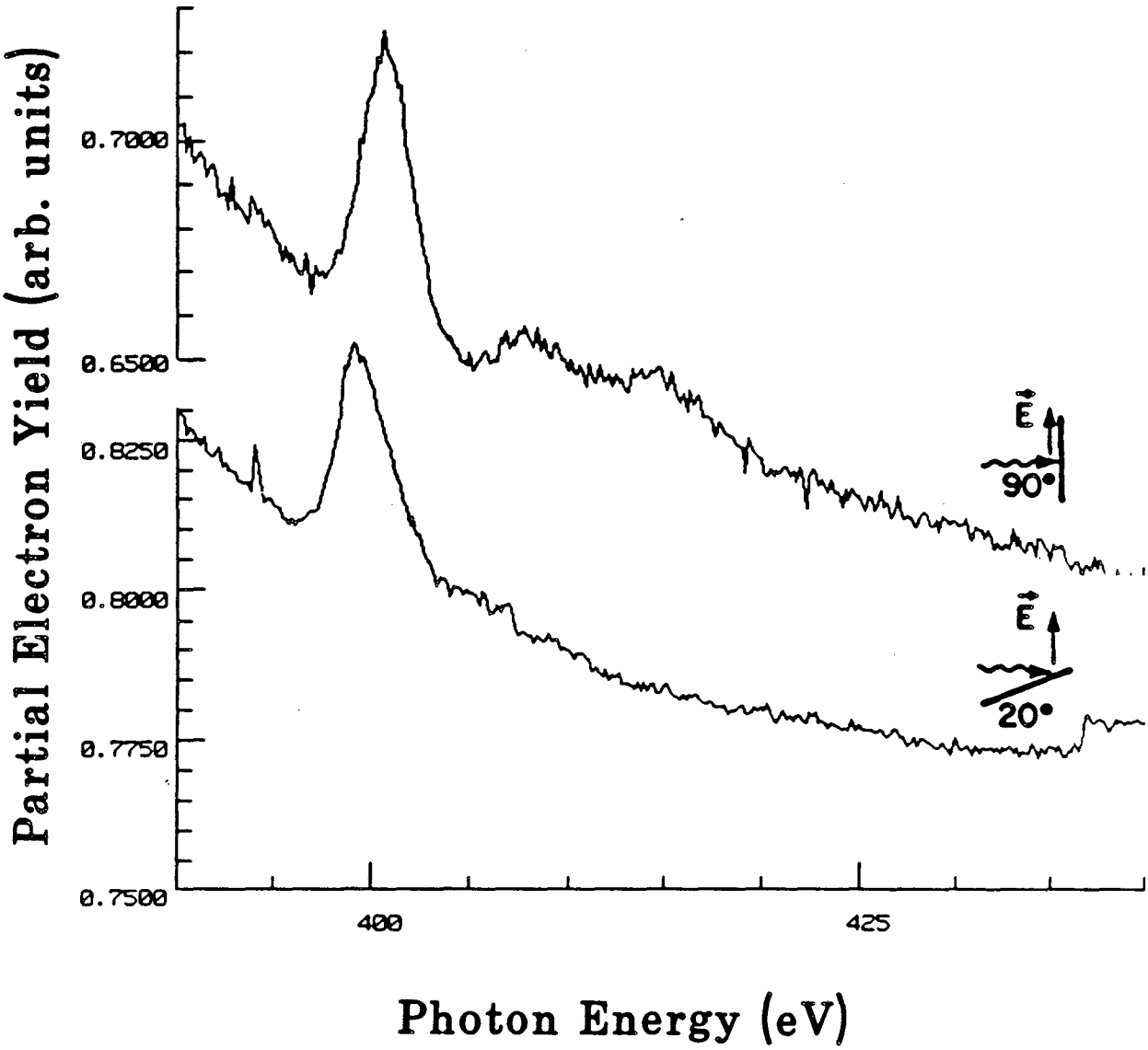

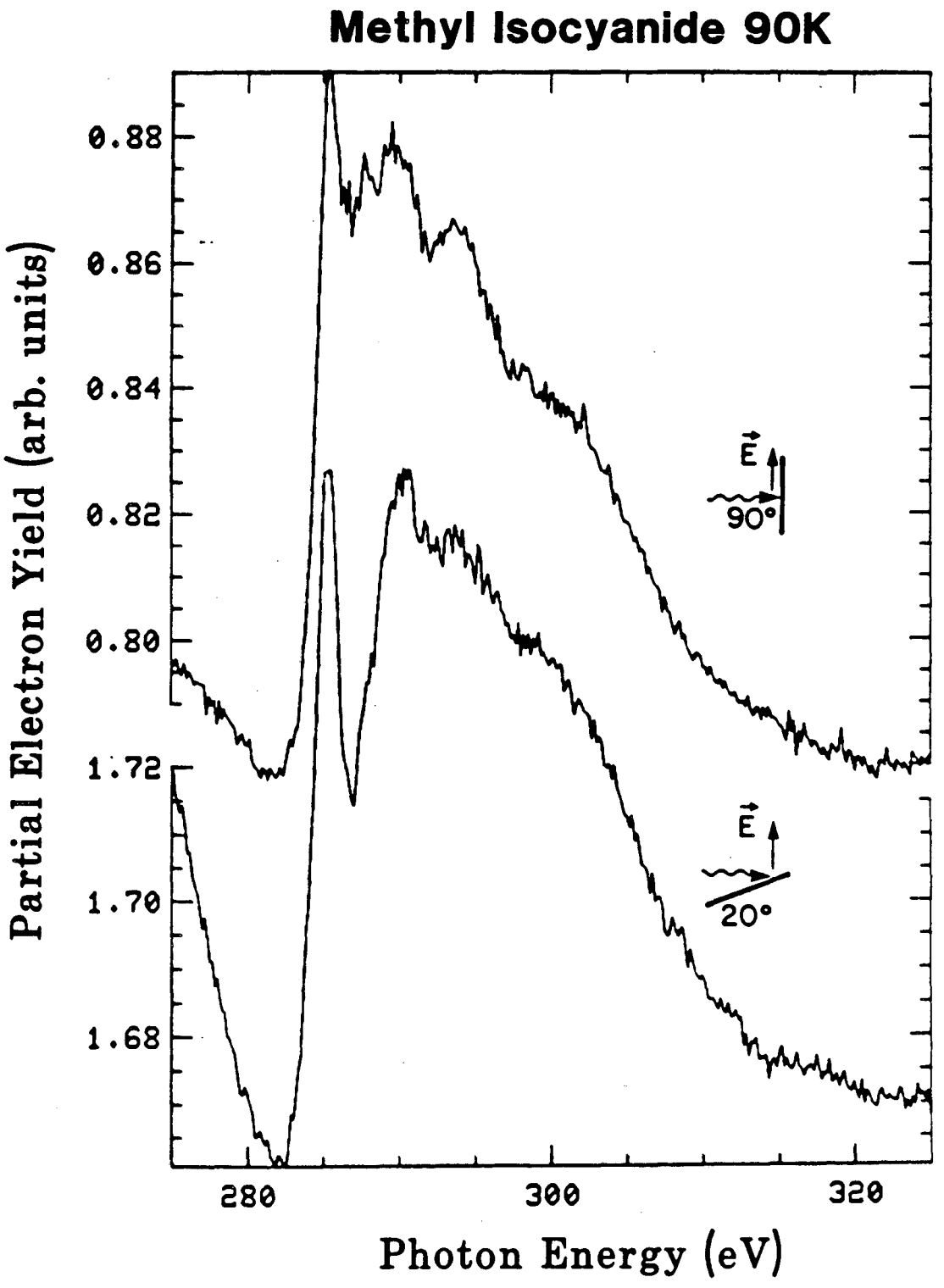
Methyl Isocyanide 90K
Partial Electron Yield (arb. units)
0.88
0.86
0.84
0.82
0.80
1.72
1.70
1.68
E
90°
E
20°
280
300
320
Photon Energy (eV)

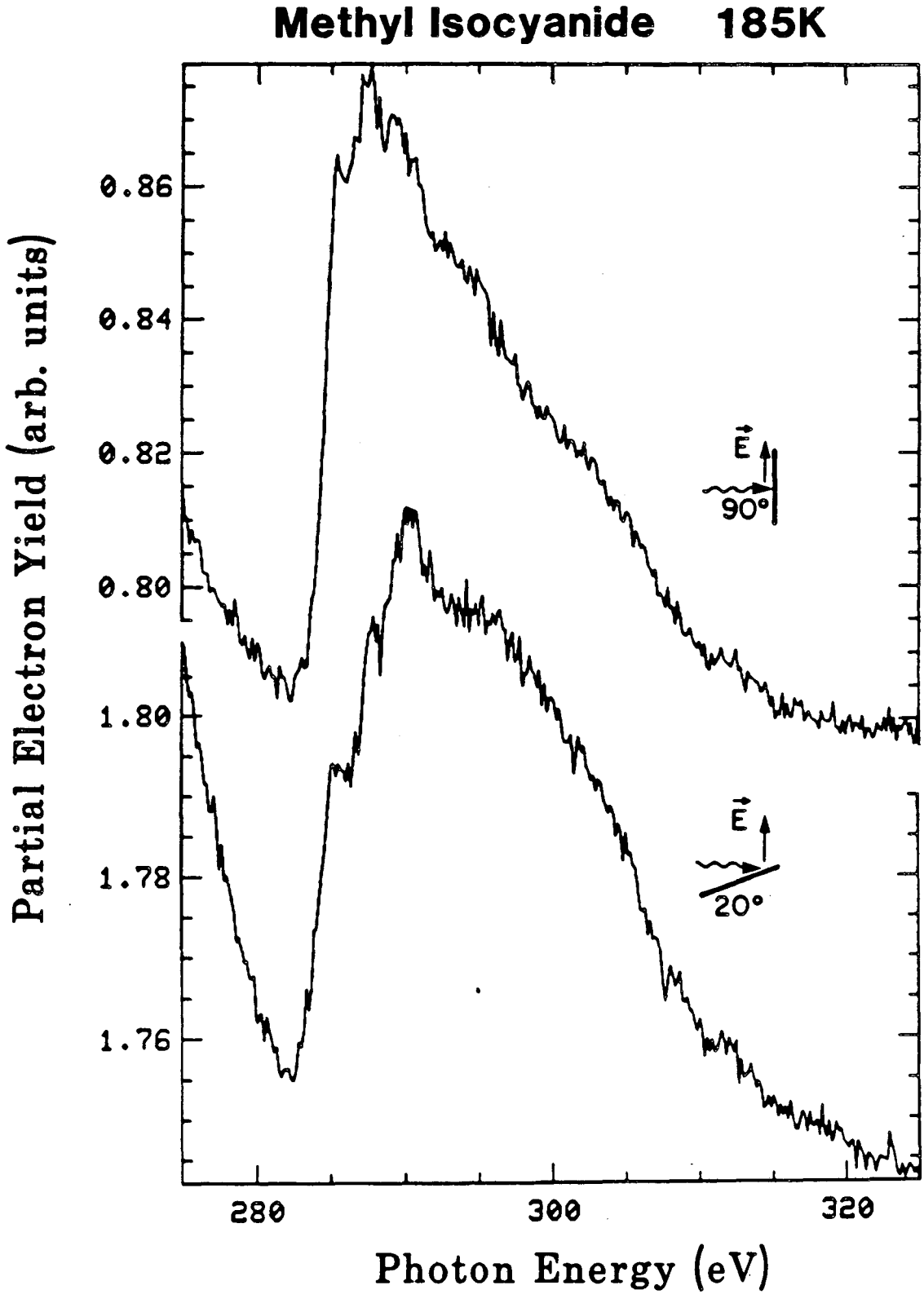
Methyl Isocyanide 185K
Partial Electron Yield (arb. units)
0.86
0.84
0.82
0.80
1.80
1.78
1.76
E
90°
E
20°
280
300
320
Photon Energy (eV)

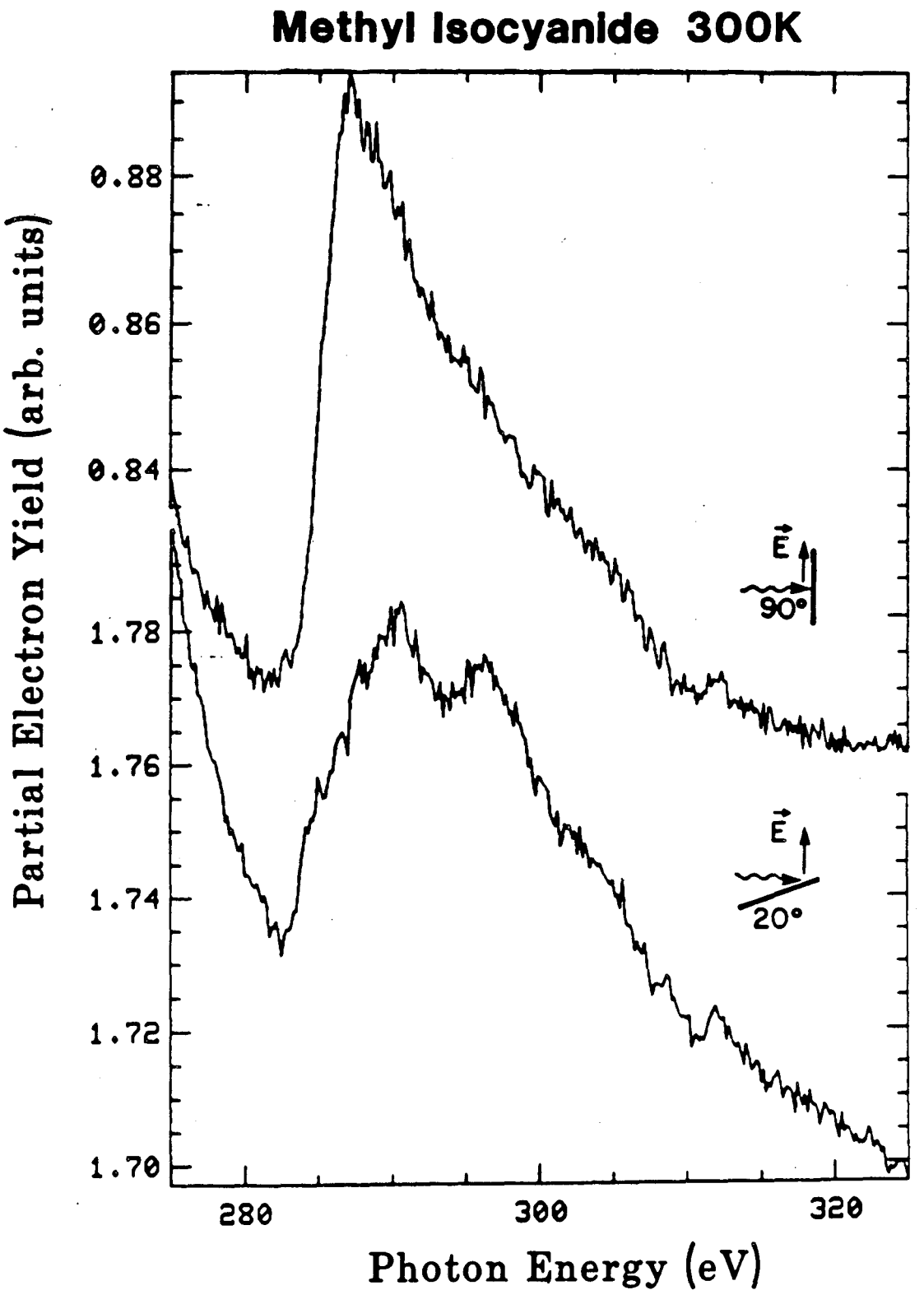
Methyl Isocyanide 300K
Partial Electron Yield (arb. units)
0.88
0.86
0.84
1.78
1.76
1.74
1.72
1.70
280
300
320
Photon Energy (eV)
E
90°
E
20°

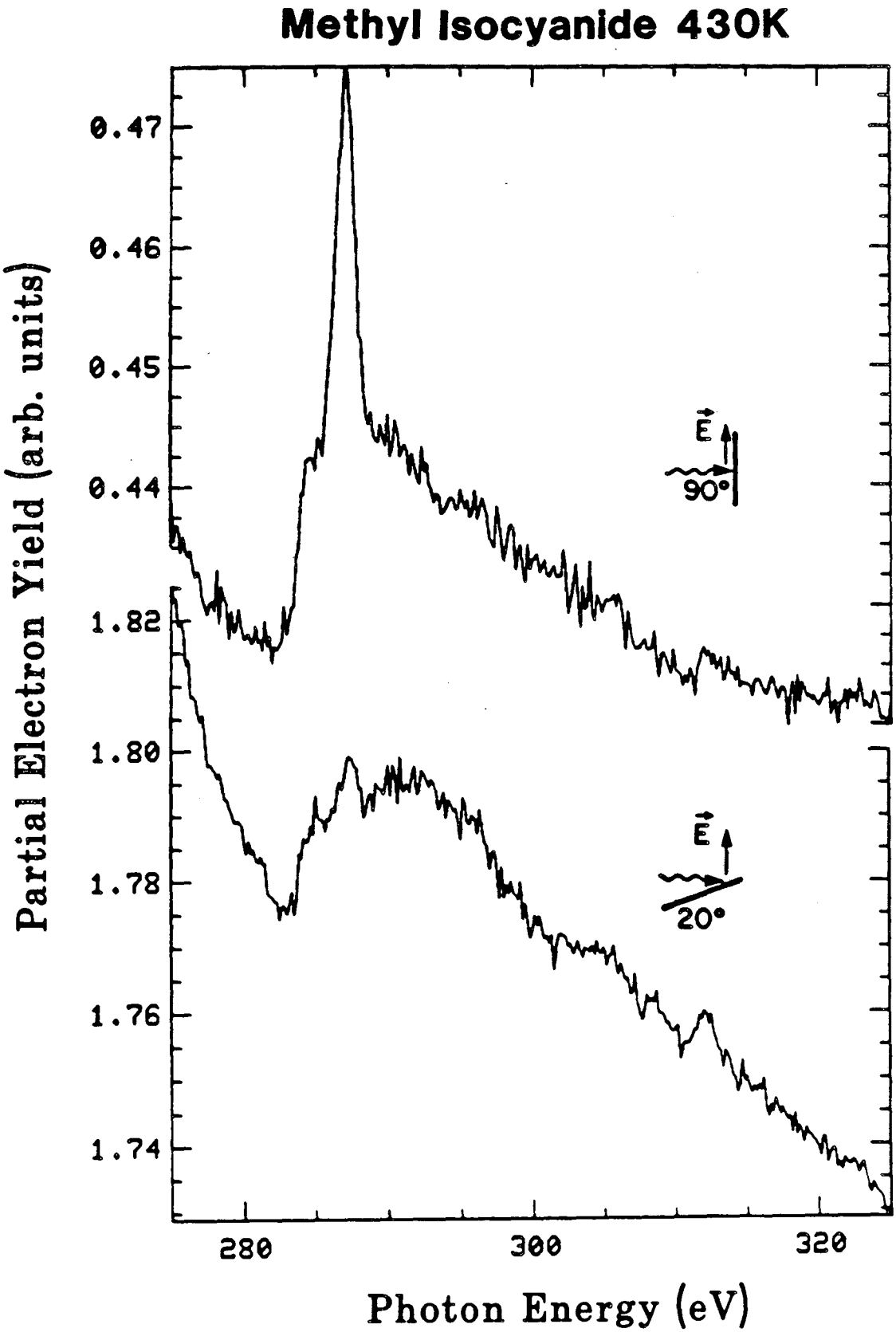
Methyl Isocyanide 430K
Partial Electron Yield (arb. units)
0.47
0.46
0.45
0.44
1.82
1.80
1.78
1.76
1.74
E
90°
E
20°
280
300
320
Photon Energy (eV)

HCN 90K

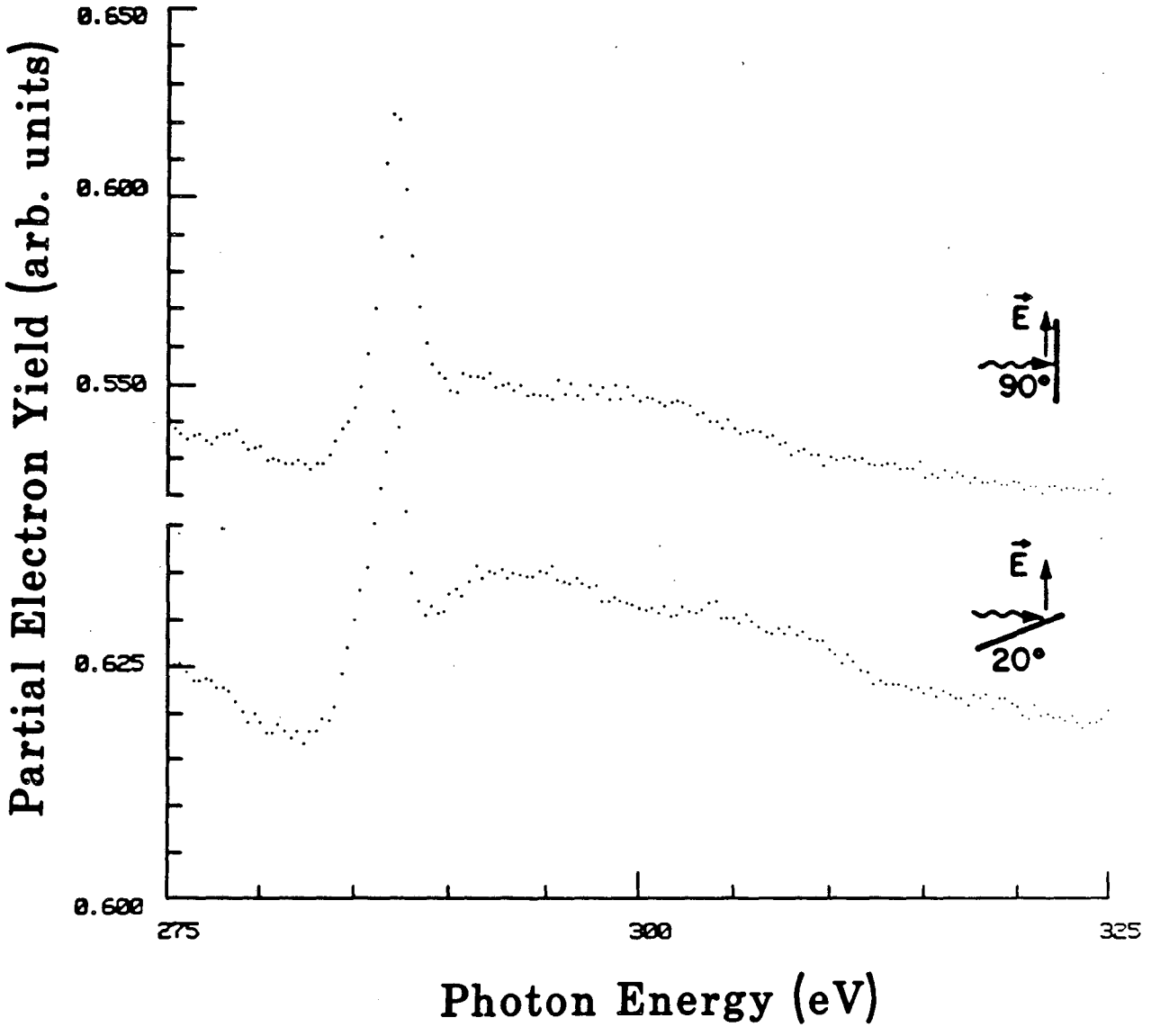
Partial Electron Yield (arb. units)
0.650
0.600
0.550
0.625
0.600
275
300
325
Photon Energy (eV)
E
90°
E
20°

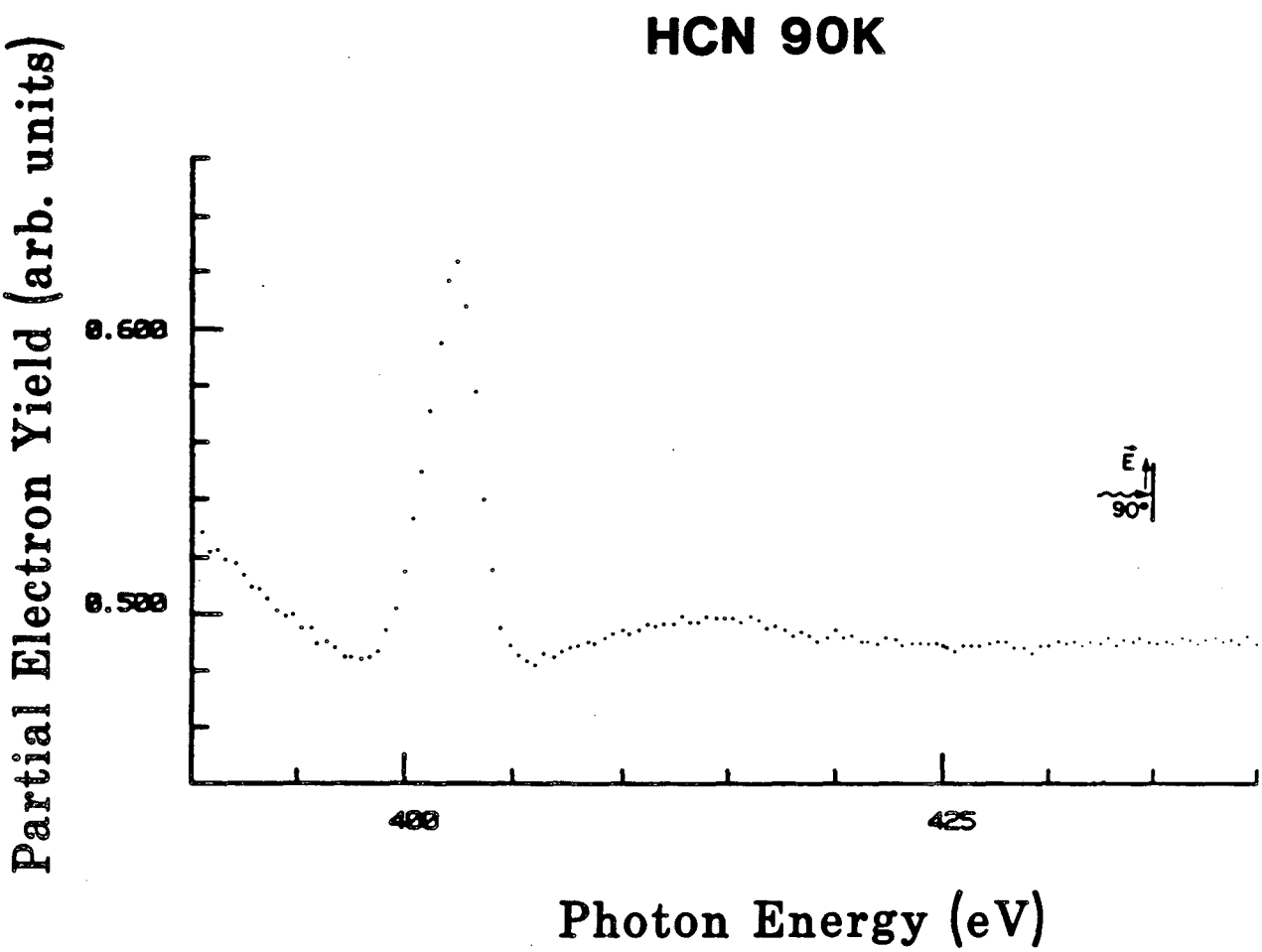
HCN 90K
Partial Electron Yield (arb. units)
0.600
0.500
400
425
Photon Energy (eV)
E
90°

HCN 130K

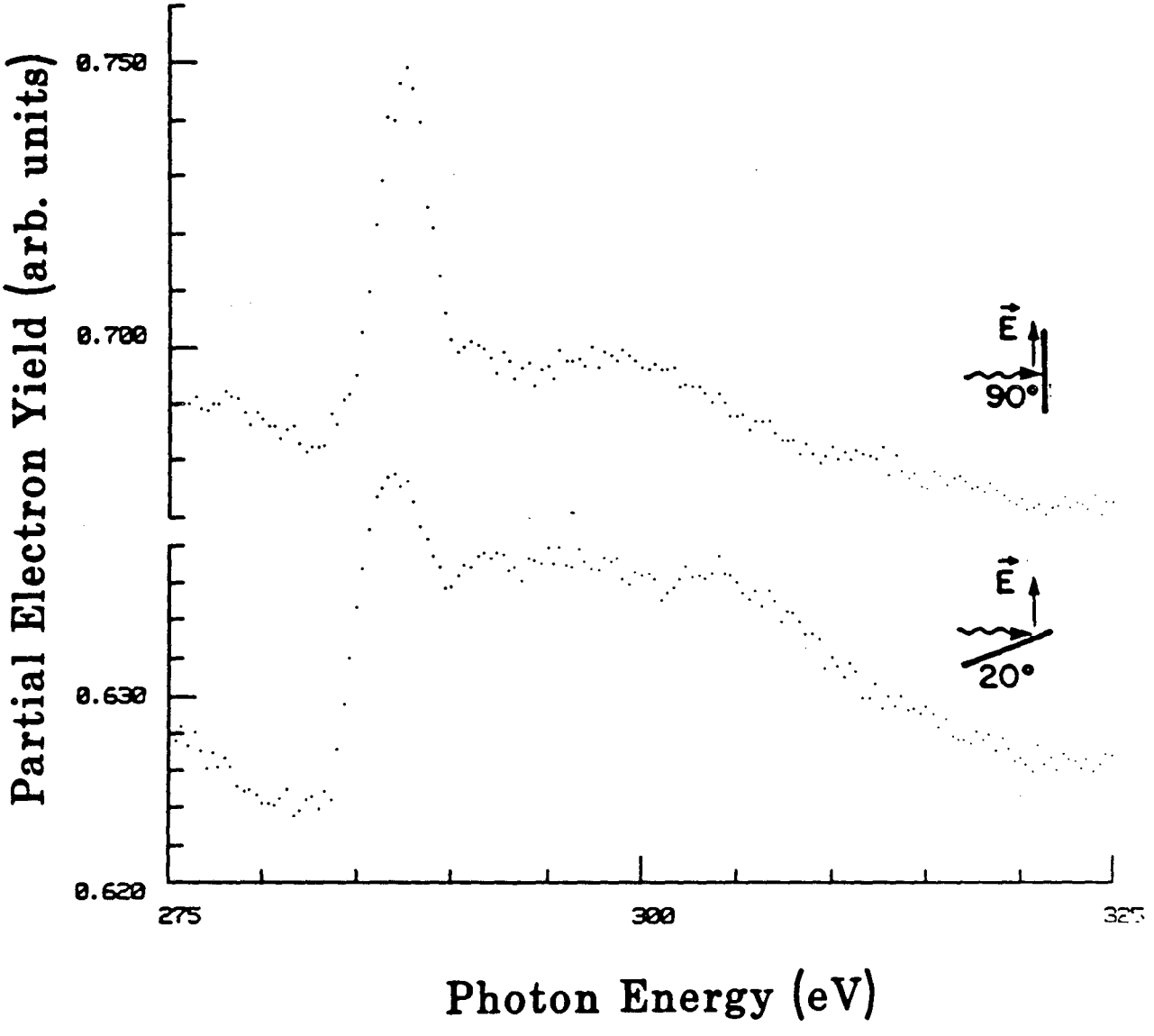
Partial Electron Yield (arb. units)
0.750
0.700
0.630
0.620
E
90°
E
20°
275
300
325
Photon Energy (eV)

HCN 130K

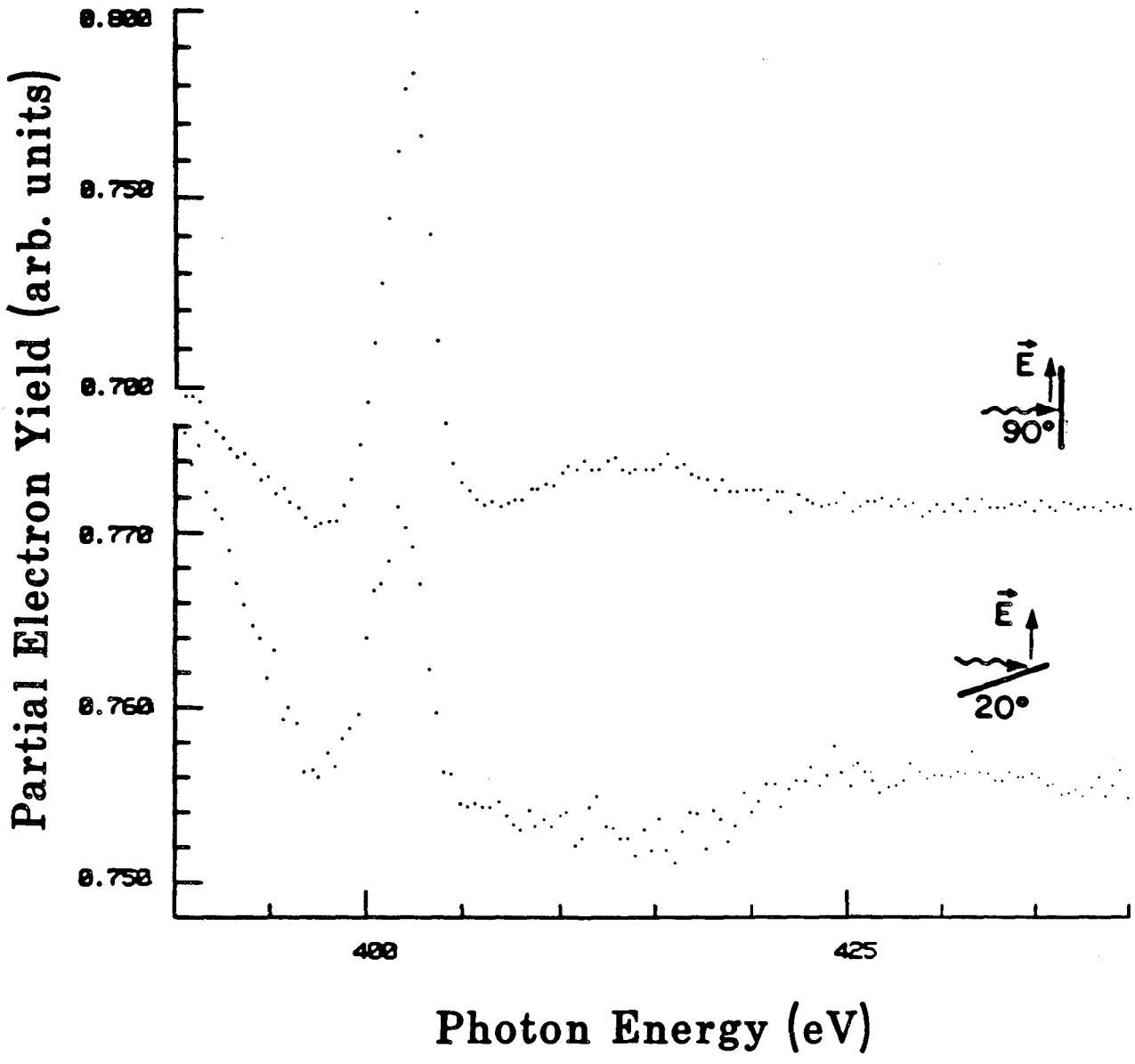
Partial Electron Yield (arb. units)
0.800
0.750
0.700
0.770
0.760
0.750
400
425
Photon Energy (eV)
E
90°
E
20°

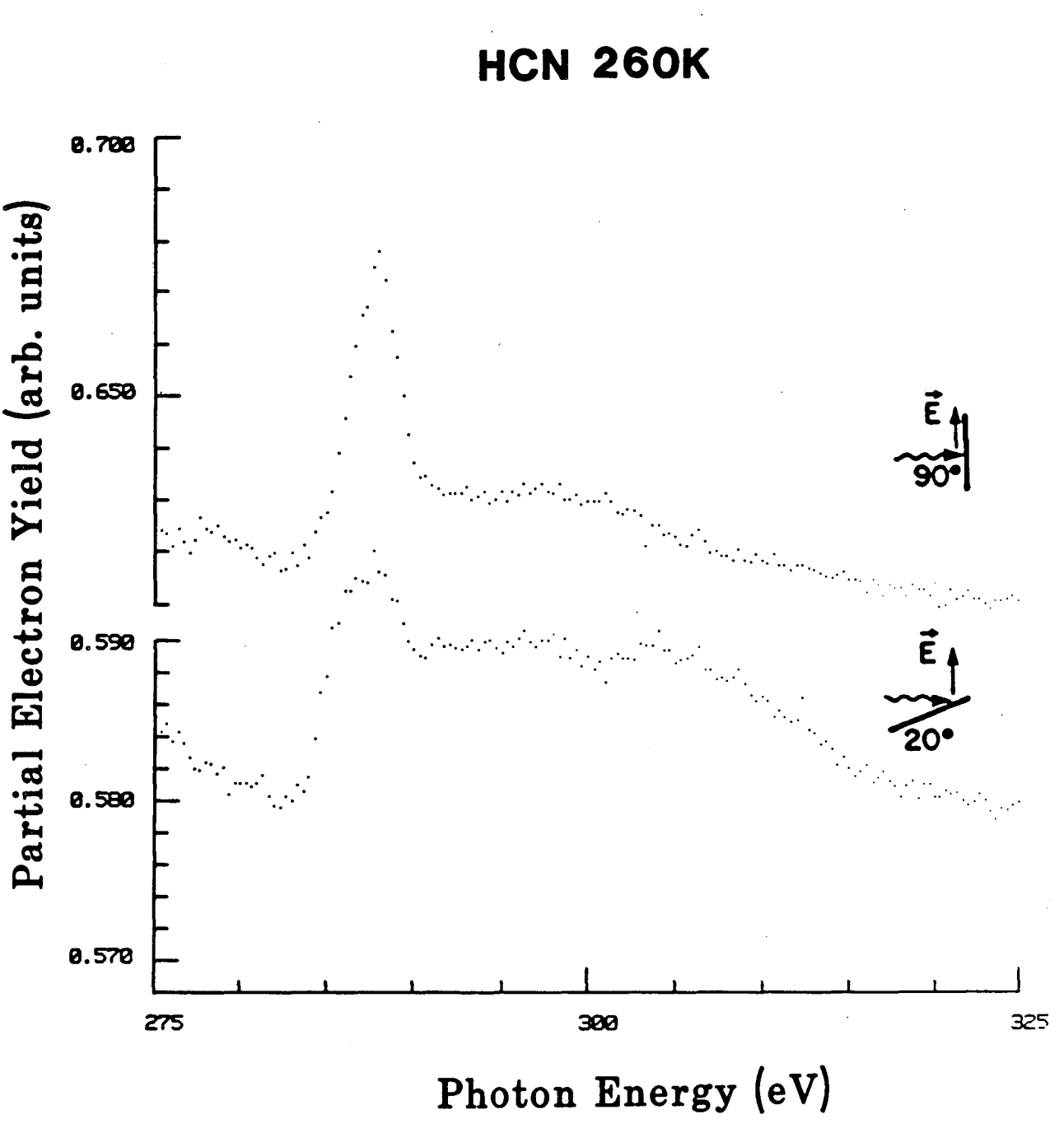
HCN 260K
Partial Electron Yield (arb. units)
0.700
0.650
0.590
0.580
0.570
E
90°
E
20°
275
300
325
Photon Energy (eV)

HCN 260K

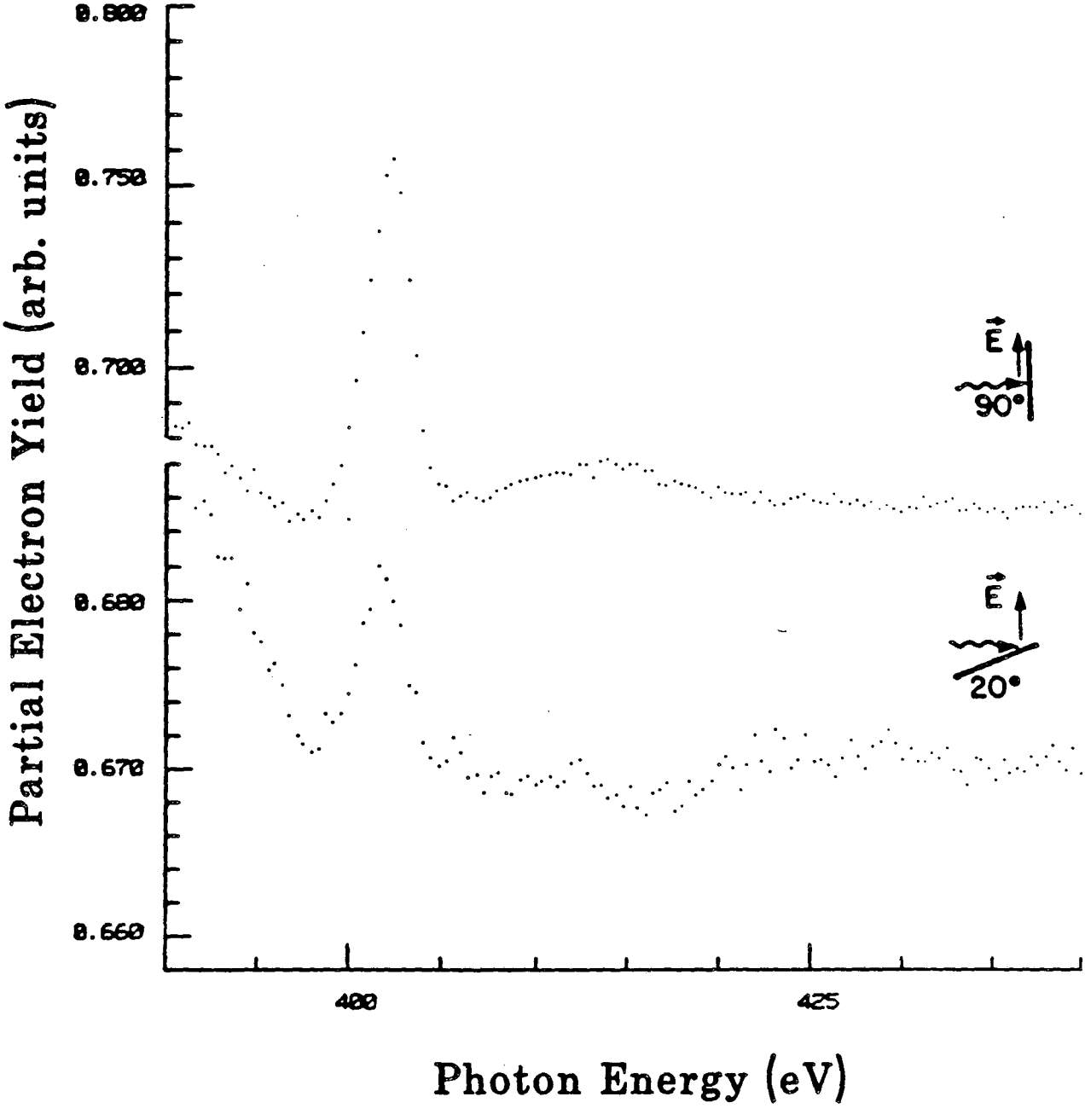
0.800
0.750
0.700
0.680
0.670
0.660
Partial Electron Yield (arb. units)
400
425
Photon Energy (eV)
E
90°
E
20°

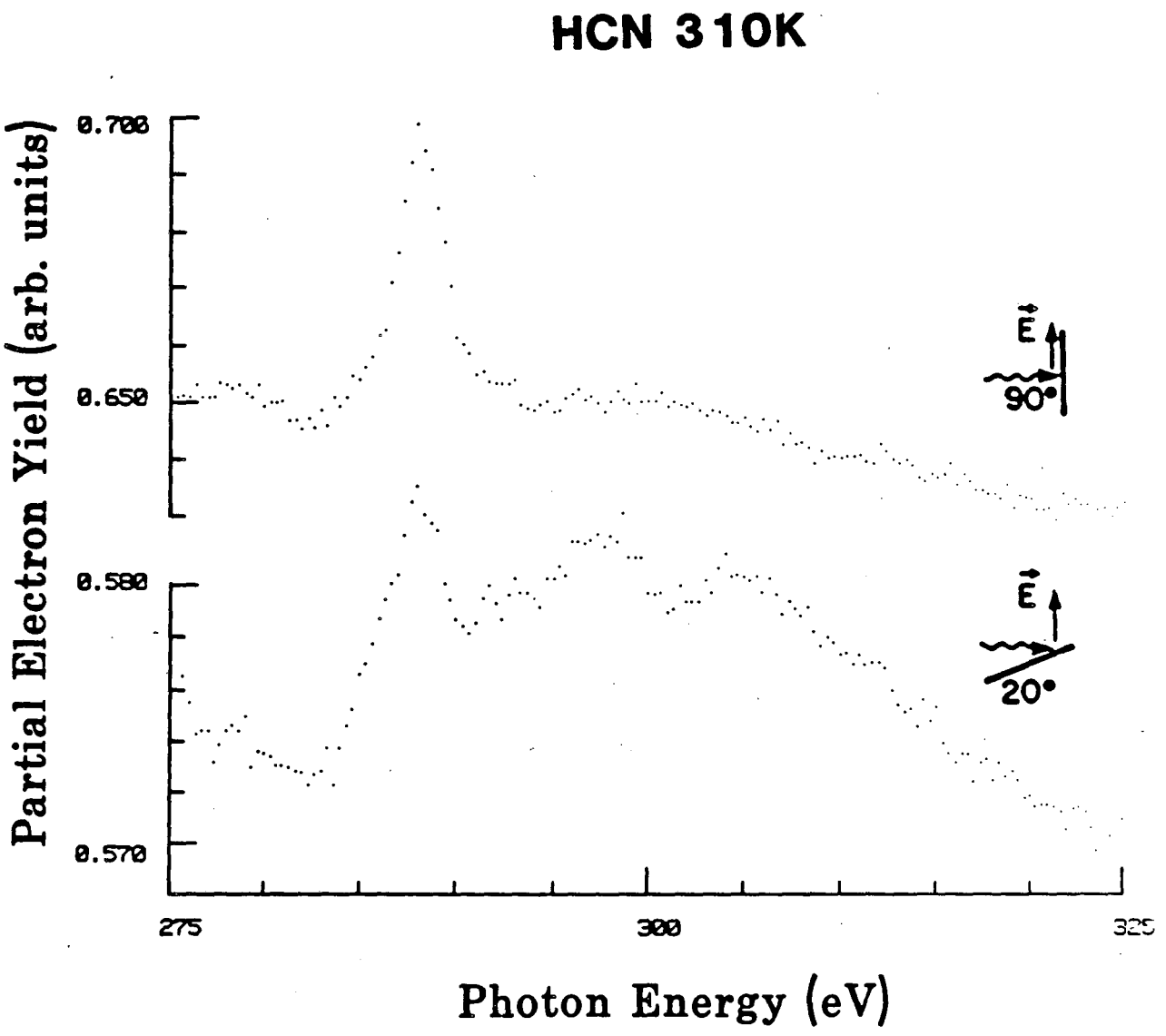
HCN 310K
Partial Electron Yield (arb. units)
0.700
0.650
0.580
0.570
E
90°
E
20°
275
300
325
Photon Energy (eV)

HCN 310K

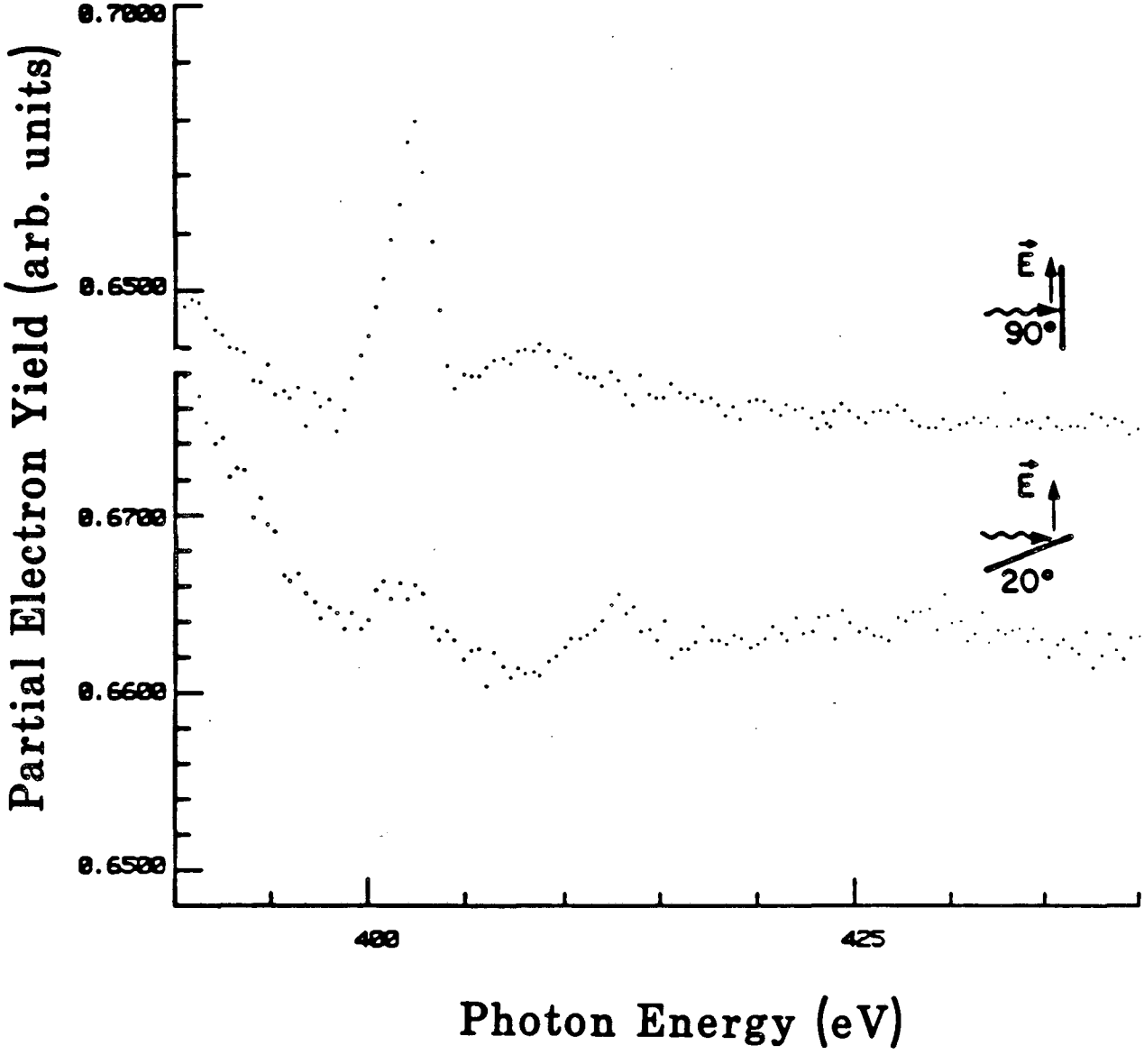
Partial Electron Yield (arb. units)
0.7000
0.6500
0.6700
0.6600
0.6500
400
425
Photon Energy (eV)
E
90°
E
20°

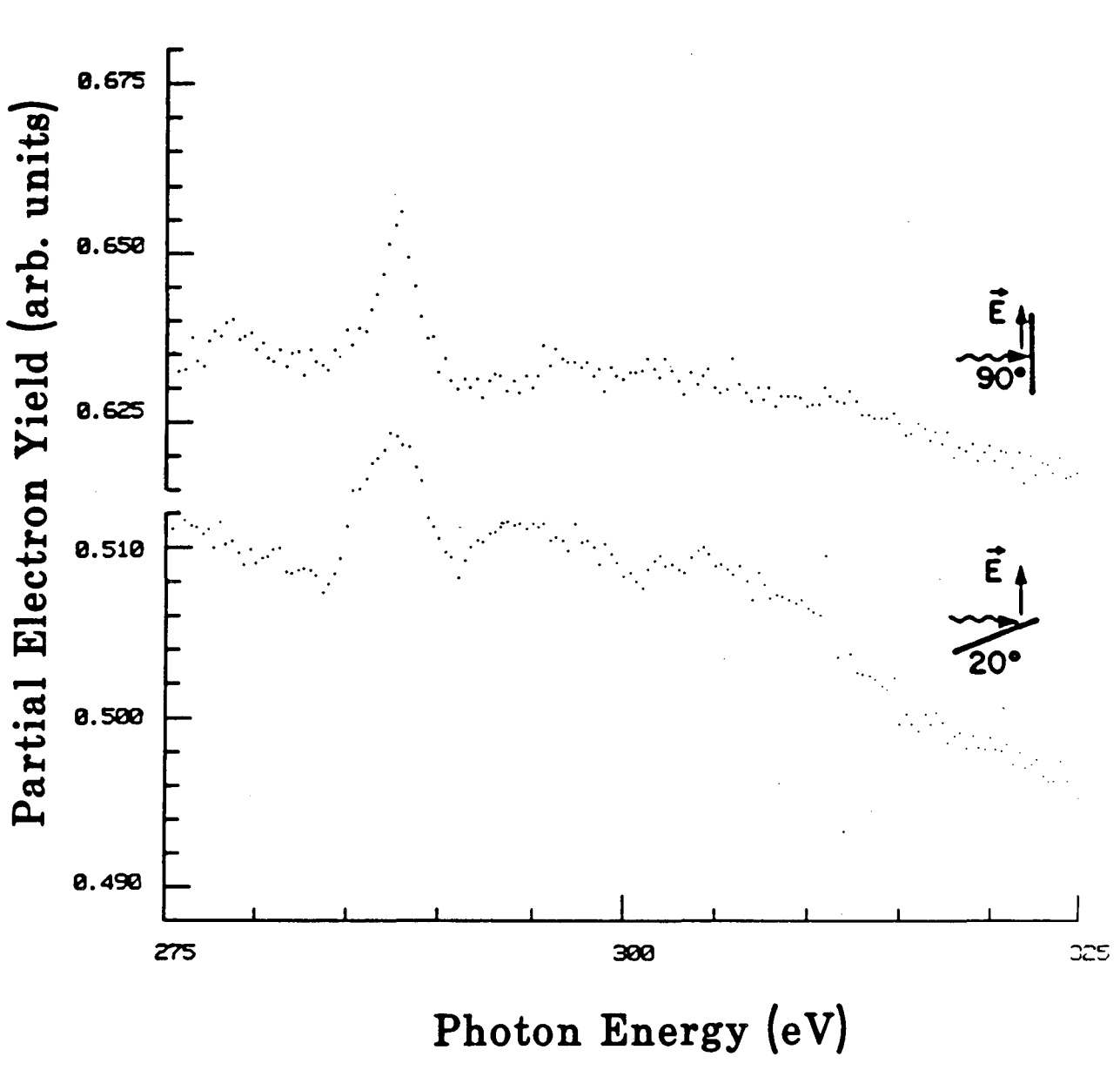
HCN 540K
Partial Electron Yield (arb. units)
0.675
0.650
0.625
0.510
0.500
0.490
E
90°
E
20°
275
300
325
Photon Energy (eV)

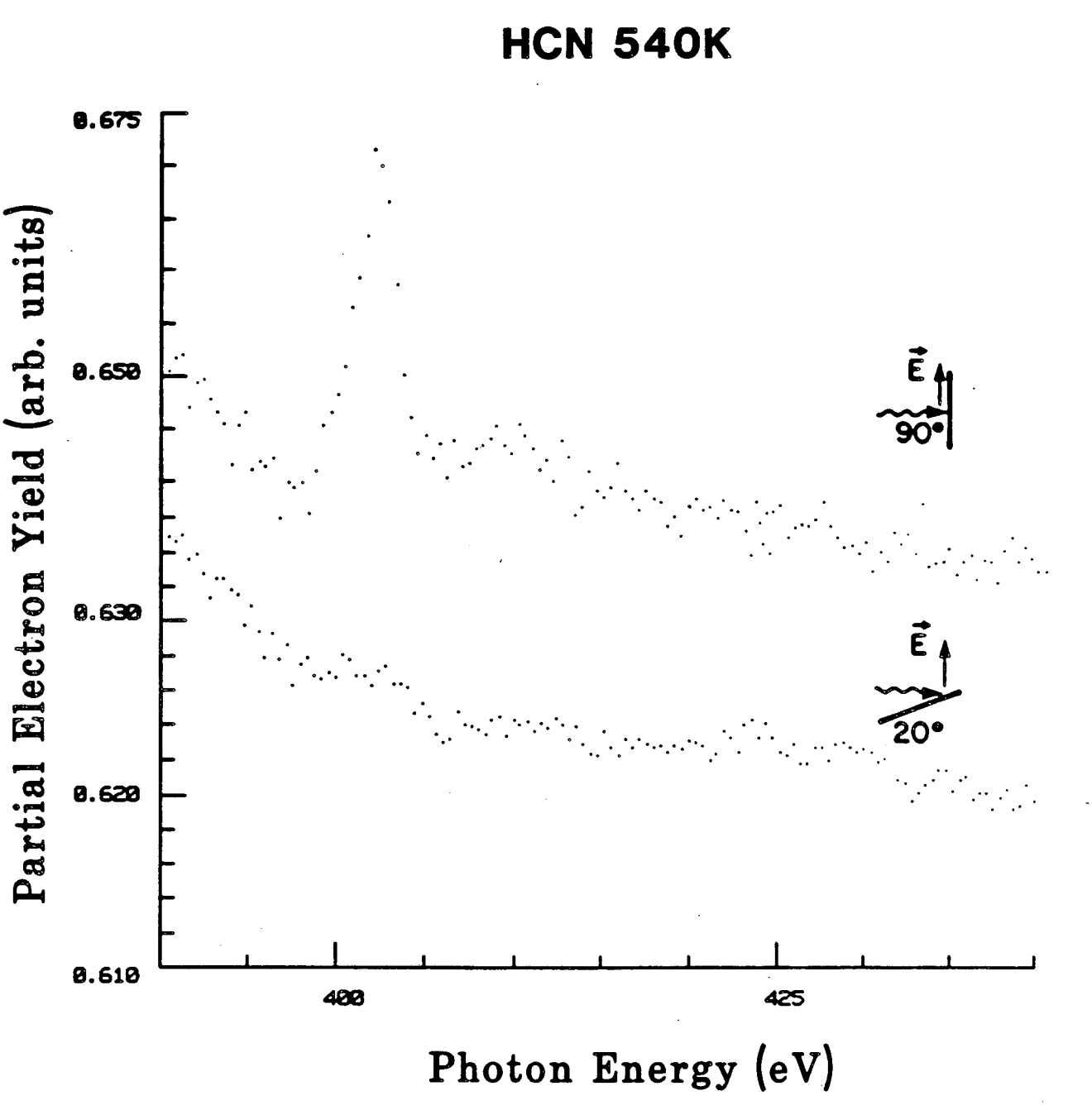
HCN 540K
Partial Electron Yield (arb. units)
0.675
0.650
0.630
0.620
0.610
400
425
Photon Energy (eV)
E
90°
E
20°

This report was done with support from the Department of Energy. Any conclusions or opinions expressed in this report represent solely those of the author(s) and not necessarily those of The Regents of the University of California, the Lawrence Berkeley Laboratory or the Department of Energy.

Reference to a company or product name does not imply approval or recommendation of the product by the University of California or the U.S. Department of Energy to the exclusion of others that may be suitable.

LAWRENCE BERKELEY LABORATORY
TECHNICAL INFORMATION DEPARTMENT
UNIVERSITY OF CALIFORNIA
BERKELEY, CALIFORNIA 94720